

NKS-426  
ISBN 978-87-7893-516-8

---

Determination of Fire Barriers reliability for fire risk  
assessment of Nuclear Power Plants.  
(FIREBAN) – Final Report

Patrick van Hees<sup>1</sup>  
Simo Hostikka<sup>2</sup>  
Topi Sikanen<sup>3</sup>  
Dan Lauridsen<sup>4</sup>  
Sebastian Levin<sup>5</sup>

<sup>1</sup>Lund University, Sweden

<sup>2</sup>Aalto University, Finland

<sup>3</sup>VTT Technical Research Institute, Finland

<sup>4</sup>DBI Danish Institute of Fire and Security Technology, Denmark

<sup>5</sup>Ringhals AB, Sweden

July 2019

## **Abstract**

Fires in nuclear power plants can be an important hazard for the overall safety of the facility. An important factor in reducing the spread of the fire is the use of fire barriers. However, it is important to be able to quantify the uncertainty of the result of the fire resistance of a fire barrier for fire risk assessment of nuclear power plants. The final report summarises the activities of the project at the different partners which means reliability of fire barriers by calculation tools, determination of uncertainty and sensitivity of input parameters with modelling of fire resistance of fire barriers.

## **Key words**

Fire, nuclear power plants, fire barriers, modelling, uncertainty

# **Determination of Fire Barriers reliability for fire risk assessment of Nuclear Power Plants. (FIREBAN) – Final Report**

*Patrick van Hees*  
*Simo Hostikka<sup>1</sup>*  
*Topi Sikanen<sup>2</sup>*  
*Dan Lauridsen<sup>3</sup>*  
*Sebastian Levin<sup>4</sup>*

---

Department of Fire Safety Engineering  
Lund University, Sweden

Brandteknik  
Lunds tekniska högskola  
Lunds universitet

Report 3225, Lund 2019

1. Aalto University, Finland
2. VTT Technical Research Centre of Finland Ltd, Finland
3. DBI Danish Institute of Fire and Security Technology,  
Denmark
4. Ringhals AB, Sweden



**Determination of Fire Barriers  
reliability for fire risk  
assessment of Nuclear Power  
Plants (FIREBAN) –  
Final Report**

**Patrick van Hees  
Simo Hostikka<sup>1</sup>  
Topi Sikanen<sup>2</sup>  
Dan Lauridsen<sup>3</sup>  
Sebastian Levin<sup>4</sup>**

1. Aalto University, Finland
2. VTT Technical Research Centre of Finland Ltd, Finland
3. DBI Danish Institute of Fire and Security Technology, Denmark
4. Ringhals AB, Sweden

**Lund 2019**

# Determination of Fire Barriers reliability for fire risk assessment of Nuclear Power Plants (FIREBAN) – Final Report

Patrick van Hees  
Simo Hostikka<sup>1</sup>  
Topi Sikanen<sup>2</sup>  
Dan Lauridsen<sup>3</sup>  
Sebastian Levin<sup>4</sup>

1. Aalto University, Finland
2. VTT Technical Research Centre of Finland Ltd, Finland
3. DBI Danish Institute of Fire and Security Technology, Denmark
4. Ringhals AB, Sweden

## Report 3225

ISSN: 1402-3504

ISRN: LUTVDG/TVBB--3225--SE

Number of pages: 26

Illustrations: Patrick van Hees, Jonathan Vallée, Topi Sikanen, Simo Hostikka

## Keywords

Fire, nuclear power plants, fire barriers, modelling, uncertainty

## Sökord

Brand, kärnkraftverk, brandväggar, modellering, osäkerhet

## Abstract

Fires in nuclear power plants can be an important hazard for the overall safety of the facility. An important factor in reducing the spread of the fire is the use of fire barriers. However, it is important to be able to quantify the uncertainty of the result of the fire resistance of a fire barrier for fire risk assessment of nuclear power plants. The final report summarises the activities of the project at the different partners which means reliability of fire barriers by calculation tools, determination of uncertainty and sensitivity of input parameters with modelling of fire resistance of fire barriers.

© Copyright: Brandteknik, Lunds tekniska högskola, Lunds universitet, Lund 2019.

---

Brandteknik  
Lunds tekniska högskola  
Lunds universitet  
Box 118  
221 00 Lund  
brand@brand.lth.se  
<http://www.brand.lth.se>

Telefon: 046 - 222 73 60

Division of Fire Safety Engineering  
Faculty of Engineering LTH  
Lund University  
P.O. Box 118  
SE-221 00 Lund, Sweden  
brand@brand.lth.se  
<http://www.brand.lth.se/english>

Telephone: +46 46 222 73 60

## Preface

This report is the final report (including all years) of the Fireban project financed by NKS under project number NKS\_R\_2016\_119, which is gratefully thanked. Furthermore, the authors would like to thank all who provided them with literature and information on the subject of fire barriers. As this project is a co-financed project the following other financing bodies are thanked:

NBSG (Nationella Brandsäkerhetsgruppen)

State Nuclear Waste Management Fund, SAFIR2018-project FIRED

NKS conveys its gratitude to all organizations and persons who by means of financial support or contributions in kind have made the work presented in this report possible.

The authors also thank all main and co-authors for their contributions in the different publications which are the basis for this final report. Sincere words of thanks are given to (alphabetical order):

Andres, B.

Bhargava, A.

Bisby, L.

Deepal, P.

Hidalgo, JP.

Johansson, N.

Livkiss, K.

Vallée, J.

Lund, May 2019.

Patrick van Hees

Simo Hostikka

Topi Sikanen

Dan Lauridsen

Sebastian Levin

### **Disclaimer**

The views expressed in this document remain the responsibility of the author(s) and do not necessarily reflect those of NKS. In particular, neither NKS nor any other organisation or body supporting NKS activities can be held responsible for the material presented in this report.



# Contents

<b><u>1. INTRODUCTION.....</u></b>	<b><u>1</u></b>
1.1. BACKGROUND.....	1
1.2. SCOPE, OBJECTIVE AND METHODS .....	2
1.3. LIMITATIONS OF THIS REPORT .....	3
<b><u>2. OVERVIEW OF THE FIREBAN PROJECT.....</u></b>	<b><u>5</u></b>
2.1. WORK PACKAGE 1: STATE-OF-THE-ART FOR FIRE BARRIER RELIABILITY ASSESSMENT.....	5
2.2. WORK PACKAGE 2: RISK-BASED ASSESSMENT OF BARRIER PERFORMANCE .....	5
2.3. WORK PACKAGE 3: RELIABILITY DETERMINATION.....	6
2.3.1. USE OF EXISTING TEST FIRE TEST DATA IN COMBINATION WITH NEW TEST DATA	6
2.3.2. USE OF STATISTICS .....	6
2.3.3. USE OF MODELLING FOR THE FIRE BARRIER PERFORMANCE ASSESSMENT.....	6
2.3.4. PRACTICAL TEST DESIGN .....	6
2.4. WORK PACKAGE 4: DISSEMINATION OF RESULTS.....	6
2.5. WORK PACKAGE 5: MANAGEMENT.....	6
<b><u>3. CONDUCTED STUDIES .....</u></b>	<b><u>9</u></b>
3.1. RELIABILITY STUDY OF FIRE BARRIERS BY CALCULATION WITH ABAQUS AND FDS [13].....	9
3.1.1. INTRODUCTION.....	9
3.1.2. OBJECTIVES.....	10
3.1.3. METHOD .....	10
3.1.4. LIMITATIONS .....	11
3.1.5. RESULTS .....	11
3.1.6. CONCLUSIONS .....	13
3.1.7. FURTHER RESEARCH .....	13
3.2. PROPAGATION OF MODEL UNCERTAINTY IN THE STOCHASTIC SIMULATIONS OF COMPARTMENT FIRE THERMAL PHENOMENA [14, 19] .....	14
3.3. UNCERTAINTIES IN MODELLING HEAT TRANSFER IN FIRE RESISTANCE TESTS: A CASE STUDY OF STONE WOOL SANDWICH PANELS [15].....	16
3.4. RESPONSE OF STONE WOOL-INSULATED BUILDING BARRIERS UNDER SEVERE HEATING EXPOSURES [16, 18] .....	16
3.5. CHARACTERIZATION OF STONE WOOL PROPERTIES FOR FIRE SAFETY ENGINEERING CALCULATIONS [17].....	17
3.6. MODEL BASED OPTIMIZATION FOR CALIBRATION OF PYROLYSIS MODELS, VTT REPORT [20] .....	17
<b><u>4. DISSEMINATION.....</u></b>	<b><u>19</u></b>
4.1. PUBLICATIONS.....	19
4.2. PARTICIPATION AT CONFERENCES.....	19
4.3. WORKSHOP ON FIRE PRA .....	20
<b><u>5. CONCLUSIONS .....</u></b>	<b><u>21</u></b>

## **REFERENCES**

### **ANNEXES**

#### **A. ACRONYMS**

**B. THESIS REPORT LTH (open access) [Reference 13]**

**C. PAPER ALTO UNIVERSITY (no open access) [Reference 14]**

**D. FIRE AND MATERIALS PAPER LIVKISS ET AL (no open ACCESS, available on request from the authors) [Reference 15]**

**E. JOURNAL OF FIRE SCIENCES ANDRES ET AL (no open ACCESS, available on request from the authors) [Reference 16]**

**F. JOURNAL OF FIRE SCIENCES LIVKISS ET AL (no open ACCESS, available on request from the authors) [Reference 17]**

**G. FIRE TECHNOLOGY PAPER PADEL AND HOSTIKKA (open access) Alto University [Reference 19]**

**H. VTT REPORT SIKANEN (open access) VTT-R-05578-18 [Reference 20]**

# 1. Introduction

## 1.1. Background

Safe shutdown of a reactor after internal or external events is a key factor in the overall safety design of a nuclear power plant. In many cases, fire is a significant event that can affect the reactor safety and the capability of safe shut down. When the event is a fire, it is not only about shutting down the facility but also prevent the destruction of critical components necessary for a safe shut down process. For prevention purposes, redundant systems are used to decrease the probability of unsuccessful shutdown processes. When analysing the fire consequences, the functional performance of components such as cables, and electronic circuits, for example, is of highest importance. With respect to fire, events can be classified in 3 major groups depending on the position of the subsystems, as illustrated in Figure 1. [1, 2, 3]. In the first class (left), the redundant systems A and B are located in the same enclosure within a fire compartment. A fire can have a great impact on one or both subsystems and the risk of loosing the redundancy is consequently high. Probability for failure might e.g. be 1 on 100 years. In the second class of events, the systems A and B are in the same fire compartment but not in the same enclosure and the risk of failure will depend on the fire spread between enclosures. Probability will be 1 on 1000 years. Finally, the subcomponents A and B can be in 2 different fire compartments, and the risk for loosing both subsystems will be due to failure of fire compartmentation, a seldom consequence, but could trigger an bigger event such as Fujiyama accident [4, 5].

The utilization of the physical separation is an important part of the defence-in-depth principle of NPP safety. The consequences of loosing the physical separation may not be well known because these events are often ignored in fire-PSA as a result of the screening process [2]. The loss of separation may take place in various ways: i) most importantly by the unavailability of barrier components (e.g. an open fire door), ii) by mechanical damage to the fire barrier or structure (e.g. by earthquake), iii) by the penetration of heat and smoke through the fire barriers (e.g. heat conduction and leakages), or iv) through the ventilation system. This project will focus on the assessment of mechanisms iii. While in the POOLFIRE project the focus was on the fire source e.g. a pool fire, and the propagation through the ventilation systems [1], it is also important to know the risk of multi-compartment failures. Risk of failure between components inside the same enclosure and compartment (Events 1 and 2) can be treated by advanced fire modelling [9] or by using engineering methods [8]. For the risk of barrier failures, the calculation methods are incomplete. Fire barriers are often tested using standard fire tests such as EN 1363-1 and standardized exposure but we do not know how they perform at different exposures or in the presence of small changes or deficiencies. A large Marie Curie project is currently conducted between DBI and Lund University to investigate the effect of different exposures [10], but for the second source of uncertainty, only little is known.

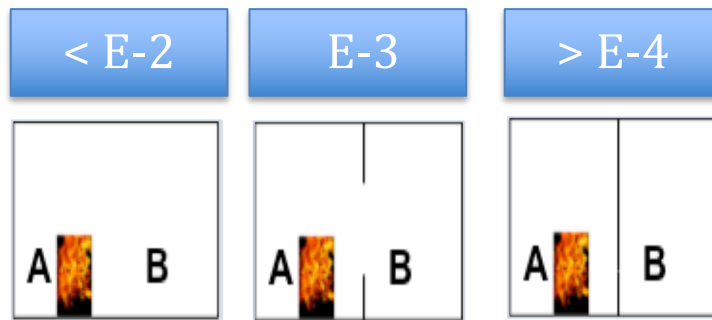


Figure 1 Example of event classification for fire incidents with probability for failure [1]

One way to determine the overall risk in a PRA analysis is by using probabilistic methods and statistics [6, 7]. For earthquake fires, some data is available [4, 5] but we also need to have the information for normal fire hazards. Another possibility is to investigate the likelihood of barrier failure using calculation methods, which predict e.g. the heat transfer in the wall or the possible leakages of gases from one compartment. This is a so-called deterministic approach, which can complement the probabilistic methods in PRA. Most of the work now has been done in predicting the result from standard fire tests according to e.g. EN 1363-1. But the links between the standard testing and modelling, risk-based design and PRA are still missing.

In a recently conducted and on-going OECD PRISME projects [3], large amount of experimental data has been gathered with respect to mechanically ventilated enclosure fires. A number of tests in the first project have been done with leakages in walls and they can give a first indication of failure rates. This international project constitutes an important and unique dataset of experiments. The focus of PRISME projects was mainly on the fire tests while the use of the test results and the validation of CFD models is a national or regional responsibility and subject to local funding.

Until now, Sweden and Finland have participated on national basis but it is clear that synergy is possible between the research groups involved in the project (Lund university, Aalto University and VTT). Activities were related to the validation of the most widely used CFD tool called FDS [9] and to the sensitivity analyses for this tool for pool fires [1]. Incorporating DBI (Danish Institute for fire and security technology) will allow for the project partners to have access to the research of 5 Marie Curie PhD students working in the Firetools project and connections with industry. The work in this project focuses on modelling the heat transfer through fire barriers. Finally, a NPP (Vattenfall Ringhals) from Sweden is involved as end-user.

## 1.2. Scope, objective and methods

The scope of the project is to investigate and assess the reliability of fire barriers in NPP during realistic fire scenarios to support the plant-scale risk assessment.

The objective is to establish data and methods to determine the conditional probabilities for failure of fire barrier. The Methods used will be statistics, literature review, calculation and specific unique designed fire tests.

### 1.3. Limitations of this report

This report should be read in conjunction with the specific report of certain work packages as well as the related scientific articles. Unless open access they are available from the authors.



## 2. Overview of the FIREBAN project

This chapter gives a short overview of the overall 3-year project. The project major core of activity is the to investigate and assess the reliability of fire barriers and will contain the following work packages. Outcomes are given below for the subsequent work packages.

### 2.1. Work package 1: State-of-the-art for fire barrier reliability assessment

The first work package will collect the state of the art on methods and experiences to determine the reliability of fire barriers. Methods used are literature review of validation data available within open literature and other projects as well as other discipline areas (e.g. mechanical stability). Use of statistics will also be considered for probability assessment. The result of this work package will be an overview of the need for possible further development and the requirements for additional data both as input data for the PSA models.

*Responsible organisations:* Aalto, VTT and Lund University

Outcome: see chapter 3 and all related articles and report which are an annex to this report

### 2.2. Work package 2: Risk-based assessment of barrier performance

In this work package, we will determine the relationship between the standard-fire based fire resistance classification and the failure risk under real fire conditions and real protection objectives.

First, the risk-based acceptance criteria will be established, as the standard criteria for test protocol do not necessary correspond to the situation at the plant. The criteria will be determined for insulation, integrity and stability, considering the different spaces to be protected, such as the cable rooms (criterion based on cable material thermal stability), and control room (life safety and working conditions).

Next, we will determine a number of risk-based fire curves for NPP rooms based on real fire scenarios. This includes for example:

- Small rooms fires
- Large rooms with local fuels
- Large rooms with plenty of fire load.

On the basis of the risk based fire curves, suggestions for practical fire test design will be presented.

*Responsible organisations:* All partners

Outcome: see chapter 3.2

---

## 2.3. Work package 3: Reliability determination

This work will contain four major routes of determination:

### 2.3.1. Use of existing test fire test data in combination with new test data

Test data from existing tests will be analysed and also unique test will be performed with small deficiency (representing cracks and lack of full insulation)

Outcome: See chapter 3.1 and 3.4

### 2.3.2. Use of statistics

Statistics data will be gathered from different sources and the input to this work is the outcome of Work package 1.

Outcome: see chapter 3.2 and 3.3.

### 2.3.3. Use of modelling for the fire barrier performance assessment.

In this case, a combination of thermal heat transfer models and CFD models such as FDS will be used. Means to integrate the reliability estimates into PRA will be proposed. In addition to the model application, we will analyse the propagation of model/parameter uncertainty to the final risk estimate.

Outcome: see chapter 3.1

### 2.3.4. Practical test design

Testing environment will be compared with realistic installations in order to document fire performance.

*Responsible organisations:* Aalto University, DBI and Lund University

Outcome: see chapter 3.4

## 2.4. Work package 4: Dissemination of results

Results from the project will be reported in scientific journals and at conferences. A small workshop for interested parties will be organised at the end of project. Due to the fact that some data from the OECD project PRISME might be used the partners will follow the rules of OECD for publication of the results. The most efficient way is to report by means of scientific papers, which are approved by the OECD project group. The co-operation with other national projects, such as the SAFIR2018 programme in Finland, will also take place in this work package.

*Responsible organisations:* All partners

Outcome: see chapter 4

## 2.5. Work package 5: Management

For the management of the project, we include activities such as communication with partners, meeting organisation, economical follow up and progress follow up. The

management work will also include the set-up of a confidentially agreement between the partners with respect to the OECD project PRISME and the FIRETOOLS project. Vattenfall Ringhals, VTT, Aalto University and LU are now part of the PRISME project but not DBI. DBI and LU are part of the Firetools project but not Aalto University and VTT. However, no hinder is foreseen in establishing this contract.

*Responsible organisation:* Lund University

Outcome: Final report



## 3. Conducted studies

This chapter summarises the studies conducted during the project.

### 3.1. Reliability study of fire barriers by calculation with ABAQUS and FDS [13]

#### 3.1.1. Introduction

In order to restrain fire spread and to contain the fire in one area, a building can be sub-divided into compartments separated from one another by fire-resisting constructions. This passive fire protection method can help by giving more time for the occupants to evacuate, by reducing the fire size thus reducing the fire service work and by reducing property damage and business interruption time. The fire resistance rating of light weight construction, especially Cold-formed light gauge steel frame (LSF) stud wall systems, has become critical to the building safety design as their use has become increasingly popular in all areas of building construction[11].

The fire resistance rating (FRR), given in unit of time, is the time for which a building element can withstand the exposure to defined heating and pressure conditions, until failure. Usually those time range between 60 min and 120 min[11]. Traditional fire resistance testing is done in furnace test and based upon ASTM standard E119 or the international standard ISO 834. According to the code EN 1363-1, the failure criterions are based on three parameters: integrity, stability and insulation[12]. The stability criterion relates to the structural capacity of the structure at elevated temperature. In this study the stability criterion will not be investigated, thus it is assumed that the walls do not collapse, do not show excessive deformation or deflection. The insulation criterion relates to the ability of a building component to restrict the heat transfer through its boundaries to a certain level. According to the EN 1363-1 code, failure of the insulation criterion is observed in two ways[12]. The code states that the specimen must maintain its function for the duration of the test without developing temperatures on its unexposed surface such as:

- An increase the average temperature above the initial average temperature by more than 140 °C, called  $T_{140}$ ;
- An increase at any location (including the roving thermocouple) above the initial average temperature by more than 180 °C, called  $T_{180}$ .

The integrity criterion represents the ability of a building component to prevent the passage, through its boundaries, of flames and hot gases and to prevent the occurrence of flames on the unexposed side. The requirements from the relevant code [2] are the following:

- Prevent the penetration of a 6 mm diameter gap gauge that can be passed through the test specimen, such that the gauge projects into the furnace, and can be moved a distance of 150 mm along the gap
- Prevent the penetration of a 25 mm diameter gap gauge that can be passed through the test specimen such that the gauge projects into the furnace.
- Prevent the ignition of a cotton pad applied for a maximum of 30 s or until ignition positioned at least 30 mm from the unexposed surface and 10 mm from the boundaries of the wall. Charring of the cotton pad without flaming or glowing shall be ignored.

In the industry the fire rated partition are built according to specifications coming from plasterboard manufacturers, providing fire resistance ratings. Those rating are based on full-scale furnace tests using the required standard. Often, the fire barriers tested in the furnace are highly optimized in order to reach the required fire resistance. The test results remain confidential and the number of samples, which fail is not documented. In practice, the construction of the fire rated barrier can slightly differ from the optimized one tested in the furnace test. Furthermore, with time, the quality of the barrier can be altered thus reducing its ability to contain the fire. This raises concerns about the reliability of fire resisting partition as an effective mean of passive fire protection. Little research has been done with respect to the impact of reduced insulation and leakage on the reliability of fire resisting partition. It is not known what kind of safety factor can be expected of fire barrier and often, the designer relies simply on the obtained rating. For this reason, research is necessary in order to determine the reliability of fire barriers.

### 3.1.2. Objectives

The first objective of this study is to show how the FRR of partitions is affected by leakage. To do this, the FRR obtained from simulations of partitions with localized leakage, distributed leakage, different leakage size and location will be compared to an airtight partition.

The second objective of this study, is to investigate the effect of a reduced thermal insulation on the FRR of partitions. Insulation can be reduced in multiple ways, the scenarios which will be investigated are: localized missing piece of different size of insulation, reduced thickness of insulation, different type of insulation, partition without insulation, hole of different size on the exposed boundary of the partition and hole through the partition. Those assumed 2 parameters and features are meant to represent ways in which a fire rated wall could be altered before being exposed to a fire.

### 3.1.3. Method

The methods that were used are hand calculations for basic heat transfer through the wall, hand calculations of infiltration and pressure inside the furnace, CFD modelling using the CFD tool - FDS and Finite element modelling using ABAQUS to replicate the standard fire furnace tests. A case study method is used in this work. More precisely, the effect on the FRR according to the insulation criterion were examined for the following parameters: The type of insulation or absence of insulation, the reduction of the insulation thickness inside the cavity, breach in the gypsum board exposed in the furnace, breach through the fire barrier and missing piece of insulation inside the cavity. Also, the effect of leakage on the FRR based on the integrity criterion was investigated assuming that the barrier leaks before it is submitted to the standard fire. Different levels of airtightness were assumed and different leakage scenario. The first scenario aims at simulating the effect of hole through the barrier. The second and third scenario was looking at the effect of leaking joint improperly sealed. In order to validate the models, comparison of model's results to experimental data of wall tested in actual furnace were made. Thus, the report also holds a study of model validity, to see whether simple calculations and modelling are able to replicate heat transfer in a furnace test.

### 3.1.4. Limitations

This study was limited to walls and did not include doors, windows, ventilation ducts. Studies were mainly done with respect to smoke leakages and reduced thermal insulation. The stability criterion relates to the structural capacity of the structure at elevated temperature. In this study the stability criterion was not investigated, thus, it is assumed that the walls do not collapse, do not show excessive deformation or deflection. Also, it is assumed that the defects and features investigated are already part of the wall before the fire. Hence this study was not looking at the deficiencies due to the fire effects.

### 3.1.5. Results

This paragraph only gives a summary of the results. More information can be found in [14].

## 1. ABAQUS simulations

The calculations were done on a light-weight stud wall system with two type of construction:

- Construction type A - 60 minutes fire resistance
- Construction type B - 120 minutes fire resistance

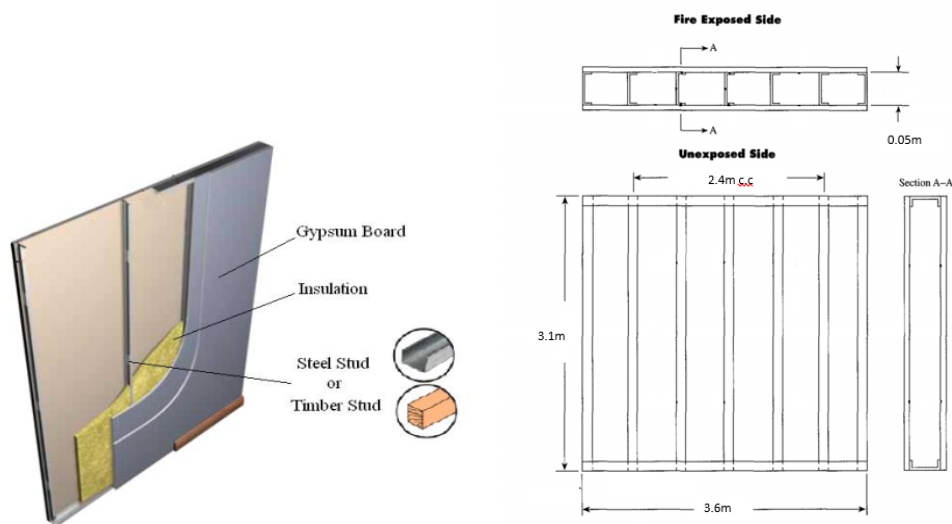


Figure 2 Schematic of the barriers used for calculations

The following different type of set-ups were tested:

- The type of insulation (uninsulated, Stone wool, Fiber glass wool)
- Reduction of the insulation thickness. 4 scenarios with stone wool (Full depth, three quarter, half and quarter)
- Presence of a hole in the exposed gypsum board. 6 models for different insulation type and for a large and small hole (50mm, 10mm radius).
- Hole through the fire barrier, with stone wool insulation. 2 models large hole 50mm radius and small hole 10mm radius.
- Missing piece of stone wool insulation of different size large part 100mm radius and small part 50mm radius.

Figure 3 shows a result of the simulation when a hole is present in the barrier construction on the exposed side.

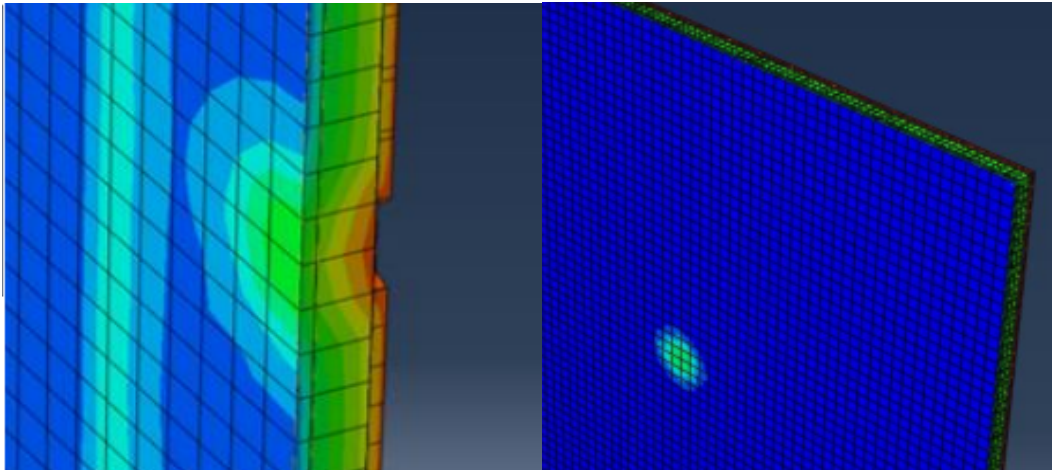


Figure 3 Example of a calculation with a hole on the exposed side.

Figure 4 shows the results of fire barriers with different insulation (left) and reduced thickness (right)

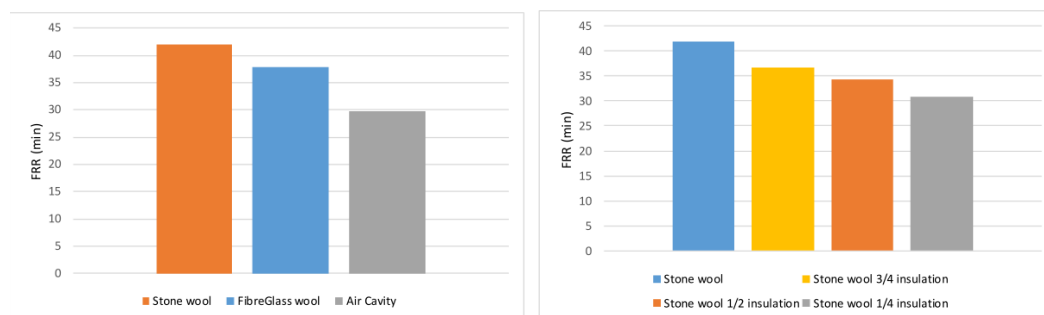


Figure 4 Results of heat transfer calculation – Reduction in FRR for two parameters.

The results can be summarised as follows:

- Barriers insulated with stone wool provided a FRR higher compared to barrier insulated with Fiberglass wool or uninsulated (air gap).
- Small or large hole on the exposed layer of the barrier insulated with stone wool, provided a FRR approx. 20% and 70% higher compared to Fiberglass and uninsulated partition, respectively.
- A hole through the partition reduced the FRR by more than 75%
- Reduction by up to 25 % of the FRR was observed for reduction of the insulation thickness by 75%.

## 2. FDS simulations

FDS simulations were performed simulating a fire barrier in front of a fire resistance furnace. Different types of leakages were simulated as can be seen in figure 5. The model was calibrated against a fire resistance test.

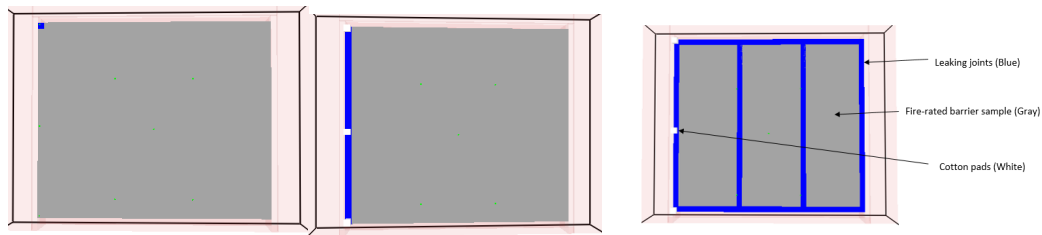


Figure 5 Different leakages: hole, (left); gap (middle); general leakage at joints(right)

The results of the FDS simulations revealed the following:

- For an average air tight construction, a leakage through a hole has a FRR 38% lower compared to leakage occurring through a joint on one side of the wall
- For an average airtight construction, a leakage through a joint on one side gives a FRR 15% lower compared to a leakage through all the joints of the wall.
- Failure was mainly due to the insulation criterion.
- A supplementary calculation using a concrete wall revealed the same results for integrity.

### 3.1.6. Conclusions

Fire rated partition are constructed according to specification taken from manufacturers. However, what happen to the FRR if the construction is built differently or is altered before it is subject to a fire. This study looked at the safety factor inherent in fire resistant structures with regards to the insulation and integrity criterion. This was done using numerical tools such as FDS for the integrity criterion and ABAQUS for the insulation criterion. No experiment was done during this study, however the models were validated using experimental data. It was found that all the tested partition with increased leakage or reduced insulation had a FRR too low to fulfill their purpose. This imply that there is no safety factor inherent in fire resistant barrier and that they should be built and kept exactly as specified by the manufacturer in order to give FRR acceptable by codes. Also, results showed that it is much more likely that the wall will fail due to the insulation criterion than due to the integrity criterion, if leakage occurs. Finally, in order for the partition to be reliable it is necessary that it is built and remains exactly as tested by the manufacturer. This work showed method to simulate fire resistance test with the help of numerical tool. This could be very useful especially when considering the high cost of testing samples in furnaces. Still, much works needs to be done in order to accurately model a fire resistance test. Experiments are needed in order to be able to validate properly the models, especially for cavity radiation and heat transfer through leakage area.

### 3.1.7. Further Research

In order to improve models on fire resistance test, further work should include the following:

- The effect on heat transfer of hot gases leaking through partition should be studied experimentally.
- The effect of heat transfer in empty cavity by radiation during a fire resistance test should be investigated. This would allow validating the numerical models and

helping to find a way to reduce the heat transfer to the unexposed gypsum layer in an empty cavity partition.

- Numerical models of thermal expansion and deformation of the partition component such as steel studs, wooden studs and gypsum board, in order to include the stability criterion.
- The impact on the fire resistance rating of lightweight partition using steel or wooden studs.
- The influence of the heat generation in some wool insulations materials and the impact on the FRR.
- The combustibility of the insulation material inside the cavity and its effect on the FRR.
- The dependency of FRR on the water movement inside the partition caused by water vaporization from the gypsum.

### 3.2. Propagation of model uncertainty in the stochastic simulations of compartment fire thermal phenomena [14, 19]

Model uncertainty affect the shape of stochastically predicted output distribution and ultimately the inferred probabilities. This problem is common in the uncertainty quantification problems where the model-errors are equally countable as input uncertainty. The validation guide of FDS presents uncertainties associated with the prediction of various output quantities. The measurement data obtained from numerous fire experiments is compared with the corresponding FDS predictions and model uncertainties are summarized in terms of systematic bias,  $\delta$  and relative standard deviation of random errors,  $\tilde{\sigma}_\epsilon$ .

With  $\delta$  and  $\tilde{\sigma}_\epsilon$ , one can improve the shape of stochastically simulated output distribution. Figure 6 illustrates this method. The error-free  $T$ , simulated,  $\hat{T}$  and corrected,  $T^*$  distributions are compared. The corrected distribution is obtained from the simulated one using,

$$T_i^* = \begin{cases} \frac{\hat{T}_i}{\delta} + \frac{n\tilde{\sigma}_\epsilon\mu_{\hat{T}}}{2} \text{ if } \frac{\hat{T}_i}{\delta} \leq \frac{\mu_{\hat{T}}}{\delta} - n\sigma_{\hat{T}} \\ \frac{\hat{T}_i}{\delta} - \frac{n\tilde{\sigma}_\epsilon\mu_{\hat{T}}}{2} \text{ if } \frac{\hat{T}_i}{\delta} > \frac{\mu_{\hat{T}}}{\delta} - n\sigma_{\hat{T}} \end{cases} \quad n = 0 \dots \infty, \quad (3.2)$$

where  $\mu_{\hat{T}}$  and  $\sigma_{\hat{T}}$  are the first and second moment of the simulated distribution.

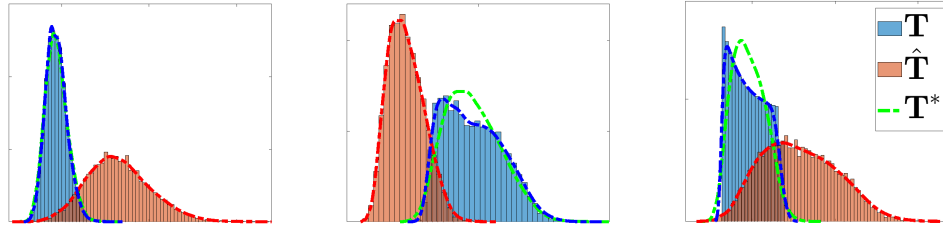


Figure 6 Examples of error-free,  $T$ , simulated,  $\hat{T}$ , and corrected,  $T^*$  distributions.

This is also illustrated using the data of a fire experiment which was carried out at VTT Building Technology in 1998. The fire experiment was carried out in a closed enclosure having one door opening to the ambient. All-together 17 tests were performed depending upon the size and the location of the fire. The Figure 7 shows the measured and predicted wall temperatures, the stochastic uncertainty and the model uncertainty.

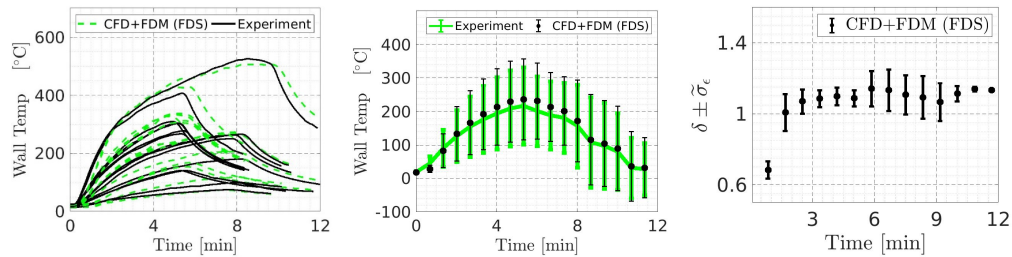


Figure 7 Left: Measured and predicted wall temperatures, Middle: Stochastic uncertainty, Right: Model uncertainty.

Figure 8 presents the probability that the wall crosses a particular temperature threshold in a given time. The probability is calculated based on the measured, predicted and corrected temperatures. The temperature correction was done using Eq. 3.2 and the constant values,  $\delta = 1.15$  and  $\tilde{\sigma}_\epsilon = 0.16$  that corresponds to peak wall temperatures.

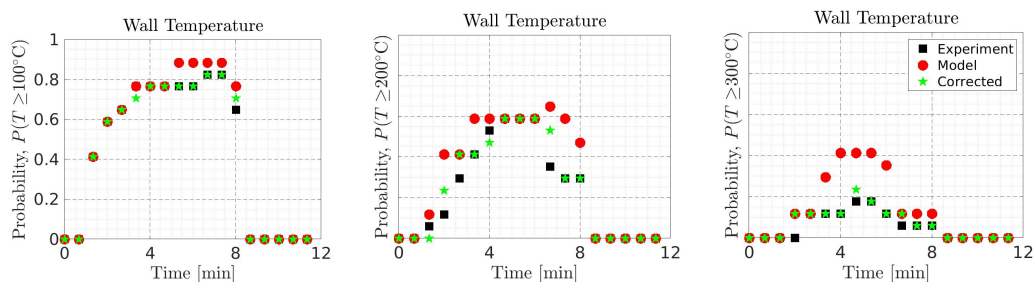


Figure 8 Probability that the wall crosses the threshold temperature in a given time. Comparison of true, simulated and corrected probabilities.

The simulated probability values are slightly higher than the experimentally observed ones. This is due to the positive bias in the temperature prediction. After compensating the effect of model uncertainty, the probability values are much close to the experimental ones. This shows that the proposed method is sufficiently effective in improving the probabilistic predictions. For the probability correction, we use the model uncertainty values obtained from the same experiment. Simulations lacking own experiment may refer to the generalized values reported in the validation guide.

### 3.3. Uncertainties in modelling heat transfer in fire resistance tests: A case study of stone wool sandwich panels [15]

Modelling fire performance of building fire barriers would allow optimising the design solutions before performing costly fire resistance tests and promote performance-based fire safety engineering. Numerical heat conduction analysis is widely used for predicting the insulation capability of fire barriers. Heat conduction analysis uses material properties and boundary condition parameters as the input. The uncertainties in these input parameters result in a wide range of possible model outcomes. In this study, the output sensitivity of a heat conduction model to the uncertainties in the input parameters was investigated. The methodology was applied to stone wool core sandwich panels subjected to the ISO 834 standard fire resistance temperature/time curve. Realistic input parameter value distributions were applied based on material property measurements at site and data available in literature. A Monte Carlo approach and a functional analysis were used to analyse the results. Overall, the model is more sensitive to the boundary conditions than to the material thermal properties. Nevertheless, thermal conductivity can be identified as the most important individual input parameter.

More information can be found in [15]. Figure 9 gives results for one of the cases.

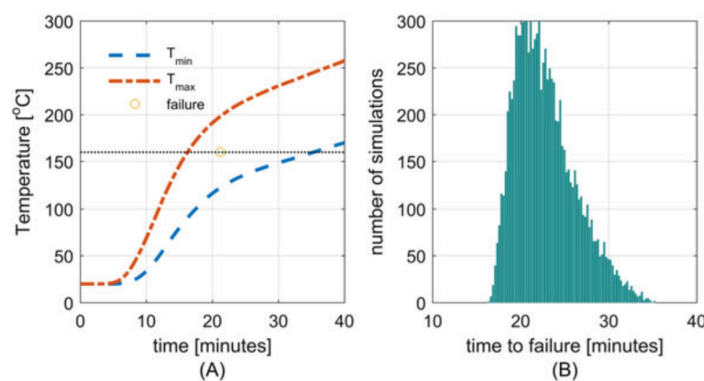


Figure 9 A, modelling results for 50 mm stone wool sandwich panel; B, time to failure distribution of 10 000 simulations

### 3.4. Response of stone wool–insulated building barriers under severe heating exposures [16, 18]

From the first modelling results described in chapter 3.1. and the corresponding uncertainty analysis conducted in chapter 3.2 it became clear that additional test data was necessary to obtain additional experimental results. Therefore, tests were conducted for stone wool–layered sandwich constructions, with either steel or gypsum claddings, tested under four different heating exposures namely 7 kW/m<sup>2</sup>

incident radiant heat flux exposure, 60 kW/m<sup>2</sup> incident radiant heat flux exposure, parametric time–temperature curve exposure and a ISO 834 standard time–temperature exposure. The test apparatuses used were an apparatus called H-TRIS [21] containing a movable radiant panel system, a mid-scale furnace (1.5 m<sup>3</sup>) and a large scale furnace (15 m<sup>3</sup>). Details of the results can be found in the paper [16]. The test

results have revealed how different phenomena such as binder reactions might occur (or not) depending on the different heating scenarios. Therefore, modelling fire scenarios (e.g. for performance-based design purposes) by using input material properties fitted for one particular fire scenario, e.g. the standard furnace exposures, might lead to incorrect predictions. These conclusions and test results gave data for further prediction in order to obtain more experiences in the fire characterization of stone wool and stone wool assemblies. One of the simulation works is given in the next chapter while specific simulation of the tests in this chapter and paper are subject to a paper which will be submitted after the project [22]. While chapter 3.5 is describing a FSE approach, chapter 3.6 is describing optimization of pyrolysis models which is a fundamental approach of modelling.

### **3.5. Characterization of stone wool properties for fire safety engineering calculations [17]**

Stone wool insulation is widely used as material in fire barrier constructions. Due to the combustion of its organic content, the temperature inside stone wool can rise above the temperature of the exposed boundary. This temperature rise is difficult to predict.

An extensive test program was performed to obtain the thermal and reaction kinetic properties of stone wool. The test methods included modified slug calorimeter, thermogravimetric analysis, differential scanning calorimetry, micro-scale combustion calorimetry and bomb calorimetry. The thermal conductivity at elevated temperatures was similar for all types. Two positive mass loss rate and heat release rate peaks were observed in temperatures between 20° C and 700° C. Reaction kinetic parameters were obtained and used in a finite difference model predicting the temperature increase in stone wool upon linear heating.

### **3.6. Model based optimization for calibration of pyrolysis models, VTT report [20]**

This report described the theoretical underpinnings of the PyroPython tool. PyroPython was born out of the need for an easier to use version of PyroPlot. Unlike Pyroplot, PyroPython aims to be agnostic of the optimization method used. Four optimization methods are supported “out of the box” current version. Adding new solvers is a fairly straightforward task.

Several optimization methods were tested on a very challenging 16 parameter pyrolysis model fitting problem. It was found that, at least for the present optimization problem, the traditional optimization methods, Nelder-Mead simplex and differential evolution have better performance than the Bayesian Optimization methodology.

This conclusion may, however, change if the optimization problem at hand would be more costly to evaluate, say a long cone calorimeter experiment or a bench scale experiment.



## 4. Dissemination

### 4.1. Publications

Following publications were obtained:

- Vallée, J. Reliability of fire barriers, Report nr 5521 Master thesis Erasmus Mundus, Lund University, 2016.
- Paudel, D., Hostikka, S., Propagation of modeling uncertainty in stochastic heat-transfer simulation using a chain of deterministic models. *Int J Uncertain Quantif* 9(1):1–14, 2019.
- Livkiss, K., Andres, B., Johansson, N., van Hees, P., Uncertainties in modelling heat transfer in fire resistance tests: A case study of stone wool sandwich panels, *Fire and Materials Journal* DOI 10.1002/fam.2419, Wiley, 2017.
- Andres, B, Hidalgo, JP, Bisby, L & van Hees, P 2017, Experimental analysis of stone wool sandwich composites exposed to constant incident heat fluxes and simulated parametric fires. in *15th International Conference and Exhibition on Fire and Materials 2017*. vol. 2, Interscience Communications Ltd, pp. 503-516, 15th International Conference and Exhibition on Fire and Materials 2017, San Francisco, United States, 2017/02/06
- Andres, B, Livkiss, K, Hidalgo, JP, van Hees, P, Bisby, L, Johansson, N & Bhargava, A, 2018, 'Response of stone wool-insulated building barriers under severe heating exposures', *Journal of Fire Sciences*, vol. 36, no. 4, pp. 315-341. <https://doi.org/10.1177/0734904118783942>
- Livkiss, K, Andres, B, Bhargava, A & van Hees, P 2018, 'Characterization of stone wool properties for fire safety engineering calculations', *Journal of Fire Sciences*, vol. 36, no. 3, pp. 202-223. <https://doi.org/10.1177/0734904118761818>
- Paudel, D. & Hostikka, S. *Fire Technol*, 2019, Propagation of Model Uncertainty in the Stochastic Simulations of a Compartment Fire, <https://doi.org/10.1007/s10694-019-00841-9>
- Andres B., Livkiss K., Bhargava A., Van Hees P., Using micro-scale and solid material data for modelling stone wool composites under heat exposures, to be submitted during 2019
- Sikanen, T., Model based optimization for calibration of pyrolysis models, VTT report VTT-R-05578-1, 2018.

### 4.2. Participation at conferences

The Firetools PhDs participated at Interflam 2016 and the Nordic Fire Safety Days in Copenhagen. The work of VTT was presented as a poster at the IAFSS conference in Lund 2017. The project leader presented the project at the NKS Stockholm NKS seminar 15-16 January 2019.

### 4.3. Workshop on Fire PRA

VTT organized a workshop on the Fire PRA, and its relation to the Fire-DID and the main PRA. This one day workshop was organized in Espoo on 25.11.2017. Topics covered in the workshop were:

- Development of deterministic analyses, including their verification and validation, and their applicability on the Fire PRA.
- Present status of Fire PRA on Finnish plants and the near plans to upgrade them.
- Main PRA and its plans: Development work needed to address the main PRA and Fire PRA inter-face.

The purpose of this workshop was to survey the companies and authorities on what they consider important topics in Fire-DID and what kind of research results they consider useful. In addition, the FDS 3D heat transfer solver was presented to the participants of the seminar.

Participants of the workshop were mainly from the NPP companies, Finnish authorities, and research organizations. After the presentations from all participating organizations, a lively discussion on research needs for fire-PRA followed. Several important issues requiring further study were identified:

- 1 Fire and smoke propagation through ventilation ducts and openings.
- 2 Fire spread from and between electrical cabinets.
- 3 Efficient screening techniques to reduce the need for detailed analyses.
- 4 Aging effects on fire barriers: Do old fire stops and fire doors still work as advertised?

From the point of view of FireBAN project, points 1 and 4 are the most relevant. One major point of the discussions on fire propagation was that, from the perspective of Fire PRA, smoke propagation is almost as important as physical flame spread. As such, the barrier considered in PRA analysis need not be a compartment wall or door, but may be an empty room between the fire and another room. VTT has participated in the OECD PRISME programs 1-2 and participates in PRISME3. The PRISME programs have provided a wealth of information on fire and smoke propagation in airtight and mechanically ventilated buildings. This information should be more efficiently communicated to the industry.

## 5. Conclusions

The report gives an overview and summary of the major achievements obtained in the FireBan project.

It is related to 9 publications and can be summarised as follows:

1. Different deficiencies in fire barrier can result in reduction of the fire resistance by up to 75 %. Deficiencies investigated were: reduced thickness of insulation, other type of insulation, holes in protection board and fire barrier and different types of leakages.
2. One can estimate the true uncertainty of the output quantity from simulated one with a priori knowledge of model uncertainty.
3. A case study of stone wool sandwich panels presents that simple statistical methods can be used to assess the most influential input parameters when modelling resistance to fire testing. For the same insulation material different tests at different exposure were performed as well as modelling. The models needed some empirical fine-tuning in order to get the appropriate input data.
4. A number of publications relate to procedures how to obtain input data for both semi-empirical and fundamental models to determine both heat transfer and pyrolysis models.

More research can be performed to further optimise the different determination methods for input, to further develop the models and also to produce full scale data for validation of the models.



## References

1. Patrick van Hees, Jonathan Wahlqvist, Simo Hostikka, Topi Sikanen, Bjarne Husted, Tommy Magnusson, Fredrik Jörud, Prediction and validation of pool fire development in enclosures by means of CFD Models for risk assessment of nuclear power plants (Poolfire) – Final Report, LUTVDG/TVBB--3183—SE, 99 pages, LTH report 3183, Lund 2014.
2. Fire Risk Analysis, Fire Simulation, Fire Spreading and Impact of Smoke and Heat on Instrumentation Electronics. State-of-the-Art Report. OECD Nuclear Energy Agency, NEA/CSNI/R(99)27, 2000, 99 p.
3. <http://www.nea.fr/jointproj/prisme.html> (downloaded 2015-10-14)
4. Sekizawa, A. and Sasaki, K. (2014). “Study on Fires Following the 2011 Great East-Japan Earthquake based on the Question- naire Survey to Fire Departments in Affected Areas,” Proceedings of the International Association for Fire Safety Science, 11th International Symposium (available at <http://www.iafss.org/publications/fss/11/100/view>).
5. Brian Meacham, Towards a Risk-Informed Performance-Based Approach for Post-Earthquake Fire Protection Design of Buildings, Proceedings of the 10th AOSFST symposium, Tsukuba Japan 2015.
6. Meacham, B.J. (1999). “International Experience in the Development and Use of Performance-Based Fire Safety Design Methods: Evolution, Current Situation, and Thoughts for the Future,” Proceedings of the International Association for Fire Safety Science, 6th International Symposium, pp.59-76.
7. Magnusson, S. E., H. Frantzich, and K. Harada, 1996, Fire Safety Design Based on Calculations: Uncertainty Analysis and Safety Verification, Fire Safety Journal, 27, pp. 305-334.
8. Johansson, N. (2015) Fire Dynamics in Multi-Room Compartment Fires. Report 1055, Department of Fire Safety Engineering, Lund University, Lund, Sweden.
9. McGrattan, K., McDermott, R., Hostikka, S., Floyd, F., “Fire Dynamics Simulator (Version 5) User’s Guide”, NIST Special Publication 1019-5, 2010.
10. <http://www.firetools-fp7.eu> (downloaded 2015-10-14).
11. P. Kolarkar and M. Mahendran, “Experimental studies of non-load bearing steel wall systems under fire conditions,” Fire Safety Journal, vol. 53, pp. 85–104, 2012.
12. British Standards Institution, “Standards Publication Fire resistance tests Part 1: General Requirements,” 2012.
13. Vallée, J. Reliability of fire barriers, Report nr 5521, Master thesis Erasmus Mundus, Lund University, <http://lup.lub.lu.se/student-papers/record/8876398>, 2016.
14. Paudel, D., Hostikka, S., Propagation of modeling uncertainty in stochastic heat-transfer simulation using a chain of deterministic models. *Int J Uncertain Quantif* 9(1):1–14, 10.1615/Int.J.UncertaintyQuantification.2018027275, 2019

- 
15. Livkiss, K., Andres, B., Johansson, N., van Hees, P., Uncertainties in modelling heat transfer in fire resistance tests: A case study of stone wool sandwich panels, *Fire and Materials Journal* DOI 10.1002/fam.2419, Wiley, 2017.
  16. Andres, B, Livkiss, K, Hidalgo, JP, van Hees, P, Bisby, L, Johansson, N & Bhargava, A 2018, 'Response of stone wool-insulated building barriers under severe heating exposures', *Journal of Fire Sciences*, vol. 36, no. 4, pp. 315-341. <https://doi.org/10.1177/0734904118783942>
  17. Livkiss, K, Andres, B, Bhargava, A & van Hees, P 2018, 'Characterization of stone wool properties for fire safety engineering calculations', *Journal of Fire Sciences*, vol. 36, no. 3, pp. 202-223. <https://doi.org/10.1177/0734904118761818>
  18. Andres, B, Hidalgo, JP, Bisby, L & van Hees, P 2017, Experimental analysis of stone wool sandwich composites exposed to constant incident heat fluxes and simulated parametric fires. in 15th International Conference and Exhibition on Fire and Materials 2017. vol. 2, Interscience Communications Ltd, pp. 503-516, 15th International Conference and Exhibition on Fire and Materials 2017, San Francisco, United States, 2017/02/06.
  19. Paudel, D. & Hostikka, S. *Fire Technology*, 2019, Propagation of Model Uncertainty in the Stochastic Simulations of a Compartment Fire, <https://doi.org/10.1007/s10694-019-00841-9>
  20. Sikanen, T., Model based optimization for calibration of pyrolysis models, VTT report VTT-R-05578-1, 2018.
  21. Maluk C, Bisby L, Krajcovic M, et al. A Heat-Transfer Rate Inducing System (H-TRIS) test method. *Fire Safety Journal*. Epub ahead of print 21 June 2016. DOI: 10.1016/j.firesaf.2016.05.001.
  22. Andres B., Livkiss K., Bhargava A., Van Hees P., Using micro-scale and solid material data for modelling stone wool composites under heat exposures, to be submitted during 2019

## Annex A Acronyms

ABAQUS: FEM Software package

Brandforsk: Swedish Board for Fire Research

CFD: Computational Fluid Dynamics

EN: European Standard

FDS: Fire Dynamics Simulator software programme

FIREBAN: Acronym for project "Determination of Fire Barriers reliability for fire risk assessment of Nuclear Power Plants"

FIREED: Acronym for project "Fire risk evaluation and Defence-in-Depth project"

FIRETOOLS: Acronym for Marie Curie project FIRETOOLS. Fire Tools is a European Industrial Doctoral Program (EID) jointly funded by European Commission and DBI under the European Union's (EU) 7th framework program under Marie Curie Actions. The overall objective of the FIRE TOOLS project is to develop tools for obtaining the fire properties and behaviour on a continuous scale for individual products, composite products and complete systems.

FRR: Fire resistance rating

FSE: Fire Safety Engineering

IRSN: Institut de radioprotection et de sûreté nucléaire

ISO: International Standardisation Organisation

LST: Light Gauge Steel Frame

NBSG: National Fire safety group (composed av SSM, SKB and nuclear power plants at Oscarshamn, Forsmark and Ringhals)

NEA: Nuclear energy agency

NKS: Nordic Nuclear Safety Research is a forum for Nordic cooperation and competence in nuclear safety, including emergency preparedness, serving as an umbrella for Nordic initiatives and interests.

NKS-R: The NKS-R programme from NKS is focused on Nordic research in the area of reactor safety including organisational issues and decommissioning of nuclear installations.

NPP: Nuclear Power Plants

OECD: Organisation for Economic Co-operation and Development

POOLFIRE: Acronym of the project Poolfire: Prediction and validation of pool fire development in enclosures by means of CFD

PRA: Probabilistic risk assessment

PSA: Probabilistic safety assessment

PRISME: The acronym PRISME comes from the French phrase propagation d'un incendie pour des scénarios multi-locaux élémentaires, which in English can be translated as "fire propagation in elementary, multi-room scenarios".

QRA: Qualitative Risk Analysis

SAFIR2018: The Finnish Research Programme on Nuclear Power Plant Safety 2015 - 2018

SKB: Svensk kärnbränslehantering AB (Swedish Nuclear Fuel and Waste Management Company)

SSM: Strålsäkerhetsmyndigheten (Swedish Radiation Protection Agency)

SVN: Apache Subversion (formerly called Subversion, command name svn) is a revision control system initiated in 2000 by CollabNet Inc. Developers use Subversion to maintain current and historical versions of files such as source code, web pages, and documentation

TS: Technical Specification

VTT: VTT Technical Research Centre of Finland Ltd

## Annex B



Lund University

Faculty of Engineering

Department: Division of Fire Safety Engineering

Year 2015-2016

**Reliability of fire barriers**

Jonathan Vallée

Promoter: Patrick Van Hees

Master thesis submitted in the Erasmus Mundus Study Programme

**International Master of Science in Fire Safety Engineering**

## DISCLAIMER

This thesis is submitted in partial fulfilment of the requirements for the degree of *The International Master of Science in Fire Safety Engineering (IMFSE)*. This thesis has never been submitted for any degree or examination to any other University/programme. The author declares that this thesis is original work except where stated. This declaration constitutes an assertion that full and accurate references and citations have been included for all material, directly included and indirectly contributing to the thesis. The author gives permission to make this master thesis available for consultation and to copy parts of this master thesis for personal use. In the case of any other use, the limitations of the copyright have to be respected, in particular with regard to the obligation to state expressly the source when quoting results from this master thesis. The thesis supervisor must be informed when data or results are used.

30-04-2016

Jonathan Vallée



Read and approved

## Summary/Abstract

*A fire barriers are widely used in the industry as a passive fire protection system. Fire barriers are built according to specifications from manufacturer after the construction was tested in full scale furnace in accordance to the appropriate codes. Those tests are made private and the test results are not published apart from the failure/success of the tested sample. In order to accurately protect the life of the occupants and the property, the fire barriers need to be built exactly as its counterpart tested in the furnace test or better. However, it is unknown how a barrier will react to having some higher leakage or lesser insulation property. This study looks at the effect of those two parameters on the fire resistance rating of fire barrier. Numerical tools, ABAQUS and FDS, were used to reproduce the furnace test. Results showed that presence of the insulation material in the cavity can improve the reliability of fire-resistant barrier with regards to the insulation criterion, especially when the fire-exposed gypsum board is breached or altered. Also, results demonstrated that for partitions with equal air tightness, leakage through holes causes earlier failures due to integrity criterion, comparing to leakage through joints or cracks.*

*Les séparations coupe-feu sont largement utilisées dans l'industrie comme système de protection passive en prévention incendie. Ces murs sont construits à partir des spécifications provenant du fabricant, obtenues suite à des essais rigoureux basé sur les normes en vigueur. Les essais sont effectués auprès de laboratoire privé et seulement le résultat final est publié (échec/succès). Afin de performé tel que prévu, le mur coupe-feu doit être construit exactement comme son homologue testé durant les essais. Cependant, il pourrait y avoir des différences entre le mur testé et le mur construit, spécialement en termes d'isolation et d'étanchéité à l'air. Ces pourquoi une étude est requise afin de connaître l'impact de ces deux propriétés sur la performance des murs coupe-feu. Pour y arriver, plusieurs simulations numériques ont été réalisées sur ABAQUS et FDS. Suite à l'analyse des résultats, il a été constaté que l'utilisation d'isolation dans la cavité murale permet d'obtenir une meilleur performance contre le feu, plus spécialement lorsqu'il y'a une brèche dans la couche de gypse situé du côté de l'incendie. De plus, avec une étanchéité à l'air équivalente, les murs dont la fuite d'air se produit par un trou ou une ouverture concentrée en un endroit précis performe moins bien dans un incendie comparé à un mur qui fuit par des joint ou par une fente distribuée le long du mur.*

## Table of contents

List of abbreviations.....	vi
List of figures and tables .....	vii
1 Introduction & Objectives.....	1
1.1 Introduction.....	1
1.2 Objectives.....	2
1.3 Methodology.....	3
1.4 Limitations.....	3
2 Heat Transfer .....	4
2.1 Radiation .....	4
2.2 Convection.....	6
2.3 Conduction .....	6
2.4 Heat flux in furnace test.....	8
3 Hot gas movement.....	9
3.1 Smoke infiltration.....	9
3.2 Air Tightness of walls.....	9
3.3 Pressure difference in a furnace .....	11
4 Fire barrier construction .....	13
4.1 Partition investigated.....	13
4.1.1 Construction type A .....	14
4.1.2 Construction type B .....	14
4.1.3 Light gauge steel frame.....	16
5 Material Properties.....	17
5.1 Thermal properties of Gypsum Board.....	17
5.1.1 Conductivity .....	18
5.1.2 Thermal capacity.....	18
5.1.3 Density .....	19
5.2 Thermal properties of insulation .....	21

5.2.1	Conductivity .....	21
5.2.2	Thermal capacity.....	22
5.2.3	Density .....	22
5.3	Thermal properties of steel.....	23
5.3.1	Conductivity .....	23
5.3.2	Thermal capacity.....	24
5.3.3	Density .....	24
5.4	Thermal property of air cavities.....	24
6	Methodology.....	26
6.1	ABAQUS Procedure .....	26
6.1.1	Geometry and Material Properties.....	26
6.1.2	Initial and Boundary Conditions .....	27
6.1.3	Interactions and assumptions.....	29
6.1.4	Mesh and Element Type .....	30
6.2	Validation of the FE model.....	32
6.3	FDS Procedure .....	34
6.3.1	Dimensions and materials.....	34
6.3.2	Temperature .....	35
6.3.3	Pressure .....	36
6.3.4	Leakage .....	36
6.3.5	Grid selection .....	38
6.4	Validation of the CFD model .....	39
6.4.1	Furnace Temperature .....	39
6.4.2	Furnace pressure distribution.....	41
6.4.3	Heat Flux at sample.....	41
7	Results and discussion .....	43
7.1	Construction Type A.....	44
7.1.1	Impact of the choice of insulation material.....	44
7.1.2	Impact of reduced amount of insulation .....	47

7.1.3	Impact of increased amount of insulation.....	50
7.1.4	Impact of hole on the exposed surface .....	52
7.1.5	Impact of the hole through the barrier .....	54
7.2	Construction Type B.....	55
7.2.1	Impact of the choice of insulation material.....	55
7.2.2	Impact of hole on the exposed surface .....	57
7.2.3	Impact of reduced amount of insulation .....	60
7.2.4	Impact of missing part of insulation .....	61
7.3	Table of results from the heat transfer simulation with ABAQUS.....	63
7.4	Impact of leakage with FDS.....	66
7.4.1	Localized leakage .....	66
7.4.2	Distributed leakage on one side .....	67
7.4.3	Distributed leakage.....	69
7.5	Discussion.....	72
7.6	Limitations and Uncertainties .....	73
8	Conclusions .....	75
9	Future Work.....	77
10	Acknowledgements.....	78
11	References .....	79
	Appendix A: FDS script file .....	I
	Appendix B: ABAQUS script file .....	XV

## **List of abbreviations**

HRRPUA – Heat Release Rate Per Unit Area

FRR – Fire Resistance Rating

NRCC – National Research Council Canada

LSF - Light gauge Steel Frame

FE – Finite Element

CFD – Computational Fluid Dynamics

ASTM – American Society for Testing and Materials

ISO – International Organization for Standardization

EN – European Standards

AAMA - American Architectural Manufacturers Association

ASHRAE – American Society of Heating, Refrigerating and Air Conditioning Engineers

NMBCC - National Model Building Code of Canada

DBI – Danish Institute of fire and security technology

## List of figures and tables

Figure 1: Heat transfer by radiation on a surface .....	5
Figure 2: Separation of surfaces into finite element .....	7
Figure 3: Heat flux measured during a furnace test (reproduced with the permission of the National Research Council of Canada).....	8
Figure 4: Typical light-weight construction assembly .....	13
Figure 5: Construction Type A.....	14
Figure 6: Construction Type B.....	14
Figure 7: Metal frame .....	15
Figure 8: joint from gypsum board .....	15
Figure 9: Conductivity of gypsum type X .....	17
Figure 10: Specific heat of gypsum board type X .....	18
Figure 11: Mass loss of gypsum board type X and Contraction of gypsum X.....	19
Figure 12: Change of density of gypsum type X .....	19
Figure 13: Conductivity of stone wool .....	20
Figure 14: Conductivity of glass fiber wool.....	21
Figure 15: Conductivity of steel .....	22
Figure 16: Specific heat of steel .....	23
Figure 17: Air density change with temperature.....	24
Figure 18: Fire barrier metal frame .....	25
Figure 19: Unexposed surface temperature.....	28
Figure 20: Exposed surface temperature .....	28
Figure 21: Temperature at the unexposed surface case a) .....	30
Figure 22: Temperature at the unexposed surface case b).....	30
Figure 23: Temperature at the unexposed surface case c) .....	31
Figure 24: Furnace modeled with FDS.....	34
Figure 25: Leakage distributed at every joints.....	36
Figure 26: Leakage distributed on one side.....	36
Figure 27: Leakage localized at the top .....	37
Figure 28: Acceptable temperature in the furnace according to EN 1363-1 .....	39
Figure 29: Average temperature versus time measured on the surface of the wall sample in FDS .....	39

Figure 30: Pressure profile in the FDS simulation.....	40
Figure 31: Distribution of the heat flux gauge (reproduced with the permission of the National Research Council of Canada) .....	41
Figure 32: Heat flux at the surface of the sample in the furnace.....	41
Figure 33: Temperature at the unexposed layer of the Wall with different types of insulation or without insulation.....	43
Figure 34: Temperature inside cross section of walls .....	44
Figure 35: FRR of each walls insulated or uninsulated .....	45
Figure 36: Temperature of the exposed side gypsum layer .....	45
Figure 37: Cross section a partition filled with fiber glass wool, after 60min .....	46
Figure 38: Wall with reduced insulation.....	47
Figure 39: Temperature in the cross section of wall with reduced insulation .....	47
Figure 40: Unexposed surface temperature of stone wool partition after 60min.....	48
Figure 41: Ratio of FRR over the expected 60min rating for partition with reduced insulation..	48
Figure 42: Temperature on unexposed surface of the wall with different position of insulation	49
Figure 43: Temperature on the unexposed side of a partition type A with 100mm stone wool insulation.....	50
Figure 44: Temperature in the cross section of a partition type A with 100mm stone wool insulation.....	50
Figure 45: Temperature on the unexposed side for insulated partition with hole on the exposed surface.....	51
Figure 46: Temperature of the partition with hole on exposed surface insulated with stone wool .....	51
Figure 47: Temperature on the unexposed side of the partition with hole on the exposed surface .....	52
Figure 48: Temperature of partition without insulation breached on exposed side .....	52
Figure 49: Temperature on the unexposed surface of a partition type A with a hole of 10mm, first and second scenario .....	53
Figure 50: Temperature on the unexposed surface of a partition type A with a hole of 50mm radius, first and second scenario .....	53
Figure 51: Temperature on the unexposed surface of wall type B with different types of insulation and without insulation.....	54
Figure 52: Temperature in the cross section of wall type B for different insulation .....	55
Figure 53: FRR for different insulation or uninsulated .....	55
Figure 54: Temperature on the unexposed side for insulated partition with hole on the exposed surface.....	56
Figure 55: Temperature of the partition with hole insulated with stone wool .....	57

Figure 56: Temperature of the partition for all types of insulation and breach of 10mm and 50mm radius.....	58
Figure 57: Temperature on the unexposed surface of wall type B with reduced insulation .....	59
Figure 58: FRR for partition with reduce insulation for type B construction .....	60
Figure 59: Temperature on the unexposed surface of wall type B with missing insulation part	60
Figure 60: The temperature of the two walls with missing portion of insulation, left 50mm radius and right 100mm radius.....	61
Figure 61: The temperature of the two walls with missing portion of insulation, left 50mm radius and right 100mm radius.....	61
Figure 62: Temperature of cotton pad scenario 1 with different level of air tightness.....	66
Figure 63: Temperature of cotton pad with time measured at the top of the sample height ....	68
Figure 64: Temperature of cotton pad with time measured at the bottom of the sample height .....	69
Figure 65: Temperature of cotton pad with time measured at the middle of the sample height	69
Figure 66: Temperature on the cotton pad after around 3600 seconds.....	72
Figure 67: Temperature on the unexposed side of the tested sample after 3600 seconds .....	73
Table 1: Leakage area for different tightness .....	11
Table 2: Thermal capacity of insulation .....	21
Table 3: Density of insulation .....	22
Table 4: Emissivity of material .....	24
Table 5: Experimental and simulation results .....	32
Table 6: Thermal properties of ceramic blanket .....	33
Table 7: Properties of propane .....	35
Table 8: Comparison of the results obtained with ABAQUS .....	65
Table 9: FRR of partition with different tightness leaking from a hole on top.....	67
Table 10: FRR of partition with different air tightness leaking from one side .....	70
Table 11: Percentage change in FRR between localized and distributed leakage .....	70
Table 12: FRR of partition with different air tightness leaking from every joints .....	71
Table 13: Percentage change in FRR between leakage in all joints and the other scenarios for the cotton pad at mid height of the furnace .....	72

# 1 Introduction & Objectives

## 1.1 Introduction

In order to restrain fire spread and to contain the fire in one area, a building can be subdivided into compartments separated from one another by fire-resisting constructions. This passive fire protection method helps to reduce the fire size which gives more time for the occupants to evacuate, eases the fire service work and decreases property damage and business interruption time. The fire resistance rating of light weight construction, especially Cold-formed light gauge steel frame (LSF) stud wall systems, has become critical to the building safety design as their use has become increasingly popular in all areas of building construction [1].

The fire resistance rating (FRR), given in unit of time, is the period of time during which a building element can withstand the exposure to defined heating and pressure conditions, until failure. Usually this time period ranges between 60min and 120 min [1]. Traditional fire resistance testing is done in furnace test and based upon the international standard ISO 834. According to the British code BS EN 1363-1, the failure criteria are based on three parameters: integrity, stability and insulation [2]. The insulation criterion relates to the ability of a building component to restrict the heat transfer through its boundaries to a certain level. According to the EN 1363-1 code, failure of the insulation criterion is observed in two ways [2]. The code states that the specimen must maintain its function for the duration of the test without developing temperatures on its unexposed surface such as:

- An increase the average temperature above the initial average temperature by more than 140 °C, called  $T_{140}$ ;
- An increase at any location (including the roving thermocouple) above the initial average temperature by more than 180 °C, called  $T_{180}$ .

The integrity criterion represents the ability of a building component to prevent the passage, through its boundaries, of flames and hot gases and to prevent the occurrence of flames on the unexposed side. The requirements from the relevant code [2] are the following:

- Prevent the penetration of a 6 mm diameter gap gauge that can be passed through the test specimen, such that the gauge projects into the furnace, and can be moved a distance of 150 mm along the gap
- Prevent the penetration of a 25 mm diameter gap gauge that can be passed through the test specimen such that the gauge projects into the furnace.

- Prevent the ignition of a cotton pad applied for a maximum of 30 s or until ignition positioned at least 30 mm from the unexposed surface and 10 mm from the boundaries of the wall. Charring of the cotton pad without flaming or glowing shall be ignored.

In the industry the fire rated partition are built according to specifications coming from manufacturers, providing fire resistance ratings. Those rating are based on full-scale furnace tests using the required standard [3]. Often, the fire barriers tested in the furnace are highly optimized in order to reach the required fire resistance. The test results remain confidential and the number of samples, which fail is not documented. In practice, the construction of the fire rated barrier can slightly differ from the optimized one tested in the furnace test. Furthermore, with time, the quality of the barrier can be altered, thus, reducing its ability to contain the fire. This raises concerns about the reliability of fire resisting partition as an effective mean of passive fire protection. Little research has been done with respect to the impact of reduced insulation and leakage on the reliability of fire resisting partition. It is not known what kind of safety factor can be expected of fire barrier and often, the designer relies simply on the obtained ratings. For this reason, research is necessary in order to determine the reliability of fire barriers.

In this report the effect of reduced integrity and insulation parameters will be investigated. In order to do so, two fire-rated barriers will be modeled with numerical tools and will be exposed to the standard fire. Then, the same barriers will be modified to exploit different features or defects, affecting the insulation or integrity criterion, and it will be exposed to the same conditions. Finally, the results will be compared to understand how those features affect the FRR. The different defects or features which will be investigated are the following: different type of insulation, different thickness of insulation, missing part of insulation, the absence of insulation, penetration through the drywall on one side or through the entire construction, infiltration of gases through cracks of different size at different location. Additionally, the report will look at the impact of the modeling techniques used such as the difference of grid size, the impact of different heat transfer modes and the assumptions taken.

## **1.2 Objectives**

The first objective of this study is to show how the FRR of partitions is affected by leakage. To do this, the FRR obtained from simulations of partitions with localized leakage, distributed leakage, different leakage size and location will be compared to an airtight partition.

The second objective of this study, is to investigate the effect of a reduced thermal insulation on the FRR of partitions. Insulation can be reduced in multiple ways, the scenarios which will be investigated are: localized missing piece of different size of insulation, reduced thickness of insulation, different type of insulation, partition without insulation, hole of different size on the exposed boundary of the partition and hole through the partition. Those assumed

parameters and features are meant to represent ways in which a fire rated wall could be altered before being exposed to a fire.

### **1.3 Method**

The methods that will be used are hand calculations for basic heat transfer through the wall, hand calculations of infiltration and pressure inside the furnace, CFD modelling using the CFD tool - FDS and Finite element modelling using ABAQUS to replicate the standard fire furnace tests. Case study method will be used in this work. More precisely, the effect on the FRR according to the insulation criterion will be examined for the following parameters: The type of insulation or absence of insulation, the reduction of the insulation thickness inside the cavity, breach in the gypsum board exposed in the furnace, breach through the fire barrier and missing piece of insulation inside the cavity. Also, the effect of leakage on the FRR based on the integrity criterion will be investigated assuming that the barrier leaks before it is submitted to the standard fire. Different level of airtightness will be assumed and different leakage scenario. The first scenario will aim at simulating the effect of hole through the barrier. The second and third scenario will be looking at the effect of leaking joint improperly sealed. In order to validate the models, comparison of model's results to experimental data of wall tested in actual furnace will be made. Thus, the report also holds a study of model validity, to see whether simple calculations and modelling are able to replicate heat transfer in a furnace test.

### **1.4 Limitations**

This study will be limited to walls and will not include doors, windows, ventilation ducts. Studies will be mainly done with respect to smoke leakages and reduced thermal insulation. The stability criterion relates to the structural capacity of the structure at elevated temperature. In this study the stability criterion will not be investigated, thus, it is assumed that the walls do not collapse, do not show excessive deformation or deflection. Also, it is assumed that the defects and features investigated are already part of the wall before the fire, this study will not be looking at the deficiencies due to the fire effects.

## 2 Heat Transfer

In order to properly model the heat transfer from the furnace to the sample, it is necessary to understand the different modes of heat transfer. There are three basic mechanisms of heat transfer, namely conduction, convection and radiation[4]. Inside the furnace the exposed surface of the partition will be affected by convection and radiation[5]. The contributions of these two modes of heat transfer are independent and must be treated separately. The total heat flux to the exposed surface in the furnace is [6]:

$$q''_{exposed\ surface} = q''_{radiation\ furnace} + q''_{convection\ furnace} \quad (1)$$

The unexposed surface of the fire barrier will be also subjected to heat transfer, but only with the ambient air outside of the furnace. The heat transfer will be done through convection with air at 20°C [7]. Radiation is not considered due to the low temperature expected on the unexposed layer and the unknown distance between the unexposed surface and other objects.

$$q''_{unexposed\ surface} = q''_{convection\ ambient} \quad (2)$$

Heat can propagate inside the barrier by different means depending on its construction. If insulation is used then heat will be transferred to the unexposed side by conduction only, but if there is an empty cavity inside the barrier then radiation is expected due to the high temperature occurring in a furnace test [8].

### 2.1 Radiation

The net radiative heat flux on a targeted surface is the difference between the absorbed incident radiation and the emitted radiation. Those two parameters depends on the emissivity/absorptivity and absolute temperature, of the surfaces involved. Indeed, as depicted in the Figure 1 (reproduced from a study of SP [5]), part of the incident radiation, coming from the surrounding, is absorbed while the rest is reflected and the surface emit radiation as well. The net radiative heat flux on a surface can be written as [5]:

$$q''_{rad} = \alpha_s q''_{inc} - q''_{emi} \quad (3)$$

The emitted radiative heat flux can be expressed according to the Stefan–Boltzmann equation[4].

$$q''_{rad} = \sigma \varepsilon T^4 \quad (4)$$

Thus the equation (3) can be written as:

$$q''_{rad} = \alpha_s q''_{inc} - \sigma \varepsilon_s T_s^4 \quad (5)$$

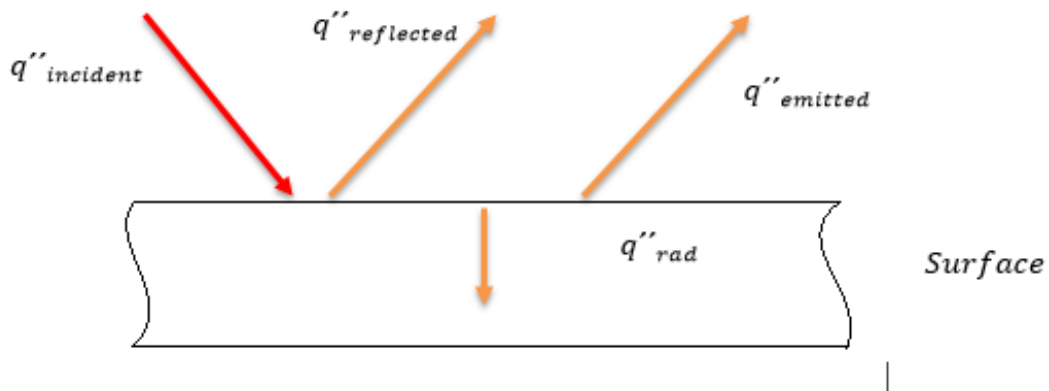


Figure 1: Heat transfer by radiation on a surface

Where

$\alpha_s$  – is the surface target absorptivity

$\varepsilon_s$  – is the emitting surface emissivity

$\sigma$  – is the Stefan–Boltzmann constant,  $5.67 \times 10^{-8} \text{ W/m}^2 \text{ K}^4$

$T_s$  – is the target surface temperature, K

However, the surface emissivity and absorptivity are considered equal according to the Kirchhoff's identity[4]. Thus the equation (5) can be rewritten as:

$$q''_{rad} = \varepsilon_s(q''_{inc} - \sigma T_s^4) \quad (6)$$

In the furnace test the incident radiation to the tested surface is emitted by the surrounding gases, by flames and by other surfaces. The heat fluxes are generally very complicated to model. Usually, a summation of the main contributions can give a good estimate of the incoming radiation [6]:

$$q''_{inc} = \sum F_i \varepsilon_i \sigma T_i^4 \quad (7)$$

Where

$\varepsilon_i$  – is the surrounding surface emissivity

$F_i$  – is the view factor involving distance and location

$T_i$  – is the surrounding surfaces, flame and gases temperature, K

The view factor for total radiation exchange between two identical, parallel, directly opposed flat plates can be assumed to be 1, when the ratio of the emitting surface dimension over the distance between surfaces is low [4]. Therefore, the heat transfer by radiation from the furnace to the exposed partition surface can be expressed as:

$$q''_{furnace} = \varepsilon_s \sigma (T_{ISO834}^4 - T_s^4) \quad (8)$$

## 2.2 Convection

Heat transfer by convection occurs between a fluid and a solid. It depends on the target geometry, adjacent fluid velocities and fluid/object temperature. Convection occurs inside the furnace between the furnace gases and the exposed surface of the sample and between the unexposed surface of the sample and the surrounding ambient temperature air, outside of the furnace. The heat transfer equation are expressed as follow [4]:

$$q''_{Exposed\ surface} = h_{exp}(T_{gases} - T_{s\_exp}) \quad (9)$$

$$q''_{Unexposed\ surface} = h_{unexp}(T_{s\_unexp} - T_{ambient}) \quad (10)$$

Where

$h_{exp}$  – is the convective heat transfer coefficient from the exposed surface, W/m<sup>2</sup>K

$h_{unexp}$  – is the convective heat transfer coefficient from the unexposed surface, W/m<sup>2</sup>K

$T_{s\_exp}$  – is the exposed surface temperature of the sample (exposed or unexposed), K

$T_{s\_unexp}$  – is the exposed surface temperature of the sample (exposed or unexposed), K

$T_{ambient}$  – is the temperature outside the furnace, K

$T_{gases}$  – is the gases temperature inside the furnace, K

The convective heat transfer coefficient,  $h$ , inside and outside the furnace will be different due to the flow conditions.

## 2.3 Conduction

Conduction only occurs inside a medium which can be a gas, liquid, or solid. The distinction between conduction and convection heat transfer is associated with whether the medium has some ordered flow or motion [9]. For very thin solids, or for conduction through solid that goes on for a long time, the process of conduction becomes stationary, and the rate of heat conducted through the solid becomes [4]:

$$q''_{cond} = \frac{k}{\delta}(T_{exp} - T_{unexp}) \quad (11)$$

Where

$\delta$  – is the thickness of the sample, m

$T_{exp}$  – is the temperature on the hot side of a sample, K

$T_{unexp}$  – is the temperature on the cold side of a sample, K

$k$  – is the conductive heat transfer coefficient, W/mK

Also a numerical solution can be used to solve heat transfer equations. For one-dimensional heat transfer, the wall needs to be represented by a series of thin, parallel elements of equal thickness, as shown in Figure 2 (reproduced from An Introduction to Fire Dynamics, Third Edition[4]). Transient heat transfer through the barrier is then calculated iteratively, by considering adjacent elements and applying the logic of Equations (12) and (13). Those equations depict the unsteady heating stage where the element numbered 3 receives heat from element 2, but loses heat to element 4. Also, at the two boundaries of the fire barrier, the conditions should be applied to reproduce the convection and the radiation heat transfer from the furnace and the room at ambient conditions. This is shown in the equations (14) and (15) [4], [10].

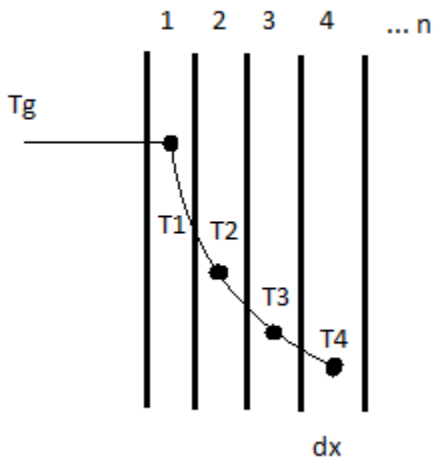


Figure 2: Separation of surfaces into finite element

$$\frac{k}{\Delta x}(T_2 - T_3) - \frac{k}{\Delta x}(T_3 - T_4) = \rho c_p \Delta x (T_3(t + \Delta t) - T_3(t)) \quad (12)$$

$$T_3(t + \Delta t) = T_3(t) + \frac{k}{\rho c_p (\Delta x)^2} (T_2 - 2T_3 + T_4) \quad (13)$$

$$T_1(t + \Delta t) = T_1(t) + \left( (h(T_{hot} - T_1) + \varepsilon_i \sigma (T_{hot}^4 - T_1^4) - \frac{k}{\Delta x} (T_1 - T_2)) \frac{2\Delta t}{\rho c_p \Delta x} \right) \quad (14)$$

$$T_m(t + \Delta t) = T_m(t) + \left( \frac{k}{\Delta x} (T_{m-1} - T_m) - (h(T_m - T_{cold})) \frac{2\Delta t}{\rho c_p \Delta x} \right) \quad (15)$$

## 2.4 Heat flux in furnace test

The total heat flux measured in an ASTM E 119 furnace test, at the National Research Council of Canada, is provided in Figure 3, for a wall furnace. The total heat fluxes were measured using a water-cooled Gardon gauge and the wall furnace was lined with ceramic fiber. The temperature was controlled with ASTM E 119 shielded thermocouples [11]. Though, the time-temperature curves are similar for ISO 834 and ASTM E119, the actual heat flux exposure early in the ASTM E 119 is more severe due to the type of thermocouples used to control the furnace. The same furnace controlled with a plate thermometer provided similar heat flux levels at times after 10 minutes [12]. This heat flux will be used later as means of validation.

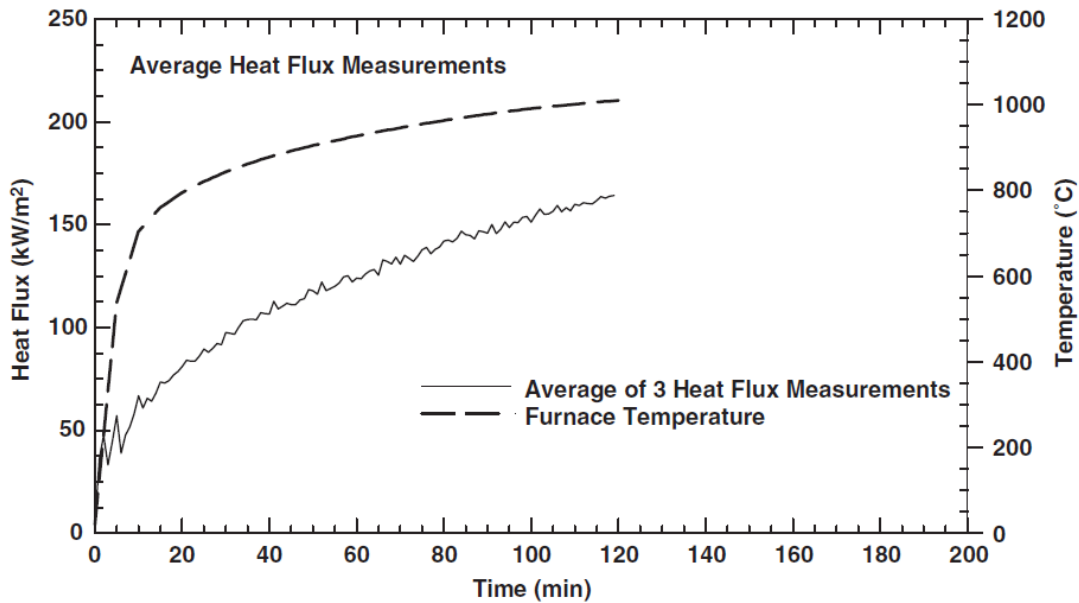


Figure 3: Heat flux measured during a furnace test (reproduced with the permission of the National Research Council of Canada)

### 3 Hot gas movement

#### 3.1 Smoke infiltration

The driving force for air movement is pressure, air moves from a location of higher pressure to a location of lower pressure. However, for air to move through a surface it needs an open area or leakage area. The total air leakage in a fire rated wall is equal to the sum of all the leakages occurring through holes and cracks in the boundaries. However, the quantity and appearance of the leakage areas is often impossible to predict since when building a fire-rated barrier the aim is not to have any leakages. Still, based on experience, a total opening area can be assumed and it is possible to estimate the total leakage through barriers. By measuring the difference in pressure across the wall from the unexposed side against the exposed side, the flow rate can be obtained from Bernoulli's equation. The orifice equation used to estimate the flow through building is presented below [13]:

$$Q = CA \sqrt{\frac{2\Delta p}{\rho}} \quad (16)$$

where

Q = volumetric airflow rate, m<sup>3</sup>/s

C = flow coefficient

A = flow area (leakage area), m<sup>2</sup>

Δ p = pressure difference across flow path, Pa

ρ = density of air entering flow path, kg/m

The flow coefficient depends on the geometry of the flow path, as well as on turbulence and friction. The number of opening also has an impact on the flow coefficient. Literature suggest a flow coefficient in the range of 0.6 to 0.7 [13].

#### 3.2 Air Tightness of walls

Fire-rated barriers should be designed and constructed to be as airtight as possible. This help to prevent any combustible gas to reach the unexposed side of the wall, thus preventing fire spread as much as possible. Nonetheless, it is not possible to build wall that's is perfectly air tight due to the presence of screws, anchors, electrical outlets, etc. Those elements create area or paths for air infiltration, even though effort is made to seal all penetration. Also, materials by themselves are never 100 % impermeable to movement of air and as such they allow for leakage, although, very low leakage.

In North America the Normalized Air Leakage Rate of Building Enclosure is used to define leakage. The average volume of air in L/s that passes through a unit area of the building enclosure in  $m^2$ , is measured and expressed in  $L/s \cdot m^2$  when the building enclosure is subjected at 75 Pa of pressure differential, in accordance with ASTM E779 [14].

The American Architectural Manufacturers Association (AAMA) suggests a maximum of  $0.3 L/s \cdot m^2$  at 75 Pa [14], while the appendix of the National Model Building Code of Canada (NMBCC) recommends a value of  $0.1 L/s \cdot m^2$  at 75 Pa [14] as a maximum allowable leakage rate. Tamura and Shaw, from the NRCC, in the 1980s measured and studied the air leakage of seven high-rise office buildings. Their conclusion was that buildings are tight if they achieve a normalized air leakage rate of  $0.5 L/s \cdot m^2$  at 75 Pa [14]. ASHRAE considered that a building is very loose when there is opening in walls equivalent to  $0.13 \times 10^{-2} m^2$ , average for values of  $0.35 \times 10^{-3} m^2$  and tight for values of  $0.17 \times 10^{-3} m^2$  per total area of wall ( $m^2$ ) [13].

With the equation (16), and the density of air at ambient temperature ( $20^\circ C$ ), the previous leakage gives the following opening area/surface ratio:

$$0.5 \frac{L}{s * m^2} = 0.0005 \frac{m^3}{s * m^2} = 0.65A \sqrt{\frac{2 * 75Pa}{1.225 \frac{kg}{m^3}}}$$

$$A = 70 \frac{mm^2}{m^2}$$

$$0.3 \frac{L}{s * m^2} = 0.0003 \frac{m^3}{s * m^2} = 0.65A \sqrt{\frac{2 * 75Pa}{1.225 \frac{kg}{m^3}}}$$

$$A = 42 \frac{mm^2}{m^2}$$

$$0.1 \frac{L}{s * m^2} = 0.0001 \frac{m^3}{s * m^2} = 0.65A \sqrt{\frac{2 * 75Pa}{1.225 \frac{kg}{m^3}}}$$

$$A = 14 \frac{mm^2}{m^2}$$

The wall area investigated will be of dimension equal to 3.6m x 3.1m. The dimensions of cracks which will be considered are presented in the following table.

Airtightness level	Leakage area (mm <sup>2</sup> )
Very loose construction	14508
Loose construction	4536
Average construction	1897
Tight construction (NRCC)	780
Tight construction (AAMA)	468
Tight construction (NMBCC)	156

Table 1: Leakage area for different tightness

### 3.3 Pressure difference in a furnace

Fully-developed fires produce a positive pressure gradient across the boundaries height, relative to ambient conditions. The pressure differential between compartment containing a fire and one containing ambient air will vary due to buoyancy of hot gases, the pressure difference can be found with the equation 17 [12],

$$\Delta p = g(\rho_a - \rho_f)h \quad (17)$$

Where

$g$  - is the gravitational constant, 9.81 m/s<sup>2</sup>

$\rho_f$  - is the gases density inside the fire compartment, kg/m<sup>3</sup>

$\rho_a$  - is the ambient air density at the same elevation, kg/m<sup>3</sup>

$h$  - is the elevation above a reference where the pressure between ambient and the compartment is equal (this reference is called the neutral plane), m

By applying the ideal gas law to equation 17, the differential pressure equation can be transformed into a temperature difference equation [12],

$$\Delta p = 352.8g \left( \frac{1}{T_a} - \frac{1}{T_f} \right) h \quad (18)$$

Where

$T_f$  - is the gas temperature inside the fire compartment, (K)

$T_a$  – is the ambient gas temperature, 293 K

The pressure found in the modeled furnace can be estimate with the equation (18), at height of 3.1m. After 2 hour of the ISO-834 standard fire the temperature inside the furnace reaches 1342 K [2] and the pressure differential is then:

$$\Delta p = 28 \text{ Pa}$$

## 4 Fire barrier construction

Fire-rated barriers may be constructed in a variety of ways. The required resistance rating will depend on the intended usage and the requirement of building codes. One of the most popular construction type of fire barrier is light weight stud wall system [1]. Lightweight partitions are usually built from various types of sheet materials, supported by timber or metal stud, with sealed joints. The cavity between the boards are filled with insulation layers or left empty. The insulation materials commonly used in the cavity are glass fibre, stone wool insulation [1]. This work will focus on LSF wall system as they are a popular types of installation [1]. Figure 4 shows a typical assembly of a light-weight partition with the insulation. The literature review of fire barrier specifications from Plasterboard manufacturer allowed to define the general component and construction specification required in order to obtain suitable fire rating.

### 4.1 Partition investigated

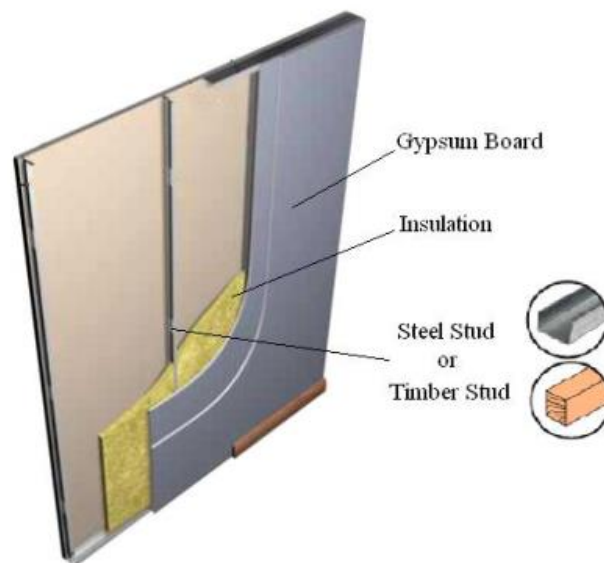


*Figure 4: Typical light-weight construction assembly*

Two different types of construction will be investigated in this project. The first one, called type A, correspond to a one hour fire resistance wall and the second construction, called type B, correspond to a two hours fire resisting wall. Construction specification of both type come from the literature review of different manufacturer.

#### 4.1.1 Construction type A

The fire barrier of type A, is built of a single layer of fire type gypsum board located on each side of the partition, 12.5mm thick. The gypsum board is supported by 50mm width, 0.5mm gauge, 'C' studs at every 600mm centres, see Figure 5. This type of construction was tested in a furnace test, without the use of any insulation, and was rated 60 minutes of fire resistance [3], [15]. This construction will be investigated with and without the use of thermal insulation. Usually, in order to achieve this resistance, the wall's joints and cracks must be sealed to prevent air infiltration. The impact of the thickness of the wall will be investigated to look at the impact on the barrier's integrity. An example of a section of the wall with and without insulation is given below.

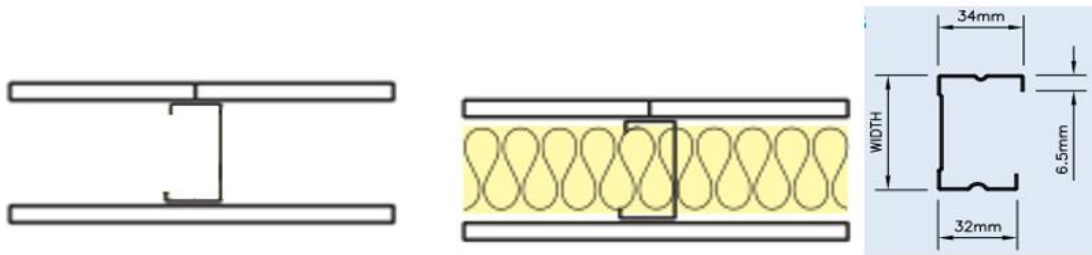


Figure 5: Construction Type A

#### 4.1.2 Construction type B

The fire barrier is built of two layers of fire type gypsum board, located on both side of the partition, 12.5mm thick. The gypsum board is supported by 50mm width, 0.5mm gauge, 'C' studs at every 600mm centres, see Figure 6. This type of construction was tested in a fire resistance test, without the use of any insulation, and was rated 120 minutes fire resistance [3], [15]. This construction was investigated with and without the use of thermal insulation. In order to achieved this resistance, the wall joints and cracks must be sealed to prevent air infiltration. The impact of the thickness of the wall will be investigated to look at the impact on the barrier's integrity. An example of a section of the wall with and without insulation is given below.

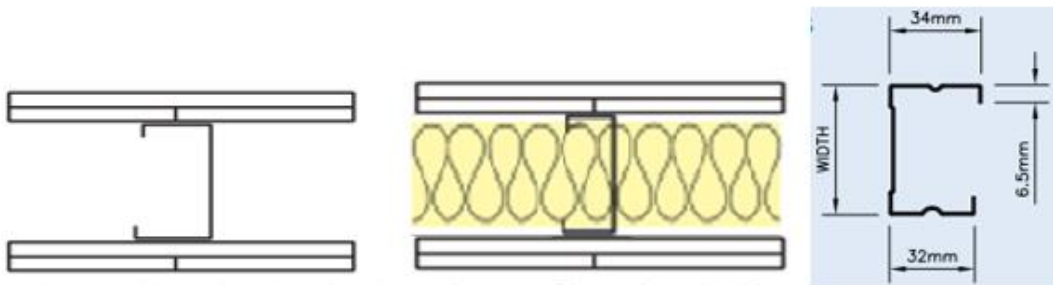


Figure 6: Construction Type B

### 4.1.3 Light gauge steel frame

The frame used to hold the insulation and on which the gypsum board is fixed to, is presented in the following picture with all related dimensions.

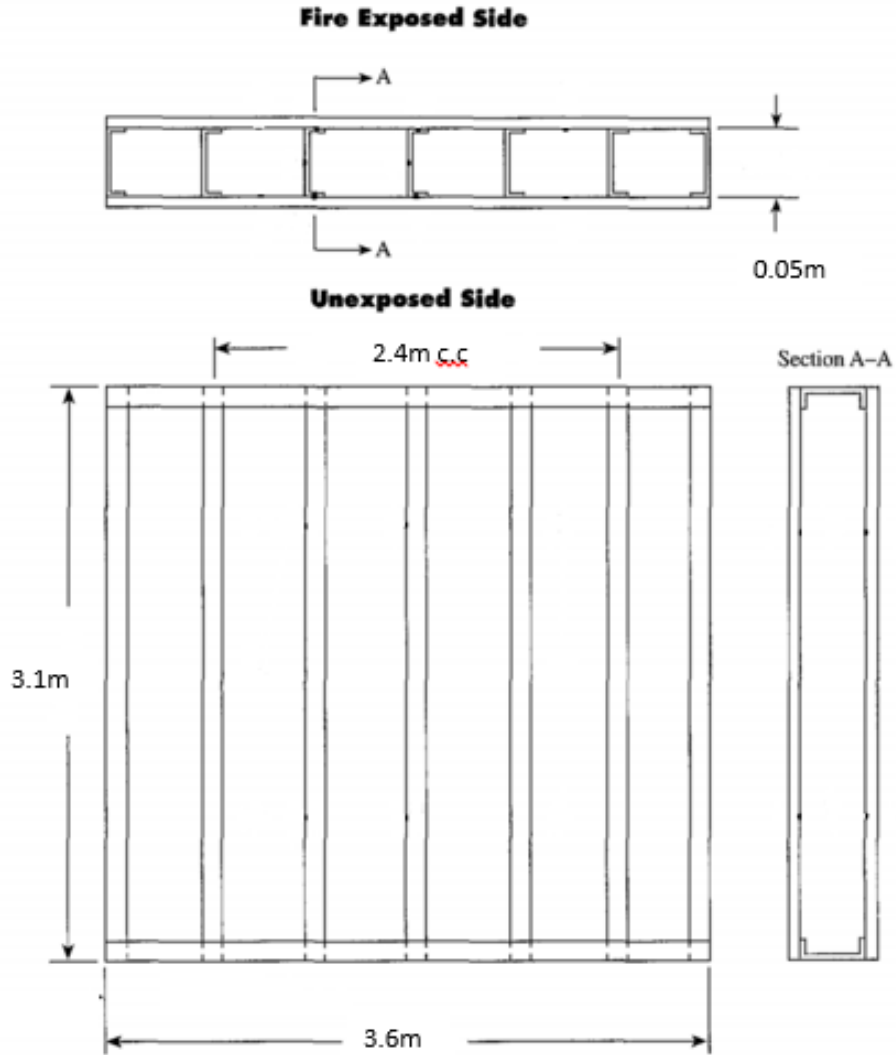


Figure 7: Metal frame

The gypsum boards are usually 1220mm wide by 3660mm long [16], this means that this wall would require 3 gypsum sheets to cover the whole surface. When using multiple sheets of gypsum, joints are formed between each sheet and the surrounding construction as well as between every two sheets. Those joints can be a source of leakage if they are not sealed properly.

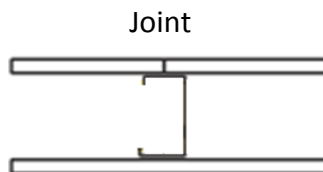


Figure 8: joint from gypsum board

## 5 Material Properties

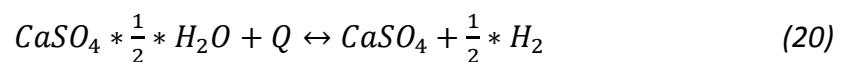
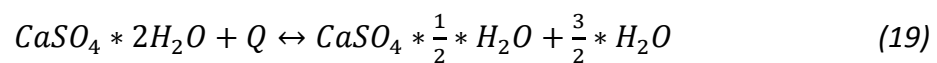
To be able to withstand the furnace increasing temperature, the partition wall must have adequate thermal properties. The properties of each layer constituting the wall are important as they help to slow down heat transfer through partitions. The material properties which should be assessed, in order to investigate the partition reliability with regards to the insulation criterion, are the density, the specific heat and the conductivity. These properties differ from one manufacturer to another, for instance gypsum board type X or Glasroc F FIRECASE. In this study the focus is not on the variation in thermal properties, but on the effects of defects affecting fire-rated barrier. Consequently, material properties will be defined in this section and will not be change in the simulation.

The specific heat or thermal capacity is a measurable physical quantity equal to the ratio of the heat added to or removed from an object to the resulting temperature change. The specific heat is measure in J/kg\*K. The thermal conductivity is a material property describing the ability to conduct heat. The thermal conductivity is measure in the units W/m\*K. The density is a material attribute defining the weight per volume of a material in kg/m<sup>3</sup>.

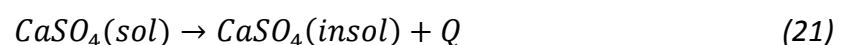
### 5.1 Thermal properties of Gypsum Board

Gypsum board is constructed of non-combustible products in which gypsum is the primary component with paper-laminated surfaces. In North America the gypsum board called Type X is used for fire barrier. This gypsum board has additives that give better fire-resistive performance compare to the regular gypsum board of the same thickness.

Gypsum is called calcium sulfate dihydrate (CaSO<sub>4</sub> 2H<sub>2</sub>O), which is a naturally occurring mineral. The water proportion is a key feature that makes gypsum a fire resistant material. When gypsum is heated, the crystalline gypsum dehydrates and water is released. This process is called Calcination and typically occur in two separate, reversible chemical reactions:



Both of these dehydration reactions are endothermic and generally occur at temperatures between 125 and 225°C. In addition to two dehydration reactions, a third exothermic reaction occurs at a temperature of around 400°C in which the molecular structure of the soluble crystal reorganizes itself into a lower insoluble energy state (hexagonal to orthorhombic) [17]:



The data used in this project is based on a paper from NIST [17], which tested the properties of different type of gypsum board under heat. The results for gypsum board type X from this paper will be used.

### 5.1.1 Conductivity

The thermal conductivity of gypsum board is a function of the temperature and heating cycle. During the first heating cycle (first time the gypsum board is being heated), the gypsum dehydrates, absorbs some of the energy, and delays the temperature rise. Results from experiment clearly show a huge differences in the thermal conductivity between first heating and second heating cycle [17]. Since it is unlikely that the gypsum board will be reused after a fire, it is reasonable to assume that the gypsum board will be at his first heating cycle. Therefore the conductivity of type x gypsum board will be taken as presented in the Figure 9 [17].

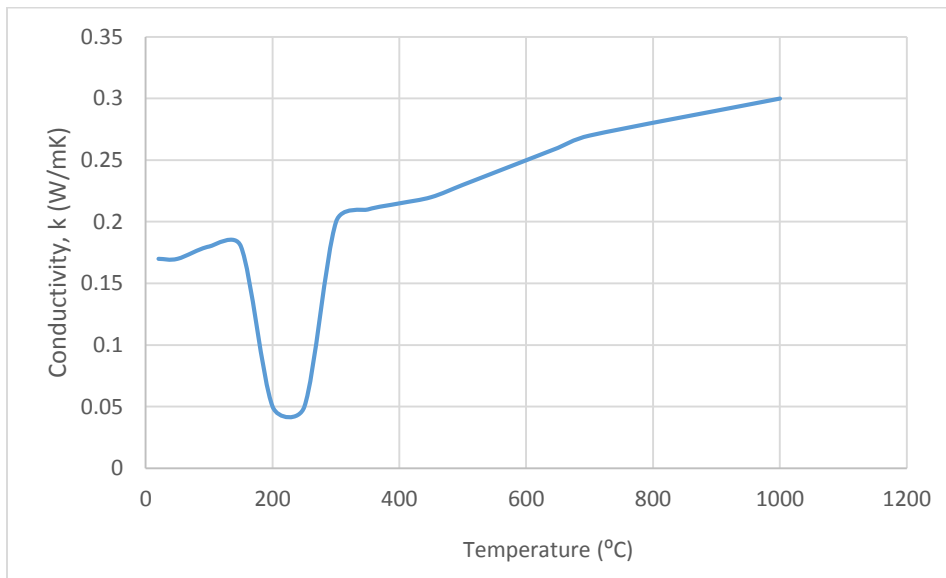


Figure 9: Conductivity of gypsum type X

### 5.1.2 Thermal capacity

The energy needed to dehydrate the gypsum has a direct effect on the gypsum board thermal capacity. This results in peaks at the moment where the dehydration reaction occurs. The tests from NIST shows relatively the same peak magnitude for different types of gypsum board tested [17]. The resulting specific heat which will be used in the models is presented in Figure 10.

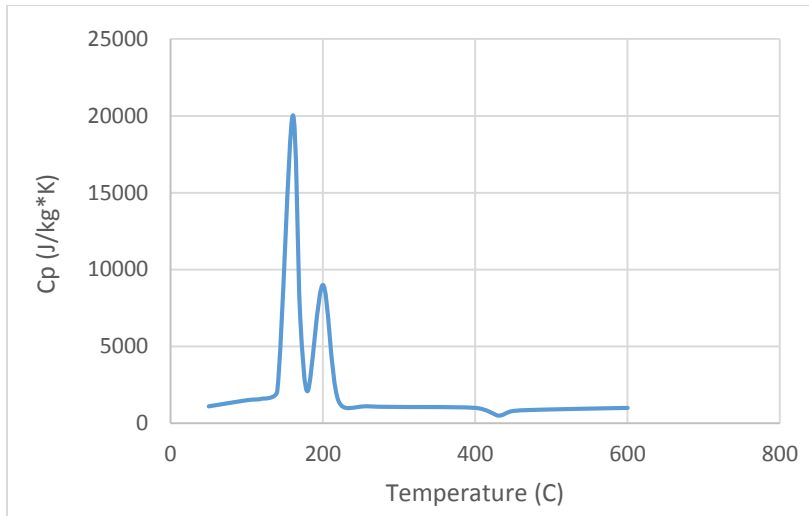


Figure 10: Specific heat of gypsum board type X

### 5.1.3 Density

At elevated temperatures, gypsum shrinks, test shows that at temperatures above 700°C, shrinkage rapidly increases. Also, experiment indicates that gypsum board loses its mechanical flexibility at about 400°C, and gradually loses its strength starting at about 500°C. Furthermore, when the gypsum board reaches temperature of 700°C, it loses all its strength. Those results suggest that screws should be able to keep gypsum board fixed to the walls for gypsum board's at temperature below 400°C and that it would tend to pull out from the screws at temperatures ranging between 600°C and 700°C [7].

In the series of tests done by NIST [17] the density of gypsum board and its mass loss was investigated. The initial density for gypsum type X is: 711kg/m<sup>3</sup>. As the temperature of the boards increases the gypsum board loses part of its mass. This occurs due to the crystallised water that evaporates. The results show that the density of gypsum boards changes significantly when the temperature increases. The mass loss was measured and is plotted as a function of temperature and shown in Figure 11. Increase of temperature also affects the size of gypsum board. Indeed, the increase of temperature in gypsum is associated with a contraction of its size, the data found for the gypsum X is presented in Figure 11. This has an effect on the opening of the fire barrier since as the board contracted it let place to gap where combustible gas can infiltrate.

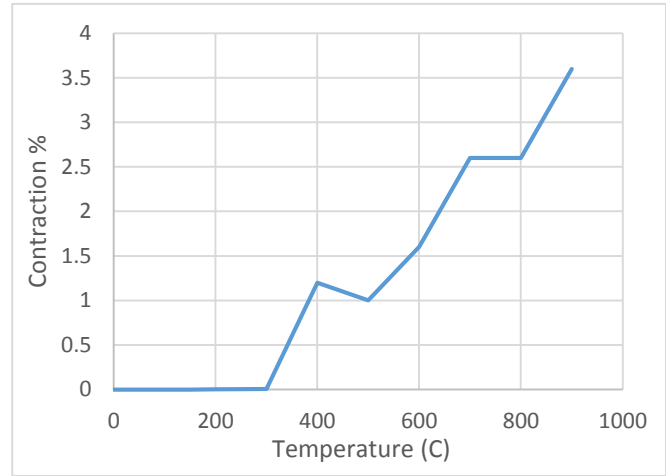
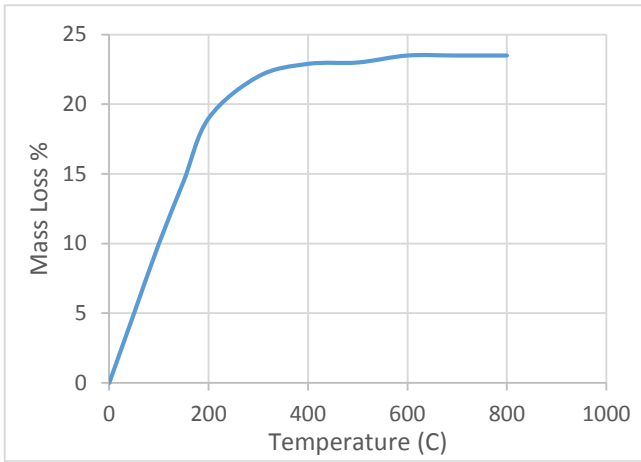


Figure 11: Mass loss of gypsum board type X and Contraction of gypsum X

With the combine effect of mass loss and contraction it is possible to estimate the change of the initial density with the increase in temperature.

$$\rho(T) = \frac{m_i - m_i * \% \text{ mass loss } (T)}{v_i - v_i * \% \text{ contraction } (T)} \quad (22)$$

The density found from the data NIST is presented in Figure 12.

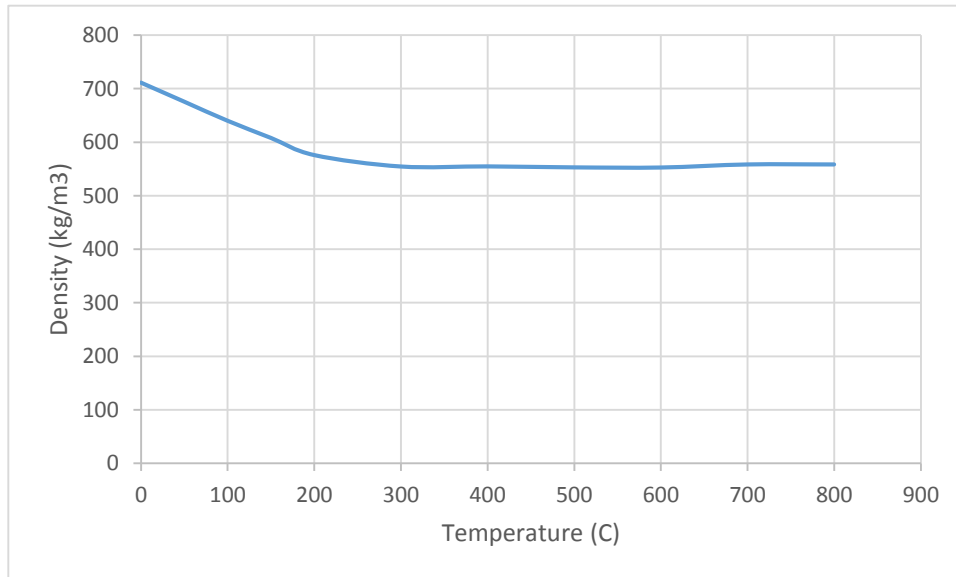


Figure 12: Change of density of gypsum type X

## 5.2 Thermal properties of insulation

In fire barriers, insulation can be used to delay the temperature rise on the unexposed side of the structure this can increase the FRR of the barrier. This study will focus on the use of stone wool and glass fiber wool, which are two insulation materials widely used in steel-framed walls [1].

### 5.2.1 Conductivity

Given sufficient time under heat, some materials undergo physical and chemical changes, which results in bonding reduction of the material and removal of successive thin layers from its surface. This process is referred to as ablation [18]. Ablation causes a reduction of the cross-sectional thickness of insulation material and therefore an increase of the heat flux across the insulation. Finite element programs such as ABAQUS, do not allow the user to simulate the change in thickness of the insulation with time. Therefore, ablation can be taken into account inside the thermal properties of materials. Past researches, simulate the effect of ablation by increasing the values of thermal conductivity with the increase of temperature [19]. Thermal conductivities as a function of temperature with consideration of ablation, can be found by the following equations [19].

Stone wool:

$$k = 0.25 + 0.00009T \quad \text{for } 20^{\circ}\text{C} \leq T \leq 550^{\circ}\text{C} \quad (23)$$

$$k = -1.1385 + 0.0026T \quad \text{for } 550^{\circ}\text{C} \leq T \leq 1200^{\circ}\text{C} \quad (24)$$

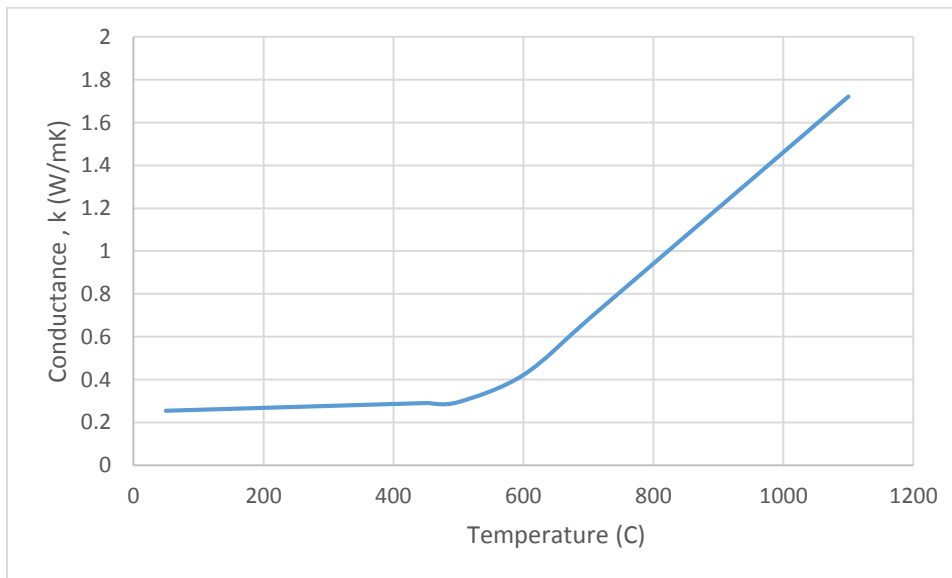


Figure 13: Conductivity of stone wool

Glassfiber:

$$k = 0.5 + 0.0002T \quad \text{for } 20^{\circ}\text{C} \leq T \leq 600^{\circ}\text{C} \quad (25)$$

$$k = -7.8 + 0.014T \quad \text{for } 600^{\circ}\text{C} \leq T \leq 700^{\circ}\text{C} \quad (26)$$

$$k = -0.08T - 54 \quad \text{for } 700^{\circ}\text{C} \leq T \leq 800^{\circ}\text{C} \quad (27)$$

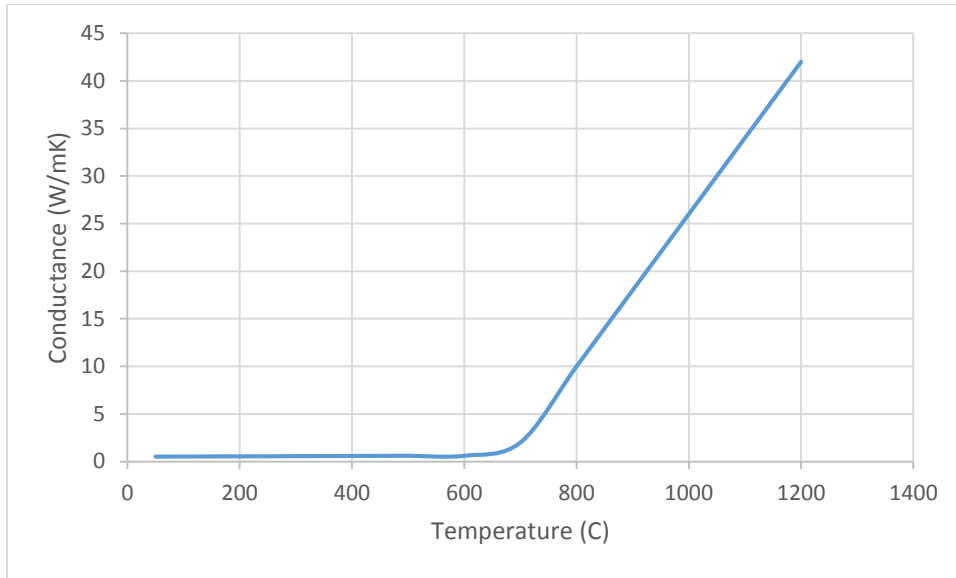


Figure 14: Conductivity of glass fiber wool

### 5.2.2 Thermal capacity

The specific heat of thermal insulation was found from experimental work [19]. This thermal property was reported to fluctuate very little with the increase of temperature [19]. The value of Stone wool and Fiber glass wool found are presented in Table 2.

	Stone wool	Fibre glass wool
<b>Thermal capacity (J/(kg° C)</b>	850	900

Table 2: Thermal capacity of insulation

### 5.2.3 Density

The density for insulation material will be assumed constant with increase of temperature because ablation is already considered in the conductivity parameter. The density used for insulation is presented in Table 3 [19].

	Stone wool	Fibre glass wool
Density (kg/m <sup>3</sup> )	100	35

Table 3: Density of insulation

### 5.3 Thermal properties of steel

In light-weight partitions, construction studs are used for structural purpose. The wall needs to maintain its stability, so studs are used throughout the length of the wall to allow the gypsum board to be mounted. Studs are generally made of wood or steel and for this project the use of steel studs will be investigated. Steel is very poor insulator, therefore it is possible that it will create a thermal bridge through the partition wall. Thermal bridges create a highly conductive parallel path through the insulation layer and allow the heat to pass to the unexposed side of the wall. Since thermal resistance of wall is an important criterion in the furnace test, it is essential that the effect of studs is considered in the models.

#### 5.3.1 Conductivity

The conductivity of steel is temperature dependent and can be found by the following equations [20]:

$$k = 54 - 0.0333T \text{ for } 20^{\circ}\text{C} \leq T \leq 800^{\circ}\text{C} \quad (28)$$

$$k = 27.3 \text{ for } 800^{\circ}\text{C} \leq T \leq 1200^{\circ}\text{C} \quad (29)$$

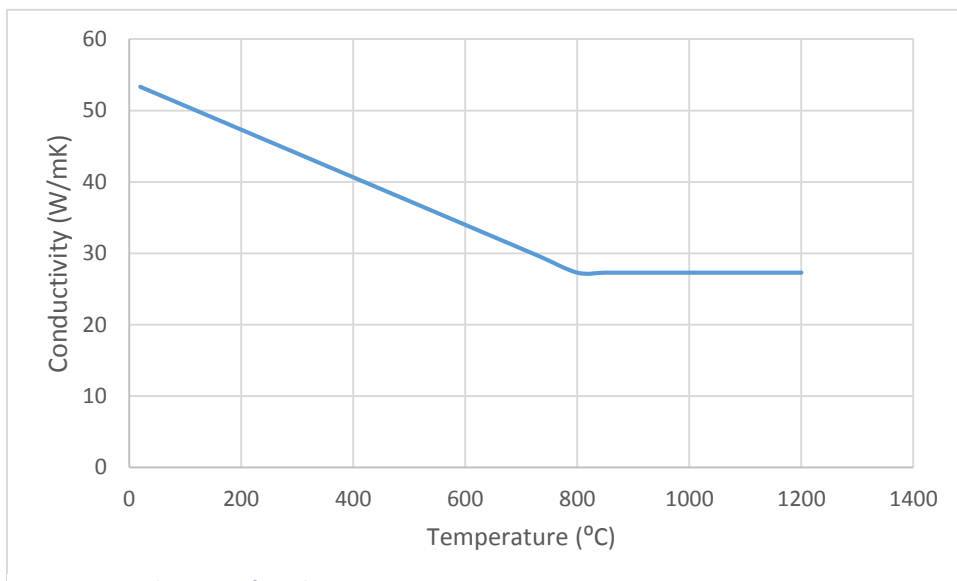


Figure 15: Conductivity of steel

### 5.3.2 Thermal capacity

The specific heat of steel is also temperature dependent and can be found by the following equations [20]:

$$C_p = 425 + 0.773T - 1.69 \times 10^{-3}T^2 + 2.22 \times 10^{-6}T^3 \quad \text{for } 20^\circ\text{C} \leq T \leq 600^\circ\text{C} \quad (30)$$

$$C_p = 666 + \frac{13002}{738-T} \quad \text{for } 600^\circ\text{C} \leq T \leq 735^\circ\text{C} \quad (31)$$

$$C_p = 545 + \frac{17820}{T-731} \quad \text{for } 735^\circ\text{C} \leq T \leq 900^\circ\text{C} \quad (32)$$

$$C_p = 650 \quad \text{for } 900^\circ\text{C} \leq T \leq 1200^\circ\text{C} \quad (33)$$

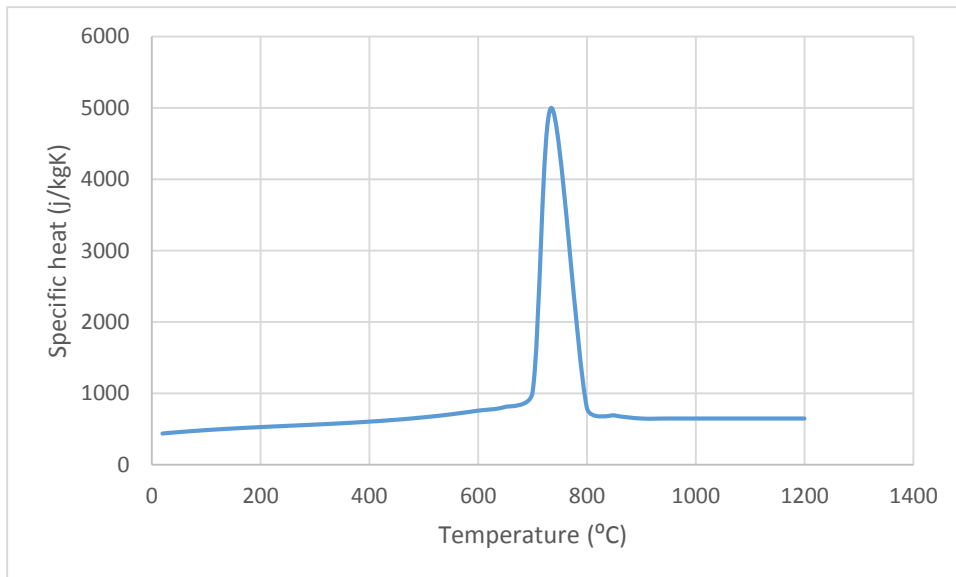


Figure 16: Specific heat of steel

### 5.3.3 Density

The density of steel can be assumed constant with changes in temperature, at  $7850\text{kg/m}^3$ [20].

## 5.4 Thermal property of air cavities

When air is enclosed in cavities of limited size, heat transfer through a partition is caused by radiation and conduction. However, due to air high resistance to heat conduction, the main heat transfer parameter to consider, for cavities, is in the form of radiation [8]. The conductivity of air can be found in different tables and depends on the temperature. At ambient temperature

(20°C) conductivity is found at values around 0,026W/m\*K and for temperature such as 600 °C at around 0.35W/m\*K [21]. The density of air also depends on the temperature and is depicted in Figure 17 [21].The heat transfer by radiation in the cavity is important to consider and it depends on the emissivity of the hot and cold surfaces. The assumed emissivity of the different layer is shown below [22].

Layer	Emissivity
Gypsum	0.8
Insulation	0.8

Table 4: Emissivity of material

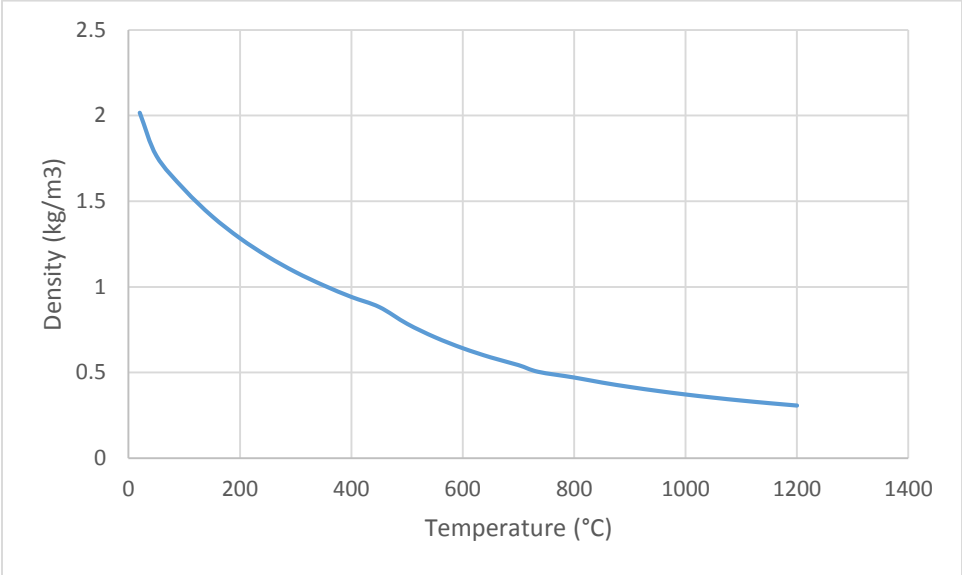


Figure 17: Air density change with temperature

## 6 Methodology

### 6.1 ABAQUS Procedure

The heat transfer which occurs in a furnace test is very complex. To investigate the effect of a reduced thermal insulation on the insulation criterion, it is necessary to have recourse to finite element method. ABAQUS allows to solve transient heat transfer on various type of construction. This can be achieved via defining a transient “Heat transfer” step in the model. The objective of this analysis is to obtain the temperatures on the unexposed side of the wall after the sample is subjected to the ISO-834 standard fire.

#### 6.1.1 Geometry and Material Properties

The geometry of the model is based on the types of construction described in section 0. Figure 18 shows the construction of the light gauge steel frame using ABAQUS.

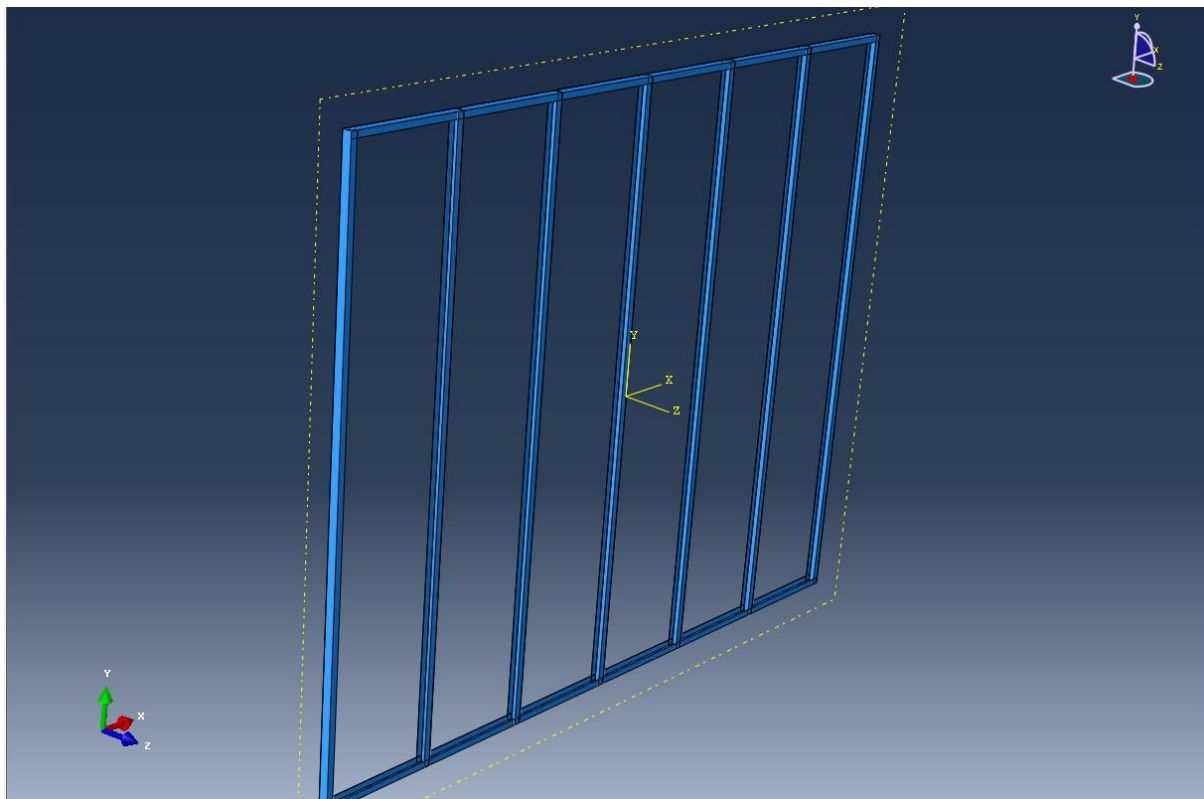


Figure 18: Fire barrier metal frame

The thermal properties of materials used in the model correspond to the one presented in section 5. ABAQUS allows defining thermal properties as function of temperature.

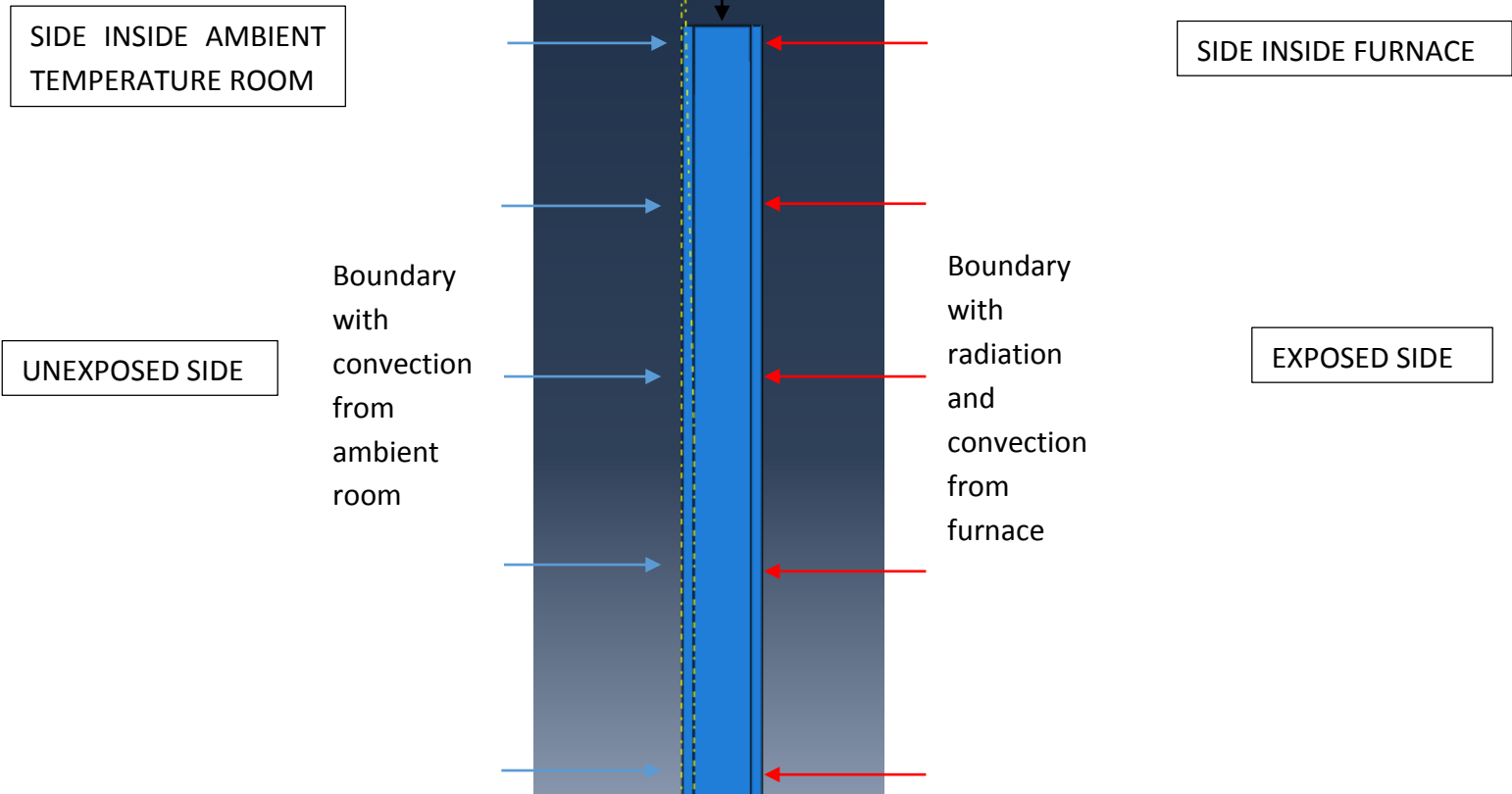
The different scenarios investigated required some changes to the original model. To test the effect of insulation, a layer of insulation filling the whole cavity was created. The insulation was in contact with the two layers of gypsum board. The thermal properties of fiberglass and

stone wool were used. Then, the thickness of the insulation was reduced to 75%, 50% and 25%, while keeping the same cavity depth. This was done to see how the FRR would change if less insulation was used in the construction of the partition, compare to the original tested in the furnace. Also, when the insulation thickness is reduced by half, two models were created. One with the insulation located on the exposed side and one on the unexposed side, this allows seeing the worst case scenario. Then, different sizes of hole in the exposed gypsum board layer were added to the original wall insulated and non-insulated to investigate the effect of breaches in the gypsum layer located in the furnace. The holes dimension used were a large hole of 50mm radius and a small hole of 10mm radius. Also, partitions with hole through were modeled to investigate the effect of penetration in fire-rated partition. Again two holes were used, one large hole of 50mm radius and one small hole 10mm radius. Finally, to investigate what would happen if at one specific location insulation would be missing, two partitions insulated with stone wool were modeled with missing piece of insulation. Round missing pieces were used of 100mm and 50mm radius. The dimension of the different features used is assumed. Indeed, other size could have been used and investigate, however it is more probable that small holes and small missing pieces of insulation will go unnoticed compare to bigger one.

### **6.1.2 Initial and Boundary Conditions**

The initial temperature of the boards was assumed to be uniform and equal to 20°C. Convection and radiation boundary conditions were defined for the surface of the wall located inside the furnace while only convection boundary conditions were defined for the surfaces of the wall outside the furnace. The boundary conditions were set using 'Interactions'. The interaction types, used for convection and radiation boundary conditions, were 'Surface film condition' and 'Surface radiation to ambient', respectively. The gypsum board on the furnace side was exposed to the standard fire temperature, and the gypsum board on the room side was exposed to a constant temperature of 20°C. The effective emissivity from the fire at the exposed surfaces was set to 0.8 [10]. The convection heat transfer coefficients were assigned according to European code on fire interaction with structures [31], i.e. 4 W/m<sup>2</sup>K for the unexposed surface and 25 W/m<sup>2</sup>K for the exposed surface. The other surfaces, which were located inside the temporary construction, are considered fully insulated since in actual test a great amount of insulation must be used to prevent the wall from leaking via the supporting construction.

Perfectly insulated boundary



To investigate if the boundary conditions used in ABAQUS are appropriate, another simulation was performed. In this simulation the surface of the wall inside the furnace is exposed to the experimental heat flux given in section 2.4. Temperatures on the unexposed and exposed gypsum surfaces of the wall were measured. The following figures show the difference between the temperatures obtained using the two methods.

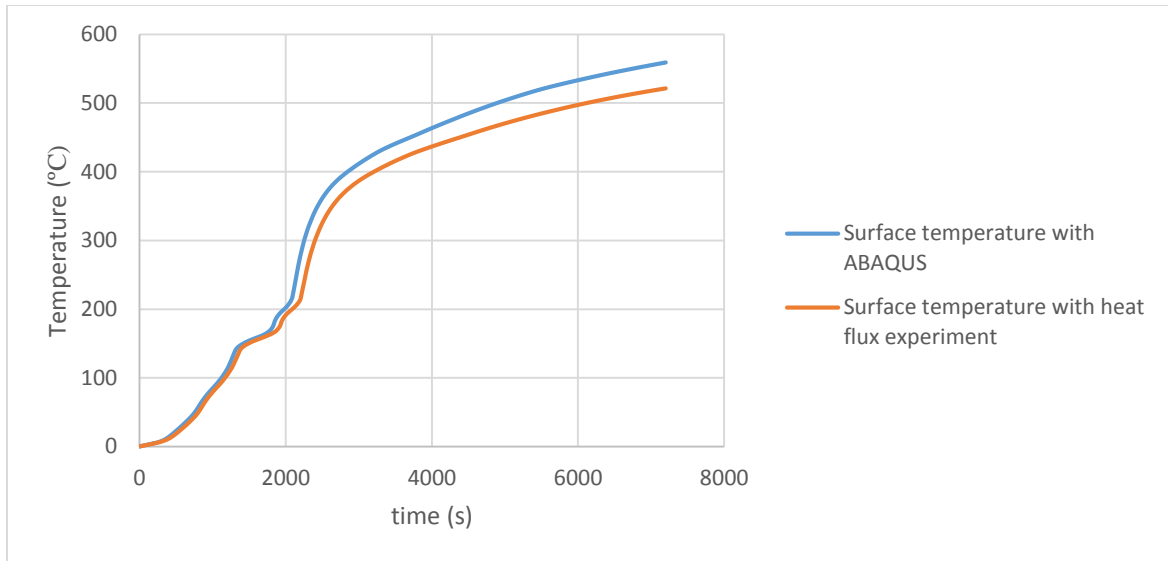


Figure 19: Unexposed surface temperature

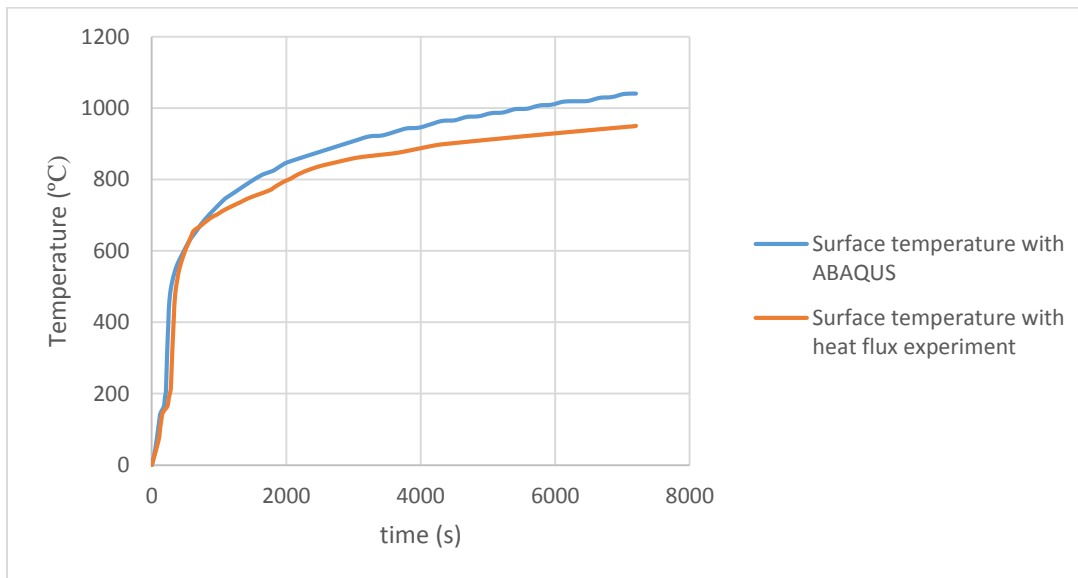


Figure 20: Exposed surface temperature

As we can see from the figures above, the modelling method used in the simulation gives slightly higher exposure temperature, but still quite similar. Therefore, the results should be considered to be conservative, especially since it is known that the ASTM E119 is also slightly more strict than the ISO 834 [12].

### 6.1.3 Interactions and assumptions

To accurately model the heat transfer inside the wall from the unexposed to the exposed surface different assumption were used. ABAQUS calculates heat transfer inside a building element with its thermal properties and conduction equation. In the model it was assumed that

the surface between different components of the wall in contact were at the same temperature. This was set using TIE interaction.

The cavity radiation was modeled with the interaction, SURFACE CAVITY RADIATION, for every scenario where a space inside the wall was not filled with insulation. ABAQUS estimate the heat transfer by radiation, in cavities, from the equation (37). The temperature and emissivity values come from the surfaces inside the cavity and F is the view factor which depends on the distance between the surfaces.

$$q''_{Cavity\ Radiation} = F\varepsilon\sigma(T_{S1}^4 - T_{S2}^4) \quad (37)$$

The conduction through air was modeled using the SURFACE TO SURFACE conduction interaction. This defines conduction between two surfaces by using the defined thermal conductivity only. This was used for every scenario where air cavity was present. Since the main heat transfer mode at elevated temperature when a cavity is present is radiation, it was assumed that the cavity do not heat up, but conduct heat through radiation and conduction. This allowed for simpler model and was the most conservative scenario. All the thermal properties defined in the section 5 were used.

#### **6.1.4 Mesh and Element Type**

For the heat transfer analysis, a standard heat transfer element type is chosen. In the ABAQUS there is no advantage in using higher order of elements than four node linear quadrilateral element, DC3D8 [30]. The number of elements is an important parameter to consider as the precision of the results will be greatly affected by this factor. The grid size across the thickness is not relevant since only the temperature at the surface is analyzed. To choose the optimum element size on the surface, a sensitivity study has been performed. For the analysis, the wall, insulated with stone wool, was selected with the following different mesh sizes:

Case a) mesh size: 0.1 m

Case b) mesh size: 0.05mm

Case c) mesh size: 0.03mm

The following figures show the difference between different grid sizes. It can be observed that the maximum temperature measured on the surface is seen from the case B (Figure 22) and does not change in case C, therefore it is not required to run simulation with a finer grid.

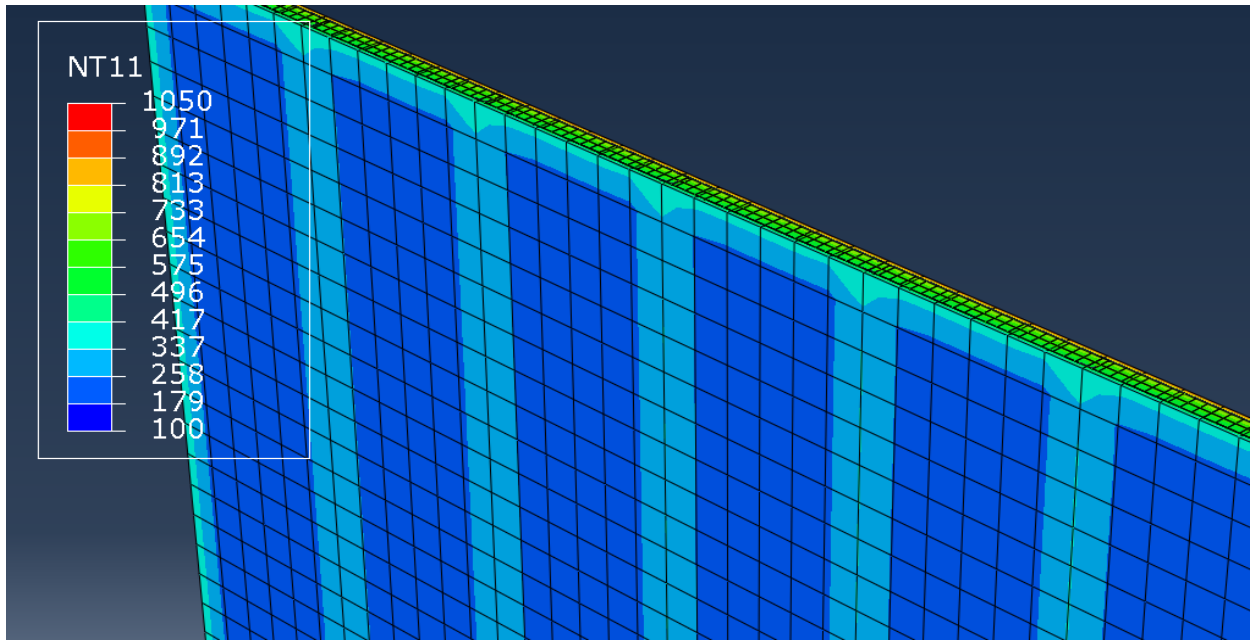


Figure 21: Temperature at the unexposed surface case a)

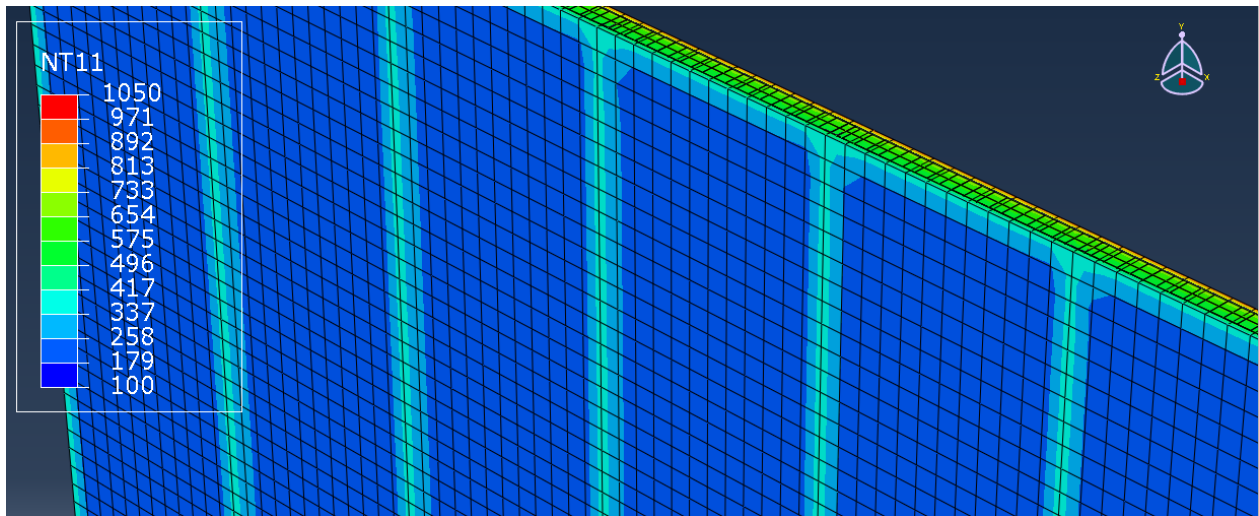


Figure 22: Temperature at the unexposed surface case b)

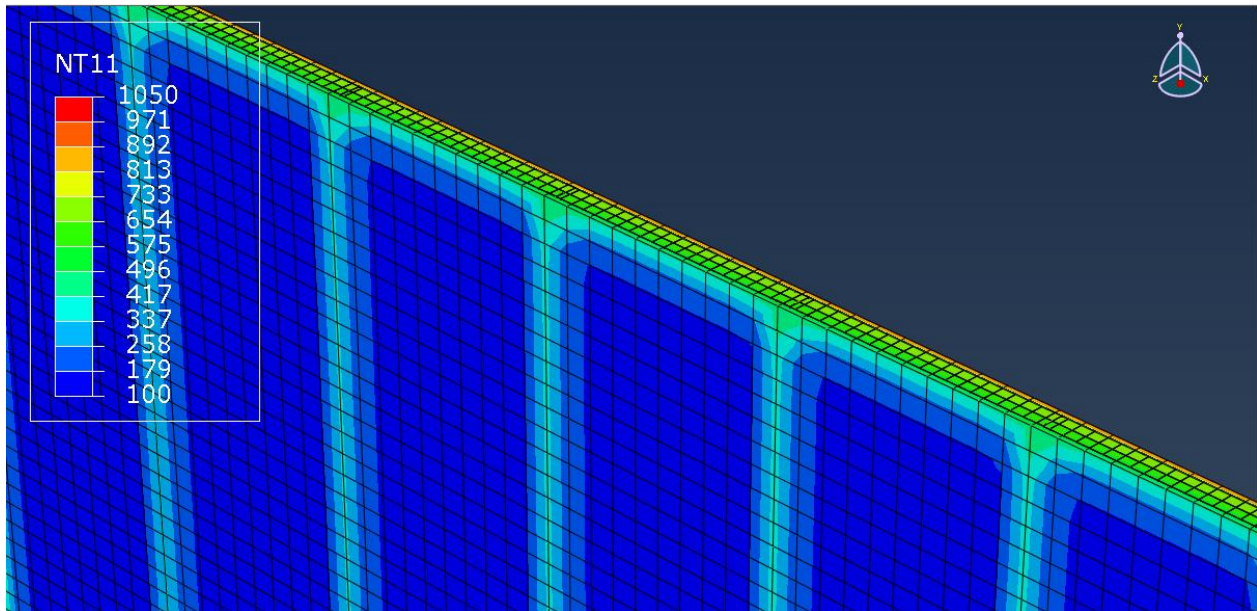


Figure 23: Temperature at the unexposed surface case c)

## 6.2 Validation of the FE model

The literature review allowed to find different experimental data on the FRR of LSF when tested in a furnace test based on codes. The literature review focused on LSF construction with the use of stone wool, fiber wool insulation and empty cavity. The FRR obtained for different test samples were compared with the results obtained with numerical model built with ABAQUS. A model, corresponding to each experimental sample, was produced in order to validate the modeling technique used in ABAQUS. Table 5 depicts the results obtained for the numerical model and the experimental data as well as the relative error of the numerical model. Some experimental FRR were given with respect to the criterion where the average temperature increased above the initial temperature by more than 140°C ( $T_{140}$ ). Other used the criterion where an increase at any location (including the roving thermocouple) above the initial average temperature was more than 180°C ( $T_{180}$ ). The information about the thickness of gypsum and insulation and the type of insulation used is given in Table 5. However, for every simulation the thermal properties used were similar to ones presented in section 5.

For example the assembly: 1 x 2 - 15.9mm gypsum 90mm air cavity, can be interpret as 1 layer of 15.9mm gypsum board exposed in the furnace – 2 layers of 15.9mm gypsum board on the cold side – Steel studs of 90mm width – Wall cavity 90mm width non insulated.

Type of assembly	Experimental test			ABAQUS	
	FRR (min)	Criterion	REF	FRR (min)	Relative error
<b>1 x 1 - 9.5mm gypsum + 50mm Stone wool insulation</b>	42, 41	T <sub>180</sub>	[32]	45	+8%
<b>1 x 1 - 12.5mm gypsum 50mm air cavity</b>	38, 33, 34, 33, 36, 36	T <sub>180</sub>	[32]	31	-11%
<b>2 x 2 - 12.5mm gypsum 50mm air cavity</b>	78, 77, 89, 91	T <sub>180</sub>	[32]	89	+6%
<b>2 x 2 - 15.9mm gypsum 90mm air cavity</b>	52 min	T <sub>140</sub>	[33]	37	-28%
<b>1 x 2 - 15.9mm gypsum 90mm air cavity</b>	66 min	T <sub>140</sub>	[33]	78	+20%

*Table 5: Experimental and simulation results*

The Table 5 shows the results of the validation test with ABAQUS. It is possible to see that the relative error obtained is generally low, ranging from 6 to 28%. The Wall with an empty cavity yields good results if compared to the data taken from the passive fire safety document from Ghent University [32]. When the model is compared with the results of SULTAN [33], the findings seems to be more confusing. The error could come from the different standard used in the experimental test, different material properties or the testing methods. However, results in the range of 6-28% are deemed acceptable considering that experiment results can differ by as much as 15% and maybe more.

### 6.3 FDS Procedure

To investigate the effect of leakage on the integrity criterion a furnace test is reproduced using the CFD tool FDS. For this purpose, the wall furnaces of the NRCC, was reproduced as precisely as possible with FDS, see Figure 24, from data [23], [11]. However, due to lack of information available, assumptions were needed. Also, the furnace was modeled to cope with the requirement of the European standard EN-1301-6, not the ASTM E119. This means that the ISO-834 temperature-time curve was used in the simulation. All parameters, assumptions and dimensions used to replicate the furnace test with FDS will be presented in this section.

#### 6.3.1 Dimensions and materials

The furnace dimensions are 3600 mm wide by 3100 mm high by 600 mm deep. The furnace walls were lined with 38-mm-thick fibrous ceramic blanket. The overall dimensions of the sample were 3600 mm wide by 3100 mm high. The fire barrier sample used correspond to the type B construction, presented in section 4. To simulate the integrity criterion, a cotton pad was modeled and positioned in front of the leakage area. The thermal properties presented in section 5 were used for all material related to the fire-rated barrier. For the thermal properties of the ceramic blanket, data from the work of Sultan [11] were used. For the cotton pad generic thermal properties were used from engineering toolbox [24], [25], [26]. The properties of the cotton pad and the ceramic blanket are presented in Table 6. The Temperature of ignition of the cotton pad was assumed to be at 400 °C as experimental results shows [12].

	<b>Ceramic fibre blanket</b>	<b>Cotton Pad</b>
<b>Thermal conductivity (W/mK)</b>	0.04	0.23
<b>Specific heat (J/kgK)</b>	1150	1339
<b>Density (kgm<sup>3</sup>)</b>	160	150

Table 6: Thermal properties of ceramic blanket

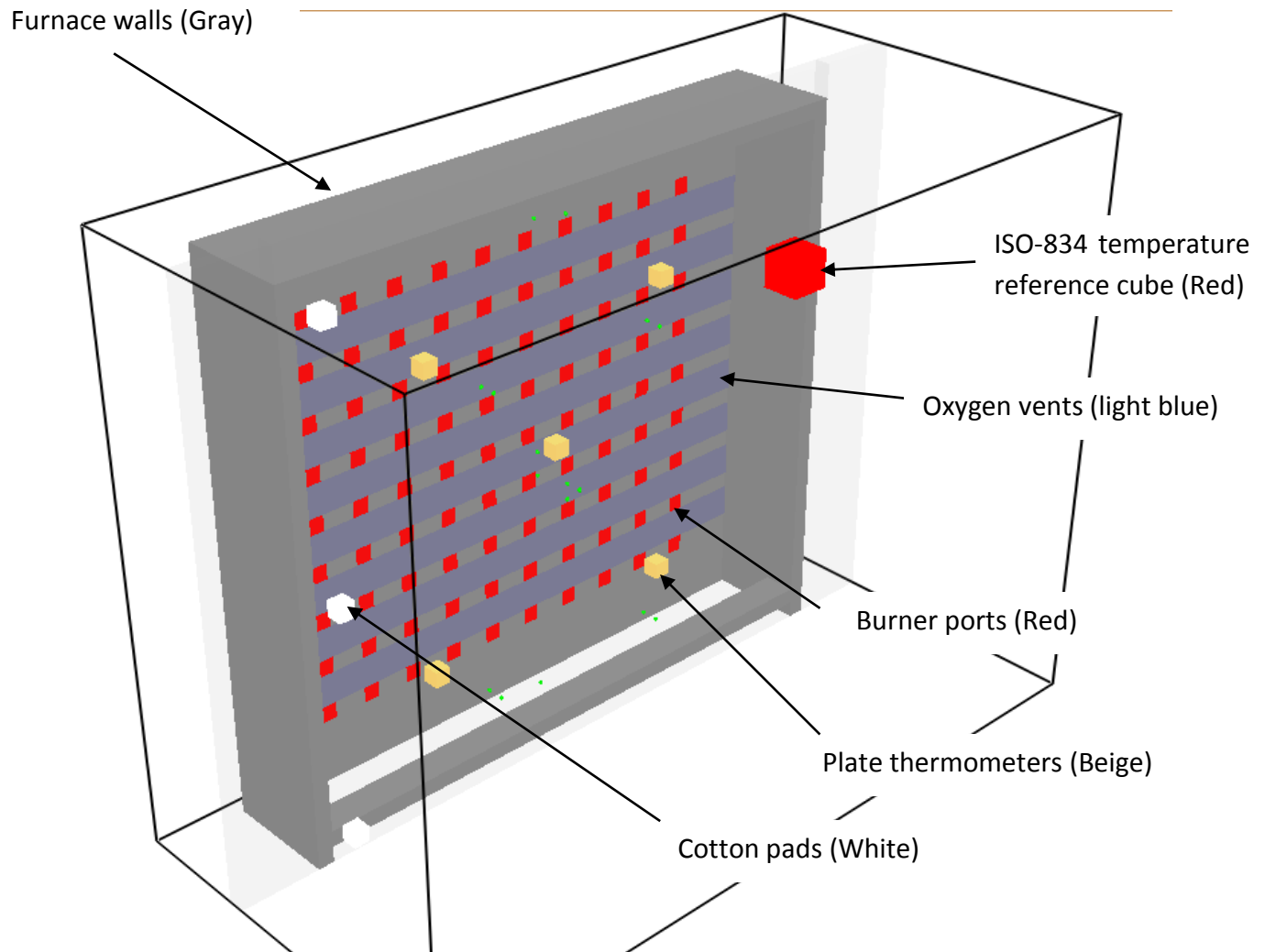


Figure 24: Furnace modeled with FDS

### 6.3.2 Temperature

Furnaces use premix air and gas burners, using different types of combustible, in order to heat up the space at the required temperature. The NRCC wall furnace, which was used as model and validation (section 2.4), has 90 propane burner ports. Those were implemented in the model as 90 vents of one grid size area with a set HRRPUA. Propane was used as fuel with the properties presented in Table 7 [27], [28]. One issues with FDS is that it is not possible to simulate pre-mixed air-fuel burners. In order to overcome this issue vents were added close to the burner ports from which air is introduced inside the furnace. Those vent are controlled, in FDS, to keep the oxygen level between 15 and 20 %. The air is introduced inside the furnace at the temperature of the ISO-834 temperature time curve, in order to reduce the extra heat necessary to warm the new air. Another major issue when it comes to modelling a fire resistance test with FDS, is to keep temperature in the furnace within the range required by the code. This was done by setting up a control system which open or close burner ports depending on the temperature inside the

furnace. The temperature is measured with plate thermometer modelled as required by the standard [2]. The plate thermometers temperature is compared to a 1 cell thick reference cube at the temperature of the standard fire. The burner ports were associated to the local plate thermometer and the ports closed if the plate thermometer temperature exceeded the reference cube's temperature and opened if the plate thermometer temperature was less than the reference cube's temperature.

Fuel	Radiative fraction (%)	Heat of combustion, $\Delta H_c$ (kJ/kg)	Soot Yield (kg/kg)
Propane	0.3	46450	0.01

Table 7: Properties of propane

### 6.3.3 Pressure

As shown in the literature review, pressure difference is very important when it comes to leakage between two compartments. Therefore, it was necessary to measure and control the pressure inside the furnace in order to keep it inside the required boundaries. The code EN-1301-6 requires that the neutral plane inside the furnace should be located 0.50 m above the bottom of the test sample and that the pressures at the top of the test sample should not exceed 20 Pa. However, other experts suggested that the neutral plane in furnace test should be maintained at the bottom of the test specimen and that the pressure in the furnace is more representative of the pressure exerted by a real fire [12]. This was estimated at 28 Pascal in section 3.3. Because of the complexity required to move the neutral plane and to keep the pressure at 20 Pascal, in FDS, the boundaries selected, for pressure at the top of the furnace, was set between 28 and 30 Pascal. Indeed, the extra air inserted inside the furnace to fix the pre-mixed burner problem, caused an increase of the internal pressure of the furnace. This made it hard to keep the pressure, inside the furnace, at 20 or even 30 Pascal. To minimize the pressure at the top of the furnace, a vent at the bottom of the furnace and a controlled vent at the top of the furnace were created. The controlled vent opened if pressure increased more than 30 Pascal and closes when pressure passed under 28 Pascal.

### 6.3.4 Leakage

There are different ways to model leakage with FDS, but since the leakage area is usually very small it was not possible to define a leak directly on the numerical mesh. A better way to handle leakage was by exploiting the HVAC model of FDS. With this feature, leakage can be presented as a large HVAC vent that connects via a very small duct linking both sides of the wall. This allows for the leakage area to be distributed over the vent area. Leakage in the simulations was modeled in three ways, with the area of leakage distributed over all the joints of the wall, over only one joint or localized in a small area. To do this, the vent area was distributed as

presented in the Figure 25, Figure 26 and Figure 27. Where blue color represent the location of the leakage through the wall.

Failure of integrity was investigated for different location on the sample: at the top, at the bottom and in the middle of the furnace. The volume flow, through a leak of certain area is given by a form of the equation (16), with the friction flow coefficient assumed to be 1 [27].

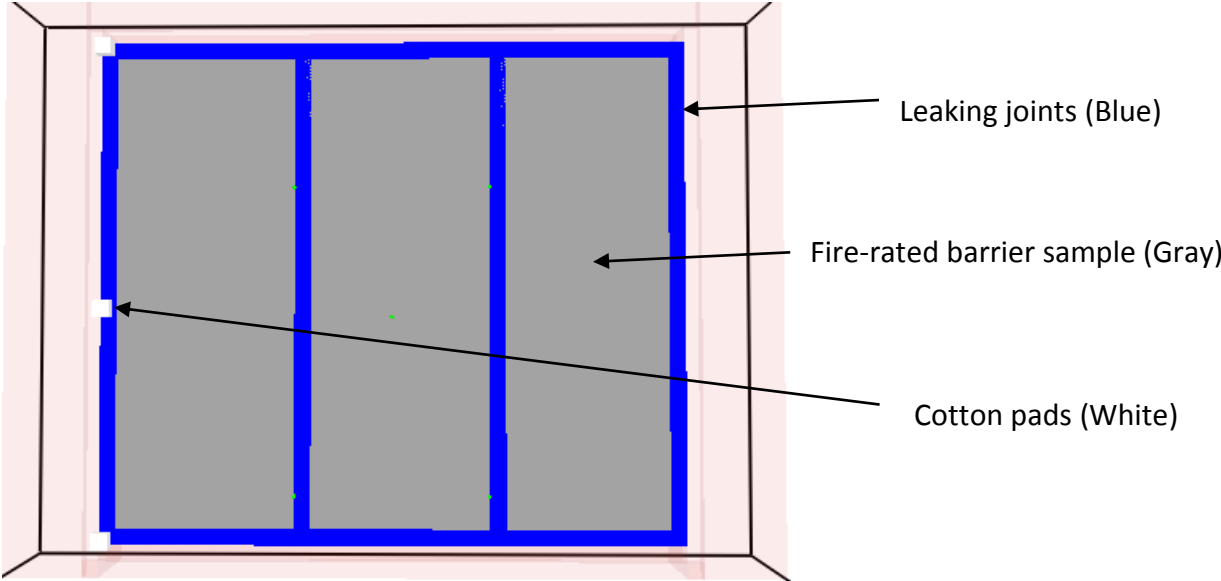


Figure 25: Leakage distributed at every joints

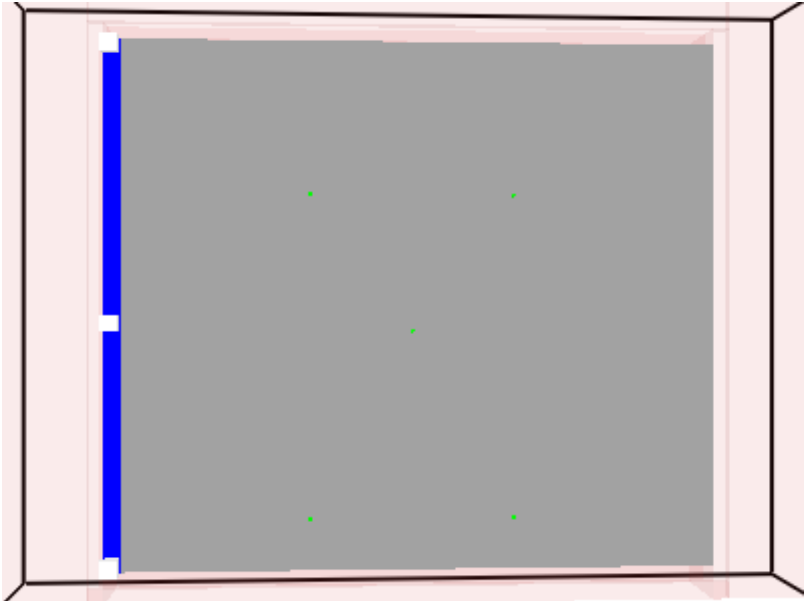


Figure 26: Leakage distributed on one side

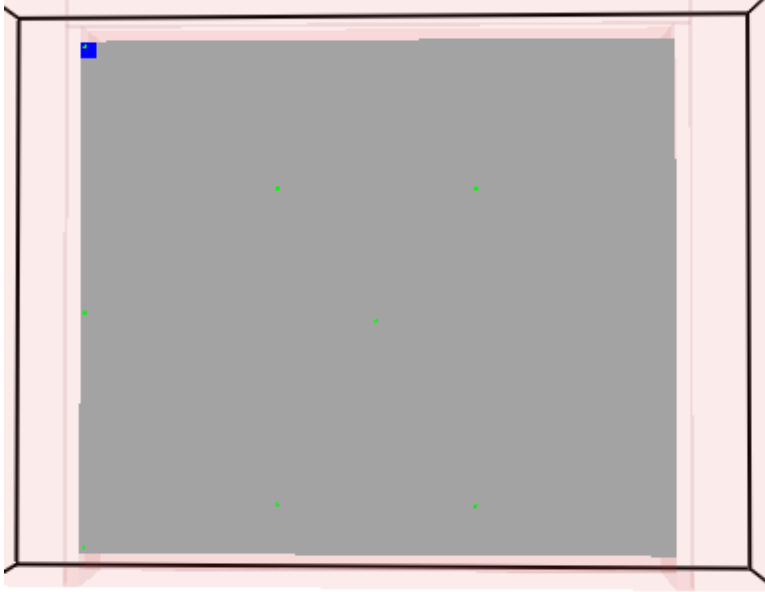


Figure 27: Leakage localized at the top

### 6.3.5 Grid selection

The duration of the fire resistance test is 7200 seconds, consequently the computational time for every simulation to be high. To decrease this time, a coarse grid was applied. However, this had an impact on the precision of the results due to increased averaging. For simulations involving buoyant plumes, a measure of how well the flow field is resolved can be used [27]. Even though, a perfect buoyant plume is not exactly used this method shall be used as a gauge to verify the grid size. This method use the characteristic fire parameter calculated with the following equation:

$$D^* = \left( \frac{\dot{Q}_{Fire}}{\rho_{\infty} c p_{\infty} T_{\infty} \sqrt{g}} \right)^{\frac{2}{5}} \quad (34)$$

Then the characteristic fire parameter shall be compared with the grid size ( $dx$ ):

$$\frac{D^*}{dx} \quad (35)$$

The U.S. Nuclear Regulatory Commission used a range of  $4 \leq \frac{D^*}{dx} \leq 16$  for their validation studies [29] and Danish best practice use  $10 \leq \frac{D^*}{dx}$ . In the simulation the HRR increases and reaches a peak located around 5500 kW, for a grid size of 100 cm, this yield  $\frac{D^*}{dx} \sim 19$ , which is over the range required by the U.S. Nuclear Regulatory Commission and as required by the Danish best practice.

## 6.4 Validation of the CFD model

In this project the furnace model will be validated against the code EN 1363-1 and experimental data. EN 1363-1 regulates how and what should be done during the furnace test so that the fire resistance test is deemed valid. Also, the heat flux at the boundary of the sample from the furnace will be compared to experimental data corresponding to the similar furnace.

### 6.4.1 Furnace Temperature

The Heating curve inside the furnace shall be controlled so that the average temperature of the furnace derived from the thermocouples follows the following relationship:

$$T = 345 \log_{10}(8t + 10) + 20 \quad (36)$$

Where

T - is the average furnace temperature, in degree Celsius;

t - is the time, in minutes.

The code stipulates that the percentage deviation in the area of the curve of the average temperature recorded by the specified furnace thermocouples versus time from the area of the standard temperature/time curve shall be [2]:

15%	<i>for</i> $5 < t \leq 10 \text{ min}$
$(15 - 0.5(t - 10))\%$	<i>for</i> $10 < t \leq 30 \text{ min}$
$(5 - 0.083(t - 30))\%$	<i>for</i> $30 < t \leq 60 \text{ min}$
2.5%	<i>for</i> $t > 60 \text{ min}$

The Temperature inside the furnace according to the code EN 1363-1 is presented in Figure 28.

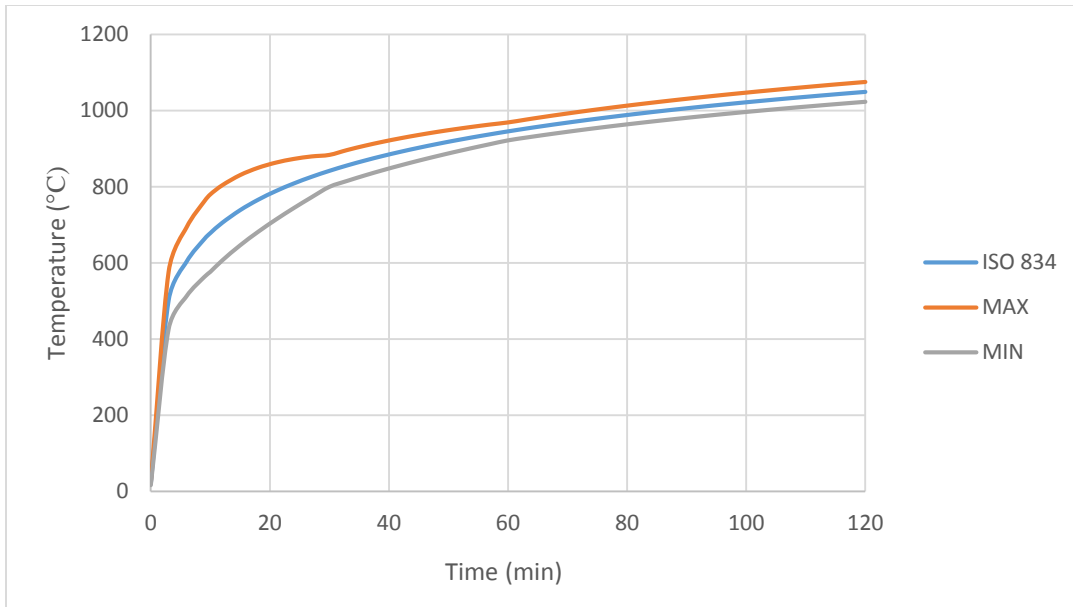


Figure 28: Acceptable temperature in the furnace according to EN 1363-1

The average temperature measured inside the FDS furnace by the plate thermometers is shown in the following graph. It is possible to see that the temperature follows the requirement of the code. The plate thermometers used are located as presented in Figure 31. It is possible to see that the temperature is within the requirement of the code.

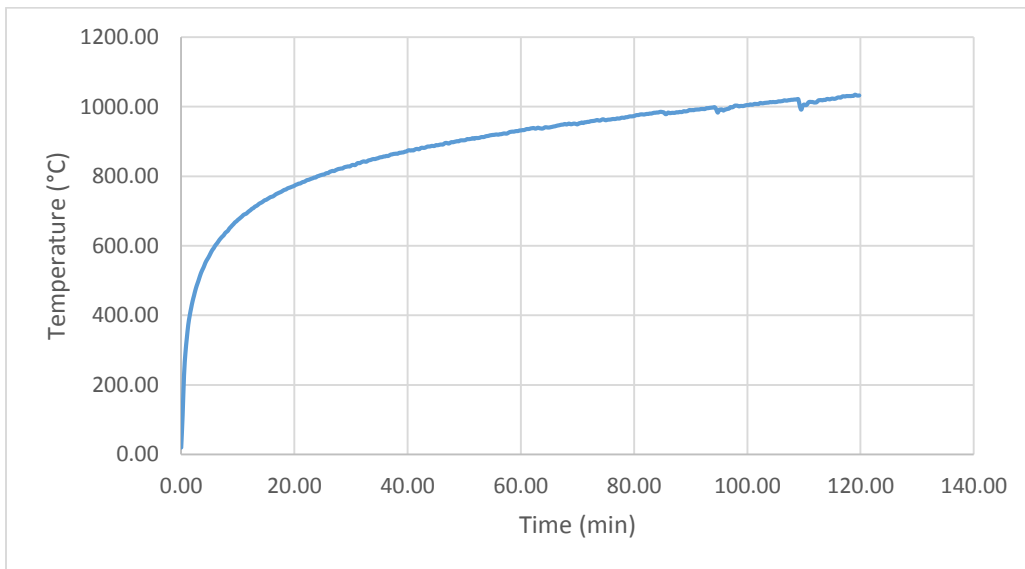


Figure 29: Average temperature versus time measured on the surface of the wall sample in FDS

### 6.4.2 Furnace pressure distribution

As mentioned in section 6.3.3, the pressure at the top of the furnace needs to stay at approx. 30 Pascal. The figure below shows the average pressure measure at the top and in the middle of the furnace.

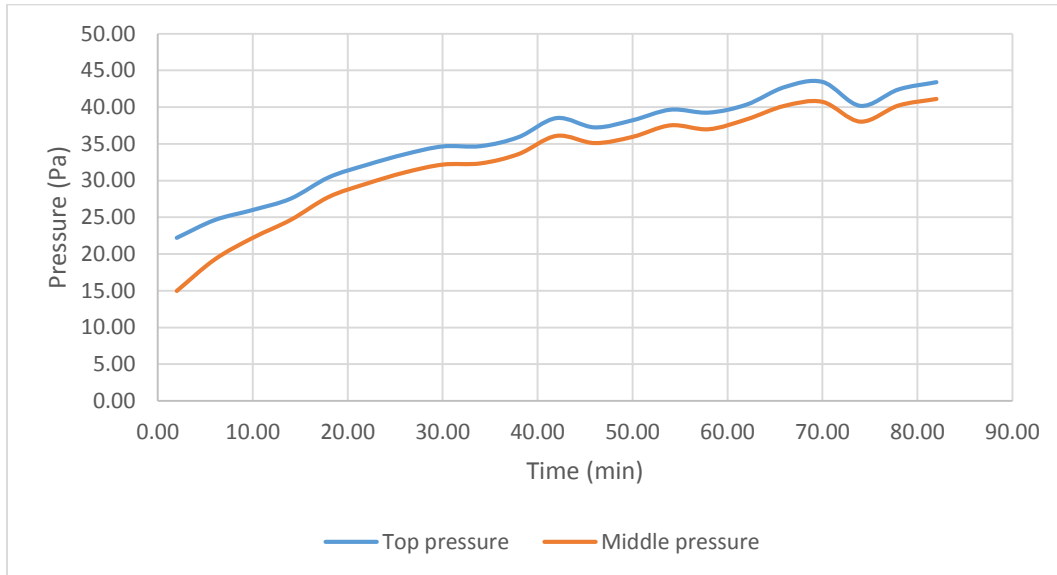


Figure 30: Pressure profile in the FDS simulation

It is possible to see that the pressure is slightly over the expected 30 Pascal so this will cause the volume flow of hot gases through the partition to increase. The impact of this pressure difference will be discussed further in the results section.

### 6.4.3 Heat Flux at sample

The total heat flux from a furnace to a sample, presented in section 2.4, will be compared to the one obtained during the simulation. The heat flux is measured by 5 gauge heat flux devices, similar to the one used in the experiment. These are located at the surface of the sample in FDS as seen Figure 31 [11]. The heat flux measured is presented in the Figure 32.

It is possible to see in the graphs that the average heat flux measured in FDS is comparable to the one obtained by SULTAN, presented in Figure 3. Although the heat flux measured in FDS is slightly higher, an increase of 10% in the heat flux was noticed.

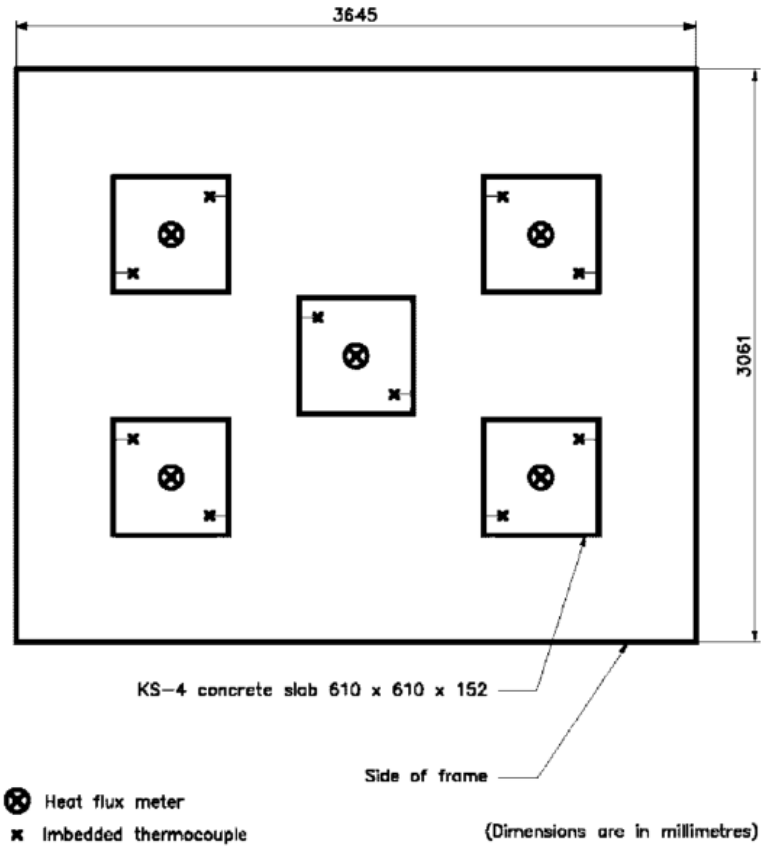


Figure 31: Distribution of the heat flux gauge (reproduced with the permission of the National Research Council of Canada)

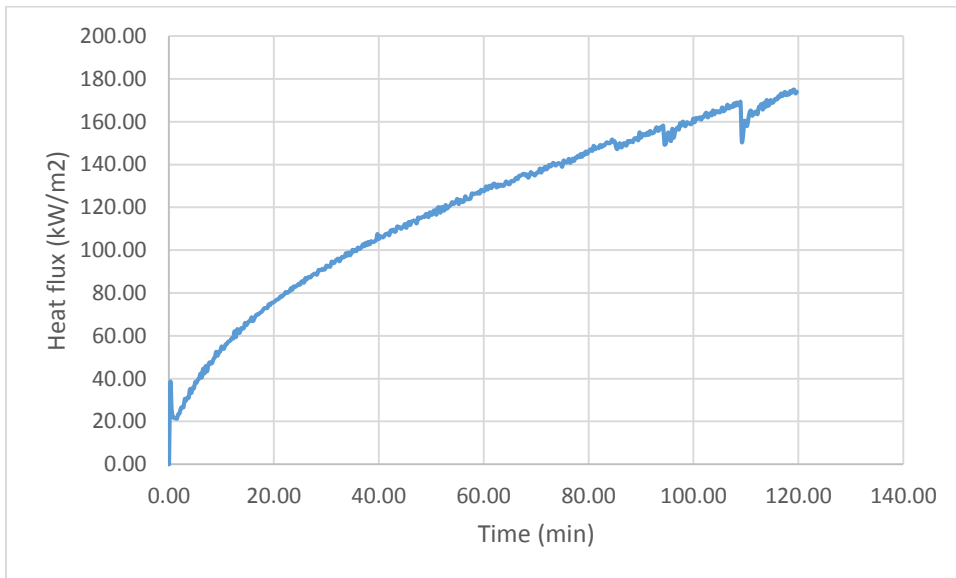


Figure 32: Heat flux at the surface of the sample in the furnace

## 7 Results and discussion

First, the results obtained from the simulations made with ABAQUS will be presented for the two type of construction and the following scenario:

- The type of insulation (Stone wool, Fiber glass wool) and uninsulated
- Reduced amount of insulation with stone wool insulation (Full depth (50mm), three quarter, half and quarter) using the same cavity depth 50mm
- When the insulation is reduced by half, the impact of the location of the insulation (exposed versus unexposed side) for the partition type A only
- Hole in the gypsum board at the exposed surface of the barrier insulated with stone wool, fiberglass wool and without insulation (Large hole 50mm radius against small hole 10mm radius).
- Hole through the fire barrier, with stone wool insulation, type A only (Large hole 50mm radius against small hole 10mm radius).
- Missing portion of stone wool insulation of different size for the partition of type B only (Large portion 100mm radius against small portion 50mm radius).

The failure criterion considered for the different partition depends on the scenario. The scenario, which leads to higher temperatures at specific locations, is considered to fail based on the criterion T180 (Holes through, holes on one side, missing portion of insulation). Other scenarios with a more uniform unexposed surface, temperature used the failure criterion T140 (reduced insulation, type of insulation).

Secondly, the results obtained from FDS concerning the integrity tests are going to be introduced. Since it is not possible to reproduce the gap gauge test, all the leakage areas were distributed over a surface limiting the width of the crack to 6mm (distributed leakage) or 25mm (localized leakage). Failure was considered once the temperature inside the cotton pad, located in front of the leakage area, reached the ignition temperature of 400 °C as obtained in experiment[12]. The scenarios considered are the following:

- Leakage localized on the surface of one cell, see Figure 27. This represents the effect of small breach or hole through the partition.
- Leakage area distributed on one side of the wall as presented in Figure 26. This represents the scenario where the sealing of the partition was not done properly at one specific location.

- Leakage area distributed over all joints of the construction, see Figure 25. This is to investigate the effect of an improper sealing work of all the joints of the partition.

## 7.1 Construction Type A

### 7.1.1 Impact of the choice of insulation material

The maximum temperature found on unexposed side of the fire resisting barrier is shown in the Figure 33 for the partitions filled with different type of insulation or empty.

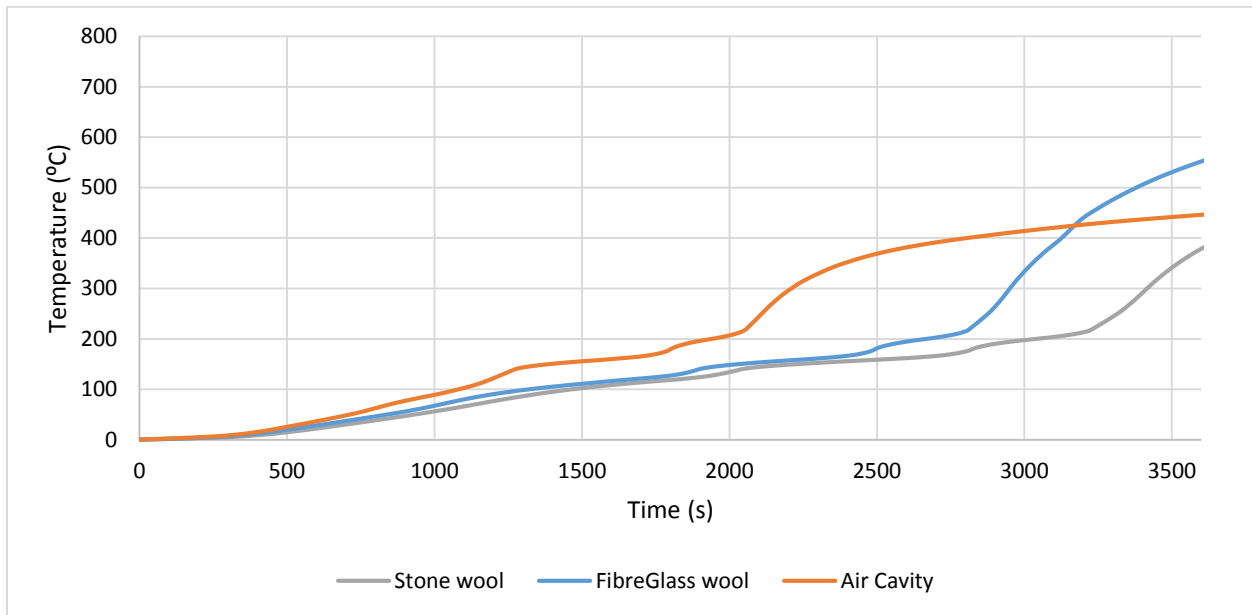


Figure 33: Temperature at the unexposed layer of the Wall with different types of insulation or without insulation

The first thing that should be noticed is that the three walls do not perform as expected. Because the FRR for all three constructions was supposed to be 60 minutes, but the temperature  $T_{180}$  was exceeded for all cases before this time, see Figure 35. Of course, the models could have been altered in order to obtain the rating specified by the manufacturer. However, it was decided to keep the method presented in section 6.1 and used in the validation section 6.1.4. The difference in the FRR obtained with ABAQUS could be explained by different properties of material or simply by the modeling method since the validation section showed error in the range of 30%. It does show however that the fire-rated barrier should not perform much more than 60 minutes in reality.

It can be observed that the wall with insulation yields better results compare to the wall without insulation in term of FRR, see also Figure 35. However, after 60min the temperature is higher for fiber glass insulation compare to an empty partition, this is due to two factors. First, as the temperature increases, the properties of fiber glass wool insulation falls, leading to higher

heat transfer by conduction as seen in section 5. Second, the heat transfer by radiation inside the empty cavity decreases, as the temperature of the gypsum layer on the cold side increases.

Also, the previous graph shows that Stone and fiber glass wool give comparable temperature until around 2500 seconds, at this point ablation of fiber glass wool causes the partition temperature to rise. Figure 35 depicts the FRR found for the different cases. The critical temperature was observed at the steel studs location for stone wool insulation (see Figure 40) and at the center point between each studs for fiber glass wool (see Figure 37). This is explained by the difference between the thermal conductivity of insulation material and steel. At high temperature the fiber glass wool conducts more heat than steel, due to ablation.

The Stone wool insulation gives the best result being able to resist 70% of the 60min expected. However, fiber glass wool and the partition without insulation are able to provide fire resistance only 62% and 55% respectively, of the expected 60min rating. Figure 34 shows the propagation of heat inside the different type of insulation after 60 min. In order the cross section are: air cavity, stone wool and fiber glass wool.

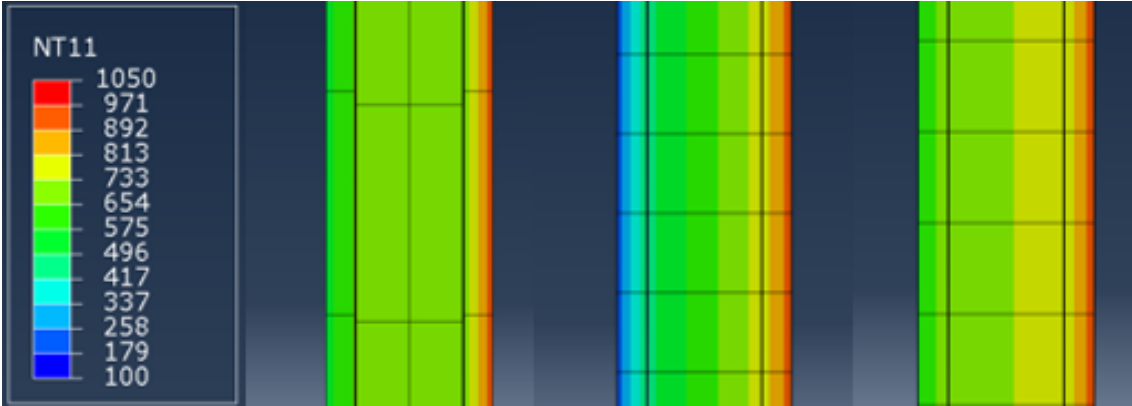


Figure 34: Temperature inside cross section of walls

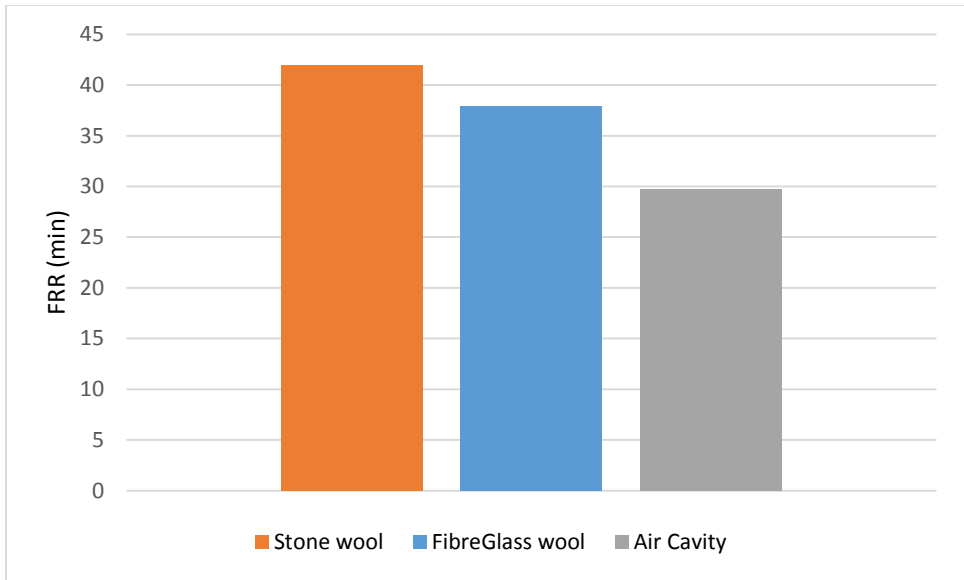


Figure 35: FRR of each walls insulated or uninsulated

One important impact of the insulation material, as it is possible to observe in Figure 34 and Figure 36, is the difference of temperature in the exposed gypsum layers. Due to insulation material, which slows down the heat transfer through the cross section of the wall, the temperature on the inside face of the exposed gypsum layer is increased, as seen below.

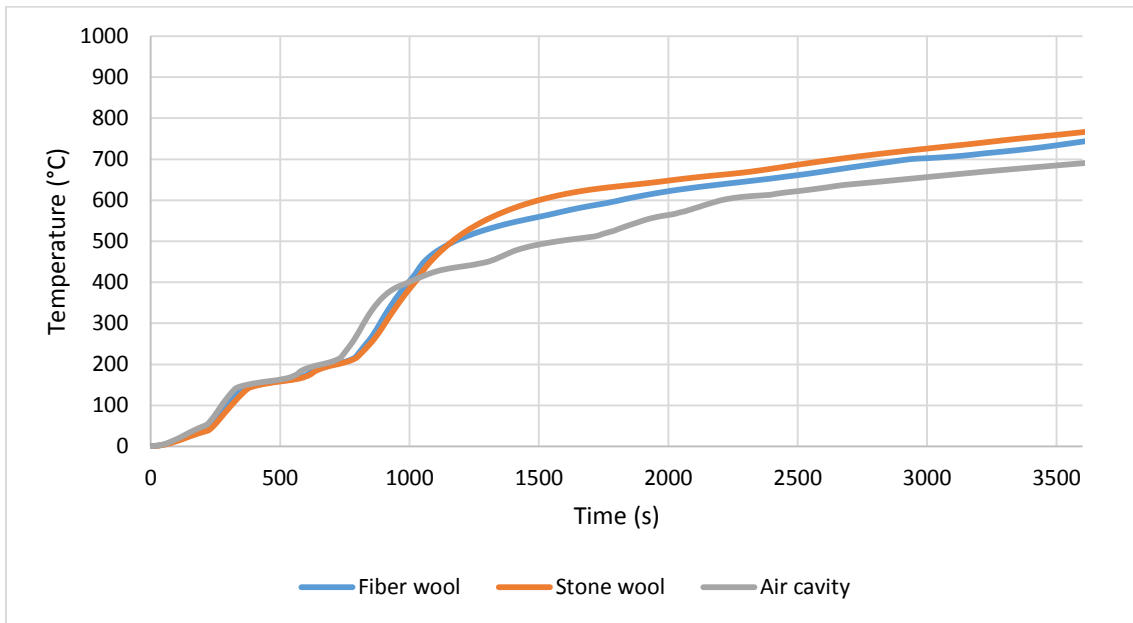


Figure 36: Temperature of the exposed side gypsum layer

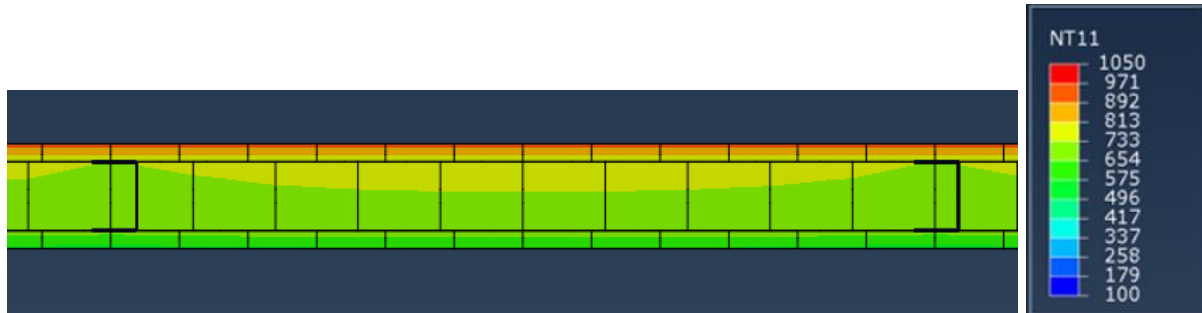


Figure 37: Cross section a partition filled with fiber glass wool, after 60min

### 7.1.2 Impact of reduced amount of insulation

The maximum temperature found on unexposed side of the fire barrier, for barrier with different thickness of insulation, is presented in Figure 38. This graph shows that the temperature on the unexposed side increases with the decrease of insulation, as expected. The increase of temperature seems proportional to the amount of insulation reduced. Figure 41 shows that the FRR is reduce by around 5% for every 25% of reduced insulation. Also, the Figure 39 shows temperature in the cross section of each scenario, after 60 min. The cross sections are introduced in this order: the color-temperature legend; the partition with 25% insulation; the partition with 50% insulation; the partition with 75% insulation; and the partition 100% insulation. We can see from this figure that in general, the cross section is hotter for scenario with reduced insulation.

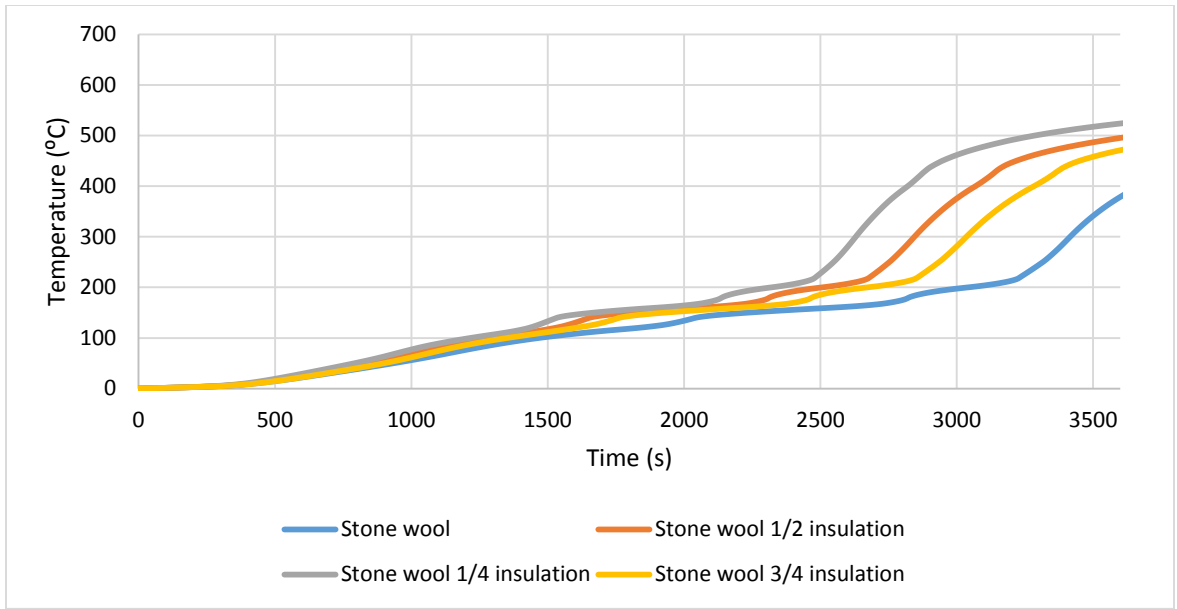


Figure 38: Wall with reduced insulation

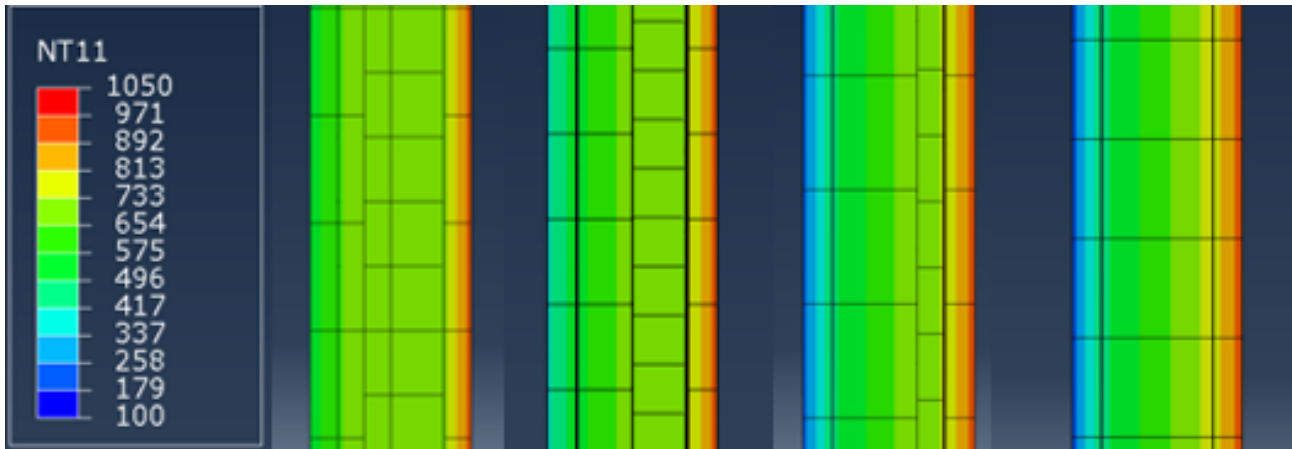


Figure 39: Temperature in the cross section of wall with reduced insulation

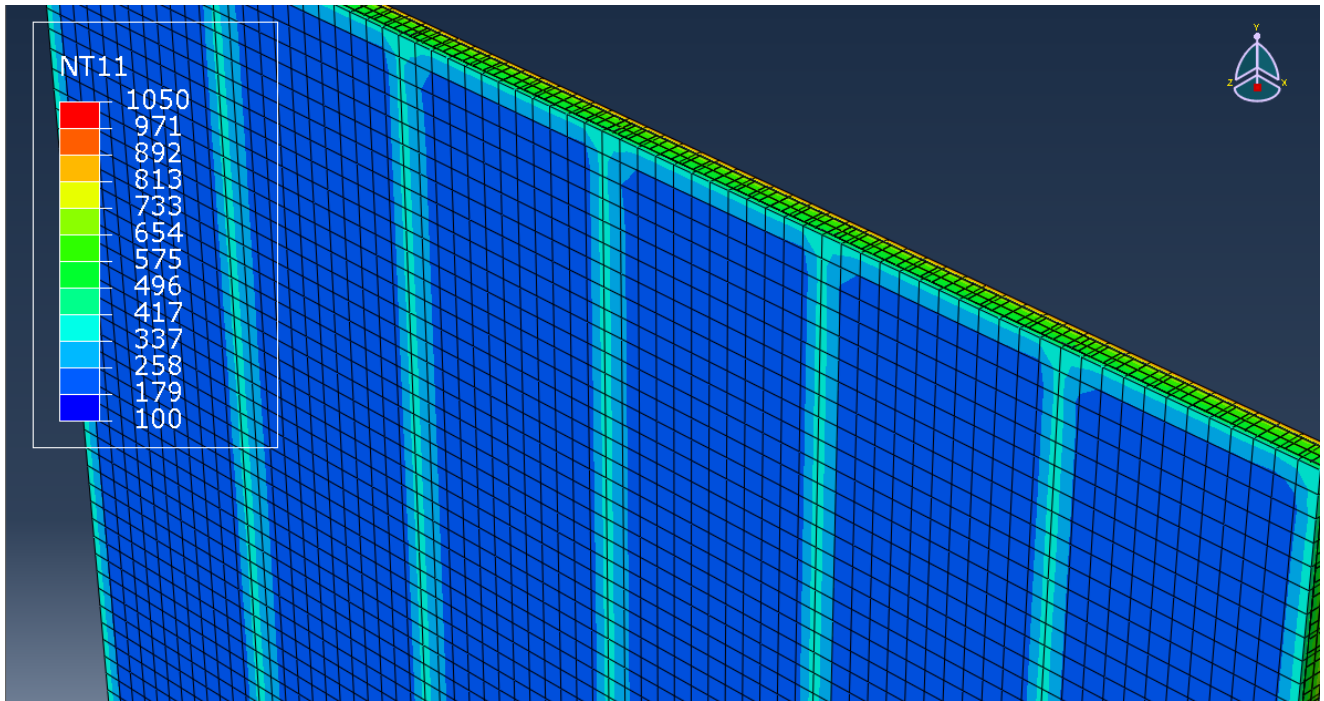


Figure 40: Unexposed surface temperature of stone wool partition after 60min

Figure 40 demonstrates the temperature on the unexposed surface of the partition insulated with 50mm of stone wool insulation, after 60min of exposure to the standard fire. As it is possible to see the maximum temperature is reached at the location of the steel studs. This is due to the high thermal conductivity of steel compare to the stone wool.

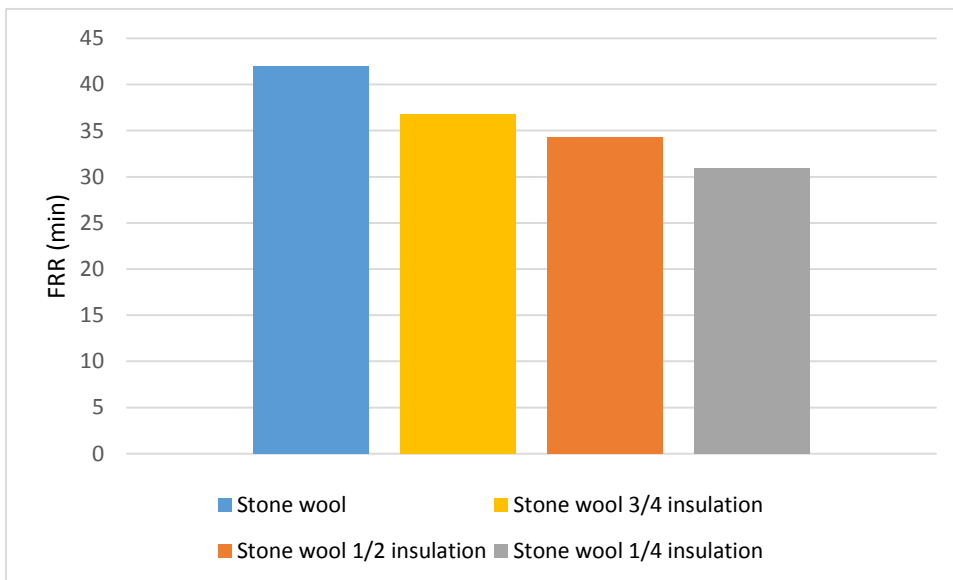


Figure 41: Ratio of FRR over the expected 60min rating for partition with reduced insulation

The following graph displays the temperature measured on the unexposed side depending on the position of insulation. The 25mm thick insulation inside the 50mm cavity was set in contact with the exposed layer of gypsum (fire side) or on the unexposed layer of gypsum (cold side).



Figure 42: Temperature on unexposed surface of the wall with different position of insulation

Figure 42 depicts that for higher temperature it is better to have insulation located on the side of the fire. This reduces the amount of cavity radiation within the construction and lower the temperature on the unexposed surface. It is possible to observe a difference of 20% in temperature on the unexposed surface, between the two cases.

### 7.1.3 Impact of increased amount of insulation

The following figure shows the temperature on the unexposed side of the partition when the insulation thickness is doubled (100mm). This will be compared later to the effect of doubling the thickness of gypsum board.

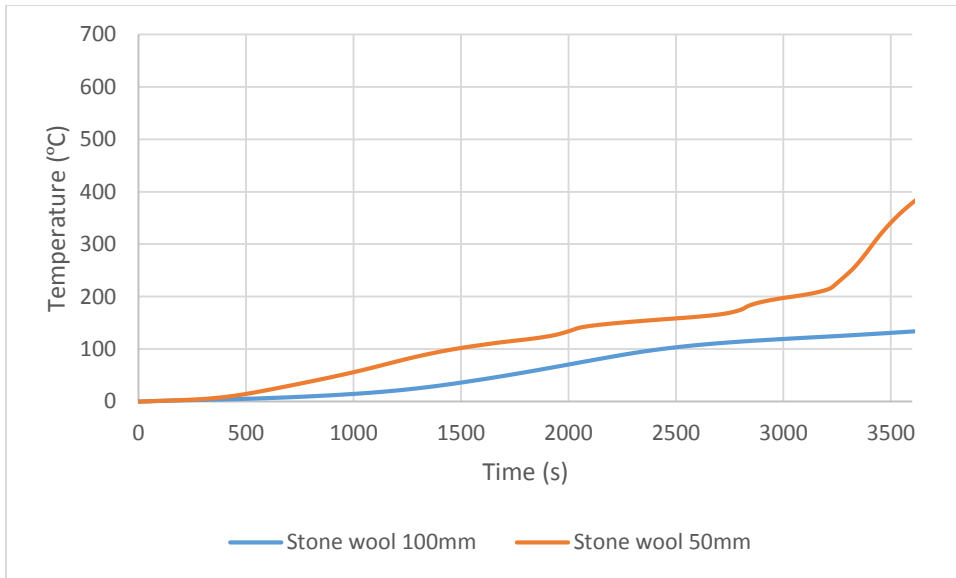


Figure 43: Temperature on the unexposed side of a partition type A with 100mm stone wool insulation

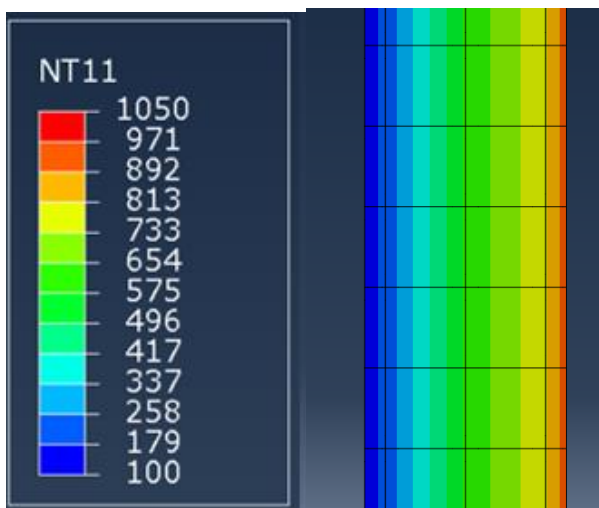


Figure 44: Temperature in the cross section of a partition type A with 100mm stone wool insulation

Figure 43 shows that when the insulation is doubled the FRR of the partition is increased by 175% passing from 43min to 75min.

### 7.1.4 Impact of hole on the exposed surface

The maximum temperature found on the unexposed side of the partition is shown in the following figures, for partition with hole on the fire-exposed surface with insulation.

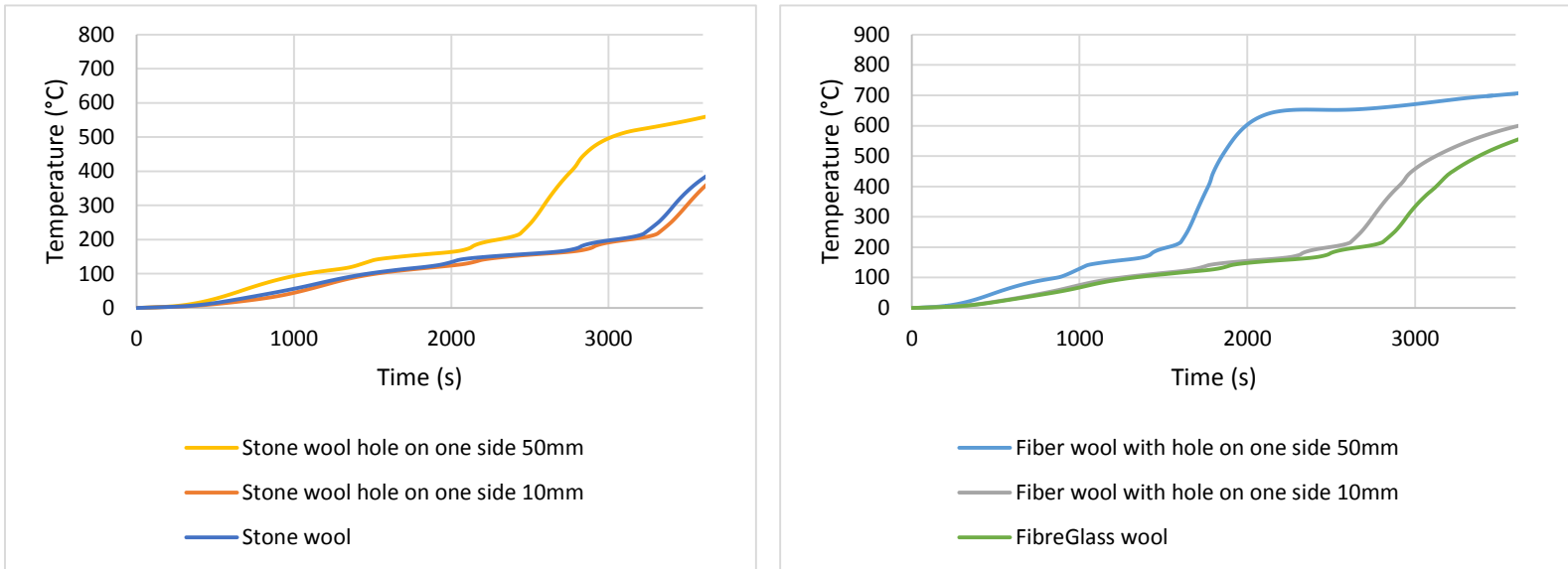


Figure 45: Temperature on the unexposed side for insulated partition with hole on the exposed surface

Figure 45 shows the impact of a hole on the exposed surface on the temperature on the unexposed surface. It can be seen that if the hole is small enough the temperature on the unexposed side will be comparable to the temperature found at the steel studs. However, if the area is increased, the heat transfer is increase and the FRR is reduced. The FRR is reduced by 20% (stone wool) and by 37% (fiber glass wool) when the diameter is increased 5 times. The following picture (Figure 46) shows the temperature through the wall insulated with stone wool, left side is a hole of 50mm radius and right side is a hole of 10mm radius.

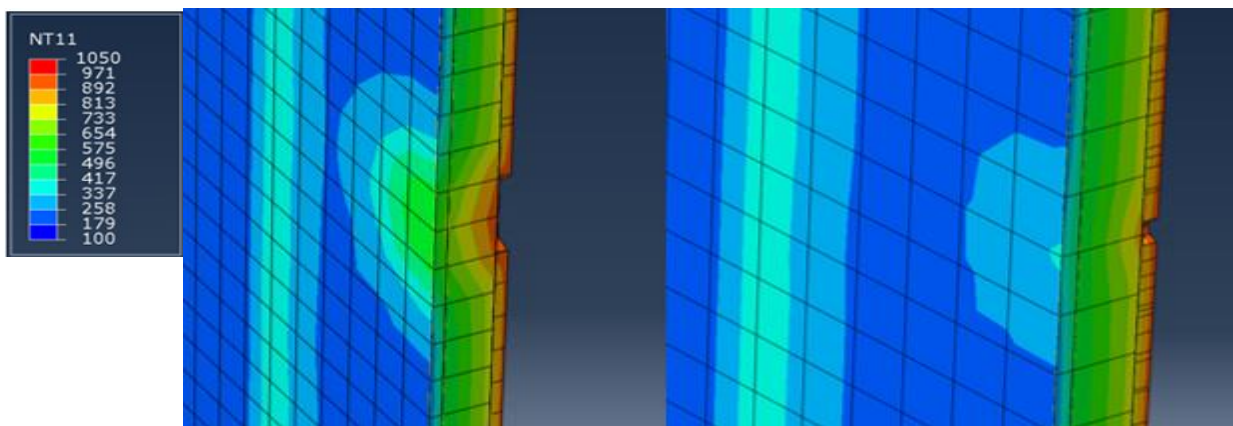


Figure 46: Temperature of the partition with hole on exposed surface insulated with stone wool

The Figure 47 shows the temperature on the unexposed surface for the different scenarios. It shows clearly that for partition without insulation the FRR is drastically reduced. A reduction of the FRR by 67% and 50% is notice for an empty partition with hole of 10mm and 50mm radius, when compare to an empty partition without hole on the exposed surface. This was expected since nothing prevents the radiation from reaching the unexposed gypsum layer, see Figure 48.

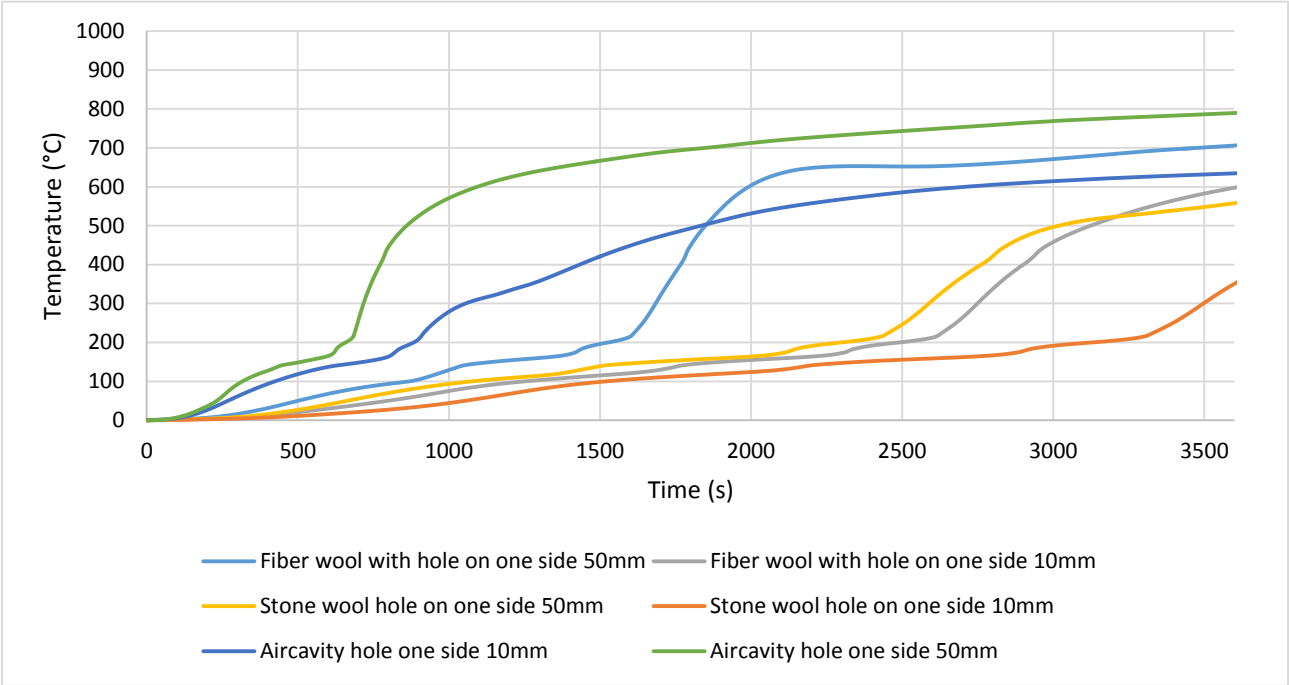


Figure 47: Temperature on the unexposed side of the partition with hole on the exposed surface

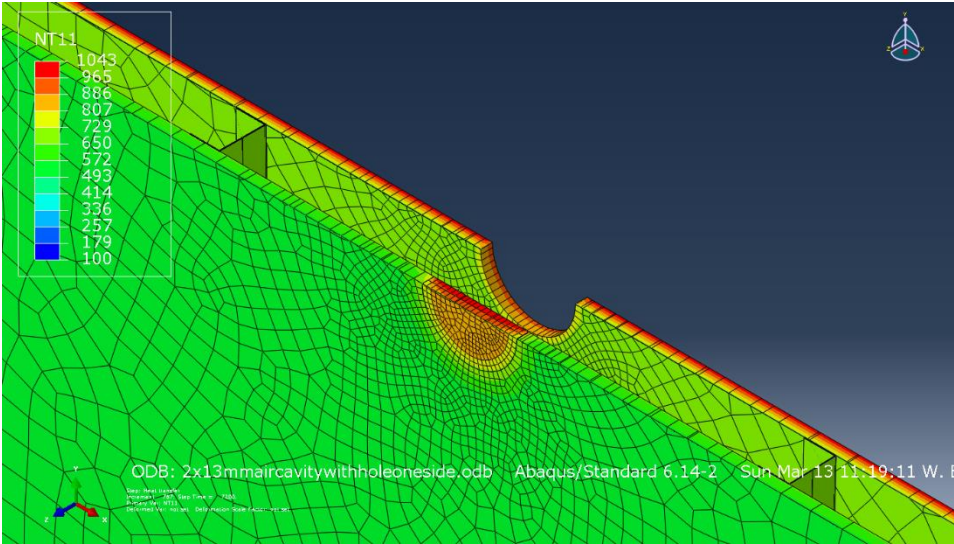


Figure 48: Temperature of partition without insulation breached on exposed side

### 7.1.5 Impact of the hole through the barrier

In this section the maximum temperature found on unexposed side of a fire rated barriers with a penetration through its boundaries is examined. For this scenario the wall insulated with stone wool was used because it was found to provide the best FRR. When the wall is breached through, it is possible to consider two scenarios. First, where the radiation and convection from hot gases affect all the area inside the hole. Second, where only the convection from the hot gases affect the area of the hole. For the first scenario the temperature at the surface will be almost equivalent to the standard temperature-time curve and therefore the FRR is as low as 5min regardless of the penetration dimension. In the second scenario the FRR is increased to around 12min also regardless of the dimension. The following pictures show the temperature on the unexposed side of the partition for both scenarios and for each penetration size (10mm, 50mm radius). On the left the pictures show the temperature with only radiation and on the right with only convection.

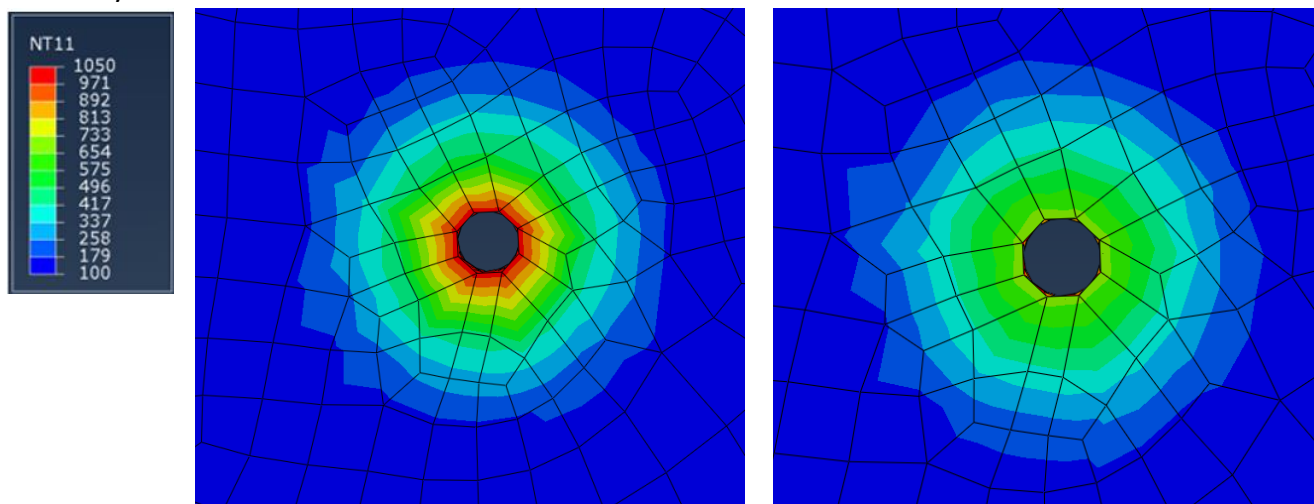


Figure 49: Temperature on the unexposed surface of a partition type A with a hole of 10mm, first and second scenario

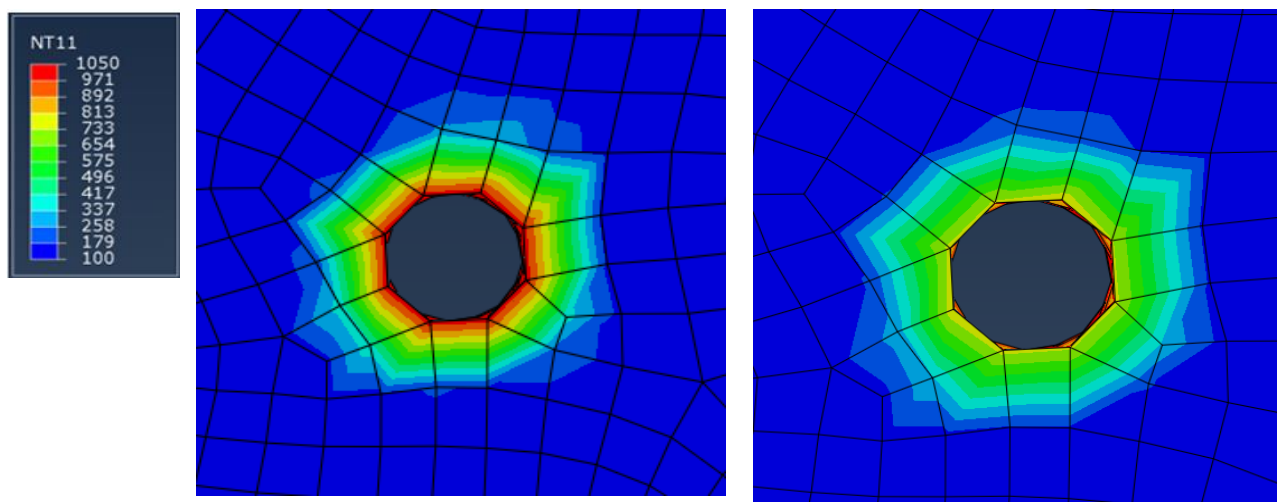


Figure 50: Temperature on the unexposed surface of a partition type A with a hole of 50mm radius, first and second scenario

## 7.2 Construction Type B

### 7.2.1 Impact of the choice of insulation material

The maximum temperature found on unexposed side of the fire-resisting barrier is shown in the Figure 51, for partitions with different type of insulation or without insulation.

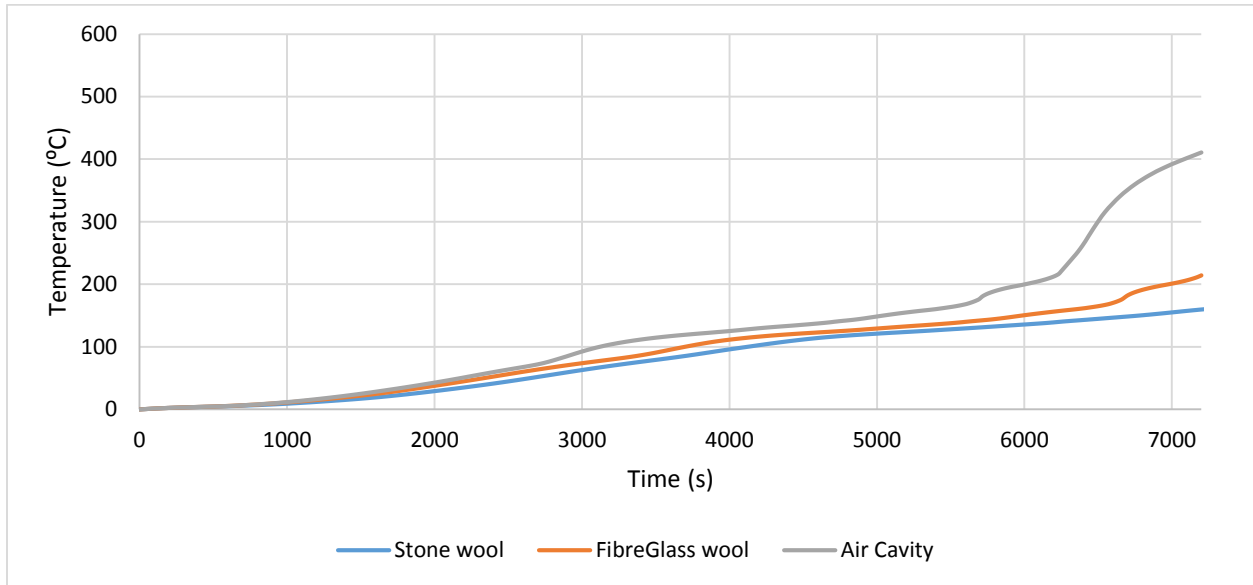


Figure 51: Temperature on the unexposed surface of wall type B with different types of insulation and without insulation

Again the fire-rated walls with different insulation do not perform as expected, still the results are closer to the manufacturer rating than the results obtained in section 7.2.1.

The previous figure shows that the temperature on the unexposed side for all three cases is within 25% difference, until approximately 83min. At this point the temperature of the wall with an empty cavity starts to increase much faster since radiation is affected by temperature at a power of 4. Figure 53 shows that the FRR for the partition insulated with stone wool is 15% higher than the fiber glass wool and 226% higher than the empty cavity. Also, the results here can be compared with the results from section 7.1.1 and it is possible to see that the FRR, with twice the thickness of drywall, increases by 280% for insulated wall and by 180% for the non-insulated wall. The Figure 52 shows the temperature at different thickness of the wall, from left to right the partition are built without insulation, with stone wool insulation and with fiber glass wool insulation.

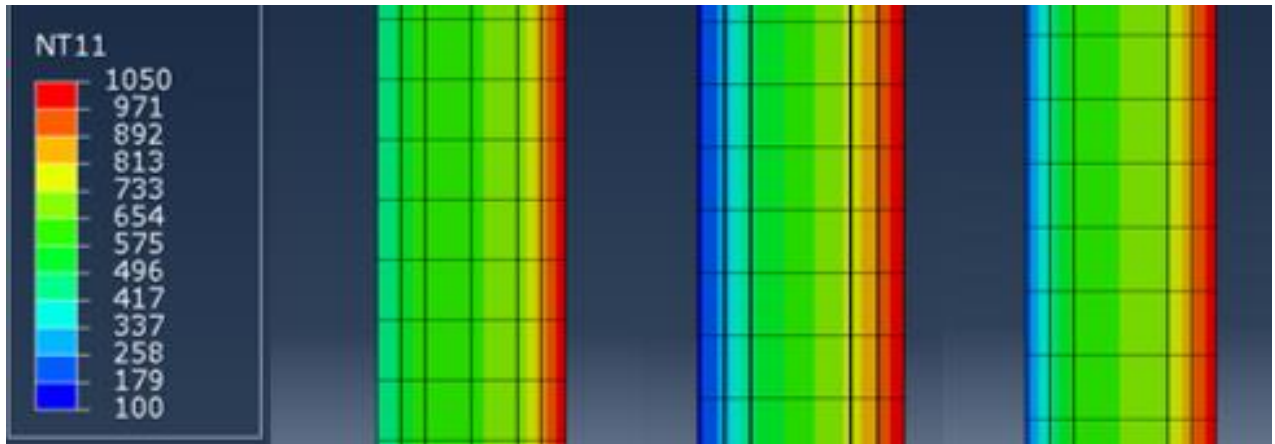


Figure 52: Temperature in the cross section of wall type B for different insulation



Figure 53: FRR for different insulation or uninsulated

### 7.2.2 Impact of hole on the exposed surface

The maximum temperature found on the unexposed side of the partition with a breach or penetration on the fire-exposed gypsum surface is shown in the following figures, for partition with and without insulation.

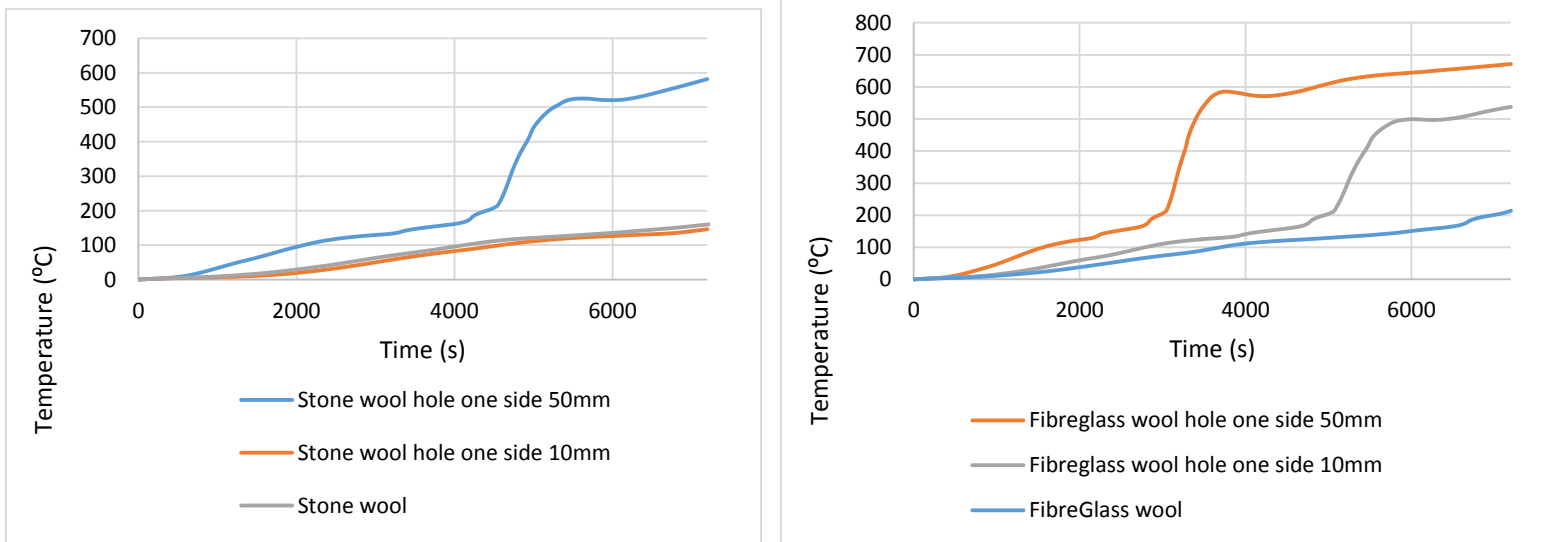


Figure 54: Temperature on the unexposed side for insulated partition with hole on the exposed surface

The two graphs above depict the difference between a wall insulated with stone or fiber glass wool. A major difference can be observed for partition with a 10mm radius penetration. For the wall with stone wool insulation the temperature at the surface remains unaffected as the temperature does not penetrate through the partition. While with fiberglass wool temperature rise very fast resulting in an early failure of the partition, a reduction of 20% of the FRR can be observed. This can also be seen in the Figure 56. For a penetration of larger dimensions, both types of insulation do not restrain the heat transfer, thus the FRR is found reduced. Still, stone wool insulation provides better fire resistance. For the larger hole, 50mm radius, a 40% and 50% reduction of the FRR can be observed for Stone wool and Fiberglass wool respectively.

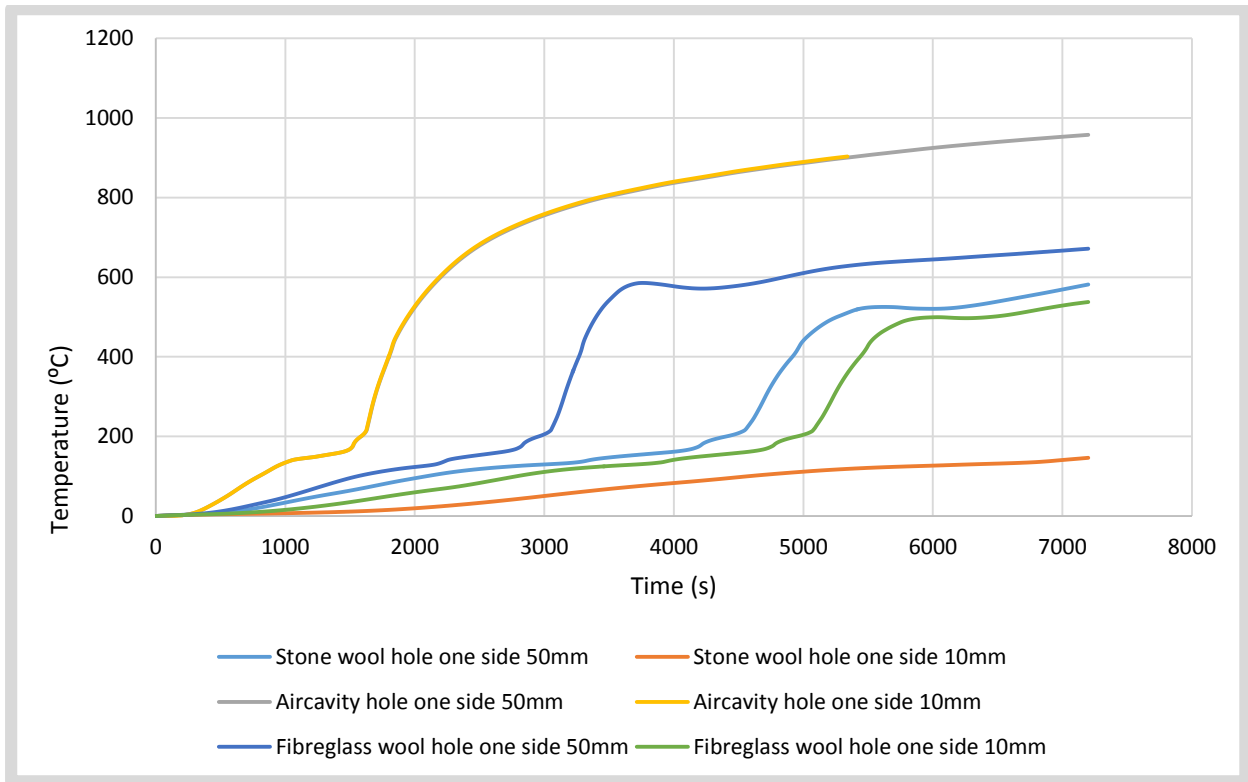


Figure 55: Temperature of the partition with hole insulated with stone wool

The figure above illustrates the temperature on the unexposed surface for the different scenarios. Again, for partition without insulation, the FRR is dramatically reduced. A reduction of the FRR by 50% is noticed for an empty partition with hole of 10mm and 50mm radius, when compare to an empty partition without hole on the exposed surface. As explain before, since nothing prevent the radiation from reaching the unexposed gypsum layer, the temperature rises very fast. This can also be seen in the following pictures.

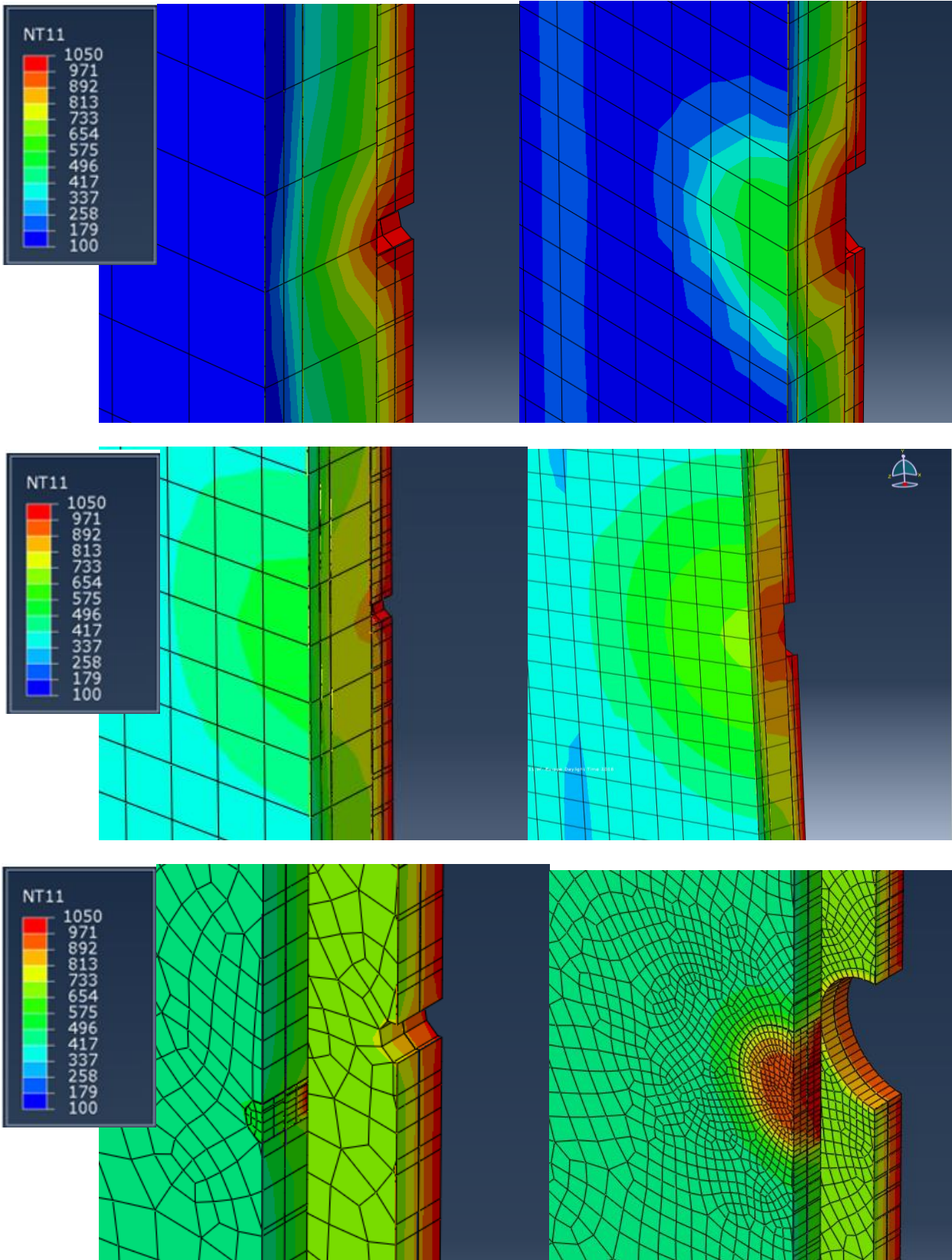


Figure 56: Temperature of the partition for all types of insulation and breach of 10mm and 50mm radius

### 7.2.3 Impact of reduced amount of insulation

The maximum temperature found on unexposed side of the barrier is shown in the figure below, for the partition with different thickness of insulation.

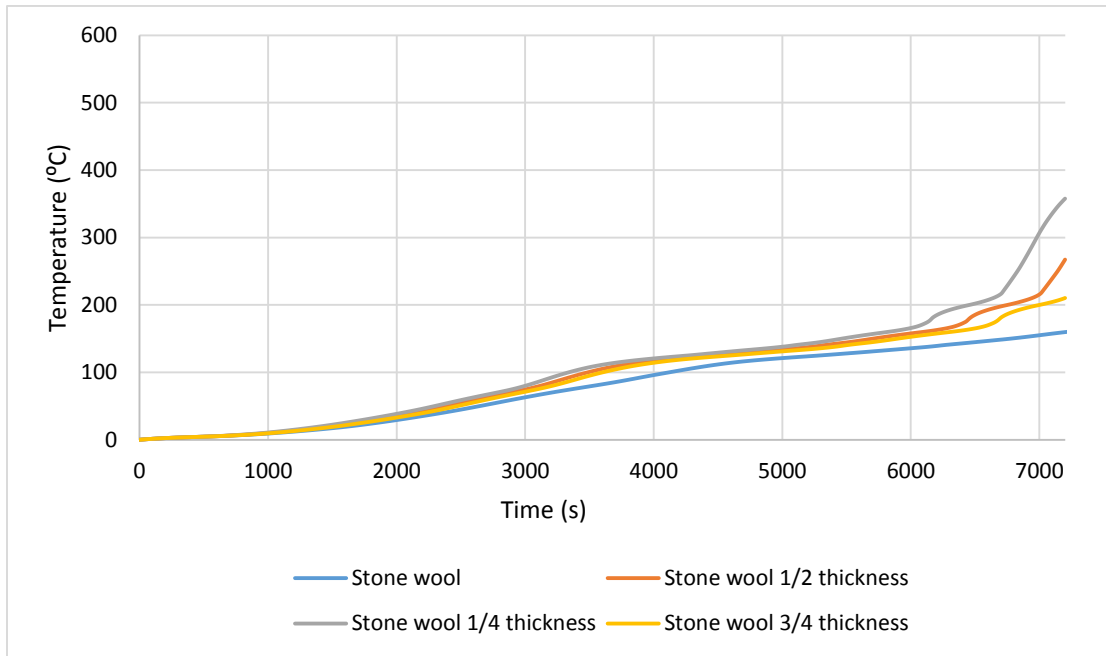


Figure 57: Temperature on the unexposed surface of wall type B with reduced insulation

Again the temperature on the unexposed side of the wall insulated with different thickness of insulation, is not significantly different, up to 80% of the test duration. Still, the FRR is slightly affected, as it can be seen from Figure 58. After 120 min the FRR is reduced by up to 20% for a 75% reduction in insulation, 15% for a 50% reduction in insulation and 12.5% for a 25% reduction in insulation. This is comparable to the data obtained with the type A construction.

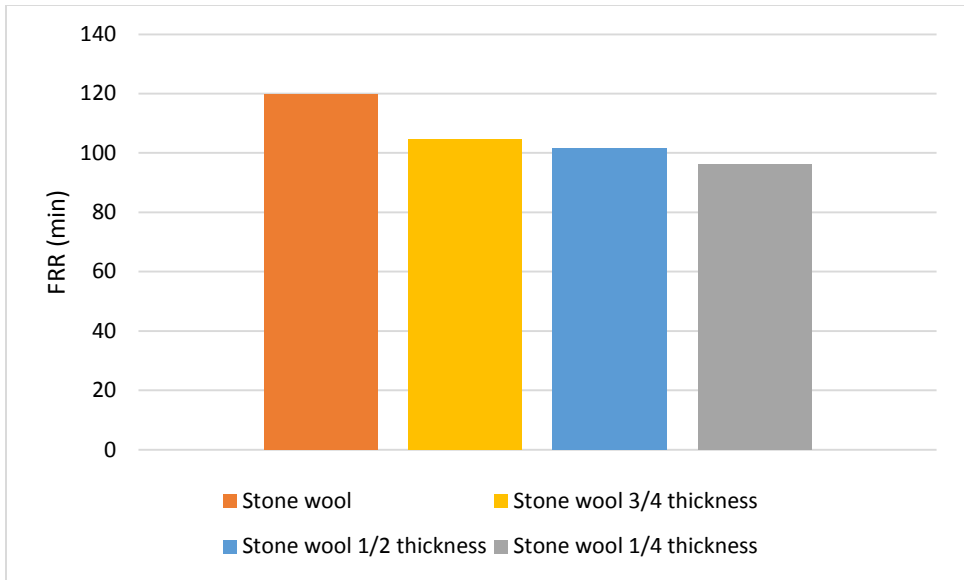


Figure 58: FRR for partition with reduce insulation for type B construction

#### 7.2.4 Impact of missing part of insulation

The maximum temperature found on unexposed side of the fire-resisting barrier is shown in Figure 59, for the barrier fully insulated against two fire barrier with missing portion of insulation.

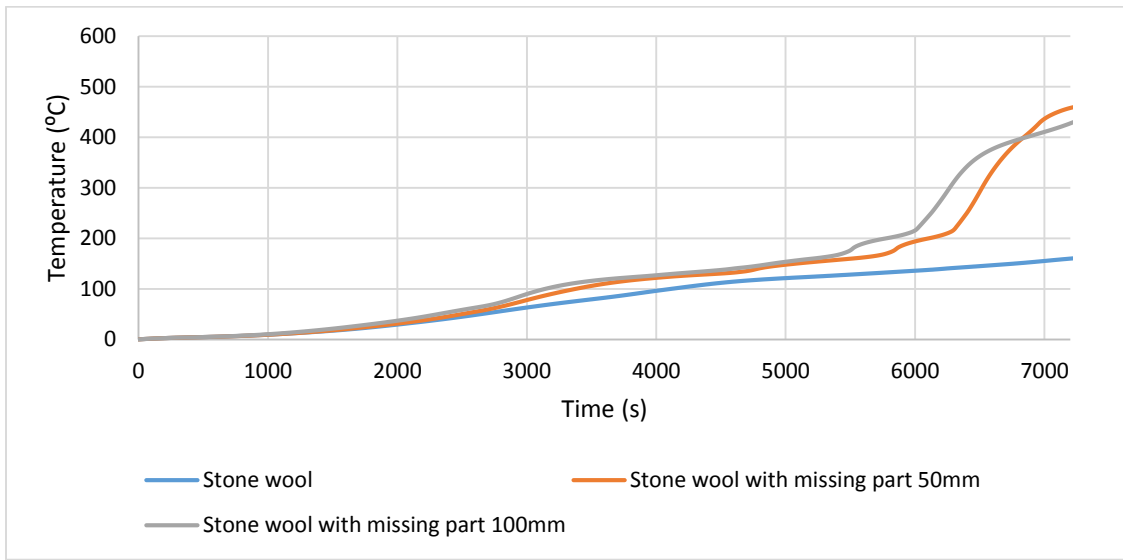


Figure 59: Temperature on the unexposed surface of wall type B with missing insulation part

As it is possible to see in the graph above and following picture, the temperature at the surface increased for the scenario with missing portion of insulation compare to the full insulated partition. Cavity radiation occurs where insulation is missing, and as seen in the previous cases, it results in higher temperature at the surface of the gypsum board. This causes the FRR to be

reduced to 96min for the wall with 100mm radius missing part and 102min for the one with 50mm radius missing part. A reduction equivalent to 20% and 15% respectively. The pictures presented below show the temperature through the partition at the location where the insulation is missing. Heat is transferred only by conduction and radiation.

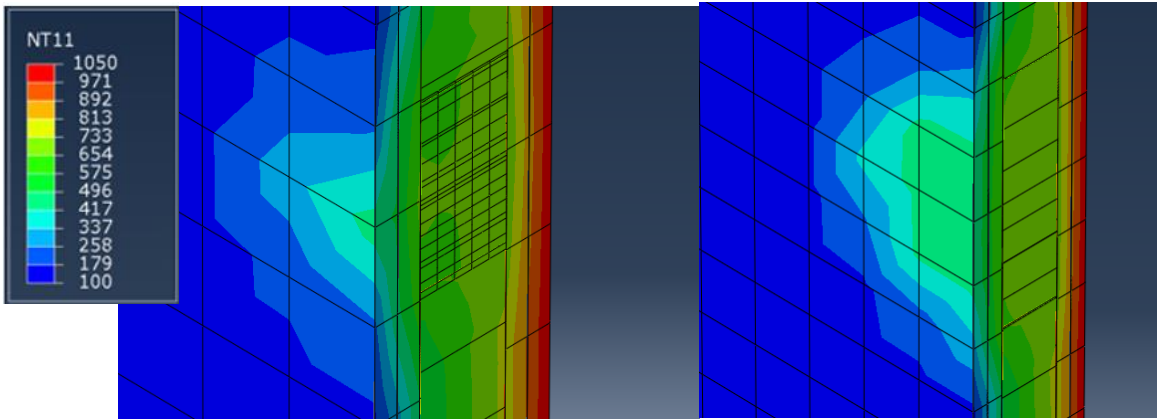


Figure 60: The temperature of the two walls with missing portion of insulation, left 50mm radius and right 100mm radius

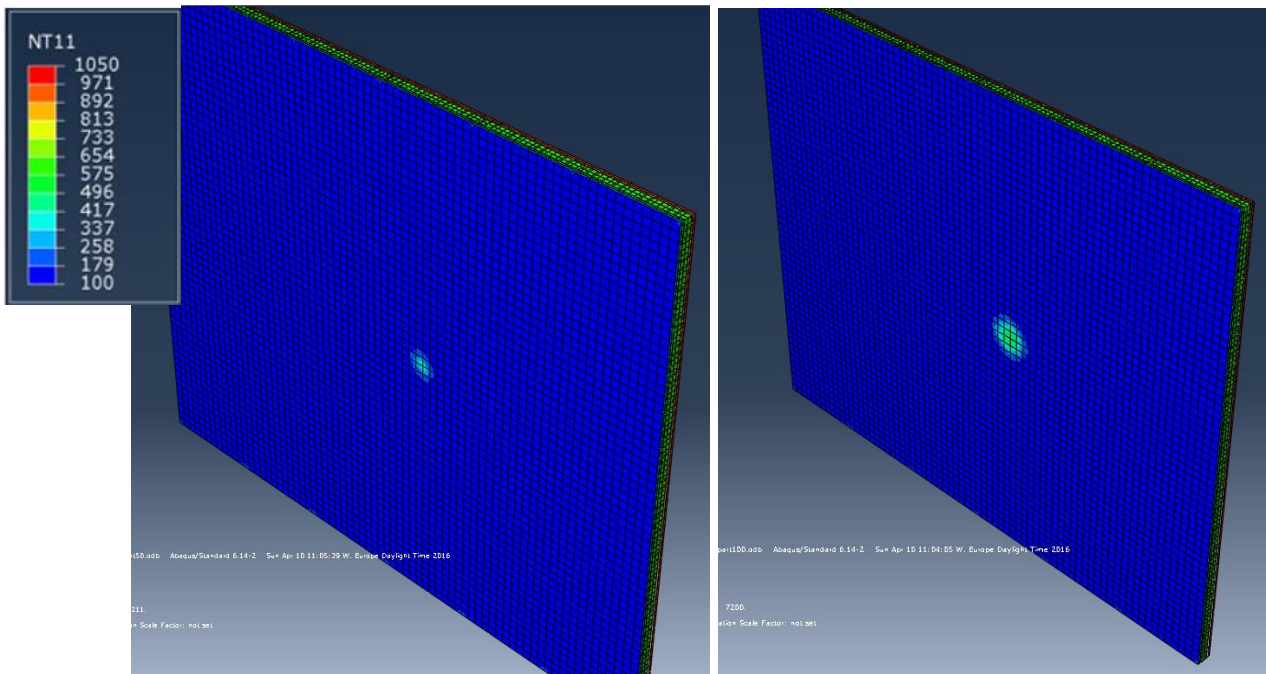


Figure 61: The temperature of the two walls with missing portion of insulation, left 50mm radius and right 100mm radius

### 7.3 Table of results from the heat transfer simulation with ABAQUS

The following table resumes the findings with ABAQUS. This table shows the reduction of the FRR of different features compare to a specific partition assembly.

Type	Partition features	Reduction of the FRR				
A/B		No reduction	Between 0- 25%	Between 25-50 %	Between 50-75 %	More 75%
Comparison with partition type A insulated with stone wool (no deficiencies)						
Type A	Empty cavity					
	Fiberglass wool					
	Stone wool insulation reduced by 25%					
	Stone wool insulation reduced by 50%					
	Stone wool insulation reduced by 75%					
	Stone wool partition exposed gypsum breach 10mm radius					
	Stone wool partition exposed gypsum breach 50mm radius					
	Hole through partition 10mm radius					
	Hole through partition 10mm radius					
Comparison with partition type A insulated with Fiberglass wool (no deficiencies)						
Type A	Empty cavity					
	Fiberglass wool partition exposed gypsum breach 10mm radius					

	Fiberglass wool partition exposed gypsum breach 50mm radius					
Comparison with partition type A uninsulated (no deficiencies)						
Type A	Empty partition exposed gypsum breach 10mm radius					
	Empty partition exposed gypsum breach 50mm radius					
Comparison with partition type A insulated with Stone wool with fire-exposed gypsum breach 10mm radius						
Type A	Fiber glass wool partition exposed gypsum breach 10mm radius					
	Empty partition exposed gypsum breach 10mm radius					
	Empty partition exposed gypsum breach 10mm radius					
Comparison with partition type A insulated with Stone wool with fire-exposed gypsum breach 50mm radius						
Type A	Fiber glass wool partition exposed gypsum breach 50mm radius					
	Empty partition exposed gypsum breach 50mm radius					
Comparison with partition type B insulated with Stone wool (no deficiencies)						
Type B	Empty cavity					
	Fiberglass wool					

	Stone wool insulation reduced by 25%		■			
	Stone wool insulation reduced by 50%		■			
	Stone wool insulation reduced by 75%		■			
	Stone wool partition exposed gypsum breach 10mm radius	■				
	Stone wool partition exposed gypsum breach 50mm radius			■		
	Hole through partition 10mm radius					■
	Hole through partition 10mm radius					■
<b>Type A</b>	Stone wool insulation				■	
Comparison with partition type B insulated with Fiberglass wool (no deficiencies)						
<b>Type B</b>	Empty cavity			■		
	Breach on exposed gypsum 10mm radius		■			
	Breach on exposed gypsum 50mm radius			■		
<b>Type A</b>	Fiberglass wool insulation				■	
Comparison with partition type B non-insulated (no deficiencies)						
<b>Type B</b>	Breach on exposed gypsum 10mm radius			■		

	Breach on exposed gypsum 50mm radius					
<b>Type A</b>	Empty Cavity					
Comparison with partition type B insulated with Stone wool with fire-exposed gypsum breach 10mm radius						
<b>Type B</b>	Fiberglass wool partition exposed gypsum breach 10mm radius					
	Empty partition exposed gypsum breach 10mm radius					
Comparison with partition type B insulated with Stone wool with fire-exposed gypsum breach 50mm radius						
<b>Type B</b>	Fiberglass wool partition exposed gypsum breach 50mm radius					
	Empty partition exposed gypsum breach 50mm radius					

Table 8: Comparison of the results obtained with ABAQUS

## 7.4 Impact of leakage with FDS

### 7.4.1 Localized leakage

Figure 62 shows the temperature at different time inside the cotton pads. The leakage was considered localized in one area, at the top of the furnace (one cell thick 100mm). The cotton pad is located in front of the leakage area, as required by the code [2]. Since the thickness of the opening should not exceed 25mm (gap gauge criteria) only the construction with an opening smaller than 2500mm<sup>2</sup> (25mm x 100mm) can be considered. This means that the very loose and loose construction are not investigated, see Table 1. The temperature of the cotton pad with time, found with the FDS models, is presented below for the fire-rated wall with different air tightness construction: Average ASHRAE, tight NRCC, tight AAMA and tight NMBCC. As mentioned in section 6.3.1 the ignition temperature assumed is 400°C.

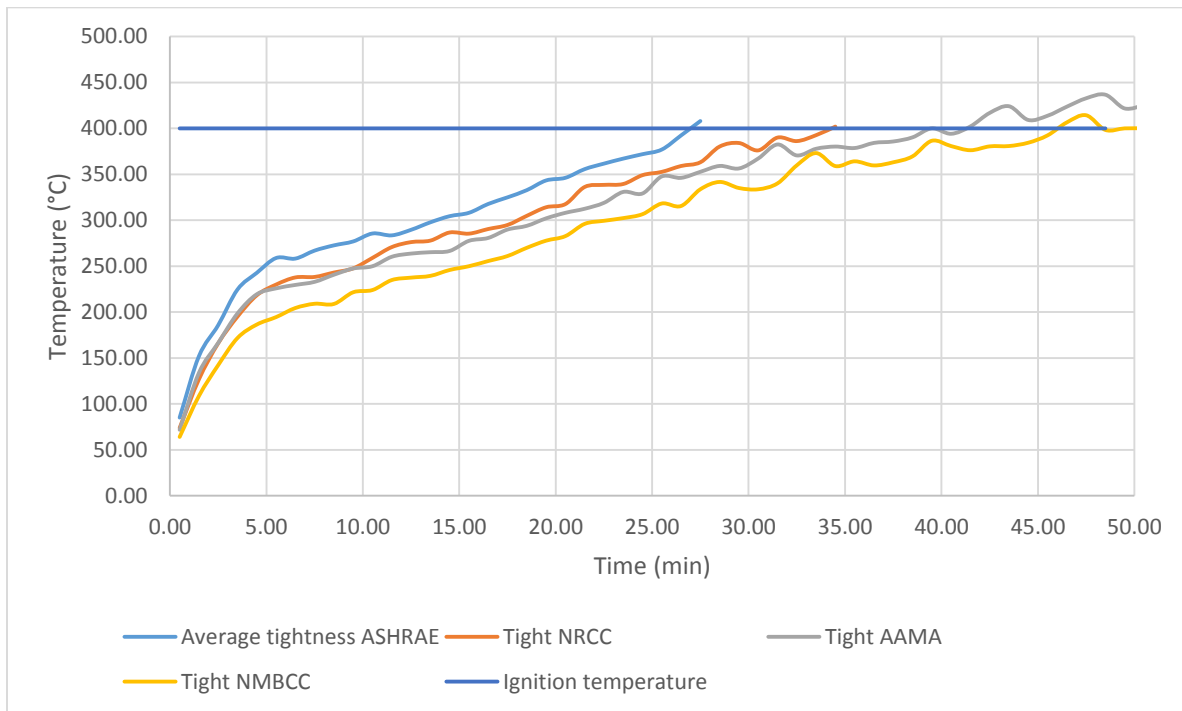


Figure 62: Temperature of cotton pad scenario 1 with different level of air tightness

Table 9 shows the FRR according to the integrity criteria of partition with localized leakage.

Scenario	Time until ignition of cotton pads (min)
Average construction	27
Tight construction (NRCC)	34
Tight construction (AAMA)	41
Tight construction (NMBCC)	46

Table 9: FRR of partition with different tightness leaking from a hole on top

As it is possible to see in the table above the FRR is reduced with an increase of the leakage volume rate. The FRR is reduced to 27min for an average construction this represents a reduction of 55% for a 60min fire-rated wall and 77% reduction for a 120min fire-rated wall. For a tight (NRCC) construction the FRR represents a reduction of 43% for a 60min fire-rated wall and 72% reduction for a 120min fire-rated wall. For a tight (AAMA) construction the FRR represents a reduction of 32% for a 60min fire-rated wall and 66% reduction for a 120min fire-rated wall. Finally, for a tight construction, according to the NMBCC, the FRR represents a reduction of 23% for a 60min fire-rated wall and 62% reduction for a 120min fire-rated wall.

#### 7.4.2 Distributed leakage on one side

The following figures show the temperature at different times inside the cotton pads, for the fire-rated partition with air tightness according to the Table 1. The leakage area, in those models, was distributed over one joint of the wall only, as seen in Figure 26. The temperature for the cotton pads was measured at different heights. One located at the floor level, the second one at mid-level and the last one at the top level of the furnace.

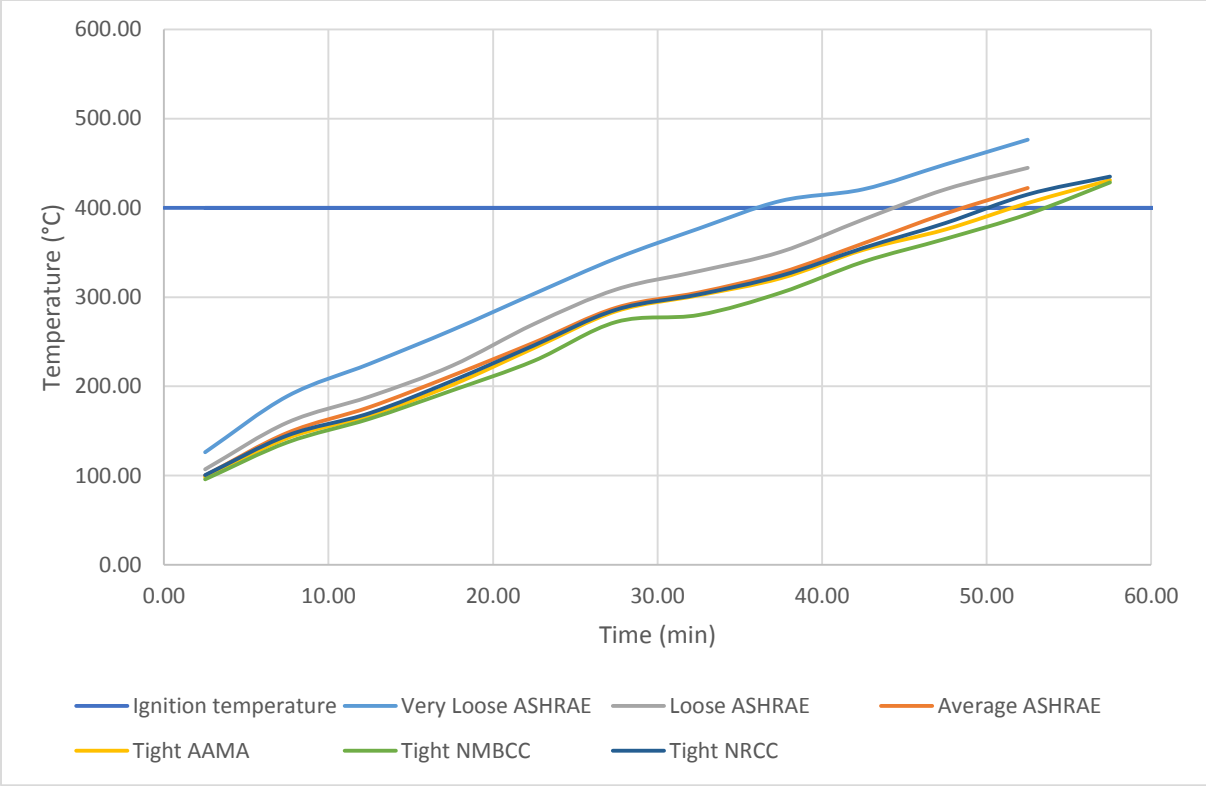


Figure 63: Temperature of cotton pad with time measured at the top of the sample height

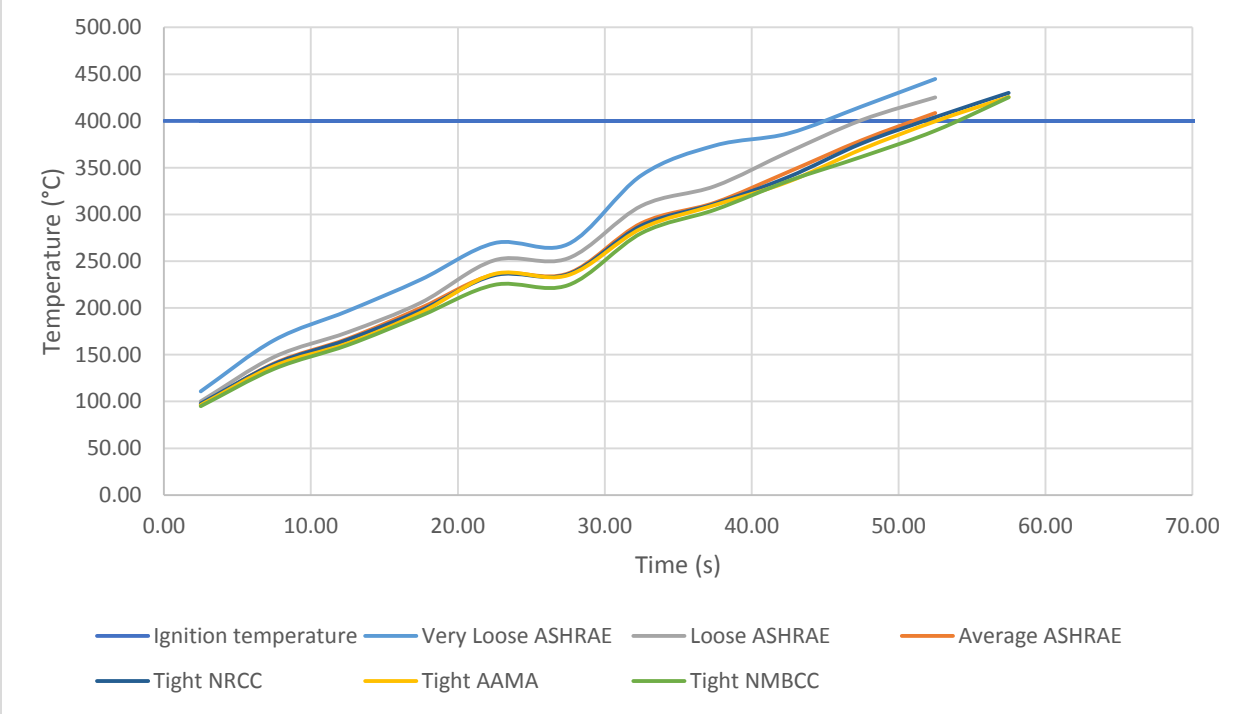


Figure 64: Temperature of cotton pad with time measured at the bottom of the sample height

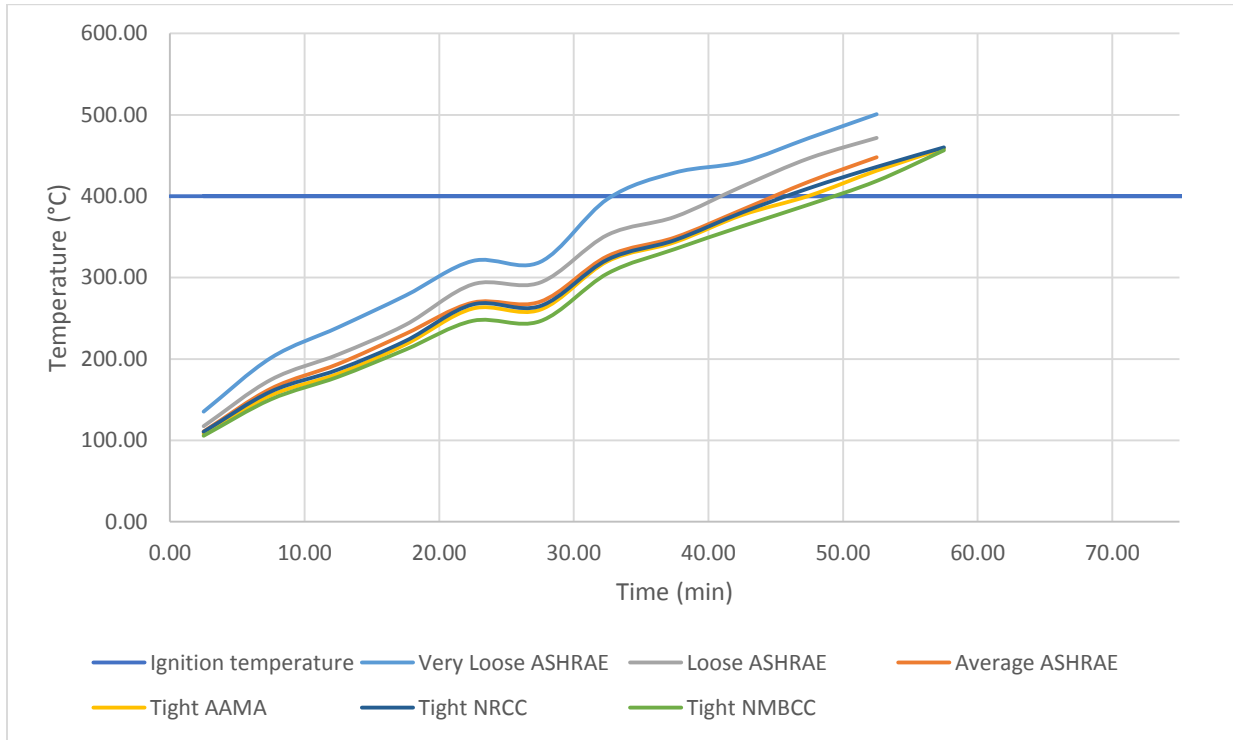


Figure 65: Temperature of cotton pad with time measured at the middle of the sample height

The Table 10 shows the time until ignition of cotton pad, for each position, taken from the graphs shown above. This time represent the time until failure according to the integrity criterion.

Scenario	Time until ignition of cotton pads (min)		
	Bottom of furnace	Middle of furnace	Top of furnace
<b>Very loose construction</b>	45	32	37
<b>Loose construction</b>	47	40	44
<b>Average construction</b>	51	44	47
<b>Tight construction (NRCC)</b>	52	46	50
<b>Tight construction (AAMA)</b>	53	48	53
<b>Tight construction (NMBCC)</b>	55	50	54

Table 10: FRR of partition with different air tightness leaking from one side

Results show, as expected, that when the leakage area increases the cotton pad reaches ignition temperature earlier, thus the FRR is reduced. This is caused by the increased quantities of hot gases allowed through the partition. Also, ignition is noticed earlier for the cotton pad located at the middle of the sample height. We can see from the Table 10 a difference of about 32% between a very loose constructions and a tight construction according to NMBCC. Moreover, if the results are compared to the one obtained with a localized leakage, section 7.4.1, we can see an increase of the FRR as presented in the Table 11, comparing to the values from Table 10 corresponding to the cotton pad in the middle of the furnace. However, the gain percentage of FRR decreases with the increase of air tightness. This implies that the leakage in a very tight construction is a less significant issue than a leakage in a loose construction.

Scenario	Increase of the FRR (%)
<b>Average construction</b>	62
<b>Tight construction (NRCC)</b>	35
<b>Tight construction (AAMA)</b>	17
<b>Tight construction (NMBCC)</b>	8

Table 11: Percentage change in FRR between localized and distributed leakage

### 7.4.3 Distributed leakage

Table 12 shows FRR for the sample with leakage area distributed over all the joints of the wall, as seen in Figure 25. The leakage area considered is presented in the Table 1.

Since, the leakage is distributed over all the joints of the wall, the volume of smoke going through the partition decreases. This causes the FRR to increase a little. The Table 12 shows a difference of 11% in the FRR between a very loose constructions and a tight construction according to NMBCC, which is less than in the previous section. Table 13 shows the increase of the FRR compare to the localized leakage, section 7.4.1, and to the distributed leakage on the right side, section 7.4.2. Leakage from every joints gives much better FRR compare to penetration, but the results do not increase much when compare to the results from section 7.4.2.

Scenario	Time until ignition of cotton pads (min)		
	Bottom of furnace	Middle of furnace	Top of furnace
<b>Very loose construction</b>	52	46	48
<b>Loose construction</b>	51	50	52
<b>Average construction</b>	54	52	54
<b>Tight construction (NRCC)</b>	54	50	54
<b>Tight construction (AAMA)</b>	54	53	54
<b>Tight construction (NMBCC)</b>	54	52	54

Table 12: FRR of partition with different air tightness leaking from every joints

Scenario	Increase of the FRR compared to section 9.3.1 (%)	Increase of the FRR compared to section 9.3.2 (%)
<b>Average construction</b>	92	18
<b>Tight construction (NRCC)</b>	47	8
<b>Tight construction (AAMA)</b>	29	10
<b>Tight construction (NMBCC)</b>	13	4

Table 13: Percentage change in FRR between leakage in all joints and the other scenarios for the cotton pad at mid height of the furnace

Figure 66 and Figure 67 show the temperature of the unexposed surface of the partition and of the surface of the cotton pad, for the scenario with leakage according to AAMA. By looking at the unexposed surface of the partition it is possible to see that the temperature on the unexposed surface is very high in the surrounding of the leakage area, compare to the rest of the sample. This causes the heat transfer by radiation to increase greatly, between the tested sample and the cotton pad. This could explain why the FRR does not change much, for very little values of leakage. Most of the heat transferred to the cotton pad seemed to be done by radiation and not by convection from hot gases. Also, this explains why the cotton pad located at the middle of the sample height gives the lower FRR. The cotton pad at this location is subjected to a higher heat flux by radiation, compare to the other two location measured.

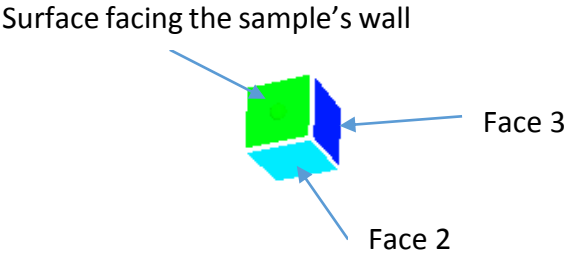


Figure 66: Temperature on the cotton pad after around 3600 seconds

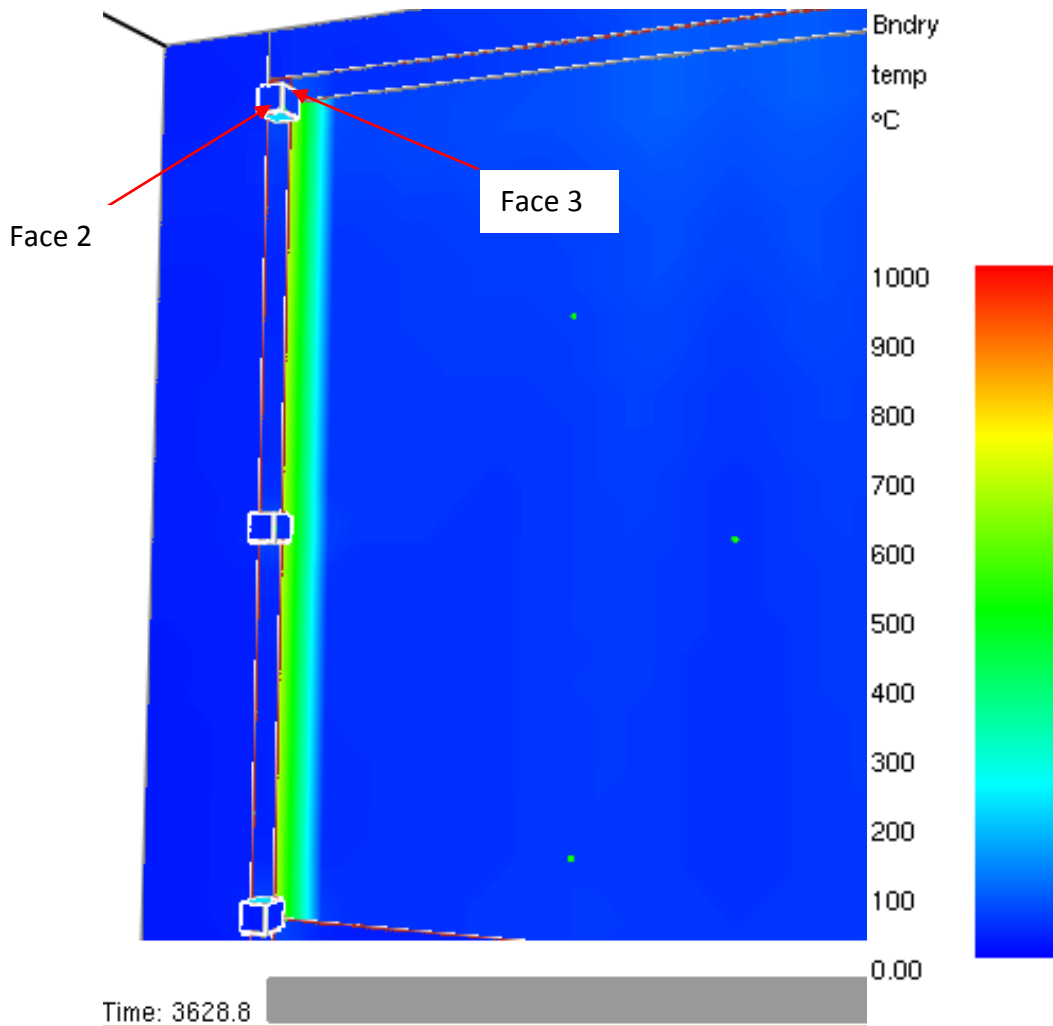


Figure 67: Temperature on the unexposed side of the tested sample after 3600 seconds

## 7.5 Discussion

The previous sections have presented simulation results in the form of time–temperature graphs, FRR-cases figures and temperature of cross section figures. Results help to understand how fire barriers are affected by different parameters. These graphs were used to describe the performance of each panel in term of insulation and integrity.

First, the impact of the thickness of plasterboard will be discussed. As seen from the data, plasterboard has a very huge impact on the FRR. By doubling the thickness of plasterboard the FRR is increase by 280%. This can be compared to insulation, which shows an increase of 175% of the FRR when the insulation is twice as thick, see section 7.1.3. Therefore, it seems more efficient for size limitation to increase the quantity of gypsum board. Still, it should be kept in mind that gypsum fails after prolonged time subjected to high temperature.

It was also found that if portion of insulation is missing from the cavity, higher temperatures are expected at the unexposed layer of gypsum, where insulation is missing. The area surrounding the location where insulation is missing is also affected as seen in Figure 56. In that area the FRR is greatly reduced, but at the other location the surface temperature remains unaffected. This is due to cavity radiation inside the empty cavity. As it will be discussed further, validation of the cavity radiation model should be done in order to express higher degree of confidence in these results.

Another important factor, which can be seen from the simulation, is the importance of insulation inside the cavity. Results show clearly that a fire resisting barrier has much more chance to withstand the fire for prolonged time if insulated. Indeed, results show lower temperature on the unexposed surface of insulated wall compare to wall with an empty cavity. Furthermore, when the plasterboard layer on the fire side is breached the temperature on the unexposed surface is directly affected. But, if insulation is used, the FRR is reduced less than a wall with an empty cavity. Since the insulation material acts as an extra surface and prevents heat from reaching the unexposed surface. This was found true especially with stone wool insulation, due to its incombustibility, represented in the simulation by lack of ablation. However, as found in section 7.1.5, if the breach reaches the surface it is not possible to prevent the heat transfer through the wall anymore and the resulting FRR falls to almost nothing. Although, the heat transfer from hot gases and from the furnace to the inside of the hole is hard to represent with exactitude in a numerical model, it is without a doubt that the partition is too compromised to be able to perform well under a fire.

On the other hand, when the wall is insulated, because of the low thermal conductivity of insulation, heat is redirected back to gypsum board exposed in the furnace. This results in the exposed gypsum layer to heat up faster, compare to a wall without insulation, as seen in Figure 36. This would result in a failure of the gypsum board faster when the wall is insulated compare to uninsulated. Indeed, as mentioned early in this work, failure of gypsum can be observed at temperature between 600°C and 700°C, therefore, the gypsum of the partition with insulation would be falling off before the partition without, thus, earlier exposing its insulation directly to the fire. Nonetheless, when failure of gypsum wall occurs it is better to have insulation in the cavity to protect the unexposed layer, otherwise the unexposed layer will quickly heat up. Regarding insulation, as it can be seen from Figure 35, stone wool reacts much better at higher temperature compare to Fiber glass wool due to the effect of ablation. Therefore, using such insulation material could be a problem if failure of the gypsum board occurs and insulation is directly exposed to the fire. But, if the gypsum layers do not fail, partition with fiberglass insulation can yield FRR similar to partition with stone wool insulation, see Figure 51. Also, other experiments on LSF showed that when the partition is insulated, lower FRR was found. This was due to bending of the partition resulting from a higher temperature in the steel stud. This could

not be analyzed during this study, but further work with ABAQUS could allow to investigate the effect of expansion and deformation of the steel studs.

Results show that the FRR of partition is greatly affected by leakage, even with tight construction. FRR of under 60min were found for all scenarios investigated, but the worst possible leakage scenario was for localized leakage area. The FRR was improved as the leakage area is reduced.

The cause of the ignition of the cotton pad seemed to be radiation from the surface of the gypsum board. Leakage through the partition increase the temperature on the unexposed surface very close to the ISO-834 and this causes the surface to radiate enough heat to the cotton pad to ignite. However, this means that the failure of the sample is more likely to be due to the insulation criterion since the unexposed reaches the maximum allowed temperature in a matter of minutes while the failure due to integrity is seen after more than 30 minutes.

## **7.6 Limitations and Uncertainties**

When looking at limitations it is important to keep in mind that the results obtained are all the results of numerical simulations. As such simulations are never an exact representation of a real scenario. Also, numerous assumptions have been taken when modeling, not only in the data used, but also in the modeling methods used. One major modeling error can be associated with the cavity radiation in the models. The radiation inside the cavity is complex and will be affected by all the numerous surfaces inside the cavity as well as their temperature. However, the model used in the simulation is rather simple and as such, more validation on this should be done before being able to use the results with more confidence. There are uncertainties related to the heat transfer method used in ABAQUS. For example it is considered that the insulation is in perfect contact with the gypsum board while, in reality, there could be a thin gap of air between which would reduce the conduction. The same could happen between the studs and the gypsum board and the two layers of gypsum board. Also, there certain concern regarding FDS simulations. Since there was no validation done on for furnace test, the severity of the fire and temperature which occurs inside a furnace could exceed the limits of FDS, consequently, the results could be inaccurate.

This study shows the advantages of using mineral wool in fire rated barrier, however, some mineral wool materials are known to cause heat generation, when submitted to external heat flux. This effect was deliberately ignored due to its complexity, but certainly it would cause the temperature on the unexposed side of the wall to rise higher than what was seen in the simulation. Some research is currently being done at DBI on this matter and maybe in the future such phenomenon could be added to simulation. Another aspect, which wasn't considered in this study, is the effect of the vaporized water from gypsum. Indeed, as mentioned in the literature review, crystalline water inside the structure of gypsum vaporized at elevated temperature and

is forced out of the gypsum board. The effect of this water movement inside the partition with regards to the FRR was not considered, a specific study should be done concerning this phenomena.

This work focused on certain features of wall such as: reduced insulation, effect of wall penetration or increased leakage, however it did not consider the impact due to change in thermal properties. Manufacturers offer very wide variety of products with very specific and different properties. As mentioned before, FRR is very dependent on the thermal properties and as such the results obtained would differ for a wall using different types of materials. For example, results from simulation using a Fiberglass wool density equal to  $100\text{kg/m}^3$  showed a reduction on the unexposed surface temperature by 12%. Still, even if the exact results would be different, the impact of the investigated features should affect the FRR in the same way. Also, there are uncertainties related to the values used, these can come from error in the measurement methodology, precision of instruments and more.

In FDS the grid dimension plays an important role in the precision of the results. The coarse grid mesh used limited the number of radiation angles, which could be used, thus affecting the heat transfer inside and outside the furnace. Also, there are uncertainties related to modeling methods used. For example, added vents used to increase oxygen inside the furnace could alter the convective heat transfer coefficient inside the furnace. Also, experimental data would be needed in order to validate the heat transfer through cracks and leakage area, in order to determine how accurate FDS is. Then, the pressure at the top of the furnace exceeds the value required by the code. This causes the exfiltration of smoke to increase as well as the heat transfer. The use of fan in FDS could help maintain the pressure at a lower level. This would require additional work and also increase the computational time. Moreover, as mentioned in the introduction, the cotton pad sample needs to be applied in front of cracks for 30 seconds, then removed. However, it was not possible to simulate this in FDS so the cotton pad was located in front of the crack for all the duration of the test. This causes the cotton pad to reach the ignition temperature faster.

## **7.7 Validity**

This work meant to give an idea on how the FRR barriers change depending on several parameters. Results provided a tendency which show how different parameter can affect the rating of barriers. Still, it is important to keep in mind that those results are valid for the case scenario considered in the scope of this work. A change in the fire-rated wall construction or in the dimension of the investigated parameters would lead to different results. For instance, concrete fire-rated wall would have a much higher thermal capacity and thus would probably take much more time to heat up. Moreover, as mentioned in the introduction, it was assumed that the wall do not collapse or deform excessively at elevated temperature. However, the type

of insulation could influence the temperature found inside the structure, as seen in section 7.1.1, thus influence the FRR based on the stability criterion.

## 8 Conclusions

Fire rated partition are built according to specifications taken from manufacturers. The objective of this work was to examine what happens to the FRR if the fire-rated barrier is built differently or is altered before it is subject to a fire. This study looked at the reliability of fire resistant structures with regards to the insulation and integrity criterion. This was done using numerical tools such as FDS for the integrity criterion and ABAQUS for the insulation criterion. No experiments were done during this study, however the models were validated using experimental data available. In general it was found that all the tested partitions with increased leakage or reduced insulation had a FRR too low to fulfill their purpose. More precisely the following elements were observed:

- For partition without deficiencies or alteration, stone wool insulation provided a FRR 13% and 40% higher compared to similar partition insulated with Fiberglass wool and uninsulated partition, respectively.
- Small breach (10mm radius) on the exposed layer of gypsum board did not affect the stone wool insulated partition, however the uninsulated partition FRR was found to be reduced by 50%. Also, when breached (10mm radius) Stone wool insulated partition provided a FRR approx. 20% and 70% higher than partition insulated with Fiberglass and uninsulated partition, respectively
- Larger breach (50mm radius) on the exposed layer of gypsum board reduced the FRR by 50% for partition with fiberglass wool and uninsulated partition and by 40% for partition with stone wool. Also, when breached (50mm radius) Stone wool insulated partition provided a FRR approx. 30% and 70% higher than partition insulated with Fiberglass and uninsulated partition, respectively
- Reduction by up to 25 % of the FRR was observed for reduction of the insulation thickness by up to 75%

Results showed that the leakage of hot gases at cracks caused the temperature on the unexposed surface to exceed the acceptable limits in a matter of minutes. Therefore, it is more likely that leaking walls will fail due to the insulation criterion rather than the integrity criterion. Still, the following observation could be made on the FRR of partition according solely to the integrity criterion.

- Leakage occurring through a hole caused a 55% reduction of the FRR, for an average air tight construction

- Leakage occurring on one side of the partition caused a 47% reduction of the FRR, for a very loose air tight construction
- Leakage occurring at all joint of the partition caused a 23% reduction of the FRR, for a very loose air tight construction

The results show clearly that in order to stay reliable, a fire-rated partition must be built and maintained as specified by the manufacturer. The results showed also that using stone wool insulation inside the cavity could help improving the FRR, based on the insulation criterion. This study showed a method to simulate fire resistance test with the help of numerical tools. This could be very useful, especially when considering the high cost of testing samples in furnaces. Still, much work needs to be done in order to accurately model a fire resistance test.

## 9 Future Work

In order to improve models on fire resistance test, further work should include the following:

- The effect on heat transfer of hot gases leaking through partition should be studied experimentally.
- The effect of heat transfer in empty cavity by radiation during a fire resistance test should be investigated. This would allow to validate the numerical models and help to find a way to reduce the heat transfer to the unexposed gypsum layer in an empty cavity partition.
- Numerical models of thermal expansion and deformation of the partition component such as steel studs, wooden studs and gypsum board, in order to include the stability criterion.
- The impact on the fire resistance rating of lightweight partition using steel or wooden studs.
- The influence of the heat generation in some woolen insulations materials and the impact on the FRR.
- The combustibility of the insulation material inside the cavity and its effect on the FRR.
- The dependency of FRR on the water movement inside the partition caused by water vaporization from the gypsum.

## **10 Acknowledgements**

The author would like to thank Rockwool for support under the form of sponsorship which allowed me to participate in the International Master of Science in Fire Safety Engineering. Also the author wishes to express his gratitude to professor Patrick Van Hees and Bjarne Husted for all their support, guidance and assistance during the master thesis process.

## 11 References

- [1] P. Kolarkar and M. Mahendran, "Experimental studies of non-load bearing steel wall systems under fire conditions," *Fire Saf. J.*, vol. 53, pp. 85–104, 2012.
- [2] British Standards Institution, "Standards Publication Fire resistance tests Part 1 : General Requirements," 2012.
- [3] CertainTeed, "Gypsum Board Systems Manual," 2012. [Online]. Available: [http://www.certainteed.com/resources/CTG\\_4080\\_Gypsum\\_Board\\_Systems\\_Manual\\_Eng.pdf](http://www.certainteed.com/resources/CTG_4080_Gypsum_Board_Systems_Manual_Eng.pdf). [Accessed: 21-Apr-2016].
- [4] D. Drysdale, "Heat Transfer," *An Introd. to Fire Dyn.*, pp. 35–82, 2011.
- [5] U. Wickström, R. Jansson, and H. Tuovinen, *Validation fire tests on using the adiabatic surface temperature for predicting heat transfer*, no. 310. 2009.
- [6] U. Wickström, *Methods for Predicting Temperatures in Fire-Exposed Structures*. 2015.
- [7] H. Takeda, "A model to predict fire resistance of non-load bearing wood-stud walls," *Fire Mater.*, vol. 27, no. 1, pp. 19–39, 2003.
- [8] S. Uvsløkk and H. Arnesen, "Thermal insulation performance of reflective material layers in well insulated timber frame structures," *8Th Symp. Build. Phys.*, 2008.
- [9] O. A. Ezekoye, "Conduction of Heat in Solids," *SFPE Handb. Fire Prot. Eng.*, vol. 5th Editio, pp. 25–52, 2015.
- [10] K. Livkiss, B. Andres, N. Johansson, and P. Van Hees, "Uncertainties in material thermal modelling of fire resistance tests," *Eur. Symp. Fire Saf. Sci.*, pp. 1–6, 2015.
- [11] M. A. Sultan, "Incident heat flux measurements in floor and wall furnaces of different sizes," *Fire Mater.*, vol. 30, no. 6, pp. 383–396, 2006.
- [12] C. Beyler, J. Beitel, N. Iwankiw, B. Lattimer, I. Hughes Associates, and N. F. P. Association, *Fire resistance testing for performance-based fire design of buildings*. 2007.
- [13] B. Park, *NFPA Standard for Smoke Control Systems 2012 Edition*. 2012.
- [14] W. Anis, "Commissioning the air barrier system," *ASHRAE J.*, vol. 47, no. 3, pp. 35–44, 2005.
- [15] R. Smith, "Passive fire protection," *Struct. Surv.*, vol. Vol. 11 Is, p. pp.142 – 149, 1993.
- [16] CertainTeed Saint Gobain, "Type X Gypsum Board." [Online]. Available: <http://www.certainteed.com/Products/313675>. [Accessed: 15-Apr-2016].
- [17] J. Lindholm, A. Brink, and M. Hupa, "Cone calorimeter – a tool for measuring heat release rate," *Finnish-Swedish Flame Days 2009*, p. 4B, 2009.
- [18] I. Rahmanian, "Thermal and Mechanical Properties of Gypsum Boards and Their Influences

- on Fire Resistance of Gypsum Board Based Systems,” 2011.
- [19] P. Keerthan and M. Mahendran, “Thermal Performance of Composite Panels Under Fire Conditions Using Numerical Studies: Plasterboards, Rockwool, Glass Fibre and Cellulose Insulations,” *Fire Technol.*, vol. 49, no. 2, pp. 329–356, 2013.
- [20] Andrew H. Buchanan, *Structural Design for Fire Safety*. 2001.
- [21] ENGINEERING TOOLBOX, “Air Properties.” [Online]. Available: [http://www.engineeringtoolbox.com/air-properties-d\\_156.html](http://www.engineeringtoolbox.com/air-properties-d_156.html). [Accessed: 06-Apr-2016].
- [22] THE ENGINEERING TOOLBOX, “Emissivity Coefficients of some common Materials,” 2016. [Online]. Available: [http://www.engineeringtoolbox.com/emissivity-coefficients-d\\_447.html](http://www.engineeringtoolbox.com/emissivity-coefficients-d_447.html). [Accessed: 06-Apr-2016].
- [23] A. Wolfenden, T. Harmathy, M. Sultan, and J. MacLaurin, “Comparison of Severity of Exposure in ASTM E 119 and ISO 834 Fire Resistance Tests,” *J. Test. Eval.*, vol. 15, no. January, pp. 371–375, 1987.
- [24] THE ENGINEERING TOOLBOX, “Thermal Conductivity of Materials and Gases.” [Online]. Available: [http://www.engineeringtoolbox.com/thermal-conductivity-d\\_429.html](http://www.engineeringtoolbox.com/thermal-conductivity-d_429.html). [Accessed: 27-Mar-2016].
- [25] ENGINEERING TOOLBOX, “Densities of Solids.” [Online]. Available: [http://www.engineeringtoolbox.com/density-solids-d\\_1265.html](http://www.engineeringtoolbox.com/density-solids-d_1265.html). [Accessed: 27-Mar-2016].
- [26] ENGINEERING TOOLBOX, “Solids - Specific Heats.” [Online]. Available: [http://www.engineeringtoolbox.com/specific-heat-solids-d\\_154.html](http://www.engineeringtoolbox.com/specific-heat-solids-d_154.html). [Accessed: 27-Mar-2016].
- [27] K. Mcgrattan and R. Mcdermott, “Fire Dynamics Simulator User ’ s Guide,” 2013.
- [28] D. Drysdale, “Fire Science and Combustion,” *An Introd. to Fire Dyn.*, pp. 1–34, 2011.
- [29] K. J. Overholt, “Simulation of a Fire in a Hillside Residential Structure - San Francisco , CA,” 1856.
- [30] M. Feng, Y. C. Wang, and J. M. Davies, “Thermal performance of cold-formed thin-walled steel panel systems in fire,” *Fire Saf. J.*, vol. 38, no. 4, pp. 365–394, 2003.
- [31] British Standards Institution, “Eurocode 1 — Actions on structures,” no. February, 2013.
- [32] A. Bruls and P. Vandeveldel, *Sécurité contre l ’ incendie dans les bâtiments*, Mai 2000. 1980.
- [33] M. A. Sultan, “A model for predicting heat transfer through noninsulated unloaded steel-stud gypsum board wall assemblies exposed to fire,” *Fire Technol.*, vol. 32, no. 3, pp. 239–

259, 1996.

## Appendix A: FDS script file

Following is the script file for the FDS furnace modeling with a very loose air tight construction leaking on one side:

```
&HEAD CHID='nrcc3'/ FURNACE TEST

FYI = 'Room and mesh definition',

&MESH ID='GRID',IJK=24,48,36,XB=0.0,2.4,-2.4,2.4,0.0,3.6/

&TIME T_END= 7200.0/ 2 hours standard fire

&MISC TMPA=20.,

&DUMP DT_DEVC=5/ DATAS EVERY 5 sec

//-----
-----//
//----- FUEL AND BURNERS PARAMETERS -----
-----//
//-----
-----//

//-- RADIATION --//

&RADI RADIATION=.TRUE.,RADIATIVE_FRACTION=0.3, NUMBER_RADIATION_ANGLES=104/

//-- FUEL DESCRIPTION --//

&REAC FUEL = 'PROPANE',

FYI = 'Propane, C_3 H_8',
C= 3.0,
H = 8.0,
O=0.0,
N=0.0,
SOOT_YIELD =0.01,
CO_YIELD =0.02,
HEAT_OF_COMBUSTION=46450.0,
IDEAL=.TRUE./

&SURF ID='FIRE',
HRRPUA=8000,
COLOR='RED'/ HRR in kW/m2

//-- BURNER PORTS --//
```



&VENT XB=0.2,0.2,0.1,0.2,1.6,1.7,SURF\_ID='FIRE' ,CTRL\_ID='VENT6' /  
&VENT XB=0.2,0.2,0.4,0.5,1.6,1.7,SURF\_ID='FIRE' , CTRL\_ID='VENT6' /  
&VENT XB=0.2,0.2,0.7,0.8,1.6,1.7,SURF\_ID='FIRE' , CTRL\_ID='VENT6' /  
&VENT XB=0.2,0.2,1.0,1.1,1.6,1.7,SURF\_ID='FIRE' , CTRL\_ID='VENT6' /  
&VENT XB=0.2,0.2,1.3,1.4,1.6,1.7,SURF\_ID='FIRE' , CTRL\_ID='VENT6' /

&VENT XB=0.2,0.2, -1.4, -1.3,1.9,2,SURF\_ID='FIRE' ,CTRL\_ID='VENT3' /  
&VENT XB=0.2,0.2, -1.1, -1.0,1.9,2,SURF\_ID='FIRE' ,CTRL\_ID='VENT3' /  
&VENT XB=0.2,0.2, -0.8, -0.7,1.9,2,SURF\_ID='FIRE' ,CTRL\_ID='VENT3' /  
&VENT XB=0.2,0.2, -0.5, -0.4,1.9,2,SURF\_ID='FIRE' ,CTRL\_ID='VENT3' /  
&VENT XB=0.2,0.2, -0.2, -0.1,1.9,2,SURF\_ID='FIRE' ,CTRL\_ID='VENT3' /  
&VENT XB=0.2,0.2,0.1,0.2,1.9,2,SURF\_ID='FIRE' , CTRL\_ID='VENT4' /  
&VENT XB=0.2,0.2,0.4,0.5,1.9,2,SURF\_ID='FIRE' ,CTRL\_ID='VENT4' /  
&VENT XB=0.2,0.2,0.7,0.8,1.9,2,SURF\_ID='FIRE' ,CTRL\_ID='VENT4' /  
&VENT XB=0.2,0.2,1.0,1.1,1.9,2,SURF\_ID='FIRE' ,CTRL\_ID='VENT4' /  
&VENT XB=0.2,0.2,1.3,1.4,1.9,2,SURF\_ID='FIRE' ,CTRL\_ID='VENT4' /

&VENT XB=0.2,0.2, -1.4, -1.3,2.2,2.3,SURF\_ID='FIRE' ,CTRL\_ID='VENT3' /  
&VENT XB=0.2,0.2, -1.1, -1.0,2.2,2.3,SURF\_ID='FIRE' ,CTRL\_ID='VENT3' /  
&VENT XB=0.2,0.2, -0.8, -0.7,2.2,2.3,SURF\_ID='FIRE' ,CTRL\_ID='VENT3' /  
&VENT XB=0.2,0.2, -0.5, -0.4,2.2,2.3,SURF\_ID='FIRE' ,CTRL\_ID='VENT3' /  
&VENT XB=0.2,0.2, -0.2, -0.1,2.2,2.3,SURF\_ID='FIRE' ,CTRL\_ID='VENT3' /  
&VENT XB=0.2,0.2,0.1,0.2,2.2,2.3,SURF\_ID='FIRE' ,CTRL\_ID='VENT4' /  
&VENT XB=0.2,0.2,0.4,0.5,2.2,2.3,SURF\_ID='FIRE' ,CTRL\_ID='VENT4' /  
&VENT XB=0.2,0.2,0.7,0.8,2.2,2.3,SURF\_ID='FIRE' ,CTRL\_ID='VENT4' /  
&VENT XB=0.2,0.2,1.0,1.1,2.2,2.3,SURF\_ID='FIRE' ,CTRL\_ID='VENT4' /  
&VENT XB=0.2,0.2,1.3,1.4,2.2,2.3,SURF\_ID='FIRE' ,CTRL\_ID='VENT4' /

&VENT XB=0.2,0.2, -1.4, -1.3,2.5,2.6,SURF\_ID='FIRE' ,CTRL\_ID='VENT3' /  
&VENT XB=0.2,0.2, -1.1, -1.0,2.5,2.6,SURF\_ID='FIRE' ,CTRL\_ID='VENT3' /  
&VENT XB=0.2,0.2, -0.8, -0.7,2.5,2.6,SURF\_ID='FIRE' ,CTRL\_ID='VENT3' /  
&VENT XB=0.2,0.2, -0.5, -0.4,2.5,2.6,SURF\_ID='FIRE' ,CTRL\_ID='VENT3' /  
&VENT XB=0.2,0.2, -0.2, -0.1,2.5,2.6,SURF\_ID='FIRE' ,CTRL\_ID='VENT3' /  
&VENT XB=0.2,0.2,0.1,0.2,2.5,2.6,SURF\_ID='FIRE' ,CTRL\_ID='VENT4' /  
&VENT XB=0.2,0.2,0.4,0.5,2.5,2.6,SURF\_ID='FIRE' ,CTRL\_ID='VENT4' /  
&VENT XB=0.2,0.2,0.7,0.8,2.5,2.6,SURF\_ID='FIRE' ,CTRL\_ID='VENT4' /  
&VENT XB=0.2,0.2,1.0,1.1,2.5,2.6,SURF\_ID='FIRE' ,CTRL\_ID='VENT4' /  
&VENT XB=0.2,0.2,1.3,1.4,2.5,2.6,SURF\_ID='FIRE' ,CTRL\_ID='VENT4' /

&VENT XB=0.2,0.2, -1.4, -1.3,2.8,2.9,SURF\_ID='FIRE' , CTRL\_ID='VENT3' /  
&VENT XB=0.2,0.2, -1.1, -1.0,2.8,2.9,SURF\_ID='FIRE' , CTRL\_ID='VENT3' /  
&VENT XB=0.2,0.2, -0.8, -0.7,2.8,2.9,SURF\_ID='FIRE' , CTRL\_ID='VENT3' /  
&VENT XB=0.2,0.2, -0.5, -0.4,2.8,2.9,SURF\_ID='FIRE' , CTRL\_ID='VENT3' /  
&VENT XB=0.2,0.2, -0.2, -0.1,2.8,2.9,SURF\_ID='FIRE' ,CTRL\_ID='VENT3' /  
&VENT XB=0.2,0.2,0.1,0.2,2.8,2.9,SURF\_ID='FIRE' ,CTRL\_ID='VENT4' /  
&VENT XB=0.2,0.2,0.4,0.5,2.8,2.9,SURF\_ID='FIRE' ,CTRL\_ID='VENT4' /  
&VENT XB=0.2,0.2,0.7,0.8,2.8,2.9,SURF\_ID='FIRE' , CTRL\_ID='VENT4' /  
&VENT XB=0.2,0.2,1.0,1.1,2.8,2.9,SURF\_ID='FIRE' , CTRL\_ID='VENT4' /  
&VENT XB=0.2,0.2,1.3,1.4,2.8,2.9,SURF\_ID='FIRE' , CTRL\_ID='VENT4' /

```
//-----  
-----//  
//----- MATERIALS AND SURFACE SETUP -----  
-----//  
//-----  
-----//
```

```
//-- SETTING UP MATERIALS --//
```

```
&MATL ID = 'MATL_FURNACE_WALL'  
CONDUCTIVITY = 0.34  
SPECIFIC_HEAT = 1  
DENSITY = 880 /
```

```
&MATL ID='COTTON PAD',  
EMISSIVITY = 0.8,  
DENSITY = 150,  
SPECIFIC_HEAT = 1.34,  
CONDUCTIVITY = 0.23,/
```

```
&MATL ID='CERAMIC BLANKET',  
EMISSIVITY = 0.8,  
DENSITY = 160,  
SPECIFIC_HEAT = 1.15,  
CONDUCTIVITY = 0.04,/
```

```
&MATL ID = 'ROCKWOOL',  
EMISSIVITY = 0.8,  
DENSITY = 711,
```

```
CONDUCTIVITY_RAMP = 'k_ramp1',
```

```
SPECIFIC_HEAT = 0.9,/
```

```
&RAMP ID='k_ramp1', T= 50., F=0.25 /  
&RAMP ID='k_ramp1', T=200., F=0.26 /  
&RAMP ID='k_ramp1', T=500., F=0.295 /  
&RAMP ID='k_ramp1', T=600., F=.42 /  
&RAMP ID='k_ramp1', T=700., F=.68 /  
&RAMP ID='k_ramp1', T=800., F=.94 /  
&RAMP ID='k_ramp1', T=900., F=1.2 /  
&RAMP ID='k_ramp1', T=1000., F=1.46 /  
&RAMP ID='k_ramp1', T=1200., F=1.98 /
```

```
&MATL ID = 'GYPSUM',  
EMISSIVITY = 0.8,  
DENSITY = 711,  
CONDUCTIVITY_RAMP = 'k_ramp2',
```

```
SPECIFIC_HEAT_RAMP = 'c_ramp2',/
```

```
&RAMP ID='c_ramp2', T= 20., F=1.000 /  
&RAMP ID='c_ramp2', T= 50., F=1.100 /  
&RAMP ID='c_ramp2', T= 100., F=1.500 /  
&RAMP ID='c_ramp2', T= 120., F=1.600 /  
&RAMP ID='c_ramp2', T= 140., F=2.100 /  
&RAMP ID='c_ramp2', T= 160., F=20.000 /  
&RAMP ID='c_ramp2', T= 170., F=7.000 /  
&RAMP ID='c_ramp2', T= 180., F=2.100 /  
&RAMP ID='c_ramp2', T= 200., F=9.000 /  
&RAMP ID='c_ramp2', T= 220., F=1.500 /  
&RAMP ID='c_ramp2', T= 260., F=1.100 /  
&RAMP ID='c_ramp2', T= 400., F=1.000 /  
&RAMP ID='c_ramp2', T= 430., F=.500 /  
&RAMP ID='c_ramp2', T= 450., F=.800 /  
&RAMP ID='c_ramp2', T= 500., F=.900 /  
&RAMP ID='c_ramp2', T= 600., F=1.000 /  
&RAMP ID='c_ramp2', T= 1200., F=1.000 /
```

```
&RAMP ID='k_ramp2', T= 20., F=0.17 /  
&RAMP ID='k_ramp2', T=50., F=0.17 /  
&RAMP ID='k_ramp2', T=100., F=0.18 /  
&RAMP ID='k_ramp2', T=150., F=0.195 /  
&RAMP ID='k_ramp2', T=200., F=0.195 /  
&RAMP ID='k_ramp2', T=250., F=0.197 /  
&RAMP ID='k_ramp2', T=300., F=0.2 /  
&RAMP ID='k_ramp2', T=350., F=0.21 /  
&RAMP ID='k_ramp2', T=400., F=0.22 /  
&RAMP ID='k_ramp2', T=450., F=0.22 /  
&RAMP ID='k_ramp2', T=500., F=0.23 /  
&RAMP ID='k_ramp2', T=550., F=0.24 /  
&RAMP ID='k_ramp2', T=600., F=0.24 /  
&RAMP ID='k_ramp2', T=650., F=0.26 /  
&RAMP ID='k_ramp2', T=700., F=0.28 /  
&RAMP ID='k_ramp2', T=1200., F=0.28 /
```

```
&MATL ID = 'MATL_MIN_WOOL_300'  
CONDUCTIVITY = 0.037  
SPECIFIC_HEAT = 0.8  
DENSITY = 300 /
```

```
&MATL ID = 'MATL_NICKEL'  
CONDUCTIVITY = 90.9  
SPECIFIC_HEAT = 0.44  
DENSITY = 8908 /
```

```
//-- SETTING UP SURFACES --//
```

```
&SURF ID = 'FURNACEWALLS',
DEFAULT=.TRUE.,
MATL_ID='CERAMIC BLANKET',
BACKING = 'INSULATED',
COLOR='BROWN',
Transparency=0.1,
THICKNESS= 0.5,/
```

```
&SURF ID = 'COTTON PAD',
DEFAULT=.TRUE.,
MATL_ID='COTTON PAD',
BACKING = 'INSULATED',
COLOR='WHITE',
THICKNESS= 0.03,/
```

```
&SURF ID = 'DRYWALL INSULATED',
DEFAULT=.TRUE.,
MATL_ID = 'GYPSUM', 'ROCKWOOL', 'GYPSUM',
BACKING = 'EXPOSED',
COLOR='GRAY',
THICKNESS = 0.025,0.045,0.025/
```

```
&SURF ID = 'PLATE_THERMOMETER'
MATL_ID(1,1) = 'MATL_NICKEL'
MATL_ID(2,1) = 'MATL_MIN_WOOL_300'
MATL_ID(3,1) = 'MATL_NICKEL'
BACKING = 'EXPOSED'
EMISSIVITY_BACK = 0.80
THICKNESS = 0.0007,0.097,0.0007 /
```

```
//-----
-----//
//----- ROOM SET UP -----
-----//
//-----
-----//
```

```
//-- FURNACE --//
```

```
FYI = 'Walls for the furnace from 0,2 to 0,8=0,60 from -1.8 to 1.8 =3,6 and
from 0.2 to 3.3 = 3,1',
```

```
&OBST XB=0.2,0.8,1.8,1.9,0.0,3.4,SURF_ID='FURNACEWALLS',/ SIDE WALL&OBST
XB=0.2,0.8,-1.8,-1.9,0.0,3.4,SURF_ID='FURNACEWALLS',/ SIDE WALL
&OBST XB=0.1,0.2,-1.9,1.9,0.0,3.4,SURF_ID='FURNACEWALLS'/ BACK WALL
```

```

&OBST XB=0.2,0.8,-1.8,1.8,0.1,0.2,SURF_ID='FURNACEWALLS' / FLOOR
&OBST XB=0.2,0.8,-1.8,1.8,3.3,3.4,SURF_ID='FURNACEWALLS' / CEILING

//-- SMOKE AND HEAT STOPER --//

&OBST XB=0.7,0.8,1.9,2.4,-0.6,3.6/
&OBST XB=0.7,0.8,-1.9,-2.4,-0.6,3.6/
&OBST XB=0.7,0.8,-1.9,1.9,-0.6,0.1/
&OBST XB=0.7,0.8,-1.9,1.9,3.4,3.6/

//-- TEST SAMPLE --//

FYI = 'Fire barrier',

&OBST XB=0.7,0.8,-1.8,1.8,0.2,3.3,SURF_ID='DRYWALL INSULATED' /

//-- COTTON PAD --//

&OBST XB=0.9,1.0,-1.7,-1.8,3.2,3.3,SURF_ID='COTTON PAD' / 1
&OBST XB=0.9,1.0,-1.7,-1.8,1.6,1.7,SURF_ID='COTTON PAD' / 2
&OBST XB=0.9,1.0,-1.7,-1.8,0.2,0.3,SURF_ID='COTTON PAD' / 3

//-- LEAKAGE --//

&VENT XB=0.7,0.7,-1.7,-1.8,0.2,3.3, SURF_ID='HVAC',ID='IN' /
&VENT XB=0.8,0.8,-1.7,-1.8,0.2,3.3, SURF_ID='HVAC',ID='OUT' /

&HVAC ID='IN',TYPE_ID='NODE',DUCT_ID='DUCT1',VENT_ID='IN' /
&HVAC ID='OUT',TYPE_ID='NODE',DUCT_ID='DUCT1',VENT_ID='OUT' /
&HVAC ID='DUCT1',TYPE_ID='DUCT',NODE_ID='IN','OUT',LENGTH=0.075
,AREA=0.014508,LOSS=1.,1./

//-- SMOKE EXCTRACTION --//

&HOLE XB=0.2,0.6,1.8,-1.8,0.1,0.2, / EXHAUST UNDER FURNACE

&HOLE XB=0.2,0.6,1.8,-1.8,3.2,3.4, CTRL_ID='EXHAUST1' / CONTROLLED EXHAUST TOP
FURNACE

//-- VENTING THE ROOM --//

&VENT MB='XMIN', SURF_ID='OPEN' /
&VENT MB='XMAX', SURF_ID='OPEN' /
&VENT MB='YMIN', SURF_ID='OPEN' /
&VENT MB='YMAX', SURF_ID='OPEN' /
&VENT MB='ZMAX', SURF_ID='OPEN' /
&VENT MB='ZMIN', SURF_ID='OPEN' /

//-- PLATE THERMOMETER OBSTRUCTION --//

```

```

&OBST XB=0.5,0.6,0.8,0.9,0.6,0.7, SURF_ID='PLATE_THERMOMETER' /
&OBST XB=0.5,0.6,-0.8,-0.9,0.6,0.7, SURF_ID='PLATE_THERMOMETER' /
&OBST XB=0.5,0.6,0.8,0.9,2.5,2.6, SURF_ID='PLATE_THERMOMETER' /
&OBST XB=0.5,0.6,-0.8,-0.9,2.5,2.6, SURF_ID='PLATE_THERMOMETER' /
&OBST XB=0.5,0.6,0.0,0.1,1.7,1.8, SURF_ID='PLATE_THERMOMETER' /

//-----
-----//
//----- CONTROLS -----
-----//
//-----
-----//

//-- PRESSURE CONTROL --//

&CTRL ID='EXHAUST1', FUNCTION_TYPE='DEADBAND', INPUT_ID='PRESSUREDEV',
ON_BOUND='UPPER', SETPOINT=28,30, LATCH=.FALSE., INITIAL_STATE=.FALSE./

//-- OXYGEN CONTROL --//

&SPEC ID='OXYGEN' / DEFINE THE OXYGEN
&SURF ID='SUPPLY',SPEC_ID='AIR', MASS_FLUX=1.0,TMP_FRONT=1050. ,
COLOR='BLUE',Transparency=0.1, RAMP_T='RAMP_ISO', / SPECIFY THE QUANTITY OF
OXYGEN INPUT kg/s
&DEVX XB=0.2,0.7,-1.8,1.8,0.2,3.2, QUANTITY='MASS FRACTION',SPEC_ID='OXYGEN',
ID='OXY', STATISTICS='MEAN' /
&CTRL ID='OXYGEN', FUNCTION_TYPE='DEADBAND', INPUT_ID='OXY',
ON_BOUND='LOWER', SETPOINT=0.18,0.20, LATCH=.FALSE.,INITIAL_STATE=.FALSE./
CONTROL THE OXYGEN LEVEL

&VENT XB=0.2,0.2,-1.8,1.8,0.8,1.0,SURF_ID='SUPPLY', CTRL_ID='OXYGEN' / SURFACE
OXYGEN IN
&VENT XB=0.2,0.2,-1.8,1.8,1.1,1.3,SURF_ID='SUPPLY', CTRL_ID='OXYGEN' / SURFACE
OXYGEN IN
&VENT XB=0.2,0.2,-1.8,1.8,1.4,1.6,SURF_ID='SUPPLY', CTRL_ID='OXYGEN' / SURFACE
OXYGEN IN
&VENT XB=0.2,0.2,-1.8,1.8,0.5,0.7,SURF_ID='SUPPLY', CTRL_ID='OXYGEN' / SURFACE
OXYGEN IN
&VENT XB=0.2,0.2,-1.8,1.8,1.7,1.9,SURF_ID='SUPPLY', CTRL_ID='OXYGEN' / SURFACE
OXYGEN IN
&VENT XB=0.2,0.2,-1.8,1.8,2.0,2.2,SURF_ID='SUPPLY', CTRL_ID='OXYGEN' / SURFACE
OXYGEN IN
&VENT XB=0.2,0.2,-1.8,1.8,2.3,2.5,SURF_ID='SUPPLY', CTRL_ID='OXYGEN' / SURFACE
OXYGEN IN
&VENT XB=0.2,0.2,-1.8,1.8,2.6,2.8,SURF_ID='SUPPLY', CTRL_ID='OXYGEN' / SURFACE
OXYGEN IN

//--TEMPERATURE CONTROL--//

```

```
/-- Hot plate in temperature control room at temperature of ISO-curve --/  
  
&SURF ID='HOT_PLATE1', TMP_FRONT=1050. , COLOR='RED', RAMP_T='RAMP_ISO', /  
&OBST XB=2.2,2.4,-0.1,0.1,3.3,3.5, SURF_ID='HOT_PLATE1' /  
&DEVC XYZ=2.3,0.0,3.4, QUANTITY='WALL TEMPERATURE', ID='TEMP_ISO1', IOR=3 /
```

```
/-- ISO Time-temp-curve --/
```

```
&RAMP ID='RAMP_ISO', T= 0000 ,F= 0 /  
&RAMP ID='RAMP_ISO', T= 0001 ,F= 0.018224171 /  
&RAMP ID='RAMP_ISO', T= 0002 ,F= 0.034418995 /  
&RAMP ID='RAMP_ISO', T= 0003 ,F= 0.048991481 /  
&RAMP ID='RAMP_ISO', T= 0004 ,F= 0.062237275 /  
&RAMP ID='RAMP_ISO', T= 0005 ,F= 0.074377916 /  
&RAMP ID='RAMP_ISO', T= 0006 ,F= 0.085583701 /  
&RAMP ID='RAMP_ISO', T= 0007 ,F= 0.095988364 /  
&RAMP ID='RAMP_ISO', T= 0008 ,F= 0.105698851 /  
&RAMP ID='RAMP_ISO', T= 0009 ,F= 0.114802024 /  
&RAMP ID='RAMP_ISO', T= 0010 ,F= 0.123369397 /  
&RAMP ID='RAMP_ISO', T= 0011 ,F= 0.131460553 /  
&RAMP ID='RAMP_ISO', T= 0012 ,F= 0.139125656 /  
&RAMP ID='RAMP_ISO', T= 0013 ,F= 0.14640734 /  
&RAMP ID='RAMP_ISO', T= 0014 ,F= 0.153342143 /  
&RAMP ID='RAMP_ISO', T= 0015 ,F= 0.159961617 /  
&RAMP ID='RAMP_ISO', T= 0016 ,F= 0.166293194 /  
&RAMP ID='RAMP_ISO', T= 0017 ,F= 0.172360878 /  
&RAMP ID='RAMP_ISO', T= 0018 ,F= 0.178185788 /  
&RAMP ID='RAMP_ISO', T= 0019 ,F= 0.183786607 /  
&RAMP ID='RAMP_ISO', T= 0020 ,F= 0.18917994 /  
&RAMP ID='RAMP_ISO', T= 0022 ,F= 0.199401914 /  
&RAMP ID='RAMP_ISO', T= 0024 ,F= 0.208953097 /  
&RAMP ID='RAMP_ISO', T= 0026 ,F= 0.217916132 /  
&RAMP ID='RAMP_ISO', T= 0030 ,F= 0.234339533 /  
&RAMP ID='RAMP_ISO', T= 0032 ,F= 0.241905044 /  
&RAMP ID='RAMP_ISO', T= 0034 ,F= 0.249096794 /  
&RAMP ID='RAMP_ISO', T= 0036 ,F= 0.255949981 /  
&RAMP ID='RAMP_ISO', T= 0038 ,F= 0.262495053 /  
&RAMP ID='RAMP_ISO', T= 0040 ,F= 0.268758528 /  
&RAMP ID='RAMP_ISO', T= 0045 ,F= 0.283331013 /  
&RAMP ID='RAMP_ISO', T= 0050 ,F= 0.296576808 /  
&RAMP ID='RAMP_ISO', T= 0055 ,F= 0.308717449 /  
&RAMP ID='RAMP_ISO', T= 0060 ,F= 0.319923233 /  
&RAMP ID='RAMP_ISO', T= 0065 ,F= 0.330327897 /  
&RAMP ID='RAMP_ISO', T= 0070 ,F= 0.340038383 /  
&RAMP ID='RAMP_ISO', T= 0075 ,F= 0.349141556 /  
&RAMP ID='RAMP_ISO', T= 0080 ,F= 0.357708929 /  
&RAMP ID='RAMP_ISO', T= 0090 ,F= 0.373465189 /  
&RAMP ID='RAMP_ISO', T= 0100 ,F= 0.387681676 /  
&RAMP ID='RAMP_ISO', T= 0110 ,F= 0.400632727 /  
&RAMP ID='RAMP_ISO', T= 0120 ,F= 0.41252532 /
```

&RAMP ID='RAMP\_ISO', T= 0130 ,F= 0.423519472 /  
&RAMP ID='RAMP\_ISO', T= 0140 ,F= 0.433741447 /  
&RAMP ID='RAMP\_ISO', T= 0150 ,F= 0.44329263 /  
&RAMP ID='RAMP\_ISO', T= 0175 ,F= 0.4647436 /  
&RAMP ID='RAMP\_ISO', T= 0200 ,F= 0.483436327 /  
&RAMP ID='RAMP\_ISO', T= 0225 ,F= 0.5 /  
&RAMP ID='RAMP\_ISO', T= 0250 ,F= 0.514870395 /  
&RAMP ID='RAMP\_ISO', T= 0275 ,F= 0.52836183 /  
&RAMP ID='RAMP\_ISO', T= 0300 ,F= 0.540708489 /  
&RAMP ID='RAMP\_ISO', T= 0325 ,F= 0.552089541 /  
&RAMP ID='RAMP\_ISO', T= 0350 ,F= 0.562645128 /  
&RAMP ID='RAMP\_ISO', T= 0375 ,F= 0.572486937 /  
&RAMP ID='RAMP\_ISO', T= 0400 ,F= 0.581705416 /  
&RAMP ID='RAMP\_ISO', T= 0425 ,F= 0.590374842 /  
&RAMP ID='RAMP\_ISO', T= 0450 ,F= 0.598556957 /  
&RAMP ID='RAMP\_ISO', T= 0500 ,F= 0.61365891 /  
&RAMP ID='RAMP\_ISO', T= 0550 ,F= 0.627340643 /  
&RAMP ID='RAMP\_ISO', T= 0600 ,F= 0.639846466 /  
&RAMP ID='RAMP\_ISO', T= 0650 ,F= 0.651362611 /  
&RAMP ID='RAMP\_ISO', T= 0700 ,F= 0.662034297 /  
&RAMP ID='RAMP\_ISO', T= 0750 ,F= 0.671976953 /  
&RAMP ID='RAMP\_ISO', T= 0800 ,F= 0.681283848 /  
&RAMP ID='RAMP\_ISO', T= 0900 ,F= 0.698283112 /  
&RAMP ID='RAMP\_ISO', T= 1000 ,F= 0.713503572 /  
&RAMP ID='RAMP\_ISO', T= 1100 ,F= 0.727282483 /  
&RAMP ID='RAMP\_ISO', T= 1200 ,F= 0.739869438 /  
&RAMP ID='RAMP\_ISO', T= 1300 ,F= 0.75145434 /  
&RAMP ID='RAMP\_ISO', T= 1400 ,F= 0.762185039 /  
&RAMP ID='RAMP\_ISO', T= 1600 ,F= 0.78153064 /  
&RAMP ID='RAMP\_ISO', T= 1800 ,F= 0.798604742 /  
&RAMP ID='RAMP\_ISO', T= 2000 ,F= 0.813885156 /  
&RAMP ID='RAMP\_ISO', T= 2200 ,F= 0.827713176 /  
&RAMP ID='RAMP\_ISO', T= 2400 ,F= 0.840341093 /  
&RAMP ID='RAMP\_ISO', T= 2600 ,F= 0.851960683 /  
&RAMP ID='RAMP\_ISO', T= 2800 ,F= 0.862721133 /  
&RAMP ID='RAMP\_ISO', T= 3000 ,F= 0.872740792 /  
&RAMP ID='RAMP\_ISO', T= 3400 ,F= 0.89092224 /  
&RAMP ID='RAMP\_ISO', T= 3800 ,F= 0.907083325 /  
&RAMP ID='RAMP\_ISO', T= 4200 ,F= 0.921628493 /  
&RAMP ID='RAMP\_ISO', T= 4600 ,F= 0.934851717 /  
&RAMP ID='RAMP\_ISO', T= 5000 ,F= 0.946973396 /  
&RAMP ID='RAMP\_ISO', T= 5500 ,F= 0.960831049 /  
&RAMP ID='RAMP\_ISO', T= 6000 ,F= 0.973483672 /  
&RAMP ID='RAMP\_ISO', T= 6500 ,F= 0.985124174 /  
&RAMP ID='RAMP\_ISO', T= 7000 ,F= 0.995902555 /  
&RAMP ID='RAMP\_ISO', T= 7200 ,F= 1 /  
&RAMP ID='RAMP\_ISO', T= 7300 ,F= 1 /

//-- Control of heater in furnace --//

```

&CTRL ID='VENT1', FUNCTION_TYPE='SUBTRACT',
INPUT_ID='TEMP_IS01','PLATE_T_01', SETPOINT=0,
LATCH=.FALSE., INITIAL_STATE=.TRUE.,TRIP_DIRECTION=-1 /
&CTRL ID='VENT2', FUNCTION_TYPE='SUBTRACT',
INPUT_ID='TEMP_IS01','PLATE_T_02', SETPOINT=0,
LATCH=.FALSE., INITIAL_STATE=.TRUE. ,TRIP_DIRECTION=-1/
&CTRL ID='VENT3', FUNCTION_TYPE='SUBTRACT',
INPUT_ID='TEMP_IS01','PLATE_T_03', SETPOINT=0,
LATCH=.FALSE., INITIAL_STATE=.TRUE.,TRIP_DIRECTION=-1 /
&CTRL ID='VENT4', FUNCTION_TYPE='SUBTRACT',
INPUT_ID='TEMP_IS01','PLATE_T_04', SETPOINT=0,
LATCH=.FALSE., INITIAL_STATE=.TRUE.,TRIP_DIRECTION=-1 /
&CTRL ID='VENT6', FUNCTION_TYPE='SUBTRACT',
INPUT_ID='TEMP_IS01','PLATE_T_05', SETPOINT=0,
LATCH=.FALSE., INITIAL_STATE=.TRUE.,TRIP_DIRECTION=-1 /

```

```

//-----
-----//
//----- MEASUREMENTS -----
-----//
//-----
-----//

```

```

//-- AVERAGE TEMPERATURE INSIDE FURNACE --//

```

```

&DEVC XB=0.2,0.7,-1.8,1.8,0.2,3.2,
QUANTITY='TEMPERATURE',ID='TEMP_FURN_TOP_AVE', STATISTICS='MEAN' /

```

```

//-- INSTRUMENT --//

```

```

&PROP ID='TC18', BEAD_DIAMETER=0.001245/
&PROP ID='HF18', BEAD_DIAMETER=0.025/

```

```

//-- PLATE THERMOMETER --//

```

```

&DEVC XYZ=0.55,0.85,0.65, QUANTITY='WALL TEMPERATURE', ID='PLATE_T_01', IOR=-
1 /
&DEVC XYZ=0.55,-0.85,0.65, QUANTITY='WALL TEMPERATURE', ID='PLATE_T_02',
IOR=-1 /
&DEVC XYZ=0.55,-0.85,2.55, QUANTITY='WALL TEMPERATURE', ID='PLATE_T_03',
IOR=-1 /
&DEVC XYZ=0.55,0.85,2.55, QUANTITY='WALL TEMPERATURE', ID='PLATE_T_04', IOR=-
1 /
&DEVC XYZ=0.55,0.05,1.75, QUANTITY='WALL TEMPERATURE', ID='PLATE_T_05', IOR=-
1 /

```

```

//-- GAUGE HEAT FLUX --//

```

```
&DEVC XYZ=0.55,0.85,0.65, QUANTITY='GAUGE HEAT FLUX', ID='PLATE_GAUGE_HF_01',  
PROP_ID='HF18',IOR=-1 /  
&DEVC XYZ=0.55,-0.85,0.65, QUANTITY='GAUGE HEAT FLUX',  
ID='PLATE_GAUGE_HF_02', PROP_ID='HF18' ,IOR=-1 /  
&DEVC XYZ=0.55,-0.85,2.55, QUANTITY='GAUGE HEAT FLUX',  
ID='PLATE_GAUGE_HF_03', PROP_ID='HF18', IOR=-1 /  
&DEVC XYZ=0.55,0.85,2.55, QUANTITY='GAUGE HEAT FLUX', ID='PLATE_GAUGE_HF_04',  
PROP_ID='HF18',IOR=-1 /  
&DEVC XYZ=0.55,0.05,1.75, QUANTITY='GAUGE HEAT FLUX', ID='PLATE_GAUGE_HF_05',  
PROP_ID='HF18', IOR=-1 /
```

```
//-- DEVICES --//
```

```
&PROP ID='TC18', BEAD_DIAMETER=0.001245/  
&PROP ID='HF18', BEAD_DIAMETER=0.025/
```

```
//-- WALL TEMPERATURE --//
```

```
&DEVC ID='TC_OUT_1',XYZ=0.8,0.6,0.5, QUANTITY='WALL TEMPERATURE' ,IOR=1/  
OUTSIDE WALL SURFACE TEMPERATURE  
&DEVC ID='TC_OUT_2',XYZ=0.8,-0.6,0.5, QUANTITY='WALL TEMPERATURE',IOR=1/  
OUTSIDE WALL SURFACE TEMPERATURE  
&DEVC ID='TC_OUT_3',XYZ=0.8,-0.6,2.4, QUANTITY='WALL TEMPERATURE',IOR=1/  
OUTSIDE WALL SURFACE TEMPERATURE  
&DEVC ID='TC_OUT_4',XYZ=0.8,0.6,2.4, QUANTITY='WALL TEMPERATURE' ,IOR=1/  
OUTSIDE WALL SURFACE TEMPERATURE  
&DEVC ID='TC_OUT_5',XYZ=0.8,0,1.6, QUANTITY='WALL TEMPERATURE' ,IOR=1/  
OUTSIDE WALL SURFACE TEMPERATURE
```

```
&DEVC ID='TC_IN_1',XYZ=0.7,0.6,0.5, QUANTITY='WALL TEMPERATURE' ,IOR=-1/  
OUTSIDE WALL SURFACE TEMPERATURE  
&DEVC ID='TC_IN_2',XYZ=0.7,-0.6,0.5, QUANTITY='WALL TEMPERATURE' ,IOR=-1/  
OUTSIDE WALL SURFACE TEMPERATURE  
&DEVC ID='TC_IN_3',XYZ=0.7,-0.6,2.4, QUANTITY='WALL TEMPERATURE' ,IOR=-1/  
OUTSIDE WALL SURFACE TEMPERATURE  
&DEVC ID='TC_IN_4',XYZ=0.7,0.6,2.4, QUANTITY='WALL TEMPERATURE' ,IOR=-1/  
OUTSIDE WALL SURFACE TEMPERATURE  
&DEVC ID='TC_IN_5',XYZ=0.7,0,1.6, QUANTITY='WALL TEMPERATURE' ,IOR=-1/  
OUTSIDE WALL SURFACE TEMPERATURE
```

```
//-- TEMPERATURE INSIDE WALL --//
```

```
&DEVC XYZ=0.7,0,1.5, QUANTITY='INSIDE WALL TEMPERATURE', DEPTH=0.005,  
IOR=1,ID='Temp 5 mm'/  
&DEVC XYZ=0.7,0,1.5, QUANTITY='INSIDE WALL TEMPERATURE', DEPTH=0.010,  
IOR=1,ID='Temp 10 mm'/  
&DEVC XYZ=0.7,0,1.5, QUANTITY='INSIDE WALL TEMPERATURE', DEPTH=0.040,  
IOR=1,ID='Temp 40 mm'/
```

```

&DEVC XYZ=0.7,0,1.5, QUANTITY='INSIDE WALL TEMPERATURE', DEPTH=0.062,
IOR=1,ID='Temp 62 mm'/

/-- COTTON PAD RADIATION TEMPERATURE READING --//

&DEVC ID='COTTON PAD RADIATIVE HEAT FLUX', QUANTITY='RADIATIVE HEAT FLUX',
XYZ=0.9,-1.75,3.25, IOR=-1/
&DEVC ID='COTTON PAD SURFACE TEMPERATURE', QUANTITY='WALL TEMPERATURE',
XYZ=0.9,-1.75,3.25, IOR=-1, /
&DEVC ID='Temp inside cotton 15 mm', QUANTITY='INSIDE WALL
TEMPERATURE', XYZ=0.9,-1.75,3.25, DEPTH=0.005, IOR=-1,/

&DEVC ID='COTTON PAD RADIATIVE HEAT FLUX 2', QUANTITY='RADIATIVE HEAT
FLUX', XYZ=0.9,-1.75,1.65, IOR=-1/
&DEVC ID='COTTON PAD SURFACE TEMPERATURE 2', QUANTITY='WALL TEMPERATURE',
XYZ=0.9,-1.75,1.65, IOR=-1, /
&DEVC ID='Temp inside cotton 15 mm 2', QUANTITY='INSIDE WALL
TEMPERATURE', XYZ=0.9,-1.75,1.65, DEPTH=0.005, IOR=-1,/

&DEVC ID='COTTON PAD RADIATIVE HEAT FLUX 3', QUANTITY='RADIATIVE HEAT
FLUX', XYZ=0.9,-1.75,0.25, IOR=-1/
&DEVC ID='COTTON PAD SURFACE TEMPERATURE 3', QUANTITY='WALL TEMPERATURE',
XYZ=0.9,-1.75,0.25, IOR=-1, /
&DEVC ID='Temp inside cotton 15 mm 3', QUANTITY='INSIDE WALL
TEMPERATURE', XYZ=0.9,-1.75,0.25, DEPTH=0.005, IOR=-1,/

/-- VELOCITY READING --//

&DEVC ID='Velocity', QUANTITY='DUCT VELOCITY',DUCT_ID='DUCT1'/
&DEVC ID='Velocity', QUANTITY='DUCT VOLUME FLOW',DUCT_ID='DUCT1'/

/-- PRESSURE READING --//

&DEVC XYZ=0.7,0.0,3.2 QUANTITY='PRESSURE', /

&DEVC XB=0.2,0.7,-1.8,1.8,3.0,3.2, QUANTITY='PRESSURE',ID='PRESSUREDEV',
STATISTICS='MEAN' /

/-- SLICE FILE --//

&SLCF PBY=0.0, QUANTITY='TEMPERATURE'/
&SLCF PBY=0.0, QUANTITY='VELOCITY',VECTOR=.TRUE./
&SLCF PBZ=0.0, QUANTITY='PRESSURE' /

/-- BOUNDARY FILE --//

&BNDF QUANTITY='RADIATIVE HEAT FLUX'/

```

&BNDF QUANTITY='RADIOMETER'/  
&BNDF QUANTITY='WALL TEMPERATURE'/

&TAIL/

## Appendix B: ABAQUS script file

Following is a sample of the INP code from ABAQUS for the partition type A insulated with stone wool. The mesh used for this INP file is coarse in order to keep the appendix short.

\*Heading

\*\* Job name: 2x13mmROCKWOOLcode Model name: Model-1

\*\* Generated by: Abaqus/CAE 6.14-2

\*Preprint, echo=NO, model=NO, history=NO, contact=NO

\*\*

\*\* PARTS

\*\*

\*Part, name="C studs"

\*Node

1,	-0.0130000003,	0.0259117652,	0.
2,	0.0185000002,	0.0259117652,	0.
3,	-0.0130000003,	0.0264117643,	0.
4,	0.0189999994,	0.0264117643,	0.
5,	0.0189999994,	-0.0235882346,	0.
6,	-0.0130000003,	-0.0235882346,	0.
7,	-0.0130000003,	-0.0227882359,	0.
8,	0.0185000002,	-0.0227882359,	0.
9,	0.0189999994,	0.00141176477,	0.
10,	0.0185000002,	0.00156176474,	0.
11,	-0.0130000003,	0.0259117652,	0.501666665
12,	0.0185000002,	0.0259117652,	0.501666665

13, -0.0130000003, 0.0264117643, 0.501666665  
14, 0.0189999994, 0.0264117643, 0.501666665  
15, 0.0189999994, -0.0235882346, 0.501666665  
16, -0.0130000003, -0.0235882346, 0.501666665  
17, -0.0130000003, -0.0227882359, 0.501666665  
18, 0.0185000002, -0.0227882359, 0.501666665  
19, 0.0189999994, 0.00141176477, 0.501666665  
20, 0.0185000002, 0.00156176474, 0.501666665  
21, -0.0130000003, 0.0259117652, 1.00333333  
22, 0.0185000002, 0.0259117652, 1.00333333  
23, -0.0130000003, 0.0264117643, 1.00333333  
24, 0.0189999994, 0.0264117643, 1.00333333  
25, 0.0189999994, -0.0235882346, 1.00333333  
26, -0.0130000003, -0.0235882346, 1.00333333  
27, -0.0130000003, -0.0227882359, 1.00333333  
28, 0.0185000002, -0.0227882359, 1.00333333  
29, 0.0189999994, 0.00141176477, 1.00333333  
30, 0.0185000002, 0.00156176474, 1.00333333  
31, -0.0130000003, 0.0259117652, 1.505  
32, 0.0185000002, 0.0259117652, 1.505  
33, -0.0130000003, 0.0264117643, 1.505  
34, 0.0189999994, 0.0264117643, 1.505  
35, 0.0189999994, -0.0235882346, 1.505  
36, -0.0130000003, -0.0235882346, 1.505

37, -0.0130000003, -0.0227882359, 1.505  
38, 0.0185000002, -0.0227882359, 1.505  
39, 0.0189999994, 0.00141176477, 1.505  
40, 0.0185000002, 0.00156176474, 1.505  
41, -0.0130000003, 0.0259117652, 2.00666666  
42, 0.0185000002, 0.0259117652, 2.00666666  
43, -0.0130000003, 0.0264117643, 2.00666666  
44, 0.0189999994, 0.0264117643, 2.00666666  
45, 0.0189999994, -0.0235882346, 2.00666666  
46, -0.0130000003, -0.0235882346, 2.00666666  
47, -0.0130000003, -0.0227882359, 2.00666666  
48, 0.0185000002, -0.0227882359, 2.00666666  
49, 0.0189999994, 0.00141176477, 2.00666666  
50, 0.0185000002, 0.00156176474, 2.00666666  
51, -0.0130000003, 0.0259117652, 2.50833344  
52, 0.0185000002, 0.0259117652, 2.50833344  
53, -0.0130000003, 0.0264117643, 2.50833344  
54, 0.0189999994, 0.0264117643, 2.50833344  
55, 0.0189999994, -0.0235882346, 2.50833344  
56, -0.0130000003, -0.0235882346, 2.50833344  
57, -0.0130000003, -0.0227882359, 2.50833344  
58, 0.0185000002, -0.0227882359, 2.50833344  
59, 0.0189999994, 0.00141176477, 2.50833344  
60, 0.0185000002, 0.00156176474, 2.50833344

61, -0.0130000003, 0.0259117652, 3.00999999  
62, 0.0185000002, 0.0259117652, 3.00999999  
63, -0.0130000003, 0.0264117643, 3.00999999  
64, 0.0189999994, 0.0264117643, 3.00999999  
65, 0.0189999994, -0.0235882346, 3.00999999  
66, -0.0130000003, -0.0235882346, 3.00999999  
67, -0.0130000003, -0.0227882359, 3.00999999  
68, 0.0185000002, -0.0227882359, 3.00999999  
69, 0.0189999994, 0.00141176477, 3.00999999  
70, 0.0185000002, 0.00156176474, 3.00999999

\*Element, type=DC3D8

1, 4, 3, 1, 2, 14, 13, 11, 12  
2, 10, 8, 5, 9, 20, 18, 15, 19  
3, 7, 6, 5, 8, 17, 16, 15, 18  
4, 4, 2, 10, 9, 14, 12, 20, 19  
5, 14, 13, 11, 12, 24, 23, 21, 22  
6, 20, 18, 15, 19, 30, 28, 25, 29  
7, 17, 16, 15, 18, 27, 26, 25, 28  
8, 14, 12, 20, 19, 24, 22, 30, 29  
9, 24, 23, 21, 22, 34, 33, 31, 32  
10, 30, 28, 25, 29, 40, 38, 35, 39  
11, 27, 26, 25, 28, 37, 36, 35, 38  
12, 24, 22, 30, 29, 34, 32, 40, 39  
13, 34, 33, 31, 32, 44, 43, 41, 42

```

14, 40, 38, 35, 39, 50, 48, 45, 49
15, 37, 36, 35, 38, 47, 46, 45, 48
16, 34, 32, 40, 39, 44, 42, 50, 49
17, 44, 43, 41, 42, 54, 53, 51, 52
18, 50, 48, 45, 49, 60, 58, 55, 59
19, 47, 46, 45, 48, 57, 56, 55, 58
20, 44, 42, 50, 49, 54, 52, 60, 59
21, 54, 53, 51, 52, 64, 63, 61, 62
22, 60, 58, 55, 59, 70, 68, 65, 69
23, 57, 56, 55, 58, 67, 66, 65, 68
24, 54, 52, 60, 59, 64, 62, 70, 69

*Nset, nset=Set-21, generate

  1, 70, 1

*Elset, elset=Set-21, generate

  1, 24, 1

** Section: STEEL

*Solid Section, elset=Set-21, material=STEEL

,

*End Part

**

*Part, name="C- Studs Bottom Top"

*Node

  1, -0.0130000003, 0.0259117652, 0.

  2, 0.0185000002, 0.0259117652, 0.

```

3, -0.0130000003, 0.0264117643, 0.  
4, 0.0189999994, 0.0264117643, 0.  
5, 0.0189999994, -0.0235882346, 0.  
6, -0.0130000003, -0.0235882346, 0.  
7, -0.0130000003, -0.0227882359, 0.  
8, 0.0185000002, -0.0227882359, 0.  
9, 0.0189999994, 0.00141176477, 0.  
10, 0.0185000002, 0.00156176474, 0.  
11, -0.0130000003, 0.0259117652, 0.515714288  
12, 0.0185000002, 0.0259117652, 0.515714288  
13, -0.0130000003, 0.0264117643, 0.515714288  
14, 0.0189999994, 0.0264117643, 0.515714288  
15, 0.0189999994, -0.0235882346, 0.515714288  
16, -0.0130000003, -0.0235882346, 0.515714288  
17, -0.0130000003, -0.0227882359, 0.515714288  
18, 0.0185000002, -0.0227882359, 0.515714288  
19, 0.0189999994, 0.00141176477, 0.515714288  
20, 0.0185000002, 0.00156176474, 0.515714288  
21, -0.0130000003, 0.0259117652, 1.03142858  
22, 0.0185000002, 0.0259117652, 1.03142858  
23, -0.0130000003, 0.0264117643, 1.03142858  
24, 0.0189999994, 0.0264117643, 1.03142858  
25, 0.0189999994, -0.0235882346, 1.03142858  
26, -0.0130000003, -0.0235882346, 1.03142858

27, -0.0130000003, -0.0227882359, 1.03142858  
28, 0.0185000002, -0.0227882359, 1.03142858  
29, 0.0189999994, 0.00141176477, 1.03142858  
30, 0.0185000002, 0.00156176474, 1.03142858  
31, -0.0130000003, 0.0259117652, 1.54714286  
32, 0.0185000002, 0.0259117652, 1.54714286  
33, -0.0130000003, 0.0264117643, 1.54714286  
34, 0.0189999994, 0.0264117643, 1.54714286  
35, 0.0189999994, -0.0235882346, 1.54714286  
36, -0.0130000003, -0.0235882346, 1.54714286  
37, -0.0130000003, -0.0227882359, 1.54714286  
38, 0.0185000002, -0.0227882359, 1.54714286  
39, 0.0189999994, 0.00141176477, 1.54714286  
40, 0.0185000002, 0.00156176474, 1.54714286  
41, -0.0130000003, 0.0259117652, 2.06285715  
42, 0.0185000002, 0.0259117652, 2.06285715  
43, -0.0130000003, 0.0264117643, 2.06285715  
44, 0.0189999994, 0.0264117643, 2.06285715  
45, 0.0189999994, -0.0235882346, 2.06285715  
46, -0.0130000003, -0.0235882346, 2.06285715  
47, -0.0130000003, -0.0227882359, 2.06285715  
48, 0.0185000002, -0.0227882359, 2.06285715  
49, 0.0189999994, 0.00141176477, 2.06285715  
50, 0.0185000002, 0.00156176474, 2.06285715

51, -0.0130000003, 0.0259117652, 2.57857132  
52, 0.0185000002, 0.0259117652, 2.57857132  
53, -0.0130000003, 0.0264117643, 2.57857132  
54, 0.0189999994, 0.0264117643, 2.57857132  
55, 0.0189999994, -0.0235882346, 2.57857132  
56, -0.0130000003, -0.0235882346, 2.57857132  
57, -0.0130000003, -0.0227882359, 2.57857132  
58, 0.0185000002, -0.0227882359, 2.57857132  
59, 0.0189999994, 0.00141176477, 2.57857132  
60, 0.0185000002, 0.00156176474, 2.57857132  
61, -0.0130000003, 0.0259117652, 3.09428573  
62, 0.0185000002, 0.0259117652, 3.09428573  
63, -0.0130000003, 0.0264117643, 3.09428573  
64, 0.0189999994, 0.0264117643, 3.09428573  
65, 0.0189999994, -0.0235882346, 3.09428573  
66, -0.0130000003, -0.0235882346, 3.09428573  
67, -0.0130000003, -0.0227882359, 3.09428573  
68, 0.0185000002, -0.0227882359, 3.09428573  
69, 0.0189999994, 0.00141176477, 3.09428573  
70, 0.0185000002, 0.00156176474, 3.09428573  
71, -0.0130000003, 0.0259117652, 3.6099999  
72, 0.0185000002, 0.0259117652, 3.6099999  
73, -0.0130000003, 0.0264117643, 3.6099999  
74, 0.0189999994, 0.0264117643, 3.6099999

75, 0.0189999994, -0.0235882346, 3.6099999  
76, -0.0130000003, -0.0235882346, 3.6099999  
77, -0.0130000003, -0.0227882359, 3.6099999  
78, 0.0185000002, -0.0227882359, 3.6099999  
79, 0.0189999994, 0.00141176477, 3.6099999  
80, 0.0185000002, 0.00156176474, 3.6099999

\*Element, type=DC3D8

1, 4, 3, 1, 2, 14, 13, 11, 12  
2, 7, 6, 5, 8, 17, 16, 15, 18  
3, 4, 2, 10, 9, 14, 12, 20, 19  
4, 10, 8, 5, 9, 20, 18, 15, 19  
5, 14, 13, 11, 12, 24, 23, 21, 22  
6, 17, 16, 15, 18, 27, 26, 25, 28  
7, 14, 12, 20, 19, 24, 22, 30, 29  
8, 20, 18, 15, 19, 30, 28, 25, 29  
9, 24, 23, 21, 22, 34, 33, 31, 32  
10, 27, 26, 25, 28, 37, 36, 35, 38  
11, 24, 22, 30, 29, 34, 32, 40, 39  
12, 30, 28, 25, 29, 40, 38, 35, 39  
13, 34, 33, 31, 32, 44, 43, 41, 42  
14, 37, 36, 35, 38, 47, 46, 45, 48  
15, 34, 32, 40, 39, 44, 42, 50, 49  
16, 40, 38, 35, 39, 50, 48, 45, 49  
17, 44, 43, 41, 42, 54, 53, 51, 52

18, 47, 46, 45, 48, 57, 56, 55, 58

19, 44, 42, 50, 49, 54, 52, 60, 59

20, 50, 48, 45, 49, 60, 58, 55, 59

21, 54, 53, 51, 52, 64, 63, 61, 62

22, 57, 56, 55, 58, 67, 66, 65, 68

23, 54, 52, 60, 59, 64, 62, 70, 69

24, 60, 58, 55, 59, 70, 68, 65, 69

25, 64, 63, 61, 62, 74, 73, 71, 72

26, 67, 66, 65, 68, 77, 76, 75, 78

27, 64, 62, 70, 69, 74, 72, 80, 79

28, 70, 68, 65, 69, 80, 78, 75, 79

\*Nset, nset=Set-21, generate

1, 80, 1

\*Elset, elset=Set-21, generate

1, 28, 1

\*\* Section: STEEL

\*Solid Section, elset=Set-21, material=STEEL

,

\*End Part

\*\*

\*Part, name=Gypsum

\*Node

1, -1.80499995, 1.505, 0.

2, -0.902499974, 1.505, 0.

3, 0., 1.505, 0.  
4, 0.902499974, 1.505, 0.  
5, 1.80499995, 1.505, 0.  
6, -1.80499995, 0.501666665, 0.  
7, -0.902499974, 0.501666665, 0.  
8, 0., 0.501666665, 0.  
9, 0.902499974, 0.501666665, 0.  
10, 1.80499995, 0.501666665, 0.  
11, -1.80499995, -0.501666665, 0.  
12, -0.902499974, -0.501666665, 0.  
13, 0., -0.501666665, 0.  
14, 0.902499974, -0.501666665, 0.  
15, 1.80499995, -0.501666665, 0.  
16, -1.80499995, -1.505, 0.  
17, -0.902499974, -1.505, 0.  
18, 0., -1.505, 0.  
19, 0.902499974, -1.505, 0.  
20, 1.80499995, -1.505, 0.  
21, -1.80499995, 1.505, 0.00949999969  
22, -0.902499974, 1.505, 0.00949999969  
23, 0., 1.505, 0.00949999969  
24, 0.902499974, 1.505, 0.00949999969  
25, 1.80499995, 1.505, 0.00949999969  
26, -1.80499995, 0.501666665, 0.00949999969

27, -0.902499974, 0.501666665, 0.00949999969  
28, 0., 0.501666665, 0.00949999969  
29, 0.902499974, 0.501666665, 0.00949999969  
30, 1.80499995, 0.501666665, 0.00949999969  
31, -1.80499995, -0.501666665, 0.00949999969  
32, -0.902499974, -0.501666665, 0.00949999969  
33, 0., -0.501666665, 0.00949999969  
34, 0.902499974, -0.501666665, 0.00949999969  
35, 1.80499995, -0.501666665, 0.00949999969  
36, -1.80499995, -1.505, 0.00949999969  
37, -0.902499974, -1.505, 0.00949999969  
38, 0., -1.505, 0.00949999969  
39, 0.902499974, -1.505, 0.00949999969  
40, 1.80499995, -1.505, 0.00949999969

\*Element, type=DC3D8

1, 6, 7, 2, 1, 26, 27, 22, 21  
2, 7, 8, 3, 2, 27, 28, 23, 22  
3, 8, 9, 4, 3, 28, 29, 24, 23  
4, 9, 10, 5, 4, 29, 30, 25, 24  
5, 11, 12, 7, 6, 31, 32, 27, 26  
6, 12, 13, 8, 7, 32, 33, 28, 27  
7, 13, 14, 9, 8, 33, 34, 29, 28  
8, 14, 15, 10, 9, 34, 35, 30, 29  
9, 16, 17, 12, 11, 36, 37, 32, 31

10, 17, 18, 13, 12, 37, 38, 33, 32

11, 18, 19, 14, 13, 38, 39, 34, 33

12, 19, 20, 15, 14, 39, 40, 35, 34

\*Nset, nset=Set-7, generate

1, 40, 1

\*Elset, elset=Set-7, generate

1, 12, 1

\*Elset, elset=\_Surf-1\_S2, internal, generate

1, 12, 1

\*Surface, type=ELEMENT, name=Surf-1

\_Surf-1\_S2, S2

\*Elset, elset=\_Surf-2\_S1, internal, generate

1, 12, 1

\*Surface, type=ELEMENT, name=Surf-2

\_Surf-2\_S1, S1

\*\* Section: GYPSUM

\*Solid Section, elset=Set-7, material=DRYWALL

,

\*End Part

\*\*

\*Part, name=Insulation

\*Node

1, -1.79999995, -1.505, 0.0500000007

2, -1.79999995, -0.501666665, 0.0500000007

3, -1.79999995, 0.501666665, 0.0500000007  
4, -1.79999995, 1.505, 0.0500000007  
5, -1.79999995, -1.505, 0.  
6, -1.79999995, -0.501666665, 0.  
7, -1.79999995, 0.501666665, 0.  
8, -1.79999995, 1.505, 0.  
9, -0.897499979, -1.505, 0.0500000007  
10, -0.897499979, -0.501666665, 0.0500000007  
11, -0.897499979, 0.501666665, 0.0500000007  
12, -0.897499979, 1.505, 0.0500000007  
13, -0.897499979, -1.505, 0.  
14, -0.897499979, -0.501666665, 0.  
15, -0.897499979, 0.501666665, 0.  
16, -0.897499979, 1.505, 0.  
17, 0.0049999989, -1.505, 0.0500000007  
18, 0.0049999989, -0.501666665, 0.0500000007  
19, 0.0049999989, 0.501666665, 0.0500000007  
20, 0.0049999989, 1.505, 0.0500000007  
21, 0.0049999989, -1.505, 0.  
22, 0.0049999989, -0.501666665, 0.  
23, 0.0049999989, 0.501666665, 0.  
24, 0.0049999989, 1.505, 0.  
25, 0.907500029, -1.505, 0.0500000007  
26, 0.907500029, -0.501666665, 0.0500000007

27, 0.907500029, 0.501666665, 0.0500000007  
28, 0.907500029, 1.505, 0.0500000007  
29, 0.907500029, -1.505, 0.  
30, 0.907500029, -0.501666665, 0.  
31, 0.907500029, 0.501666665, 0.  
32, 0.907500029, 1.505, 0.  
33, 1.809999994, -1.505, 0.0500000007  
34, 1.809999994, -0.501666665, 0.0500000007  
35, 1.809999994, 0.501666665, 0.0500000007  
36, 1.809999994, 1.505, 0.0500000007  
37, 1.809999994, -1.505, 0.  
38, 1.809999994, -0.501666665, 0.  
39, 1.809999994, 0.501666665, 0.  
40, 1.809999994, 1.505, 0.

\*Element, type=DC3D8

1, 9, 10, 14, 13, 1, 2, 6, 5  
2, 10, 11, 15, 14, 2, 3, 7, 6  
3, 11, 12, 16, 15, 3, 4, 8, 7  
4, 17, 18, 22, 21, 9, 10, 14, 13  
5, 18, 19, 23, 22, 10, 11, 15, 14  
6, 19, 20, 24, 23, 11, 12, 16, 15  
7, 25, 26, 30, 29, 17, 18, 22, 21  
8, 26, 27, 31, 30, 18, 19, 23, 22  
9, 27, 28, 32, 31, 19, 20, 24, 23

10, 33, 34, 38, 37, 25, 26, 30, 29

11, 34, 35, 39, 38, 26, 27, 31, 30

12, 35, 36, 40, 39, 27, 28, 32, 31

\*Nset, nset=Set-1, generate

1, 40, 1

\*Elset, elset=Set-1, generate

1, 12, 1

\*Elset, elset=\_Surf-1\_S3, internal, generate

1, 12, 1

\*Surface, type=ELEMENT, name=Surf-1

\_Surf-1\_S3, S3

\*Elset, elset=\_Surf-2\_S5, internal, generate

1, 12, 1

\*Surface, type=ELEMENT, name=Surf-2

\_Surf-2\_S5, S5

\*\* Section: STONE WOOL

\*Solid Section, elset=Set-1, material="STONE WOOL"

,

\*End Part

\*\*

\*\*

\*\* ASSEMBLY

\*\*

\*Assembly, name=Assembly

\*\*

\*Instance, name="Gypsum out", part=Gypsum

0., 0., -0.0095

\*End Instance

\*\*

\*Instance, name="Gypsum In", part=Gypsum

0., -4.22503145705837e-18, -0.06900000000000001

\*End Instance

\*\*

\*Instance, name=C-1, part="C studs"

0., 1.50499999999988, -0.0359117647423686

0., 1.50499999999988, -0.0359117647423686, 1., 1.50499999999988, -  
0.0359117647423686, 90.

\*End Instance

\*\*

\*Instance, name=C-2, part="C studs"

-1.78599999999984, -1.50500000000012, -0.0359117647423685

-1.78599999999984, -1.50500000000012, -0.0359117647423685, -1.78599999999984, -  
0.797893188768337, 0.671195046489412, 180.

\*End Instance

\*\*

\*Instance, name=C-3, part="C studs"

1.78599999999984, 1.50499999999988, -0.0359117647423685

1.78599999999984, 1.50499999999988, -0.0359117647423685, 2.78599999999984,  
1.50499999999988, -0.0359117647423685, 90.

\*End Instance

\*\*

\*Instance, name=C-1-lin-2-1, part="C studs"

0.6, 1.50499999999988, -0.0359117647423684

0.6, 1.50499999999988, -0.0359117647423684, 1.6, 1.50499999999988, -  
0.0359117647423684, 90.

\*End Instance

\*\*

\*Instance, name=C-1-lin-3-1, part="C studs"

1.2, 1.50499999999988, -0.0359117647423684

1.2, 1.50499999999988, -0.0359117647423684, 2.2, 1.50499999999988, -  
0.0359117647423684, 90.

\*End Instance

\*\*

\*Instance, name=C-1-lin-2-1-1, part="C studs"

-0.6, 1.50499999999988, -0.0359117647423684

-0.6, 1.50499999999988, -0.0359117647423684, 0.4, 1.50499999999988, -  
0.0359117647423684, 90.

\*End Instance

\*\*

\*Instance, name=C-1-lin-3-1-1, part="C studs"

-1.2, 1.50499999999988, -0.0359117647423684

-1.2, 1.50499999999988, -0.0359117647423684, -0.2, 1.50499999999988, -  
0.0359117647423684, 90.

\*End Instance

\*\*

\*Instance, name=C-Bottom-1, part="C- Studs Bottom Top"

1.80500000000016, -1.48599999999988, -0.0359117647423686

1.80500000000016, -1.48599999999988, -0.0359117647423686, 2.38235027955221, -  
2.06335027955192, -0.613262044294411, 119.999999109416

\*End Instance

\*\*

\*Instance, name=C-Top-2, part="C- Studs Bottom Top"

1.80500000000016, 1.48599999999988, -0.0330882352576318

1.80500000000016, 1.48599999999988, -0.0330882352576318, 1.22764972044812,  
0.908649720447835, 0.54426204429441, 119.999999109416

\*End Instance

\*\*

\*Instance, name=Insulation-1, part=Insulation

-0.00500000000016421, -4.88498130835066e-15, -0.0595000000000001

\*End Instance

\*\*

\*Nset, nset=Set-1, instance="Gypsum out", generate

1, 20, 1

\*Elset, elset=Set-1, instance="Gypsum out", generate

1, 12, 1

\*Nset, nset=Set-2, instance="Gypsum out", generate

1, 40, 1

\*Nset, nset=Set-2, instance="Gypsum In", generate

1, 40, 1

\*Elset, elset=Set-2, instance="Gypsum out", generate

1, 12, 1

\*Elset, elset=Set-2, instance="Gypsum In", generate

1, 12, 1

\*Nset, nset=Set-3, instance="Gypsum In", generate

21, 40, 1

\*Elset, elset=Set-3, instance="Gypsum In", generate

1, 12, 1

\*Elset, elset=\_CP-1-C-1\_S3, internal, instance=C-1, generate

1, 21, 4

\*Surface, type=ELEMENT, name=CP-1-C-1

\_CP-1-C-1\_S3, S3

\*Elset, elset="\_CP-1-Gypsum out\_S1", internal, instance="Gypsum out", generate

1, 12, 1

\*Surface, type=ELEMENT, name="CP-1-Gypsum out"

"\_CP-1-Gypsum out\_S1", S1

\*Elset, elset=\_CP-2-C-2\_S3, internal, instance=C-2, generate

1, 21, 4

\*Surface, type=ELEMENT, name=CP-2-C-2

\_CP-2-C-2\_S3, S3

\*Elset, elset="\_CP-2-Gypsum out\_S1", internal, instance="Gypsum out", generate

1, 12, 1

\*Surface, type=ELEMENT, name="CP-2-Gypsum out"

"\_CP-2-Gypsum out\_S1", S1

\*Elset, elset=\_CP-3-C-3\_S3, internal, instance=C-3, generate

1, 21, 4

\*Surface, type=ELEMENT, name=CP-3-C-3

\_CP-3-C-3\_S3, S3

\*Elset, elset="\_CP-3-Gypsum out\_S1", internal, instance="Gypsum out", generate

1, 12, 1

\*Surface, type=ELEMENT, name="CP-3-Gypsum out"

"\_CP-3-Gypsum out\_S1", S1

\*Elset, elset=\_CP-4-C-1-lin-2-1\_S3, internal, instance=C-1-lin-2-1, generate

1, 21, 4

\*Surface, type=ELEMENT, name=CP-4-C-1-lin-2-1

\_CP-4-C-1-lin-2-1\_S3, S3

\*Elset, elset="\_CP-4-Gypsum out\_S1", internal, instance="Gypsum out", generate

1, 12, 1

\*Surface, type=ELEMENT, name="CP-4-Gypsum out"

"\_CP-4-Gypsum out\_S1", S1

\*Elset, elset=\_CP-5-C-1-lin-3-1\_S3, internal, instance=C-1-lin-3-1, generate

1, 21, 4

\*Surface, type=ELEMENT, name=CP-5-C-1-lin-3-1

\_CP-5-C-1-lin-3-1\_S3, S3

\*Elset, elset="\_CP-5-Gypsum out\_S1", internal, instance="Gypsum out", generate

1, 12, 1

\*Surface, type=ELEMENT, name="CP-5-Gypsum out"

"\_CP-5-Gypsum out\_S1", S1

\*Elset, elset=\_CP-6-C-1-lin-2-1-1\_S3, internal, instance=C-1-lin-2-1-1, generate

1, 21, 4

\*Surface, type=ELEMENT, name=CP-6-C-1-lin-2-1-1

\_CP-6-C-1-lin-2-1-1\_S3, S3

\*Elset, elset="\_CP-6-Gypsum out\_S1", internal, instance="Gypsum out", generate

1, 12, 1

\*Surface, type=ELEMENT, name="CP-6-Gypsum out"

"\_CP-6-Gypsum out\_S1", S1

\*Elset, elset=\_CP-7-C-1-lin-3-1-1\_S3, internal, instance=C-1-lin-3-1-1, generate

1, 21, 4

\*Surface, type=ELEMENT, name=CP-7-C-1-lin-3-1-1

\_CP-7-C-1-lin-3-1-1\_S3, S3

\*Elset, elset="\_CP-7-Gypsum out\_S1", internal, instance="Gypsum out", generate

1, 12, 1

\*Surface, type=ELEMENT, name="CP-7-Gypsum out"

"\_CP-7-Gypsum out\_S1", S1

\*Elset, elset=\_CP-8-C-Bottom-1\_S3, internal, instance=C-Bottom-1, generate

1, 25, 4

\*Surface, type=ELEMENT, name=CP-8-C-Bottom-1

\_CP-8-C-Bottom-1\_S3, S3

\*Elset, elset="\_CP-8-Gypsum out\_S1", internal, instance="Gypsum out", generate

1, 12, 1

\*Surface, type=ELEMENT, name="CP-8-Gypsum out"

"\_CP-8-Gypsum out\_S1", S1

\*Elset, elset=\_CP-9-C-Top-2\_S4, internal, instance=C-Top-2, generate

2, 26, 4

\*Surface, type=ELEMENT, name=CP-9-C-Top-2

\_CP-9-C-Top-2\_S4, S4

\*Elset, elset="\_CP-9-Gypsum out\_S1", internal, instance="Gypsum out", generate

1, 12, 1

\*Surface, type=ELEMENT, name="CP-9-Gypsum out"

"\_CP-9-Gypsum out\_S1", S1

\*Elset, elset="\_CP-10-Gypsum out\_S1", internal, instance="Gypsum out", generate

1, 12, 1

\*Surface, type=ELEMENT, name="CP-10-Gypsum out"

"\_CP-10-Gypsum out\_S1", S1

\*Elset, elset=\_CP-10-Insulation-1\_S3, internal, instance=Insulation-1, generate

1, 12, 1

\*Surface, type=ELEMENT, name=CP-10-Insulation-1

\_CP-10-Insulation-1\_S3, S3

\*Elset, elset=\_CP-11-C-1\_S4, internal, instance=C-1, generate

3, 23, 4

\*Surface, type=ELEMENT, name=CP-11-C-1

\_CP-11-C-1\_S4, S4

\*Elset, elset="\_CP-11-Gypsum In\_S2", internal, instance="Gypsum In", generate

1, 12, 1

\*Surface, type=ELEMENT, name="CP-11-Gypsum In"

"\_CP-11-Gypsum In\_S2", S2

\*Elset, elset=\_CP-12-C-2\_S4, internal, instance=C-2, generate

3, 23, 4

\*Surface, type=ELEMENT, name=CP-12-C-2

\_CP-12-C-2\_S4, S4

\*Elset, elset="\_CP-12-Gypsum In\_S2", internal, instance="Gypsum In", generate

1, 12, 1

\*Surface, type=ELEMENT, name="CP-12-Gypsum In"

"\_CP-12-Gypsum In\_S2", S2

\*Elset, elset=\_CP-13-C-3\_S4, internal, instance=C-3, generate

3, 23, 4

\*Surface, type=ELEMENT, name=CP-13-C-3

\_CP-13-C-3\_S4, S4

\*Elset, elset="\_CP-13-Gypsum In\_S2", internal, instance="Gypsum In", generate

1, 12, 1

\*Surface, type=ELEMENT, name="CP-13-Gypsum In"

"\_CP-13-Gypsum In\_S2", S2

\*Elset, elset=\_CP-14-C-1-lin-2-1\_S4, internal, instance=C-1-lin-2-1, generate

3, 23, 4

\*Surface, type=ELEMENT, name=CP-14-C-1-lin-2-1

\_CP-14-C-1-lin-2-1\_S4, S4

\*Elset, elset="\_CP-14-Gypsum In\_S2", internal, instance="Gypsum In", generate

1, 12, 1

\*Surface, type=ELEMENT, name="CP-14-Gypsum In"

"\_CP-14-Gypsum In\_S2", S2

\*Elset, elset=\_CP-15-C-1-lin-3-1\_S4, internal, instance=C-1-lin-3-1, generate

3, 23, 4

\*Surface, type=ELEMENT, name=CP-15-C-1-lin-3-1

\_CP-15-C-1-lin-3-1\_S4, S4

\*Elset, elset="\_CP-15-Gypsum In\_S2", internal, instance="Gypsum In", generate

1, 12, 1

\*Surface, type=ELEMENT, name="CP-15-Gypsum In"

"\_CP-15-Gypsum In\_S2", S2

\*Elset, elset=\_CP-16-C-1-lin-2-1-1\_S4, internal, instance=C-1-lin-2-1-1, generate

3, 23, 4

\*Surface, type=ELEMENT, name=CP-16-C-1-lin-2-1-1

\_CP-16-C-1-lin-2-1-1\_S4, S4

\*Elset, elset="\_CP-16-Gypsum In\_S2", internal, instance="Gypsum In", generate

1, 12, 1

\*Surface, type=ELEMENT, name="CP-16-Gypsum In"

"\_CP-16-Gypsum In\_S2", S2

\*Elset, elset=\_CP-17-C-1-lin-3-1-1\_S4, internal, instance=C-1-lin-3-1-1, generate

3, 23, 4

\*Surface, type=ELEMENT, name=CP-17-C-1-lin-3-1-1

\_CP-17-C-1-lin-3-1-1\_S4, S4

\*Elset, elset="\_CP-17-Gypsum In\_S2", internal, instance="Gypsum In", generate

1, 12, 1

\*Surface, type=ELEMENT, name="CP-17-Gypsum In"

"\_CP-17-Gypsum In\_S2", S2

\*Elset, elset=\_CP-18-C-Bottom-1\_S4, internal, instance=C-Bottom-1, generate

2, 26, 4

\*Surface, type=ELEMENT, name=CP-18-C-Bottom-1

\_CP-18-C-Bottom-1\_S4, S4

\*Elset, elset="\_CP-18-Gypsum In\_S2", internal, instance="Gypsum In", generate

1, 12, 1

\*Surface, type=ELEMENT, name="CP-18-Gypsum In"

"\_CP-18-Gypsum In\_S2", S2

\*Elset, elset=\_CP-19-C-Top-2\_S3, internal, instance=C-Top-2, generate

1, 25, 4

\*Surface, type=ELEMENT, name=CP-19-C-Top-2

\_CP-19-C-Top-2\_S3, S3

\*Elset, elset="\_CP-19-Gypsum In\_S2", internal, instance="Gypsum In", generate

1, 12, 1

\*Surface, type=ELEMENT, name="CP-19-Gypsum In"

"\_CP-19-Gypsum In\_S2", S2

\*Elset, elset="\_CP-20-Gypsum In\_S2", internal, instance="Gypsum In", generate

1, 12, 1

\*Surface, type=ELEMENT, name="CP-20-Gypsum In"

"\_CP-20-Gypsum In\_S2", S2

\*Elset, elset=\_CP-20-Insulation-1\_S5, internal, instance=Insulation-1, generate

1, 12, 1

\*Surface, type=ELEMENT, name=CP-20-Insulation-1

\_CP-20-Insulation-1\_S5, S5

\*Elset, elset=\_Surf-1\_S2, internal, instance="Gypsum out", generate

1, 12, 1

\*Surface, type=ELEMENT, name=Surf-1

\_Surf-1\_S2, S2

\*Elset, elset=\_Surf-2\_S1, internal, instance="Gypsum In", generate

1, 12, 1

\*Surface, type=ELEMENT, name=Surf-2

\_Surf-2\_S1, S1

\*Elset, elset=\_Surf-3\_S1, internal, instance="Gypsum In", generate

1, 12, 1

\*Surface, type=ELEMENT, name=Surf-3

\_Surf-3\_S1, S1

\*\* Constraint: CP-1-Gypsum out-C-1

\*Tie, name="CP-1-Gypsum out-C-1", adjust=yes, type=SURFACE TO SURFACE

CP-1-C-1, "CP-1-Gypsum out"

\*\* Constraint: CP-2-Gypsum out-C-2

\*Tie, name="CP-2-Gypsum out-C-2", adjust=yes, type=SURFACE TO SURFACE

CP-2-C-2, "CP-2-Gypsum out"

\*\* Constraint: CP-3-Gypsum out-C-3

\*Tie, name="CP-3-Gypsum out-C-3", adjust=yes, type=SURFACE TO SURFACE

CP-3-C-3, "CP-3-Gypsum out"

\*\* Constraint: CP-4-Gypsum out-C-1-lin-2-1

\*Tie, name="CP-4-Gypsum out-C-1-lin-2-1", adjust=yes, type=SURFACE TO SURFACE

CP-4-C-1-lin-2-1, "CP-4-Gypsum out"

\*\* Constraint: CP-5-Gypsum out-C-1-lin-3-1

\*Tie, name="CP-5-Gypsum out-C-1-lin-3-1", adjust=yes, type=SURFACE TO SURFACE  
CP-5-C-1-lin-3-1, "CP-5-Gypsum out"

\*\* Constraint: CP-6-Gypsum out-C-1-lin-2-1-1

\*Tie, name="CP-6-Gypsum out-C-1-lin-2-1-1", adjust=yes, type=SURFACE TO SURFACE  
CP-6-C-1-lin-2-1-1, "CP-6-Gypsum out"

\*\* Constraint: CP-7-Gypsum out-C-1-lin-3-1-1

\*Tie, name="CP-7-Gypsum out-C-1-lin-3-1-1", adjust=yes, type=SURFACE TO SURFACE  
CP-7-C-1-lin-3-1-1, "CP-7-Gypsum out"

\*\* Constraint: CP-8-Gypsum out-C-Bottom-1

\*Tie, name="CP-8-Gypsum out-C-Bottom-1", adjust=yes, type=SURFACE TO SURFACE  
CP-8-C-Bottom-1, "CP-8-Gypsum out"

\*\* Constraint: CP-9-Gypsum out-C-Top-2

\*Tie, name="CP-9-Gypsum out-C-Top-2", adjust=yes, type=SURFACE TO SURFACE  
CP-9-C-Top-2, "CP-9-Gypsum out"

\*\* Constraint: CP-10-Insulation-1-Gypsum out

\*Tie, name="CP-10-Insulation-1-Gypsum out", adjust=yes, type=SURFACE TO SURFACE  
"CP-10-Gypsum out", CP-10-Insulation-1

\*\* Constraint: CP-11-Gypsum In-C-1

\*Tie, name="CP-11-Gypsum In-C-1", adjust=yes, type=SURFACE TO SURFACE  
CP-11-C-1, "CP-11-Gypsum In"

\*\* Constraint: CP-12-Gypsum In-C-2

\*Tie, name="CP-12-Gypsum In-C-2", adjust=yes, type=SURFACE TO SURFACE  
CP-12-C-2, "CP-12-Gypsum In"

\*\* Constraint: CP-13-Gypsum In-C-3

\*Tie, name="CP-13-Gypsum In-C-3", adjust=yes, type=SURFACE TO SURFACE

CP-13-C-3, "CP-13-Gypsum In"

\*\* Constraint: CP-14-Gypsum In-C-1-lin-2-1

\*Tie, name="CP-14-Gypsum In-C-1-lin-2-1", adjust=yes, type=SURFACE TO SURFACE

CP-14-C-1-lin-2-1, "CP-14-Gypsum In"

\*\* Constraint: CP-15-Gypsum In-C-1-lin-3-1

\*Tie, name="CP-15-Gypsum In-C-1-lin-3-1", adjust=yes, type=SURFACE TO SURFACE

CP-15-C-1-lin-3-1, "CP-15-Gypsum In"

\*\* Constraint: CP-16-Gypsum In-C-1-lin-2-1-1

\*Tie, name="CP-16-Gypsum In-C-1-lin-2-1-1", adjust=yes, type=SURFACE TO SURFACE

CP-16-C-1-lin-2-1-1, "CP-16-Gypsum In"

\*\* Constraint: CP-17-Gypsum In-C-1-lin-3-1-1

\*Tie, name="CP-17-Gypsum In-C-1-lin-3-1-1", adjust=yes, type=SURFACE TO SURFACE

CP-17-C-1-lin-3-1-1, "CP-17-Gypsum In"

\*\* Constraint: CP-18-Gypsum In-C-Bottom-1

\*Tie, name="CP-18-Gypsum In-C-Bottom-1", adjust=yes, type=SURFACE TO SURFACE

CP-18-C-Bottom-1, "CP-18-Gypsum In"

\*\* Constraint: CP-19-Gypsum In-C-Top-2

\*Tie, name="CP-19-Gypsum In-C-Top-2", adjust=yes, type=SURFACE TO SURFACE

CP-19-C-Top-2, "CP-19-Gypsum In"

\*\* Constraint: CP-20-Insulation-1-Gypsum In

\*Tie, name="CP-20-Insulation-1-Gypsum In", adjust=yes, type=SURFACE TO SURFACE

"CP-20-Gypsum In", CP-20-Insulation-1

\*End Assembly

\*Amplitude, name="Heat flux", time=TOTAL TIME

0.,	0.,	600.,	0.357142857,	1200.,	0.428571429,	1800.,	0.5
2400.,	0.642857143,	3000.,	0.714285714,	3600.,	0.714285714,	4200.,	0.785714286
4800.,	0.857142857,	5400.,	0.885714286,	6000.,	0.928571429,	6600.,	0.96
7200.,	1.						

\*Amplitude, name="ISO 834", time=TOTAL TIME

0.,	0.02,	180.,	0.48,	360.,	0.57,	540.,	0.63
720.,	0.67,	900.,	0.7,	1080.,	0.73,	1260.,	0.75
1440.,	0.77,	1620.,	0.79,	1800.,	0.8,	1980.,	0.82
2160.,	0.83,	2340.,	0.84,	2520.,	0.85,	2700.,	0.86
2880.,	0.87,	3060.,	0.88,	3240.,	0.89,	3420.,	0.89
3600.,	0.9,	3780.,	0.91,	3960.,	0.91,	4140.,	0.92
4320.,	0.93,	4500.,	0.93,	4680.,	0.94,	4860.,	0.94
5040.,	0.95,	5220.,	0.95,	5400.,	0.96,	5580.,	0.96
5760.,	0.97,	5940.,	0.97,	6120.,	0.98,	6300.,	0.98
6480.,	0.98,	6660.,	0.99,	6840.,	0.99,	7020.,	1.
7200.,	1.						

\*\*

\*\* MATERIALS

\*\*

\*Material, name=Air

\*Conductivity

0.0243, 0.

0.0257, 20.

0.0271, 40.

0.0285, 60.

0.0299, 80.

0.0314,100.

0.0328,120.

0.0343,140.

0.0358,160.

0.0372,180.

0.0386,200.

0.0421,250.

0.0454,300.

0.0485,350.

0.0515,400.

\*Density

1.293, 0.

1.205, 20.

1.127, 40.

1.067, 60.

1., 80.

0.946,100.

0.898,120.

0.854,140.

0.815,160.

0.779,180.

0.746,200.

0.675,250.

0.616,300.

0.566,350.

0.524,400.

\*Specific Heat

1005., 0.

1005., 20.

1005., 40.

1009., 60.

1009., 80.

1009.,100.

1013.,120.

1013.,140.

1017.,160.

1022.,180.

1026.,200.

1034.,250.

1047.,300.

1055.,350.

1068.,400.

\*Material, name=DRYWALL

\*Conductivity

0.17, 20.

0.17, 50.

0.18, 100.

0.18, 150.

0.05, 200.

0.05, 250.

0.2, 300.

0.21, 350.

0.215, 400.

0.22, 450.

0.23, 500.

0.24, 550.

0.25, 600.

0.26, 650.

0.27, 700.

0.3, 1000.

\*Density

711., 0.

675.45, 50.

639.9, 100.

607.905, 150.

575.922, 200.

554.608, 300.

554.839, 400.

553.,500.

552.759,600.

558.434,700.

558.434,800.

\*Specific Heat

1000., 20.

1100., 50.

1500.,100.

1600.,120.

2100.,140.

20000.,160.

7000.,170.

2100.,180.

9000.,200.

1500.,220.

1100.,260.

1000.,400.

500.,430.

800.,450.

900.,500.

1000.,600.

\*Material, name="FIBRE WOOL"

\*Conductivity

0.51, 50.

0.524, 100.

0.524, 120.

0.528, 140.

0.532, 160.

0.534, 170.

0.536, 180.

0.54, 200.

0.544, 220.

0.58, 400.

0.586, 430.

0.59, 450.

0.6, 500.

0.6, 600.

2., 700.

10., 800.

18., 900.

26., 1000.

34., 1100.

42., 1200.

\*Density

35.,

\*Specific Heat

900.,

\*Material, name=STEEL

\*Conductivity

53., 20.

52., 50.

51., 100.

49., 150.

47., 200.

46., 250.

44., 300.

42., 350.

41., 400.

39., 450.

37., 500.

36., 550.

34., 600.

32., 650.

31., 700.

30., 735.

27., 800.

27., 850.

27., 900.

27., 950.

27.,1000.

27.,1050.

27.,1100.

27.,1150.

27.,1200.

\*Density

7850.,

\*Specific Heat

440., 20.

460., 50.

488., 100.

510., 150.

530., 200.

547., 250.

565., 300.

584., 350.

606., 400.

633., 450.

667., 500.

708., 550.

760., 600.

814., 650.

1008., 700.

5000., 735.

803., 800.

695., 850.

650., 900.

650., 950.

650.,1000.

650.,1050.

650.,1100.

650.,1150.

650.,1200.

\*Material, name="STONE WOOL"

\*Conductivity

0.2545, 50.

0.259, 100.

0.2608, 120.

0.2626, 140.

0.2644, 160.

0.2653, 170.

0.2662, 180.

0.268, 200.

0.2698, 220.

0.286, 400.

0.2887, 430.

0.2905, 450.

0.295, 500.

0.4215, 600.

0.6815, 700.

0.9415, 800.

1.2015, 900.

1.4615,1000.

1.7215,1100.

1.9815,1200.

\*Density

100.,

\*Specific Heat

900.,

\*\*

\*\* INTERACTION PROPERTIES

\*\*

\*Surface Interaction, name=Conduction

1.,

\*Gap Conductance

0.0257, 0., 20.

0., 1., 20.

0.0271, 0., 40.

0., 1., 40.

0.0285, 0., 60.

0., 1., 60.

0.0299, 0., 80.

0., 1., 80.

0.0314, 0.,100.

0., 1.,100.

0.0328, 0.,120.

0., 1.,120.

0.0343, 0.,140.

0., 1.,140.

0.0358, 0.,160.

0., 1.,160.

0.0372, 0.,180.

0., 1.,180.

0.0386, 0.,200.

0., 1.,200.

0.0421, 0.,250.

0., 1.,250.

0.0454, 0.,300.

0., 1.,300.

0.0485, 0.,350.

0., 1.,350.

0.0515, 0.,400.

0., 1.,400.

\*\*

\*\* PHYSICAL CONSTANTS

\*\*

\*Physical Constants, absolute zero=-273., stefan boltzmann=8.67e-08

\*\* -----

\*\*

```
** STEP: Heat transfer
**
*Step, name="Heat transfer", nlgeom=NO, inc=1000000
*Heat Transfer, end=PERIOD, deltmx=10000.
100., 7200., 0.01, 100.,
**
** INTERACTIONS
**
** Interaction: Cold Convection
*Sfilm
Surf-1, F, 20., 4.
** Interaction: Hot Convection
*Sfilm, amplitude="ISO 834"
Surf-2, F, 1049., 25.
** Interaction: Radiation
*Sradiate, amplitude="ISO 834"
Surf-3, R, 1049., 0.8
**
** OUTPUT REQUESTS
**
*Restart, write, frequency=0
**
** FIELD OUTPUT: F-Output-1
**
```

\*Output, field, variable=PRESELECT

\*Output, history, frequency=0

\*End Step

## Annex G



# Propagation of Model Uncertainty in the Stochastic Simulations of a Compartment Fire

*Deepak Paudel, Aalto University, Espoo, Finland*

*Simo Hostikka\* , Fire Safety Engineering, Aalto University, Espoo, Finland*

**Received:** 17 October 2018/**Accepted:** 28 February 2019

**Abstract.** Model validation and probabilistic simulations are routinely used for quantifying the uncertainties originating from the numerical models and their inputs, respectively. How the two uncertainty types combine in the context of fire risk analyses is not well understood. In this work, we study the propagation of modeling uncertainty to the predicted distributions of probabilistic fire simulations using model validation data representing an uncertain compartment fire scenario. The wall temperatures are predicted in three different ways: one using a coupled model in which the input is the fire heat release rate, and two models using a standalone conduction solver and either experimentally or numerically (CFD) determined heat flux as a boundary condition. Using the predicted wall temperatures, we calculated demonstrative wall failure probabilities assuming different critical threshold temperatures. We propose a simple method for correcting the simulated distributions and probabilities towards the experimentally observed ones. The simulation results with the Fire Dynamics Simulator show that the obtained uncertainties of this particular validation set are similar to the ones reported in the validation guide. In average, the most accurate model over-predicts wall temperature by  $\sim 5.0\%$  and the prediction uncertainty for both gas phase and solid phase temperature is  $\sim 10\%$ . The wall temperatures predicted from the measured heat-fluxes show higher modeling uncertainty than the ones predicted by a coupled model of the entire gas-wall system. The proposed correction method is shown to improve the accuracy of the predicted distributions for internal wall temperatures at different times. In practical applications, this would lead to more accurate estimates of the time-dependent failure probabilities.

**Keywords:** Uncertainty propagation, Compartment fire, Modeling uncertainty

## 1. Introduction

With an aim to enable the performance-based design of fire safety, the development and validation of essential computational tools is underway. In about a half-century, in this context, numerous simulation tools emerged. Some of them primarily evolved to solve the fire-related problems, while others are general purpose tools that now include the fire simulation module. Among them, the tools adopting the well-known integration techniques such as the finite difference method

---

\* Correspondence should be addressed to: Simo Hostikka, E-mail: [simo.hostikka@aalto.fi](mailto:simo.hostikka@aalto.fi)



(FDM) and finite volume method (FVM) are the fire dynamics simulator (FDS), fireFOAM and ANSYS Fluent. The validity and modeling uncertainty of these tools for fire engineering calculations has been investigated and reported by numerous studies. For example, using FDS, Lee [1] accurately simulated the tunnel fires, Shen [2] and Drean [3] predicted the building fires and Yu [4] simulated the momentum-driven jet flows. Similarly, using fireFOAM, Zadeh [5] predicted the turbulent air plume induced ceiling jet and using ANSYS fluent Jujuly [6] simulated the liquefied natural gas (LNG) pool fire.

All numerical models have a certain modeling uncertainty; i.e. the model cannot capture the actual physical phenomenon perfectly. For a particular output, the modeling uncertainty should be quantified in a meaningful way. In fire safety engineering, the most common practice is to express it as a measure of systematic and random deviation from the experimentally observed value. For example, in the validation guide of FDS, the modeling uncertainty is presented for various output quantities. The data obtained from numerous fire experiments are compared with the corresponding model simulations and the model uncertainty is quantified in terms of systematic bias and the second central moment of random errors. These two parameters represent the trending error property of the model, hence can be used to estimate the prediction uncertainty resulting from using the tool [7, 8].

The fire simulation tools have been reported to be used also in the probabilistic analysis. For example, Matala [9] used FDS to study the performance of cables in the tunnel fires, Hietaniemi [10] used it to study the performance of load-bearing wood beams in the building fires, Ayala [11] used it for the stochastic simulations of atrium fires, and Anderson [12] used the CFAST zone model to estimate the community-averaged extent of fire damage in homes. The main task in such an analysis is to calculate the output uncertainty corresponding to the given input uncertainty. The term “output uncertainty” can be used in the case of non-parametric analysis as well but should not be confused with the one used for the parametric analysis. McGrattan [13] presents a method to estimate the output uncertainty based on the available information of the model uncertainty. In his method, the output uncertainty is the interpretation of normally distributed random errors around a single unbiased output. In other words, it is simply the representation of the possible modeling uncertainty resulting from using the tool. In the parametric analysis, the output uncertainty is rather the desired quantity, and should not be dependent on the modeling uncertainty but only the input parameter uncertainty. The problem not addressed in the above-mentioned and similar other studies is that the stochastically inferred output uncertainty is inevitably a combination of both input and modeling uncertainties, being possibly very different from the true output uncertainty [14, 15].

In this study, we present an uncertainty model that can be used to obtain the true output uncertainty from the stochastically simulated one. We use the model to illustrate how the model uncertainty propagates together with parameter uncertainty. We demonstrate this using the validation data representing the uncertain scenarios of the compartment fire. A set of real fire experiments with three varying parameters represents the stochastic set of simulations. Finally, we present

that the model uncertainty metrics can be used to statistically compensate for their effect in a probability calculation. Unlike in the previous works, where the uncertainties are usually presented for the peak values, we present the uncertainty pertaining to each time instance of the output.

## 2. Uncertainty Modeling

### 2.1. Parameter Uncertainty

If the inputs of a mathematical model are uncertain then the outputs will be uncertain too. This uncertainty propagation depends upon the characteristics of the model itself. The expression of uncertainty in output,  $T = f(\mathbf{X})$ ,  $f$  being continuous and one time differentiable function, can be derived by Taylor expanding  $T$  about its mean and utilizing the definition of standard deviation in  $T$  [16]. The first order approximation is,

$$\sigma_T^2 = \mathbf{J}^T \Sigma^X \mathbf{J}, \tag{1}$$

where  $\sigma_T^2$  represents variance in  $T$ ,  $\Sigma^X$  is variance-covariance matrix of the input vector,  $\mathbf{X}$ , and  $\mathbf{J} = (J_1, J_2, J_3 \dots)$ ,  $J_i = \partial f / \partial X_i$ . If the input variables,  $\mathbf{X}$ , are independent of each other then the Eq. 1 would simply reduce to

$$\sigma_T^2 = \left| \frac{\partial f}{\partial X_1} \right|^2 \sigma_{X_1}^2 + \left| \frac{\partial f}{\partial X_2} \right|^2 \sigma_{X_2}^2 + \left| \frac{\partial f}{\partial X_3} \right|^2 \sigma_{X_3}^2 + \dots \tag{2}$$

Figure 1 depicts the uncertainty propagation for a simple model,  $T = \pi X$ . A normally distributed output,  $T \sim \mathcal{N}(\pi 10, \pi^2)$ , is obtained for a normally distributed input,  $X \sim \mathcal{N}(10, 1)$ . For complex and non-linear problems, such derivation is mathematically challenging, therefore, stochastic methods are adopted. Some

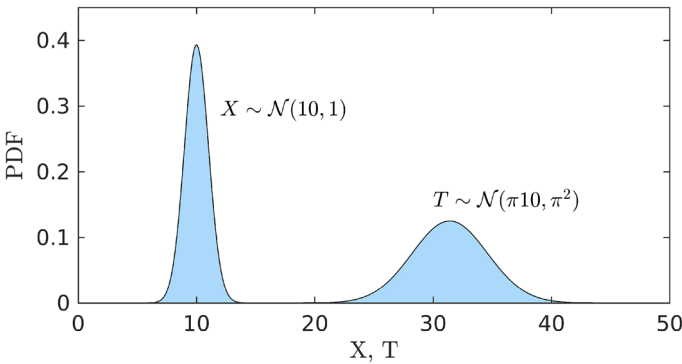


**Figure 1. Input and output distribution for  $T = \pi X$ . The mean and variance of  $X$  is 10 and 1 respectively.**

examples of stochastic methods are Monte-Carlo (MC), Latin hypercube sampling (LHS) and Fourier amplitude sensitivity test (FAST) [17–19].

### 2.2. Combining Model and Parameter Uncertainty

The model uncertainty can be decomposed into two components: systematic bias and random error [7]. The systematic bias is assumed to be a measure of the multiplicative factor by which the observed output is away from the true value. On average, it is the ratio of observed and true output. The random error is assumed to be an additive error that makes the observed output to fluctuate around the true value. We assume that these parameters can be determined for each output parameter, and are constants for a specific type of fire scenario.

The output for a simulation model,  $T = f(X)$ , with systematic bias,  $\delta$ , and random error,  $\epsilon$ , is

$$\hat{T} = \delta \cdot T + \epsilon, \tag{3}$$

where  $\hat{T}$  is the simulated quantity and  $T$  is the true quantity. Here, the  $T$  and  $\epsilon$  are independent and the mean of  $\epsilon$  is zero. For such conditions, the mean and variance of the observed quantity can be written as,

$$\mu_{\hat{T}} = \delta \cdot \mu_T \quad \text{and} \quad \sigma_{\hat{T}}^2 = \delta^2 \cdot \sigma_T^2 + \sigma_{\epsilon}^2. \tag{4}$$

Where  $\mu_T$  and  $\sigma_T^2$  are the mean and variance of the true quantity and  $\sigma_{\epsilon}^2$  is the variance of the random error. The derivation for these expressions can be found in the Appendix A.

For a normally distributed output,  $T$ , Table 1 lists the expressions of distributions in the presence or absence of model uncertainty. Figure 2 shows the histogram plots for specific values of  $\delta$  and  $\sigma_{\epsilon}$ . The left figure compares the effect of only the bias, the middle one compares the effect of only the random error, and the right one compares the effect of both. Figures show that the bias simply shifts the distribution, while the random error widens it.

**Table 1**  
**The Output Distribution in Presence or Absence of Error**

S.N.	Distribution of $\hat{T}$	Condition	Description
1	$\mathcal{N}(\mu_T, \sigma_T^2)$	$\delta = 1, \sigma_{\epsilon} = 0$	No model uncertainty (blue)
2	$\mathcal{N}(\delta \cdot \mu_T, \delta^2 \cdot \sigma_T^2)$	$\delta \neq 1, \sigma_{\epsilon} = 0$	Presence of bias
3	$\mathcal{N}(\mu_T, \sigma_T^2 + \sigma_{\epsilon}^2)$	$\delta = 1, \sigma_{\epsilon} \neq 0$	Presence of random error
4	$\mathcal{N}(\delta \cdot \mu_T, \delta^2 \cdot \sigma_T^2 + \sigma_{\epsilon}^2)$	$\delta \neq 1, \sigma_{\epsilon} \neq 0$	Presence of both

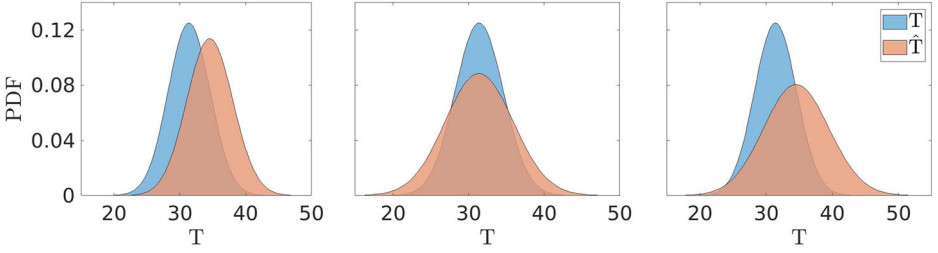


**Figure 2.** The simulated and true output distribution for, **Left:  $\delta=1.1$ ,  $\sigma_\epsilon=0$** , **Middle:  $\delta=1$ ,  $\sigma_\epsilon=\pi$**  and **Right:  $\delta=1.1$ ,  $\sigma_\epsilon=\pi$** .

### 2.3. Correction of Output Distribution

If the prior information of  $\delta$  and  $\sigma_\epsilon$  is available, one can correct the simulated output towards the true one. The corrected moments,  $\mu_T$  and  $\sigma_T$ , can be derived from Eq. 4. The corrected distribution is then the distribution generated using the corrected moments. The cumulative distribution function (CDF) of the corrected values can be obtained by substituting  $\mu_T$  and  $\sigma_T$  into the general expression of CDF. For Gaussian distribution, the CDF is

$$\Phi(T) = 1 - \frac{1}{2} \operatorname{erfc} \left( \frac{\delta \cdot T - \mu_{\hat{T}}}{\sqrt{2(\sigma_{\hat{T}}^2 - \sigma_\epsilon^2)}} \right). \quad (5)$$

This method works well for the output distributions that can be represented by the first two moments, e.g., Gaussian and uniform. When the shape of the output distribution cannot be well represented by the first two moments, the output distribution can be corrected using

$$T = \frac{1}{\delta} \left[ \mu_{\hat{T}} + (\hat{T} - \mu_{\hat{T}}) \sqrt{1 - \left( \frac{\sigma_\epsilon}{\sigma_{\hat{T}}} \right)^2} \right], \quad (6)$$

where  $T$  is the corrected realization corresponding to the observed realization,  $\hat{T}$ . The derivation for this expression can be found in Appendix A.

We illustrate the correction method using two arbitrarily chosen examples [20]. In one of the examples, both the simulated and the true distribution are Gaussian, while in the remaining one, the distribution shape is irregular. First, we calculate the correction parameters,  $\delta$  and  $\sigma_\epsilon$ , by comparing the simulated and true values,

$$\delta = \frac{\mu_{\hat{T}}}{\mu_T}, \quad \text{and} \quad \sigma_\epsilon = \left[ \frac{1}{N-1} \sum_{i=1}^N (\hat{T}_i - \delta \cdot T_i)^2 \right]^{\frac{1}{2}}, \quad (7)$$

where  $\hat{T}_i$  and  $T_i$  are the  $i$ th realization of the simulated and the true quantity respectively and  $N$  is the sample size. Then, using the correction parameters we estimate the true shape from the simulated one.

Figure 3 shows the true, simulated and corrected distributions along with CDF. In the upper plots, the dotted line represents the distribution generated using Eq. 5 and the continuous line represents the distribution generated using Eq. 6. Plots indicate that both methods work well with the normally distributed output. For irregularly distributed outputs, as expected, the estimation is better with Eq. 6. The maximum difference between the CDF of true and the corrected distribution is  $\sim 0.05$  and  $\sim 0.01$  respectively for Eqs. 5 and 6. Even with Eq. 6, complete trace-backing is not possible because the random error that occurred per realization cannot be known.

### 2.4. Sampling Uncertainty

In the stochastic analysis, the inferred moments and the probabilities depend upon the sample size and sampling method. This is known as sampling uncertainty. Figure 4 illustrates such uncertainty using one of the examples presented in the previous section. The simulated distribution  $\hat{T}$ , corrected distribution,  $T$ , and the 95%

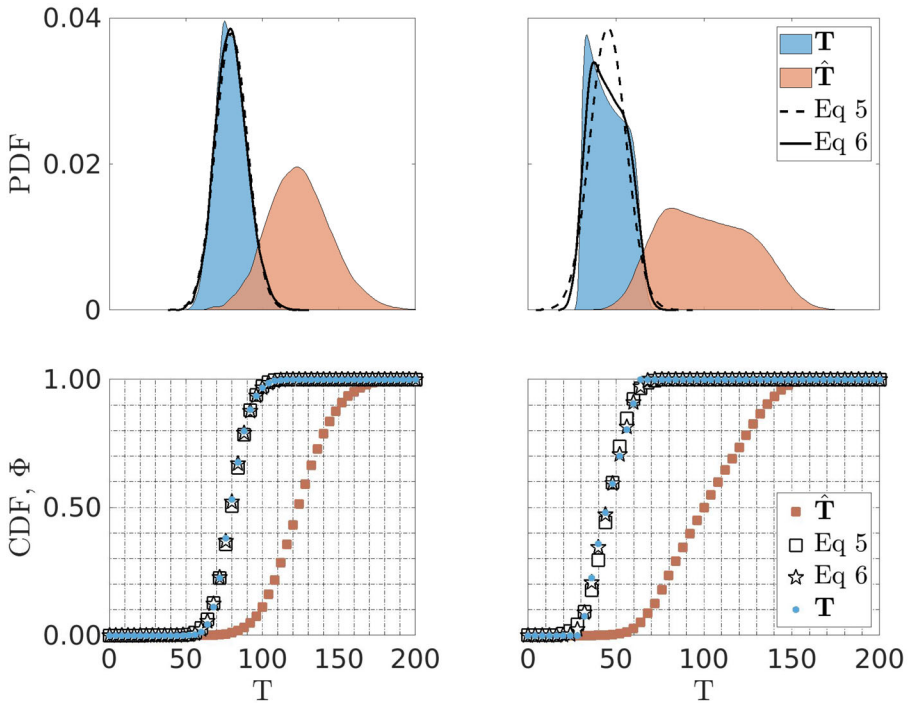


**Figure 3. Upper: The true,  $T$ , simulated,  $\hat{T}$ , and corrected distributions. Lower: Corresponding cumulative density functions.**

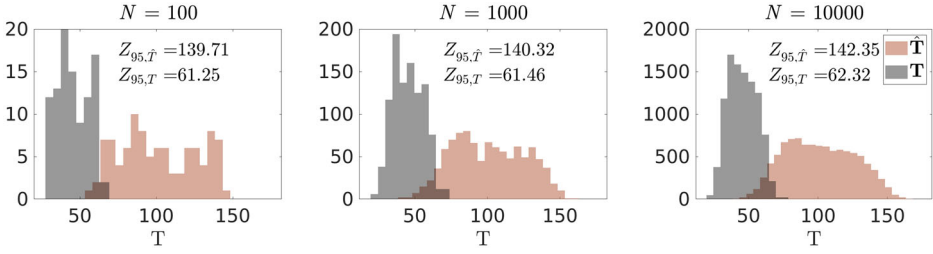


**Figure 4. The distributions of simulated values,  $\hat{T}$ , corrected values,  $T$ , and 95% fractiles for three different sample sizes  $N=100$ ,  $1000$  and  $10,000$ .**

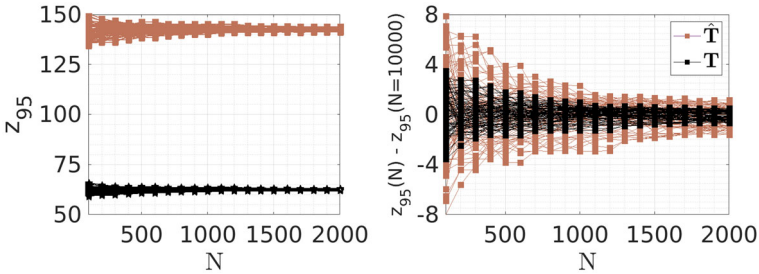


**Figure 5. Left: The 95% fractiles value,  $z_{95}$ , of the simulated,  $\hat{T}$ , and corrected,  $T$ , distributions for different sample size,  $N$ . Right: The difference of  $z_{95}(N)$  and the converged value,  $z_{95}(N=10,000)$ .**

fractiles values,  $z_{95}$ , are presented for sample sizes  $N=100$ ,  $1000$  and  $10,000$ . Higher sample size well represents the distribution and  $z_{95}$  values increases with the increase in the sample size.

The sampling uncertainty can be presented as  $\pm$  bounds from the corrected value. For example, if the probability inferred from the corrected distribution is  $p$ , then the probability is  $p \pm \Delta p$ , where  $\Delta p$  is the sampling uncertainty. The sampling uncertainty for simple MC simulation having sample size  $N$  is  $z_a \sqrt{p(1-p)/N}$ , where  $z_a$  is a multiplier number that determines the level of confidence [21]. For 99% level of confidence  $z_a$  is 2.58. For LHS, such analytical expression is not available, and a separate convergence analysis is needed. Figure 5 shows the result of the convergence analysis carried out for the distributions presented in Fig. 4. The left plot shows  $z_{95}(N)$ . The right plot shows their difference with the converged value,  $z_{95}(N=10,000)$ , and the maximum bound represents the sampling uncertainty. With  $N = 1000$ , the corrected  $z_{95}$  and the sampling uncertainty are 61 and 2 respectively. This means the 95% fractiles value is  $61 \pm 2$ .

### 3. FDS Model Validation

#### 3.1. Validation Experiment

In October of 1998, a series of fire test was carried out at VTT Building Technology with an aim to produce a set of data for validation of fire models [22]. The tests were conducted in a compartment,  $10 \times 7 \times 5 \text{ m}^3$ , having one door opening to the large fire testing hall. The walls and ceiling were made of lightweight concrete and the floor was made of normal concrete. Figure 6 depicts one of the test setups with a fire plume and measurement devices. Table 2 lists the material properties and the thickness of the obstructions.

Systematic variations of fire size and locations were made to determine their effect on the fire environment. The selected fire locations are indicated in Fig. 6 and the test series are summarized in Table 3. Test 10 and 14 were for calibrations, and hence not included in the table.

The fire source was n-Heptane circular steel pool placed over a load cell measuring mass loss rate. Water was used under n-Heptane to stabilize the fire. The free height from the water surface to pool edge was 0.13 m. The free height from the fuel surface to pool edge was 0.11 m in most of the tests.

Burning rates, gas temperatures, wall temperatures, and heat fluxes were measured during the tests. There were 30 thermocouples to measure hot gas

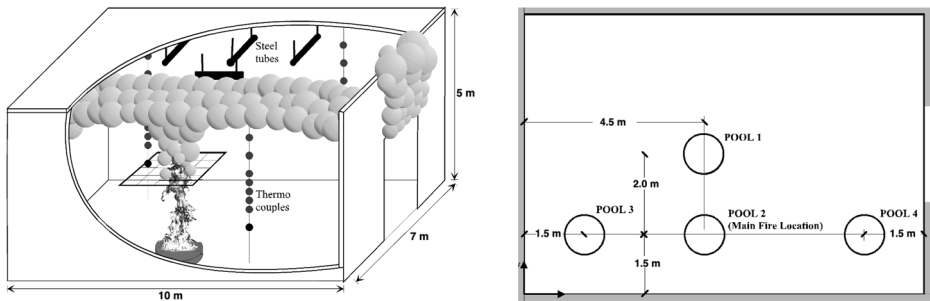


**Figure 6. Left: Schematic diagram representing the fire experiment. Right: The selected pool locations.**

**Table 2**  
**Material Properties and Thickness of Compartment Objects**

Item	Material	Thickness $l$ (m)	Density $\rho$ ( $\text{kgm}^{-3}$ )	Specific heat $c_p$ ( $\text{Jkg}^{-1}\text{K}^{-1}$ )	Thermal conductivity $k$ ( $\text{WK}^{-1}\text{m}^{-1}$ )
Walls	Lightweight concrete	0.25	475	1150	0.08
Ceiling	Lightweight concrete	0.3	475	1150	0.08
Floor	Concrete	0.3	2280	1040	1.8

**Table 3**  
**Fire Test Series: Fire Size, Fire Location and Opening Door Width**

Test No.	Pool location	Pool diameter (m)	Pool Area (m <sup>2</sup> )	Duration (min)	Door width (m)
Test 0	2	0.71	0.4	4:00	2.4
Test 1	2	0.71	0.4	4:00	2.4
Test 2	2	0.71	0.4	8:27	2.4
Test 3	2	0.88	0.6	7:45	2.4
Test 4	2	0.88	0.6	7:55	2.4
Test 5	2	0.88	0.6	8:14	2.4
Test 6	3	0.88	0.6	7:55	2.4
Test 7	1	0.88	0.6	8:00	2.4
Test 8	1	0.88	0.6	7:45	2.4
Test 9	4	0.88	0.6	7:18	2.4
Test 11	2	1.17	1.0	5:15	2.4
Test 12	2	1.17	1.0	5:07	2.4
Test 13	2	1.17	1.0	5:21	2.4
Test 15	1	1.17	1.0	5:15	2.4
Test 16	1	1.17	1.0	5:20	1.2
Test 17	2	1.17	1.0	5:20	1.2
Test 18	2	1.17	1.0	5:29	1.2
Test 19	2	1.60	2.0	5:30	2.4
Test 20	2	1.60	2.0	9:30	2.4

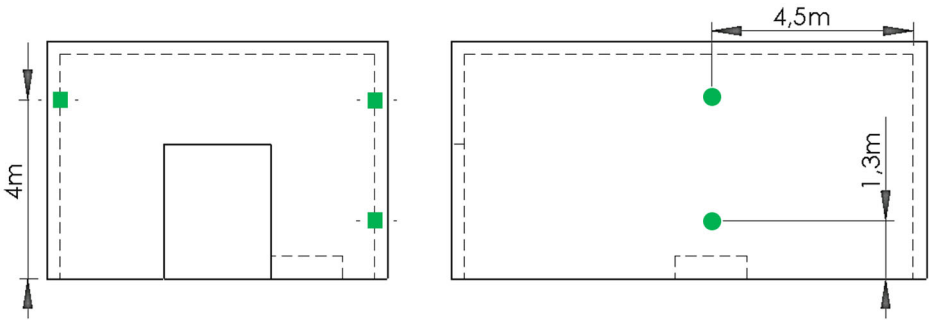


**Figure 7. The locations of the block of thermocouples placed to measure the inside wall temperatures.**

layer(HGL) temperature, 46 thermocouples to measure ceiling jet temperature, 25 thermocouples to measure plume temperature, 5 heat-flux gages to measure the heat flux on the wall and 9 thermocouples to measure the inside wall temperature. Figure 7 shows the three locations where the inside wall temperatures were measured. At each location, a light-weight concrete block with three thermocouples was placed in order to measure the temperatures at varying depths from the inner wall surface.

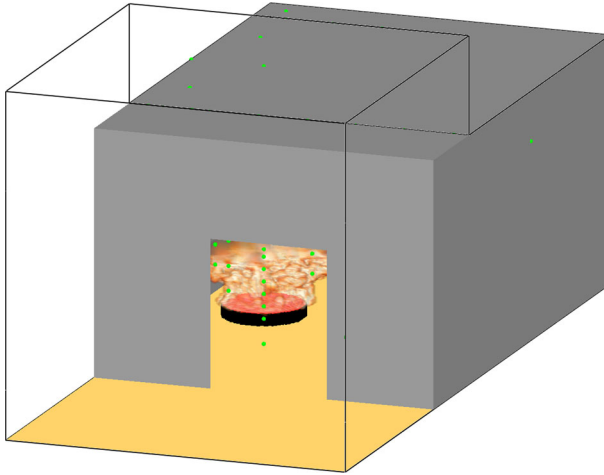


**Figure 8. 3D representation of the computational setup.**

### 3.2. FDS Model

The fire experiment was modeled using FDS version 6.5.3. Figure 8 shows the 3D representation of the simulation domain with transparent gas region and the gray structural region. The fire driven flows in the gas region were simulated by numerically solving the weakly compressible form of the Navier–Stokes equations. The governing equations are presented in Technical Reference Guide of FDS [23]. The heat-transfer in the structural region was simulated by numerically solving the one-dimensional heat-conduction equation

$$\rho c_p \frac{\partial T}{\partial t} = \frac{\partial}{\partial x} \left( k \frac{\partial T}{\partial x} \right), \quad (8)$$

with boundary conditions

$$\begin{aligned} -k \frac{\partial T}{\partial x} &= q'' \Big|_{x=0}, \\ -k \frac{\partial T}{\partial x} &= -h(T - T_\infty) - e\sigma(T^4 - T_\infty^4) \Big|_{x=l}, \end{aligned} \quad (9)$$

where  $x$  is the wall/ceiling depth from the heat-exposed surface.  $l$  represents the wall/ceiling thickness such that the hot-side and cold side surface are at  $x = 0$  and  $x = l$  respectively.  $q''$  is the interface heat-flux,  $e$  is the emissivity,  $T_\infty$  is the ambient temperature and the field variable  $T(x, t)$  represents the wall temperature. The density,  $\rho$ , the specific heat capacity,  $c_p$ , and the thermal conductivity,  $k$ , are assumed to be constant. The heat transfer coefficient,  $h$ , at the front and the back of the wall is calculated based on a combination of natural and forced convection correlations [23].

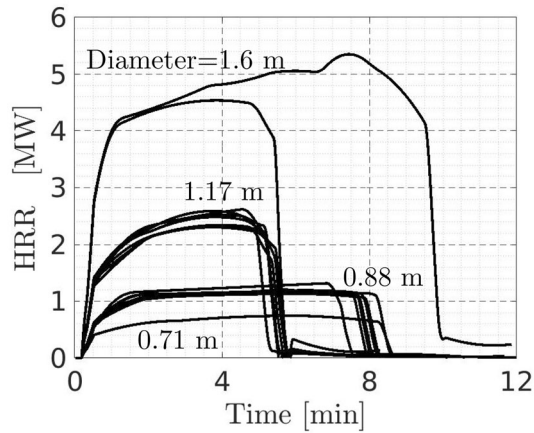


**Figure 9. The specified heat release rate for different tests. Four test groups based on the pool diameter.**

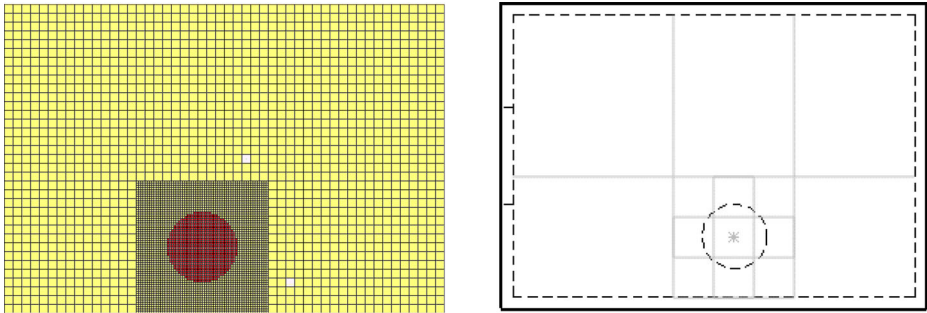


**Figure 10. Left: Discretization of the gas domain. Right: Decomposition of the gas domain for parallel computing.**

The fire source was modeled as a circular burner with an appropriate heat release rate (HRR), corresponding to a fuel inflow boundary condition. Figure 9 shows the specified HRR for the tests. The text in the figure indicates four different test groups having the same pool diameter. The pool front surface temperature was specified to follow the same trend as HRR, starting from the room temperature at  $t = 0$  and increasing to a peak value of  $98.4^{\circ}\text{C}$  at the time of the peak HRR, and staying in that value until the end of the simulation. To account for the incomplete combustion, soot yield was set to 2%.

Figure 10 depicts the discretization of the gas domain. To accurately resolve the cylindrical shape of the heat source, the computational cells near the heat source is refined to 5 cm. The cell size in the rest of the region is 10 cm. Similarly, the right side in Fig. 11 depicts the discretization of the 1D heat-conduction model. To resolve the spacing (0.5 mm) between the thermocouples measuring the wall

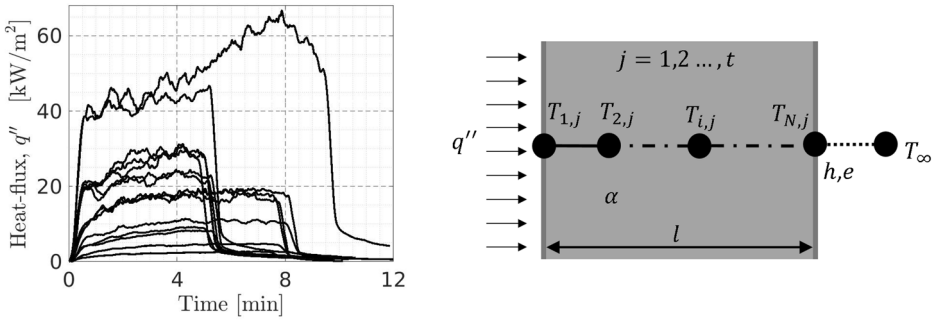


**Figure 11. Left: Boundary heat-fluxes for the standalone analysis. Right: Schematic diagram representing the heat conduction model.**

temperatures, the compartment wall (0.3 m thick ) is discretized into 1000 grid points with finer spacing close to the surfaces.

The simulation was carried out using a distributed-memory computer. We used two steps to decompose the simulation domain. First, the entire compartment is divided into  $6 \times 5 = 30$  mesh regions. The right side in Fig. 10 shows the bottom six of them, the view from the top. Then, for the bottom layer, one of the mesh regions is further divided into nine regions. This results all together  $29 + 9 = 38$  individual mesh regions. It applies to all tests except the ones in which the pool is located in the middle of the compartment. For these cases, the gas domain is divided into  $9 \times 5 = 45$  mesh regions with one of them further divided into nine, resulting all together  $44 + 9 = 53$  individual mesh regions. In both cases, there are two additional mesh region covering the outside geometry, see Fig. 8. Each mesh region used one core and 500 MB memory from a CPU. The models representing all 17 tests were computed at the same time and the total computation time was  $\sim 6$  h.

### 3.3. Standalone Analysis

Excluding the gas phase computation, we carry out a separate analysis to predict the compartment wall thermal response. In this case, the heat-diffusion in the wall is simulated in response to a pre-defined boundary heat-flux that represent the possible fire scenario.

Figure 11 shows a schematic diagram of the standalone model. The left figure shows the Gauge heat-flux,  $q''$ , measured during the experiment and  $\alpha = k/(\rho c_p)$  indicates the wall material property.  $i = 1, 2, \dots, N$  and  $j = 1, 2, \dots$  represent the spatial and temporal discretization with  $N$  nodes and  $t$  time steps respectively. The cold-side boundary condition is both convective and radiative heat flux with a heat transfer coefficient  $h$  and emissivity  $e$  respectively. The wall temperatures,  $T_{i,j}$ , were predicted in response to the heat-flux obtained in two different ways; (i) measured during the experiment,  $q''_{Exp}$ , (ii) predicted from the (CFD + FDM) coupled analysis,  $q''_{FDS}$ .

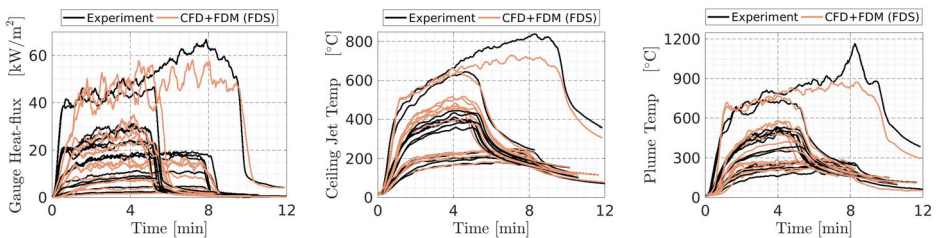
We compare the solutions of the coupled model and the standalone model to find out how the different error types propagate to the wall temperature predictions. If, for instance,  $q''_{\text{Exp}}$  was error-free and there was no error in interpretation of  $q''_{\text{Exp}}$  as a boundary condition, then the standalone model with  $q''_{\text{Exp}}$  boundary conditions should be more accurate than the coupled model. This is due to the fact that, in the coupled model, both input uncertainties (most importantly fuel mass loss rate) and the gas phase model uncertainty propagate to the wall temperature prediction. In general, the measurement uncertainty of  $q''_{\text{Exp}}$  is higher than the measurement uncertainty of the fuel mass loss rate [22], and the relative performance of the different modeling techniques is not obvious. In addition, comparing the coupled model uncertainties against the standalone model with  $q''_{\text{FDS}}$  boundary condition will indicate how much error is generated by the process of interpreting specified (measured or predicted) heat fluxes as a boundary condition for the numerical model.

## 4. Results

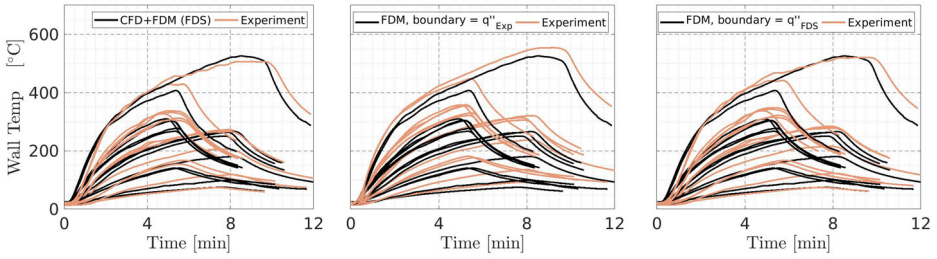
### 4.1. Measured and Predicted Outputs

Figure 12 compares several predicted and measured quantities. The Gauge Heat-flux corresponds to the one measured on the side wall 1.35 m above the floor and 4.5 m from the back wall. Most of the predicted and measured curves are overlapping with each other. The curves with highest values correspond to the test no 20. For this test, a noticeable discrepancy can be seen in the beginning and around 8 min. The experimental uncertainty in this test may also be higher than average as the temperatures were significantly higher, and as there was only one repetition of this particular scenario.

Figure 13 show the measured and predicted inside wall temperatures for the three versions of the heat flux boundary condition. Figure 14 show the times at which the inside wall temperature exceeds a given threshold,  $T_{\text{cr}}$  °C. The maximum value of the temperature measured during the experiment was 500°C, and the horizontal axis of the lower plots is normalized by this maximum value, i.e.,  $T_{\text{cr}}/500$ . Most of the curves showing the threshold times do not reach the end because the peak temperature value for those test is below 500°C. The results indi-



**Figure 12. The predicted and measured, Left: Heat-flux, Middle: Ceiling jet temperature and Right: Plume temperature.**



**Figure 13. Predicted and measured inside wall temperature. Left: CFD+FDM coupled model. Middle: Standalone model with boundary,  $q''_{Exp}$ . Right: Standalone model with boundary,  $q''_{FDS}$ .**

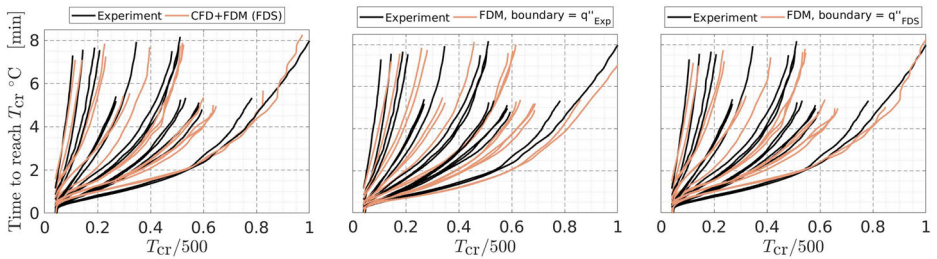


**Figure 14. Predicted and measured time at which the wall crosses  $T_{cr}$  °C . Left: CFD+FDM coupled model. Middle: Standalone model with boundary,  $q''_{Exp}$ . Right: Standalone model with boundary,  $q''_{FDS}$ .**

cate that the coupled model predictions overlap more to the measured values than the predictions from the standalone model with  $q''_{Exp}$  boundary condition. Although the discrepancy in temperatures is small, the discrepancy in times to reach a threshold temperature are sometimes very high, especially when the threshold is close to a semi-steady temperature of the particular experiment.

#### 4.2. Modeling Uncertainty

Table 4 lists the bias,  $\delta$ , and the second central moments of random errors,  $\sigma_\epsilon$ , calculated following the methods explained in [7]. The  $\delta$  represents the average deviation of model prediction from the measured value. The random errors are presented as a relative term, i.e.,  $\tilde{\sigma}_\epsilon = \sigma_\epsilon / \mu_{\hat{y}}$ .  $\tilde{\sigma}_\epsilon\{E\}$  represent the random experimental errors and  $\tilde{\sigma}_\epsilon\{M\}$  represent the random model errors. For the calculation, we used all the measurement points mentioned in Sect. 3.1. Appendix B shows the scatter plots. The uncertainty values obtained from the current experiment are close to the ones reported in the FDS Validation Guide, except for the Gauge Heat Flux output quantity. The model uncertainty and the systematic bias for the Gauge Heat flux are higher than those reported in the Validation Guide.

In addition to the discretization scheme explained in Sect. 3.2, we studied how the mesh configurations affected the uncertainties (Table 5). The corresponding

**Table 4**  
**Experimental Uncertainty, Modeling Uncertainty and Systematic Bias: Comparison Between the Current Experiment and the Validation Guide**

Output quantity	Current experiment			Validation guide		
	$\tilde{\sigma}_\epsilon\{E\}$	$\tilde{\sigma}_\epsilon\{M\}$	$\delta$	$\tilde{\sigma}_\epsilon\{E\}$	$\tilde{\sigma}_\epsilon\{M\}$	$\delta$
HGL temperature	0.04	0.04	1.01	0.07	0.12	1.07
Ceiling jet temperature	0.07	0.07	1.04	0.13	0.14	1.06
Plume temperature	0.07	0.09	0.98	0.07	0.22	1.09
Adiabatic surface Temp	0.07	0.12	0.99	0.07	0.17	1.04
Gauge heat-flux	0.11	0.85	0.98	0.11	0.27	1.00
Wall temperature						
CFD + FDM (FDS)	0.07	0.12	1.05	–	–	–
FDM, boundary = $q''_{Exp}$	0.07	0.10	1.15	–	–	–
FDM, boundary = $q''_{FDS}$	0.07	0.17	1.07	–	–	–

**Table 5**  
**Uncertainties in Wall Temperature Prediction for Different Mesh Configurations**

Burner shape	Mesh type	Mesh configuration		Uncertainty	
		Near the burner (cm)	Rest of the region (cm)	$\tilde{\sigma}_\epsilon\{M\}$	$\delta$
Cylindrical	Multi-size	5	10	0.12	1.05
Cylindrical	Multi-size	5	20	0.15	1.05
Rectangular	Uniform	10	10	0.16	1.15
Rectangular	Uniform	20	20	0.17	1.05

scatters plots are shown in Appendix C. The first configuration is the one that we explained in Sect. 3.2. In the second configuration, the 10 cm mesh region was made coarse, down to 20 cm. In the remaining two configurations, uniform cell size was used in the entire gas domain and the cylindrically shaped burner was simplified to a rectangle shape. For cylindrical shaped burner and multi-mesh configuration, the bias remains unchanged. For the rectangular burner, the bias increases despite the mesh refinement. This is due to the imperfect modeling of the burner vent area. The vent area is poorly represented when the burner surface is not perfectly aligned with the mesh face. For the coarse mesh, the effective vent area can be lower than the specified value. This results in a lower HRR and ultimately the lower bias.

Figure 15 visualizes the model uncertainty as a function of time.  $\delta$  and  $\tilde{\sigma}_\epsilon$  were calculated, using Eq. 7 at each time, by comparing the measured and predicted temperatures presented in Fig. 12. The plots show that on average, Gauge heat-fluxes are underestimated, while Ceiling Jet and Plume temperatures are overestimated. The Gauge heat-fluxes have higher random components than the Ceiling jet temperatures and Plume temperatures. Most importantly, we see that the

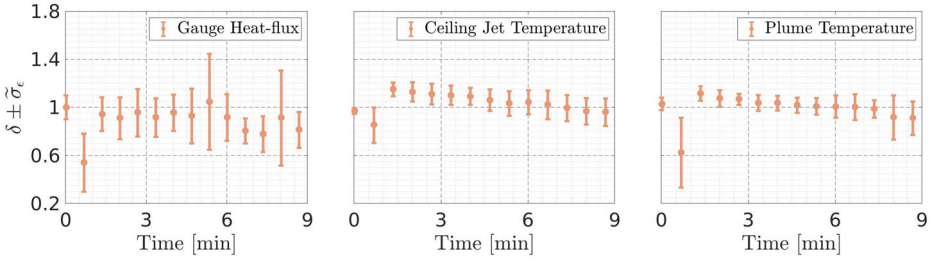


**Figure 15. Model uncertainty in the prediction of, Left: Gauge heat-flux, Middle: Ceiling jet temperature and Right: Plume temperature.**

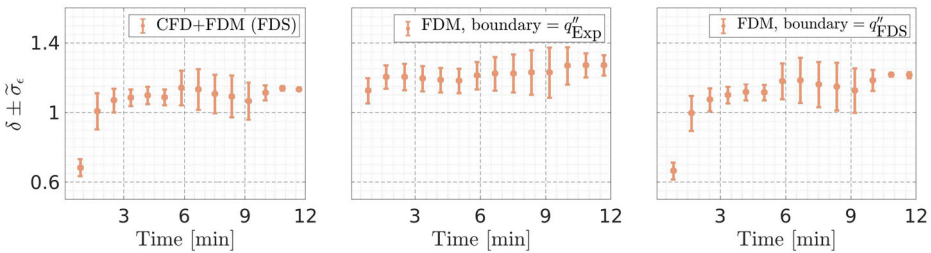


**Figure 16. Model uncertainty in the prediction of wall temperature. Left: CFD+FDM coupled model. Middle: Standalone model with boundary,  $q''_{Exp}$ . Right: Standalone model with boundary,  $q''_{FDS}$ .**

model uncertainties at different time instances are not identical to those calculated at the time of the peak output.

Figures 16 and 17 show the  $\delta$  and  $\tilde{\sigma}_\epsilon$  calculated based on the wall temperatures and threshold times presented in Figs. 13 and 14 respectively. The plot indicates that the wall temperatures on average are overestimated. Due to this, the predicted times are underestimated. In the models based on the FDS gas phase, the early transient temperatures are underestimated, and threshold times hence overestimated. The effect is much less in the right-most plot (standalone model with  $q''_{Exp}$  boundary condition), indicating that either the HRR boundary condition or CFD solution introduces a temporal delay in the early phase. Comparison of the coupled and standalone analysis predictions over the entire time period, however, indicates that the modeling uncertainty is higher for the latter one. Furthermore, the modeling uncertainty is higher for boundary flux  $q''_{Exp}$ . We therefore conclude that, for the wall temperature prediction, the propagation of gas-phase modeling uncertainty is less harmful than the propagation of heat-flux measurement uncertainty. Better predictions can be achieved with the coupled analysis.

### 4.3. Measured and Predicted Moments

The model uncertainty metrics presented in Figs. 15 and 16 are relative quantities and do not visualize well the quality of parameter uncertainties. Figure 18 com-

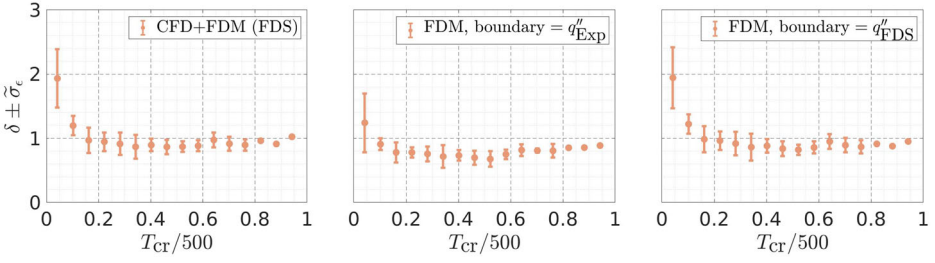


**Figure 17. Model uncertainty in the prediction of threshold time. Left: CFD+FDM coupled model. Middle: Standalone model with boundary,  $q''_{Exp}$ . Right: Standalone model with boundary,  $q''_{FDS}$ .**

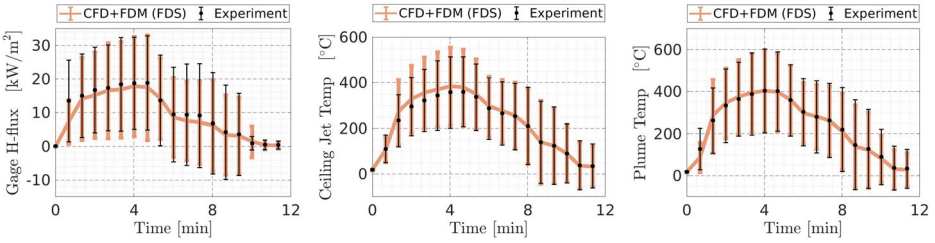


**Figure 18. The two moments of the predicted and measured outputs. Left: Gauge heat-flux, Middle: Ceiling jet temperature and Right: Plume temperature.**

compares the measured and the predicted outputs in terms of their first two moments. The line or dot represents the first moment and the half-length of the error bar represent the second moment. Plots show that the measured and the predicted values are close to each other. In average, the first moments of the ceiling jet temperatures and plume temperatures are slightly over-predicted and the first moments of Gauge Heat-fluxes are slightly under-predicted. In most of the plots, the error bar after 8 minutes extends towards the negative axis. This is because after 8 minutes, the mean is close to zero and the standard deviation is high, see Figs. 12 and 13.

Figures 19 and 20 respectively show the first two moments of wall temperatures and the times at which the wall crosses the threshold temperature,  $T_{cr}$  °C. In average, the wall temperatures are slightly overpredicted and because of this, the times are underpredicted. Overall, the simulated first two moments are close to the observed one.

#### 4.4. Temperature and Probability Correction

Assuming that the wall fails when it crosses a given temperature threshold, the failure probability would be the fraction of the number of the test cases in which the wall temperature rises above this threshold. We now try to understand how the modeling uncertainty in temperatures propagates to such a probability and

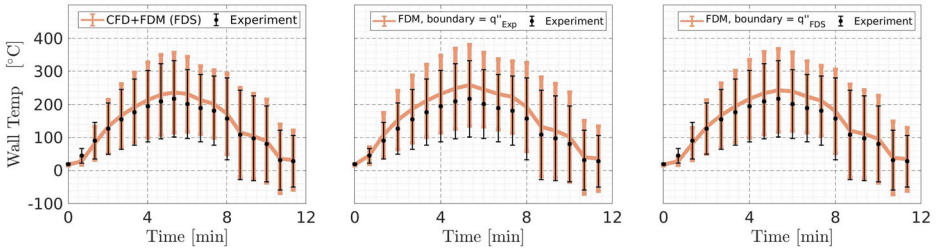


**Figure 19. The first two moments of the predicted and measured wall temperatures. Left: CFD+FDM coupled model. Middle: Standalone model with boundary,  $q''_{Exp}$ . Right: Standalone model with boundary,  $q''_{FDS}$ .**

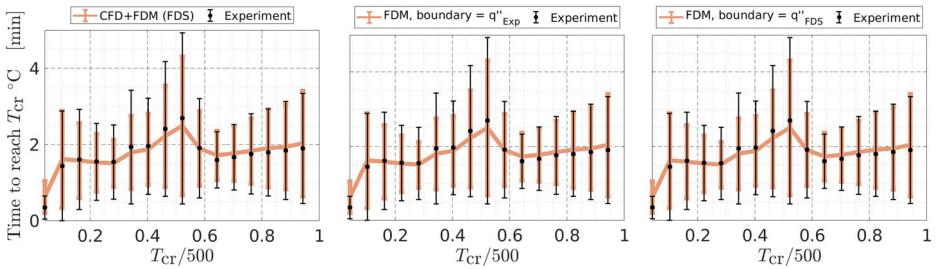


**Figure 20. The first two moments of the predicted and measured times at which the wall crosses  $T_{cr}$  °C . Left: CFD+FDM coupled model. Middle: Standalone model with boundary,  $q''_{Exp}$ . Right: Standalone model with boundary,  $q''_{FDS}$ .**

how it can be corrected. As the temperature predictions of the previous section were indistinctly close to the measurements, it became very difficult to demonstrate the corrections of probabilities. We, therefore, used the results corresponding to the mesh configuration with the highest modeling uncertainty.

In Figure 21, the upper plots show the predicted, measured and the corrected wall temperatures at three different times for each of the tests. The corrected temperature were obtained using Eq. 6 and single values of model uncertainty parameters ( $\delta = 1.15$ ,  $\tilde{\sigma}_\epsilon\{M\} = 0.16$ , see Table 5). We see that where the prediction and measurement are apart, the corrected value is usually closer to the measurement.

The lower plots of Figure 21 show the failure probabilities at different times for three different threshold temperatures. Initially, the walls are at ambient temperature and probabilities are zero. The probabilities increase as the number of tests exceeding the given threshold increases. The upper middle plot shows the temperatures at 4 min. At this time, the number of temperatures above 100°C is 13 for the predicted, corrected as well as the measured quantities. Therefore the probability is,  $13/17 \sim 0.8$  (lower left plot). The number of points crossing 300°C, however, is 7 for the predicted, 3 for the corrected and 2 for the measured quantities,

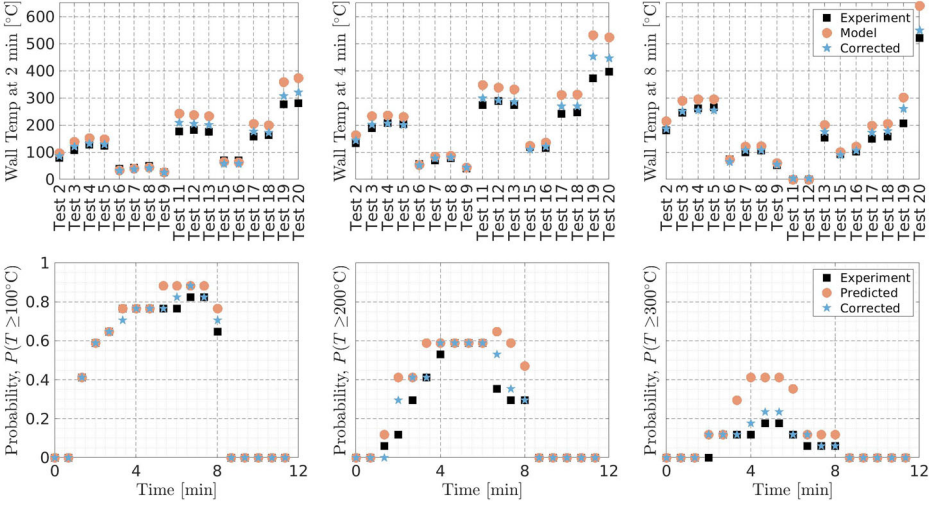


**Figure 21. Upper: The predicted, measured and corrected wall temperatures. Lower: Probability that the wall crosses a given threshold in a given time.**

therefore the probabilities are  $7/17 \sim 0.4$ ,  $3/17 \sim 0.15$  and  $2/17 \sim 0.1$  respectively (lower right plot).

The predicted probabilities are higher than the measured ones. The corrected probability values are closer to the measured ones. Even though the real modeling uncertainty varies with respect to time, the probability correction carried out using the generalized (constant) value was effective at each time instance. This indicates that the model uncertainty values can be generalized for the failure probability correction. Here we used the uncertainty parameters obtained from the same campaign that we used for testing the method. In the validation guide, however, the uncertainty parameters are calculated from the result of numerous fire experiments, hence representing more generalized values.

#### 4.5. Stochastic Analysis

In this study, the variation of fire size, the pool area, pool location and the width of the opening door represent the input parameter uncertainty. For stochastic inputs listed in Table 6, we carry out MC simulation using the model having uniform cell of size of 10 cm. The sampling size,  $N$ , is 100 and the sampling method is LHS. The selected fire type is t-square fire. For such fire, HRR is calculated using fire growth time,  $t_g$ , and peak HRR as

$$\text{HRR}(t) = \min \left( 1000 \left( \frac{t}{t_g} \right)^2, \text{maxHRR} \right) [\text{kW}], \quad (10)$$

where  $t$  is time in second.

**Table 6**  
**Mean, Range and the Type of Distribution Representing the Input Stochastic**

Input parameters	Distribution	Mean	Lower value	Upper value	Unit
Maximum HRR	Uniform	–	950	5400	(kW)
Growth time, $t_g$	Triangular	75	30	150	(s)
Fuel layer thickness	Uniform	–	20	50	(mm)
Pool diameter	Uniform	–	0.7	1.6	(m)
Pool location, x	Uniform	–	1.5	8.5	(m)
Pool location, y	Uniform	–	1.5	3.5	(m)
Opening door width	Uniform	–	1.2	2.4	(m)

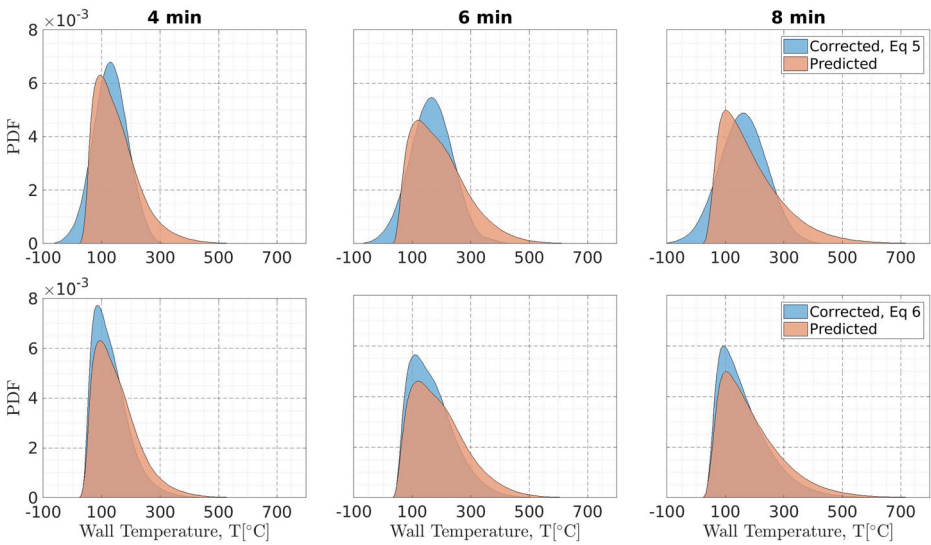


**Figure 22. Predicted and corrected probability density of wall temperatures at different times. Upper: Correction using Eq. 5. Lower: Correction using Eq. 6.**

Figure 22 compares the predicted and corrected probability density for wall temperatures. The correction is based on the average value of the model uncertainty, ( $\delta = 1.15$ , and  $\tilde{\sigma}_\epsilon\{M\} = 0.16$  see Table 5). The plot shows that the correction assuming Gaussian shape is not appropriate for wall temperatures, i.e., the distribution reaches negative axis. The correction using Eq. 6, however, narrows the width of the distribution without deviating significantly from the observed shape.

Figure 23 shows the contour plot for the CDF,  $\Phi$ , of wall temperatures. The vertical axis shows the temperature range, the horizontal axis shows the time and the embedded text show the  $\Phi$  values. The left plot shows the predicted values.

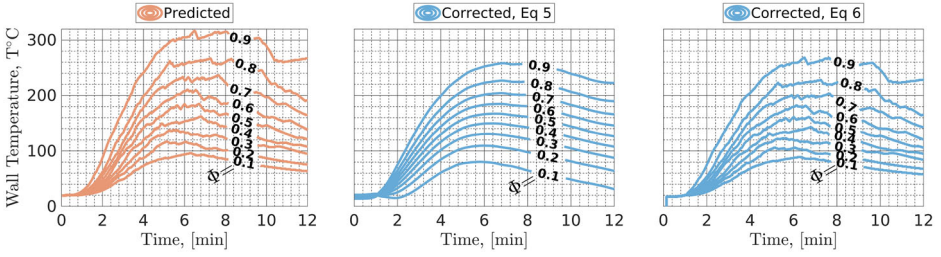


**Figure 23. CDF,  $\Phi$ , of wall temperatures. Left: Predicted. Middle: Corrected according to Eq. 5. Right: Corrected according to Eq. 6.**

The middle and right plots show the corrected values calculated according to Eqs. 5 and 6 respectively.

Assuming that the wall fails when it crosses a given temperature threshold, the failure probability would be the fraction of the number of the test cases in which the wall temperature rises above this threshold. From the above CDF plots one can infer the failure probability. For example, the predicted probability that the wall temperature rises above  $100^{\circ}\text{C}$  before 6 min is  $1-0.1 \sim 0.9$ , where as the corrected probability is  $1-0.2 \sim 0.8$ . Similarly the predicted probability for wall to rise above  $200^{\circ}\text{C}$  before 6 min is  $1-0.6 \sim 0.4$  and the corrected probability is  $1-0.7 \sim 0.3$ . The predicted probabilities are higher than the measured ones. This is due to bias in the temperature prediction.

## 5. Discussion

The study propose correction, Eqs. 5 and 6, for the stochastically simulated output,  $\hat{T}$ , based on the requirement that the corrected quantity,  $T$ , and the random error,  $\epsilon$ , are independent of each other and the mean of  $\epsilon$  is zero. In general, the output and the total error are dependent and the mean of the total error may not be zero. The significance of the uncertainty model presented in this study is that the total error is decomposed into a dependent constant, i.e., the ratio of simulated and corrected mean,  $\delta = \mu_{\hat{T}}/\mu_T$ , and a random component,  $\epsilon = \hat{T} - \delta \cdot T$ , which implies that the mean of  $\epsilon$  must be zero.

In this study, the correction method is illustrated using the true and observed data that are perfectly aligned in time. Figure 24 demonstrate the applicability of the method when data are shifted in time. It is found that the corrected probability density for wall temperatures shifted up to 5 s backward or forward perfectly overlaps with the corrected probability density for wall temperatures that are not shifted in time. Upper and lower plots compare the probability density of the wall temperatures shifted backward by 10 s and 1 min respectively. Plots show that there is an acceptable difference in probability density when the wall temperatures are shifted by 10 s. For 1 min shift, however, the difference is significant. The method, therefore, may not work when the data are significantly shifted in time.

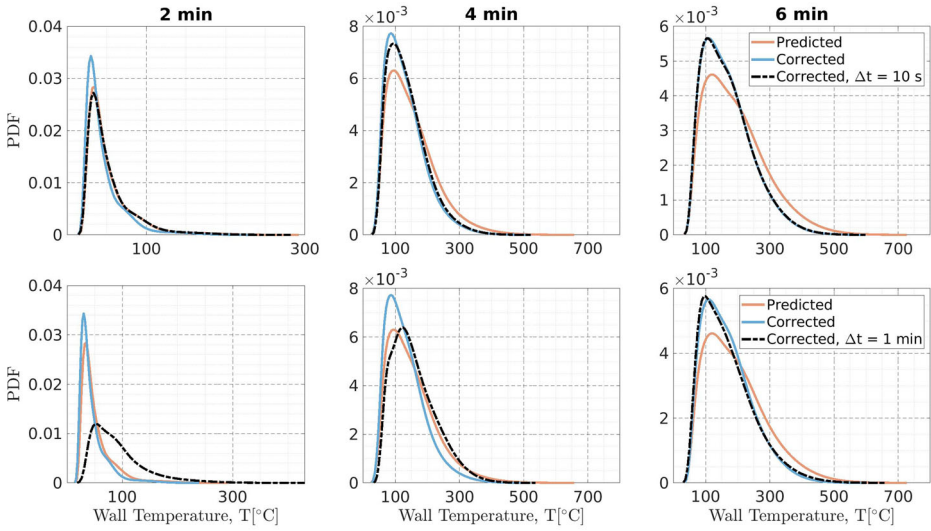


**Figure 24. Corrected probability density of wall temperature for the data that are shifted in time by  $\Delta t$ . Upper:  $\Delta t = 10$  s. Lower:  $\Delta t = 1$  min.**

In Sect. 4.2 we conclude that the coupled analysis approach for wall temperatures prediction is more accurate than the standalone approach. This could be confusing as the random model errors,  $\tilde{\sigma}_\epsilon\{M\}$ , presented in Table 4 is lowest for standalone model with boundary  $q''_{Exp}$ . The basis for this reasoning is the comparatively high bias values for standalone model with boundary  $q''_{Exp}$  presented in Table 4 and the first two plots in Figure 16. Similarly, the average model uncertainty values presented in Table 4 may not fully comply with the values presented in Figs. 15 and 16. This is because the values in Table 4 are based on the peak values of all measurement points, while the ones presented in Figs. 15 and 16 correspond to the measured and predicted outputs presented in Figs. 12 and 13 respectively, i.e., one measurement point located at the side wall 1.3 m from floor and 4.5 m from the back wall.

Finally, the study presents predicted and corrected CDF of wall temperatures calculated for the input stochastics listed in Table 6. The proposed correction method handles only one type of different uncertainties appearing in a probabilistic simulation with deterministic models. Other uncertainty types, input uncertainty and sampling uncertainty deserve their own studies when aiming at accurate fire risk analyses. Figure 25 presents an overall procedure for uncertainty management in the stochastic simulation. Estimation of input uncertainty distribution is crucially important for the simulation outcome and can require significant effort if the number of uncertain parameters is high. Luckily, in a nonlinear system, such as fire, the number of dominating input parameters is usually small [24]. For sampling uncertainty, the convergence of the distribution moments can be studied, as explained in Sect. 2.4. This would be very expensive if a complex numerical

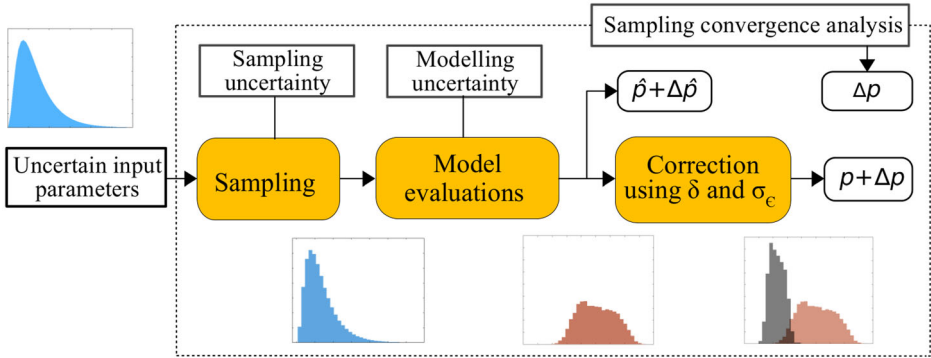


**Figure 25. Schematic diagram showing the procedure of uncertainty management in the stochastic simulations.**

method such as CFD is being used. Means to quantify the sampling convergence in LHS could possibly be developed using surrogate models, such as the response surface method.

## 6. Conclusion

In this work, we show that the model uncertainties based on the peak outputs and the current experimental data are similar to the ones estimated from the FDS validation database. The coupled analysis (FDS alone) had the smallest model uncertainties in wall temperatures. The higher uncertainties in the standalone analyses were caused by the high uncertainties of the heat flux, i.e. additional uncertainty propagation. The model uncertainties were found to vary over time, however, the probability correction using the generalized uncertainty parameters was effective at each time instance. The model uncertainties reported in the context of a model validation can be, therefore, used for correcting the output distributions resulting from parameter (input) uncertainty. Nevertheless, the proposed method for the model uncertainty compensation may not be effective when the model uncertainty cannot be generalized. Further work is needed to study the effect of Latin hypercube sampling uncertainty in failure probability calculation. Also, validation using larger experimental datasets and a wider range of output quantities would be valuable.

## Acknowledgements

Open access funding provided by Aalto University. This work has been funded by the State Nuclear Waste Management Fund of Finland in the scope of the

SAFIR-programs, the Finnish Fire Protection Fund (Palosuojelurahasto), Raken-  
nustuotteiden laatu Säätiö SR and Nordic Nuclear Safety Research (NKS).

## Open Access

This article is distributed under the terms of the Creative Commons Attribution 4.0 International License (<http://creativecommons.org/licenses/by/4.0/>), which permits unrestricted use, distribution, and reproduction in any medium, provided you give appropriate credit to the original author(s) and the source, provide a link to the Creative Commons license, and indicate if changes were made.

## Appendix 1: Estimation of True Distribution

In Sect. 2.2 we presented the uncertainty model which includes a constant multi-  
plicative term  $\delta$  and the random additive term  $\epsilon$ ,

$$\hat{T} = \delta \cdot T + \epsilon. \quad (11)$$

Satisfying Eq. 11 with mean we get,

$$\mu_{\hat{T}} = \delta \cdot \mu_T + \mu_{\epsilon}.$$

The mean of the random errors is zero,  $\mu_{\epsilon} = 0$ , hence,

$$\mu_{\hat{T}} = \delta \cdot \mu_T \quad (12)$$

Squaring both side of Eq. 11 and taking average,

$$\overline{\hat{T}^2} = \overline{\delta^2 \cdot T^2 + 2\delta \cdot T \cdot \epsilon + \epsilon^2}.$$

$T$  and  $\epsilon$  are independent of each other and  $\mu_{\epsilon} = 0$   $\overline{\delta \cdot T \cdot \epsilon} = 0$ . This results,

$$\sigma_{\hat{T}}^2 + \mu_{\hat{T}}^2 = \delta^2 \cdot \sigma_T^2 + \delta^2 \cdot \mu_T^2 + \sigma_{\epsilon}^2.$$

Using  $\mu_{\hat{T}} = \delta \mu_T$  from Eq. 12 we get,

$$\sigma_{\hat{T}}^2 = \delta^2 \cdot \sigma_T^2 + \sigma_{\epsilon}^2. \quad (13)$$

Next we estimate the true output  $T$  from the simulated output,  $\hat{T}$  using the con-  
stant coefficients  $\alpha$  and  $\beta$ .

$$T = \alpha \cdot \hat{T} + \beta. \quad (14)$$

To obtain  $\alpha$  and  $\beta$ , we use the expression of the mean and variance, Eqs. 12 and 13, respectively. Using the mean,

$$\begin{aligned}\mu_T &= \alpha \cdot \mu_{\hat{T}} + \beta, \\ \beta &= \frac{\mu_{\hat{T}}}{\delta} - \alpha \cdot \mu_{\hat{T}}.\end{aligned}\tag{15}$$

Similarly, using the expression of variance,

$$\begin{aligned}\sigma_T^2 &= \frac{1}{\delta^2} [\sigma_{\hat{T}}^2 - \sigma_\epsilon^2], \\ \bar{T}^2 - \mu_T^2 &= \frac{1}{\delta^2} [\sigma_{\hat{T}}^2 - \sigma_\epsilon^2].\end{aligned}$$

Squaring both side of Eq. 14 and replacing  $T^2$ ,

$$\begin{aligned}\overline{\alpha^2 \cdot \hat{T}^2 + 2\alpha \cdot \beta \cdot \hat{T} + \beta^2} - \frac{\mu_{\hat{T}}^2}{\delta^2} &= \frac{1}{\delta^2} [\sigma_{\hat{T}}^2 - \sigma_\epsilon^2], \\ \alpha^2 (\sigma_{\hat{T}}^2 + \mu_{\hat{T}}^2) + 2\alpha \cdot \beta \cdot \mu_{\hat{T}} + \beta^2 - \frac{\mu_{\hat{T}}^2}{\delta^2} &= \frac{1}{\delta^2} [\sigma_{\hat{T}}^2 - \sigma_\epsilon^2].\end{aligned}\tag{16}$$

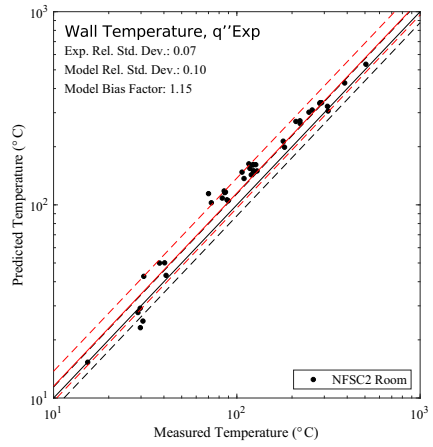
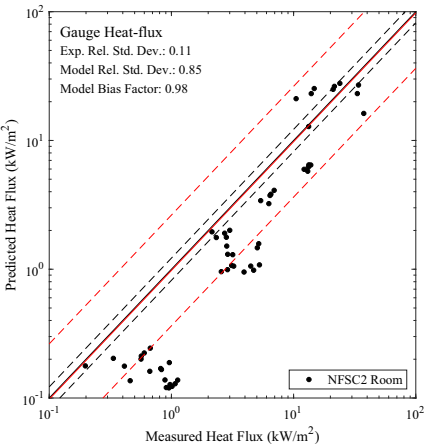
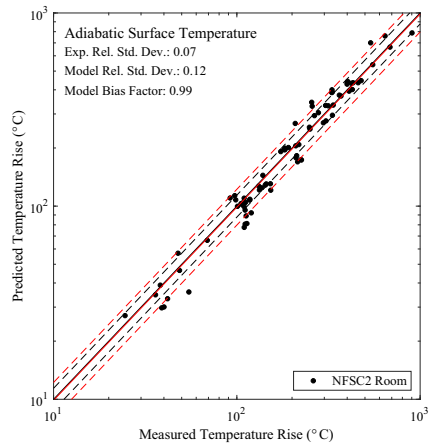
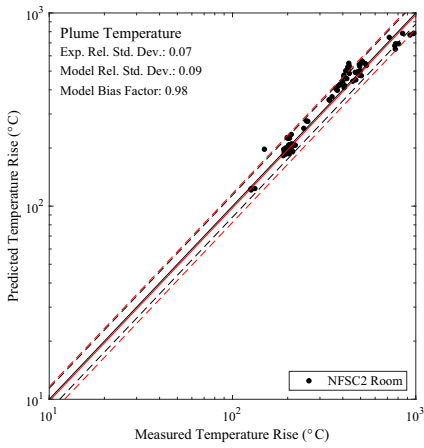
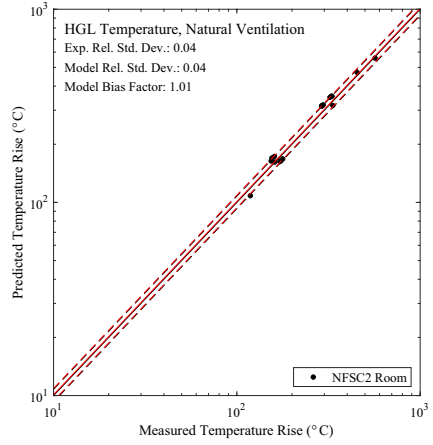
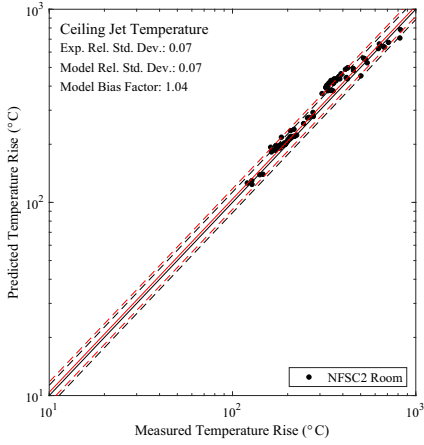
Now  $\alpha$  and  $\beta$  can be solved from Eqs. 15 and 16,

$$\alpha = \frac{1}{\delta} \sqrt{1 - \left(\frac{\sigma_\epsilon}{\sigma_{\hat{T}}}\right)^2}\tag{17}$$

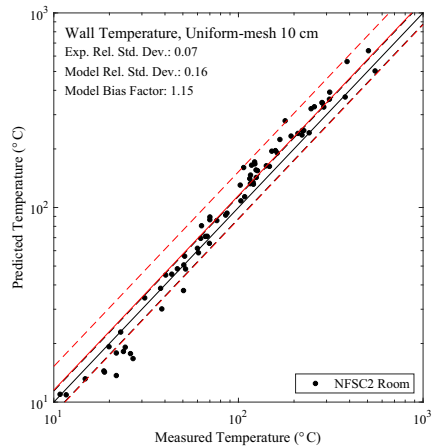
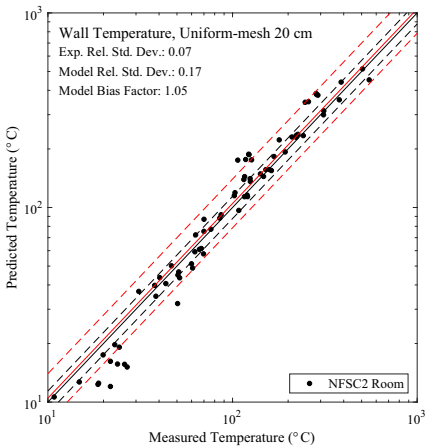
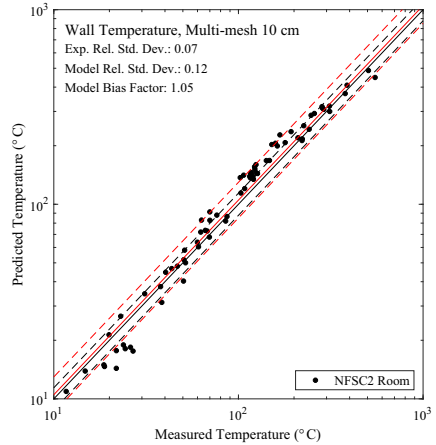
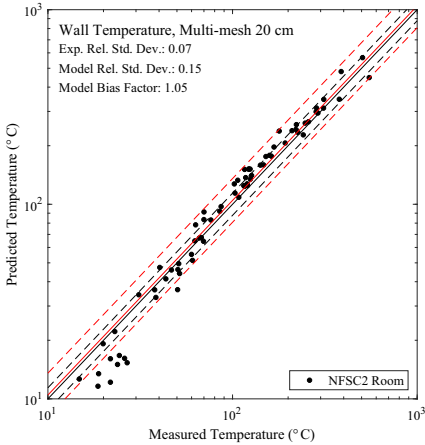
Replacing  $\alpha$  and  $\beta$  in in Eq. 14,

$$T = \frac{1}{\delta} \left[ \mu_{\hat{T}} + (\hat{T} - \mu_{\hat{T}}) \sqrt{1 - \left(\frac{\sigma_\epsilon}{\sigma_{\hat{T}}}\right)^2} \right]\tag{18}$$

## **Appendix 2: Uncertainty Metrics Showing the Measured and Predicted Outputs**



## Appendix 3: Uncertainty Metrics Showing the Measured and Predicted Wall Temperatures for Different Mesh Configurations

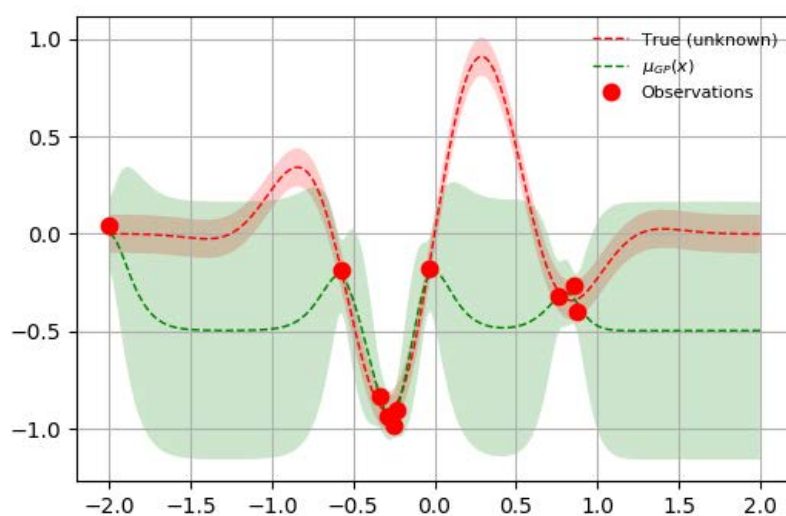


## References

1. Lee SR, Ryou HS (2006) A numerical study on smoke movement in longitudinal ventilation tunnel fires for different aspect ratio. *Build Environ* 41(6):719–725
2. Shen TS, Huang YH, Chien SW (2008) Using fire dynamic simulation (fds) to reconstruct an arson fire scene. *Build Environ* 43(6):1036–1045
3. Drean V, Schillinger R, Leborgne H, Auguin G, Guillaume E (2018) Numerical simulation of fire exposed facades using LEPIR II testing facility. *Fire Technol* 54(1):1–24
4. Yu LX, Beji T, Maragkos G, Liu F, Weng MC, Merci B (2018) Assessment of numerical simulation capabilities of the fire dynamics simulator (fds 6) for planar air curtain flows. *Fire Technol* 54(3):583–612

5. Zadeh SE, Maragkos G, Beji T, Merci B (2016) Large eddy simulations of the ceiling jet induced by the impingement of a turbulent air plume. *Fire Technol* 52(6):2093–2115
6. Jujuly MM, Rahman A, Ahmed S, Khan F (2015) Lng pool fire simulation for domino effect analysis. *Reliab Eng Syst Saf* 143(1):19–29
7. McGrattan K, Toman B (2011) Quantifying the predictive uncertainty of complex numerical models. *Metrologia* 48(3):173
8. McGrattan K, Hostikka S, Floyd J, Baum H, Rehm RG, Mell W, McDermott R (2013) Fire dynamics simulator, technical reference guide, volume 3: validation. National Institute of Standards and Technology, Maryland. NIST Special Publication 1018
9. Matala A, Hostikka S (2011) Probabilistic simulation of cable performance and water-based protection in cable tunnel fires. *Nucl Eng Des* 241(12):5263–5274
10. Hietaniemi J (2007) Probabilistic simulation of fire endurance of a wooden beam. *Struct Saf* 29(4):322–336
11. Ayala P, Cantizano A, Sánchez-Úbeda E, Gutiérrez-Montes C (2017) The use of fractional factorial design for atrium fires prediction. *Fire Technol* 53(2):893–916
12. Anderson A, Ezekoye OA (2018) Quantifying generalized residential fire risk using ensemble fire models with survey and physical data. *Fire Technol* 54(3):715–747
13. McGrattan K, Peacock R, Overholt K (2016) Validation of fire models applied to nuclear power plant safety. *Fire Technol* 52(1):5–24
14. Liang B, Mahadevan S (2011) Error and uncertainty quantification and sensitivity analysis in mechanics computational models. *Int J Uncertain Quantif* 1(2):147–161
15. Olsson K, Anderson J, Lange D (2017) Uncertainty propagation in FE modeling of a fire resistance test using fractional factorial design based model reduction and deterministic sampling. *Fire Saf J* 91(1):517–523
16. Hamilton WC (1964) *Statistics in physical sciences*. Ronald Press Co., New York
17. Robert C, Casella G (2013) *Monte Carlo statistical methods*. Springer, Berlin
18. Iman R, Davenport J, Zeigler D (1980) *Latin hypercube sampling (a program users guide): Technical report sand79-1473*, Sandia Laboratories, Albuquerque, NM
19. Suard S, Hostikka S, Baccou J (2013) Sensitivity analysis of fire models using a fractional factorial design. *Fire Saf J* 62(1):115–124
20. Paudel D, Hostikka S (2019) Propagation of modeling uncertainty in stochastic heat-transfer simulation using a chain of deterministic models. *Int J Uncertain Quantif* 9(1):1–14
21. Crow EL (1956) Confidence intervals for a proportion. *Biometrika* 43(3/4):423–435
22. Hostikka S, Kokkala M, Vaari J (2001) Experimental study of the localized room fires: NFSC2 test series. Technical Research Centre of Finland, VTT Research Notes 2104. 49 p
23. McGrattan K, Hostikka S, McDermott R, Floyd J, Weinschenk C, Overholt K (2013) Fire dynamics simulator, technical reference guide, volume 1: mathematical model. National Institute of Standards and Technology, Maryland. NIST Special Publication 1018
24. Hostikka S, Keski-Rahkonen O (2003) Probabilistic simulation of fire scenarios. *Nucl Eng Des* 224(3):301–311

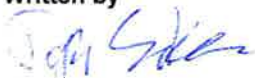
## Annex H



## Model based optimization for calibration of pyrolysis models

Authors: Topi Sikanen

Confidentiality: Public

<b>Report's title</b>	
Model based optimization for calibration of pyrolysis models	
<b>Customer, contact person, address</b>	<b>Order reference</b>
SAFIR2018 programme	
<b>Project name</b>	<b>Project number/Short name</b>
Fire Risk Evaluation and Defence-in-depth (FIRED)	110308/FIRED
<b>Author(s)</b>	<b>Pages</b>
Topi Sikanen	18/
<b>Keywords</b>	<b>Report identification code</b>
Pyrolysis, Optimization, Parameter Identification, Bayesian Optimization	VTT-R-05578-18
<b>Summary</b>	
<p>This report describes a tool for pyrolysis model parameter identification called "PyroPython". PyroPython is successor to the pyroplot tool that was developed in earlier SAFIR projects. The motivation for writing a new tool was to make it faster and more accessible. Python was chosen as the programming language of the project due to the rich open source scientific computing ecosystem available for python.</p> <p>Unlike pyroplot, which used genetic algorithms for optimizing the model parameters, PyroPython aims to be agnostic to the choice of optimizer. At the time of writing, the software support Bayesian Optimization (BO), optimization by multistart method using a derivative free optimization algorithm (Nelder-Mead) using multiple random starts, differential evolution and random sampling.</p> <p>Usage of BO for parameter identification is novel aspect of PyroPython tool. Bayesian optimization involves fitting a response surface model to model evaluations and using the response surface to explore promising solution candidates.</p> <p>The PyroPython tool is released as open source software and is available from <a href="https://github.com/Pyroid/PyroPython">https://github.com/Pyroid/PyroPython</a>. The documentation can be found at <a href="http://pyroid.github.io/">http://pyroid.github.io/</a>.</p>	
<b>Confidentiality</b>	Public
Espoo 2.11.2018	
<b>Written by</b>	<b>Reviewed by</b>
	
Topi Sikanen	Anna Matala
Senior Research Scientist	Senior Research Scientist
<b>Accepted by</b>	
	
Eila Lehmus	
Research Team Leader	
<b>VTT's contact address</b>	
Anna Matala, P.O. Box 1000, FI-2044 VTT, Finland	
<b>Distribution (customer and VTT)</b>	
VTT, SAFIR2018	
<p><i>The use of the name of VTT Technical Research Centre of Finland Ltd in advertising or publishing of a part of this report is only permissible with written authorisation from VTT Technical Research Centre of Finland Ltd.</i></p>	

## Contents

---

Preface.....	2
Contents.....	3
1. Introduction.....	4
2. Parameters needed by pyrolysis models.....	5
2.1 Reaction kinetic scheme .....	5
2.2 Kinetic parameters.....	6
2.3 Thermophysical parameters .....	6
2.4 Connection between hyperparameter optimization and pyrolysis model selection ....	7
3. Parameter identification as optimization problem .....	7
3.1 Evaluating fit .....	7
3.2 Bayesian Optimization .....	8
3.3 Other Optimization methods .....	11
4. Determining pyrolysis parameters for synthetic model of birch wood. ....	12
4.1 Comparison of optimization methods .....	13
4.1.1 Error reduction per function evaluation.....	13
4.1.2 Quality of the solutions.....	15
5. Conclusions .....	18
References.....	18

## 1. Introduction

---

Predicting flame spread and solid ignition require the use of models describing the thermal degradation of solids under external heat flux. In the fire research community, such models are called pyrolysis models. Increasingly complex computational pyrolysis models have been proposed, from simple one-dimensional models to three-dimensional models incorporating material deformation and gas flow in the pores of porous materials.

In theory, including more and more physics in the model should allow one to predict the pyrolysis behaviour of materials with greater and greater accuracy. However, each new equation added to the model invariably comes with a number of parameters that usually cannot be determined directly from experiment.

Often the lack of experimental data for parameters is circumvented by use of inverse modelling. In inverse modelling, we take a pyrolysis model (or any simulator) that is able to model the experiment and try to work out the parameters that reproduce the experimental data.

In their study, Bal and Rein (2015), showed that models with widely different levels of complexity (3 to 30 free parameters) could produce results with similar accuracy when the parameters of each model were tuned by inverse modelling.

From a mathematical point of view, inverse modelling in the context of parameter identification for pyrolysis models is a regression problem. As such, the issues in model selection are similar to the problem of model selection in statistics.

This report describes the theoretical background for pyrolysis model parameter identification tool "PyroPython". PyroPython is successor to the "pyroplot" tool that was developed in earlier SAFIR projects. The motivation for writing a new tool was to make it faster and more accessible. Python was chosen as the programming language of the project due to the rich open source scientific computing ecosystem available for python. The user guide for pyropython is available at <http://pyrold.github.io>. This report focuses on the algorithms used and their comparison.

## 2. Parameters needed by pyrolysis models

---

### 2.1 Reaction kinetic scheme

In general, all the pyrolysis models used in fire simulations are simplifications of the reality. In a real degradation process several reactions occur simultaneously, some releasing fuel or inert gas to the gas phase, and some being phase change reactions. In predicting flame spread the most important characteristic is the mass loss and related fuel gas release.

The level of complexity of the model depends on the end application and the preferences of the modeller. There are three basic types of reaction schemes (see Figure 2-1): Parallel, Consecutive and Competing.

*Parallel* reaction scheme means that the material can be divided into two (or more) pseudo-components which degrade independently from each other. The reactions may or may not occur at the same temperature. A good example would be a wood sample including some amount of humidity. The sample would consist of a pseudo-component A (water) and pseudo-component B (wood polymer), which both undergo their own reactions depending on the temperature and their parameters.

*Consecutive* reaction scheme means that the material first degrades into another material, and then the second material degrades further to another material. An example of this could be a wood that first degrades into char, and then in the presence of oxygen and high temperatures converts to ash.

*Competing* reaction scheme is probably the most common in the nature, but less used in the pyrolysis modelling as it is more difficult to observe from the experimental data. It means that the material has two (or more) alternative reaction mechanisms (in this case, two sets of pyrolysis parameters) depending on the ambient conditions (temperature, oxygen content etc.). An example of this would be, once again, wood pyrolysis. According to di Blasi (diBlasi 1998), the in low temperatures the intermolecular dehydration dominates the process, while in high temperatures the dominant process is the depolymerisation reaction. The result of these reactions can be either char and fuel gas, or tar, respectively.

Often the selected reaction path can include a combination of these three. In some cases the choice is simple, e.g. in case of bound water it makes sense to use the parallel scheme. In some other cases the choice is not clear at all, or it doesn't matter; often equally well-fitting solutions can be found with different reaction paths. What has to be kept in mind is that the estimated parameters are always linked to the used reaction path - they do not have any physical meaning alone.

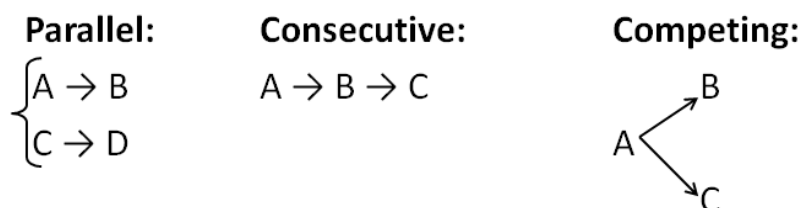


Figure 2-1. Reaction scheme options.

## 2.2 Kinetic parameters

In FDS, reaction rates are calculated using the Arrhenius equation

$$r_{ij} = A_{ij} \left( \frac{\rho_{s,i}(t)}{\rho_s(0)} \right)^{N_{s,ij}} \exp\left(-\frac{E_{ij}}{RT}\right) \quad 1$$

where  $A$  ( $s^{-1}$ ) is the pre-exponential factor,  $E$  (kJ/kmol) is the activation energy and  $N$  is the reaction order. Subscript  $i$  denotes the  $i^{\text{th}}$  material component and  $j$  the  $j^{\text{th}}$  reaction.  $\rho_{s,i}$  is the solid density of the component, and  $\rho_{s,0}$  is the original density of the layer. The solid phase heat conduction is solved in one dimension, according to the heat conduction equation.

The local densities of the material components then evolve according to

$$\frac{\partial}{\partial t} \left( \frac{\rho_{s,i}(t)}{\rho_s(0)} \right) = \sum_{j=1}^{N_{r,i}} r_{ij} + S_i, \quad 2$$

where  $N_{r,i}$  and  $S_i$  are the number of reactions and production rate for the  $i$ :th material component, respectively. The production rate can be calculated as

$$S_i = \sum_{n=1}^{N_m} \sum_{j=1}^{N_{r,m}} \gamma_{i,nj} r_{nj} \quad 3$$

where  $\gamma_{i,nj}$  is the yield of material component  $i$  from the  $j$ :th reaction of the  $n$ :th material component.

## 2.3 Thermophysical parameters

The temperature in the solid is solved from the heat conduction equation

$$\rho_s c_s \frac{\partial T_s}{\partial t} = \nabla \cdot k \nabla T + \dot{q}_s''' \quad 4$$

where  $T$  is temperature and  $c$  and  $k$  are the specific heat and thermal conductivity, respectively. The chemical source term  $\dot{q}_s'''$  contains the heats of reaction  $H_r$ , and is calculated as

The solid density is the sum of the composite densities

$$\rho_s = \sum_{n=1}^{N_m} \rho_n Y_n \quad 5$$

where  $Y_n$  is the mass fraction of the  $n$ :th material component. The thermal properties of the solid are determined in a similar manner.  $k_s = \frac{\sum_{n=1}^{N_m} X_n k_{s,n}}{\sum_{n=1}^{N_m} \rho_{s,n} c_{s,n}}$ ;  $\rho_s c_s =$  6

where  $X_n$  is the volume fraction of the  $n$ :th component.

## 2.4 Connection between hyperparameter optimization and pyrolysis model selection

In machine learning literature “hyperparameter optimization” refers to optimizing the parameters of machine learning algorithm or model. Examples of hyperparameters are

1. Number of layers and neurons in a neural net
2. Learning rate parameters used to teach the neural net
3. Parameters of kernel functions

The problem of hyperparameter optimization is also closely related to the model selection problem in statistics. A commonly used method for model selection is Cross Validation. Cross Validation works as follows

1. Suppose you have a set of observations  $X$
2. Split the test data into “training” set and “testing” set.
3. Train the model using the “training” set. Evaluate the predictive capability of the model on the “testing” set.
4. Repeat steps 2-3 with a different split of training and test sets a number of times
5. The best model is the one that has best performance outside the training set

“All models are wrong but some models are useful”. In this case “useful” is defined as a model that has good generalization capability (low error on the test set). In the machine learning world cross validation is a common method of combating overfitting.

## 3. Parameter identification as optimization problem

---

From mathematical point of view, the problem of determining the optimal parameters  $\theta$  parameters for model  $M$ , can be formulated as an optimization problem

$$\theta^* = \arg \min_{\theta} e(M(\theta)) \quad 7$$

### 3.1 Evaluating fit

Pyropython evaluates model fit as a convex combination of individual error measures:

$$e(\theta) = \sum_{i=1}^{N_{var}} \beta_i f(\theta) \quad 8$$

Here  $N_{var}$  refers to number of variables (e.g. temperature, mass loss rate),  $\beta_i$  is a weight given for variable  $i$ . By default, Pyropython uses an objective function based on standardized moments:

$$f(\boldsymbol{\theta}) = \sum_{j=1}^{N_{obs,i}} \alpha_{i,j} \frac{|y_{sim,i,j}(\boldsymbol{\theta}) - y_{exp,i,j}|^p}{\sigma_{exp,i}^p} \quad 9$$

In the above equation,  $N_{obs,i}$  is the number of observations for variable  $i$ ,  $\alpha_{i,j}$  is the weight given to observation  $j$  of variable  $i$ . In the fraction on the RHS,  $y_{exp,i,j}$  refers to experimental observation and  $y_{sim,i,j}(\boldsymbol{\theta})$  is the simulation model prediction with parameter vector  $\boldsymbol{\theta}$ . The exponent  $p$  is a user defined constant with  $p=1$  corresponding to absolute deviation and  $p=2$  to squared error. In the nominator  $\sigma_{exp,i}$  is the standard deviation of experimental observations. Unless stated otherwise,  $\beta_i = 1/N_{var}$  and  $\alpha_{i,j} = 1$  for the remainder of this document

Note that using  $\sigma_{exp,i}$  in Eq 97 has a similar effect as standardizing all variables before taking the differences (with unnecessary subscripts omitted for clarity):

$$\frac{|y_{sim} - y_{exp}|^p}{\sigma_{exp}^p} = \left| \frac{y_{sim}}{\sigma_{exp}} - \frac{y_{exp}}{\sigma_{exp}} \right|^p = \left| \frac{y_{sim} - \mu_{exp}}{\sigma_{exp}} - \frac{y_{exp} - \mu_{exp}}{\sigma_{exp}} \right|^p \quad 10$$

Here  $\mu_{exp}$  is the mean value of the experimental data and  $\frac{y_{exp} - \mu_{exp}}{\sigma_{exp}}$  is the standardized version of the experimental data (mean is 0 and variance is 1). This alleviates problems with trying to fit based on several variables with different magnitudes.

Other possibilities available in pyropython are the “relative deviation” and “gpyro” error measures. The “relative deviation” is given by

$$f(\boldsymbol{\theta}) = \sum_{j=1}^{N_{obs,i}} \alpha_{i,j} \frac{|y_{sim,i,j}(\boldsymbol{\theta}) - y_{exp,i,j}|}{|y_{exp,i,j}| + \varepsilon}, \quad 11$$

where  $\varepsilon$  is a small positive constant to avoid division by zero. The “gpyro” measure is negative of the fitness measure used in the software Gpyro (Lautenberger, 2009)

$$f(\boldsymbol{\theta}) = - \sum_{j=1}^{N_{obs,i}} \alpha_{i,j} \frac{|y_{exp,i,j}|}{|y_{sim,i,j}(\boldsymbol{\theta}) - y_{exp,i,j}| + \varepsilon |y_{exp,i,j}|}, \quad 12$$

In the limit  $\varepsilon \ll 0$  the “gpyro” measure is simply the inverse of the relative deviation. In testing no gain was found from using Eqs 119 or 1210 over Eq. 97.

## 3.2 Bayesian Optimization

In PyroPython, we implemented an optimization method that has not, as far as we know, been used in determining pyrolysis model parameters.

In their seminal paper, Jones et al. (1998) proposed an algorithm for “global optimization of blackbox functions”. Since then, the method they proposed has been employed for example in aerodynamic shape optimization and identifying model hyper parameters for machine learning methods. We will first describe the basic procedure and then proceed with the details

Bayesian Optimization is a form of sequential model based optimization. The general procedure of Bayesian optimization is as follows:

1. Evaluate the function to be minimized at a number of points sampled randomly from the search space
2. Fit a probabilistic model  $\mu(\boldsymbol{\theta})$  to the observed values  $y(\boldsymbol{\theta})$ .

3. Based on the probabilistic model, choose promising points where to evaluate the objective function.

The original and perhaps still most used, probabilistic model is the Gaussian Process<sup>1</sup>. However, any probabilistic model can be used in Step 2 of the above process. The important point is that the model should return both the prediction  $\mu(\theta)$  as well confidence interval on that prediction  $\sigma(\theta)$ . *Scikit-optimize* also provides decision tree based ensemble surrogate. Models available at the time of writing are Random Forests (RF), Gradient Boosted Regression Trees (GBRT) and Extra Randomized Trees (ET). These models work by combining several individual decision trees by some form of *bagging* or *boosting*, see e.g. Hastie et al. (2009) for tutorial on Tree based models.

The novelty of Bayesian optimization when compared to any response surface method comes from utilizing the confidence intervals of the probabilistic model. Figure 3-1 shows data points with a fitted Gaussian process and associated confidence intervals.

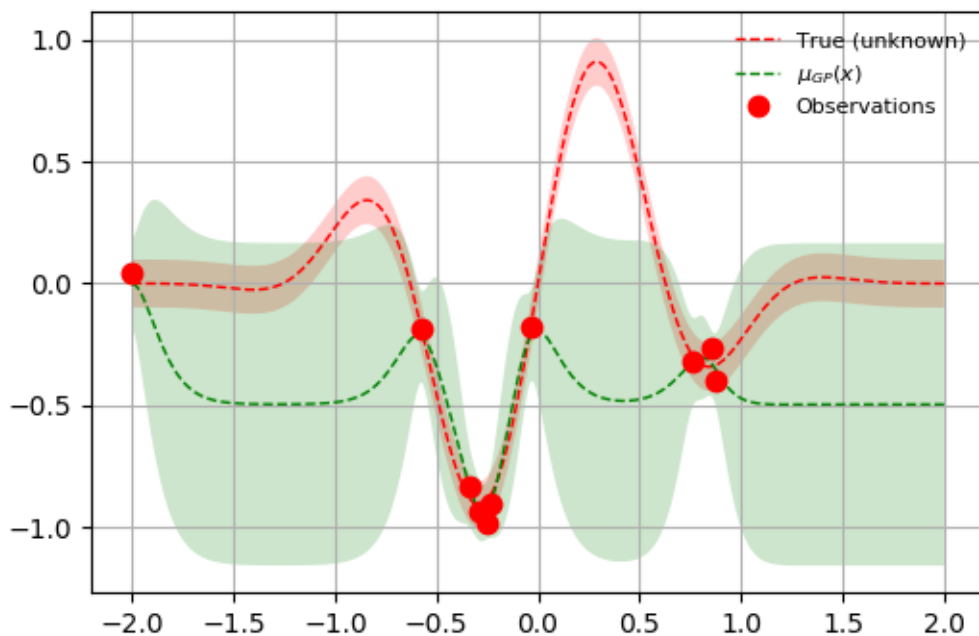


Figure 3-1 Gaussian process model fitted to a unknown function, based on noisy measurements. The green band shows the confidence interval  $\sigma(\theta)$  of the GP regression and the slashed green line shows the expected value of the GP,  $\mu(\theta)$ .

When determining where to evaluate the objective function next, two choices are obvious

1. *Exploitation*: Search for the minimum of  $\mu(\theta)$ .
2. *Exploration*: Explore regions where  $\mu(\theta) - \sigma(\theta)$  is small.

The first choice is equivalent to simply minimizing the fitted function, while the latter choice leads one to evaluate the objective function at regions of space yet unexplored. In BO algorithms, Step 3 is of the general algorithm usually involves minimizing a so-called *acquisition function*  $u(\theta)$ . Acquisition functions usually come with parameters to tune the

<sup>1</sup> See, e.g. . <http://www.gaussianprocess.org/gpml/>

balance between *exploration* (Choice 2) and *exploitation* (Choice 1). Several types of acquisition functions have been defined in the literature. We only consider 2:

1. Expected Improvement (EI):

$$u(\theta) = E[\mu(\theta) - \mu(\theta^*)] \quad 13$$

2. Lower Confidence Bound:

$$u(\theta) = \mu(\theta) - \kappa\sigma(\theta) \quad 14$$

In the above  $\theta^*$  is the best parameter combination seen thus far and  $\kappa$  is a free parameter. Unless stated otherwise we set  $\kappa = 1.96$ .

The expected improvement can be evaluated analytically, if we assume the surrogate is a Gaussian Process (see Jones,1999):

$$u(\theta) = \begin{cases} (\mu(\theta) - \mu(\theta^*) - \xi)\Phi(Z) + \sigma(\theta)\phi(Z) & \text{if } \sigma(\theta) > 0 \\ 0 & \text{if } \sigma(\theta) = 0 \end{cases} \quad 15$$

$$Z = \begin{cases} \frac{(\mu(\theta) - \mu(\theta^*) - \xi)}{\sigma(\theta)} & \text{if } \sigma(\theta) > 0 \\ 0 & \text{if } \sigma(\theta) = 0 \end{cases}$$

Here  $\Phi$  and  $\phi$  are the CDF and pdf of the standard normal distribution, respectively. The free parameter,  $\xi$ , controls the trade-off between exploration and exploitation. Higher values favour more exploration of the parameter space, while lower values favour exploitation of the surrogate model. The default value of  $\xi$  is 0.01.

Figure 3-2 shows the progress of the BO algorithm after evaluating 5 random starting points<sup>2</sup>. The left figure on the top row shows the situation after first fitting the GP surrogate to the 5 randomly sampled observations. The right figure on the top row shows the values of the EI acquisition function for this surrogate. The maximum of the acquisition function is shown with the blue dot. The maximum coincides with the global minimum of the objective function.

On the second row we have evaluated the objective function at the point suggested by the maximum of the EI function on the first row. Now the GP surrogate is fitted again to all points evaluated thus far. Based on this new surrogate we get new values for the acquisition function (left figure of the middle row). Maximizing the acquisition function leads to a new suggested point, again near the global optimum. This process is then repeated in the last row.

After the third iteration, the local optima have been very thoroughly sampled and consequently the confidence interval of the GP surrogate is small. This leads the algorithm to explore other regions of the objective function as shown by the suggested sampling points on rows 4 and 5.

Figure 3-2 shows very clearly, that the BO algorithm may find the global optimum, even if the GP surrogate is not good model of the true objective function everywhere.

<sup>2</sup> This example is adapted from <https://scikit-optimize.github.io/notebooks/bayesian-optimization.html>

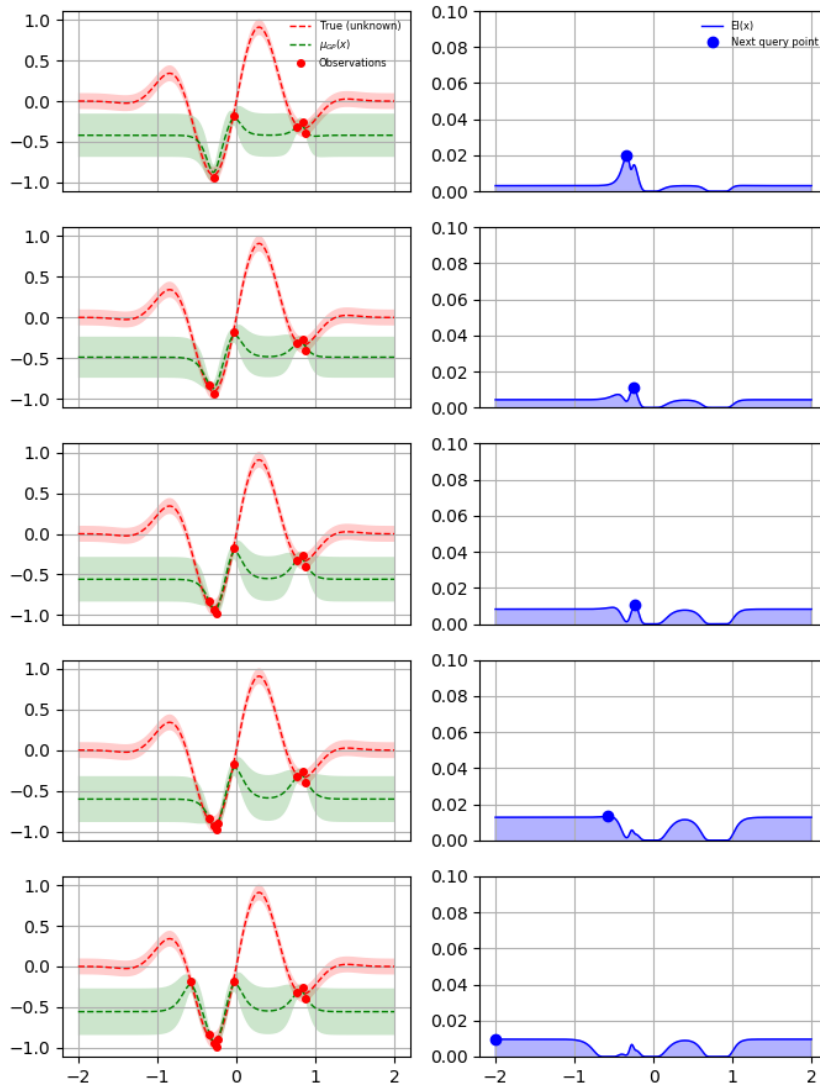


Figure 3-2 Progress of BO algorithm after 5 random starting points. On the left: The true objective function in red, the GP model of the objective function in green. On the right, the EI acquisition function (Eq. 1513). The blue dot shows the maximum of the acquisition function.

### 3.3 Other Optimization methods

Bayesian optimization is best suited for problems that fulfil the following criteria:

1. The function to be minimized is “black box”, i.e, derivative information is not available or is difficult to obtain
2. The function to be minimized is *expensive*

### 3. Function evaluations may be noisy.

Objective functions based on FDS (or any other simulator run by PyroPython) always fulfil criteria 1. FDS often fulfils Criteria 2, at least starting from the size of a cone-calorimeter simulation. The same can be said about Criteria 3, at least for simulations involving the gas phase, FDS results include noise (but not much).

Sometimes, the objective function is not quite so noisy or expensive, but still “black-box”. For these situations, PyroPython offers “multistart” optimization by Nelder-Mead method (as implemented in Scipy.optimize). Nelder-Mead method is a derivative free (“black box”) optimization method that has linear convergence rate. There are no global convergence proofs for Nelder-Mead. In fact it is known not to converge to a local minimizer for some objective functions. However it has been found very successful in practice.

In addition to the BO and multistart methods, PyroPython also allows one to search for the minimum using random sampling. This is useful as a baseline comparison for optimization methods.

## 4. Determining pyrolysis parameters for synthetic model of birch wood.

As an example, we determine the kinetic and thermal parameters of Birch Wood needed by FDS condensed phase model. The experimental data used for fitting was created by running FDS with the chosen “True” value. The example is based on the Birch\_TGA\_Example available in the PyroPython repository<sup>3</sup>.

*Table 4.1 The True parameter values and optimization bounds for the synthetic optimization test*

Parameter	True value	Bounds for optimization	
		min	max
<b>YWATER</b>	0.024	0.01	0.06
<b>LOGAW</b>	23	21	24
<b>EW</b>	140	130	160
<b>LOGA_SELLU</b>	11.45	10	12
<b>E_SELLU</b>	167	160	180
<b>NS_SELLU</b>	0.62	0.5	1.0
<b>LOGA_HEMISELLU</b>	10.7	10	12
<b>E_HEMISELLU</b>	140	130	150
<b>NS_HEMISELLU</b>	1	0.5	2.0
<b>YGAS_HS</b>	0.997	0.8	1.0

<sup>3</sup> [https://github.com/Pyrold/PyroPython/blob/master/examples/Birch\\_TGA\\_Example/](https://github.com/Pyrold/PyroPython/blob/master/examples/Birch_TGA_Example/)

<b>LOGA_LIGNIN</b>	9.2	8	10
<b>E_LIGNIN</b>	150	140	160
<b>YGAS_LIGNIN</b>	0.5	0.3	0.6

## 4.1 Comparison of optimization methods

### 4.1.1 Error reduction per function evaluation

This section presents results from a computational experiment comparing different optimization methods for determination of kinetic parameters. The problem considered in this experiment is determination of kinetic parameters for birch wood pyrolysis (Grønli scheme). Experimental data consists of TGA data at four different heating rates. The PyroPython input files and experimental data files are available in the PyroPython repository. The achieved MSE is recorded as a function of number of function evaluations. In this context “function evaluation” means running FDS on all the templates (4 heating rates) and evaluating the objective function.

*Table 4.2 Settings for the computational experiment comparing optimization methods.*

<b>Label</b>	<b>Estimator</b>	<b>Acquisition function</b>	<b>Optimizer</b>
<b>GP</b>	Gaussian Process	EI	scikit-optimize
<b>ET</b>	Extra randomized Trees	EI	scikit-optimize
<b>Nelder-Med</b>	NA	NA	Melder-Mead
<b>Differential evolution</b>	NA	NA	differential evolution
<b>Ransom sampling</b>	NA	NA	dummy

The experiment compares four optimization methods:

1. ET: Bayesian optimization with Extra randomized Trees regressor.
2. GP: Bayesian optimization with Gaussian process regressor
3. N-M: Nelder mead simplex
4. DE: Differential evolution

The experimental procedure was as follows:

1. Create a common set of initial designs using LHS sampling and evaluate the objective function for these. The size of the initial population was 150 points.
2. Run optimization methods 1-3 using this initial data. The differential evolution algorithm implementation in scipy does not support giving the initial design so the algorithm determined its own initial population
3. Record the best objective value (MSE) for up to 1000 function evaluations

Figure 4-1 shows convergence plots for Bayesian Optimization with two different regressors and two traditional optimization methods (Nelder-Mead and Differential evolution). The

continuous lines show the median of MSE from all the runs while the shaded area shows the range of minimum and maximum.

For the present case, in terms of improving MSE per function evaluation, best optimizers are (from best to worst):

1. Nelder-Mead simplex
2. BO with Gaussian Process regressor
3. Differential evolution
4. BO with extra trees regressor
5. Random sampling (dummy)

The poor performance of Differential Evolution algorithm can be compensated for by exploiting parallelism. The implementation of the Differential Evolution algorithm employed here does not lend itself to parallelization so the parallelism aspect was not explored. However, the speedup should be approximately linear in the number of cores used. In contrast the Nelder-Mead simplex cannot be parallelized at all and parallelization of the BO algorithms is still an open research question.

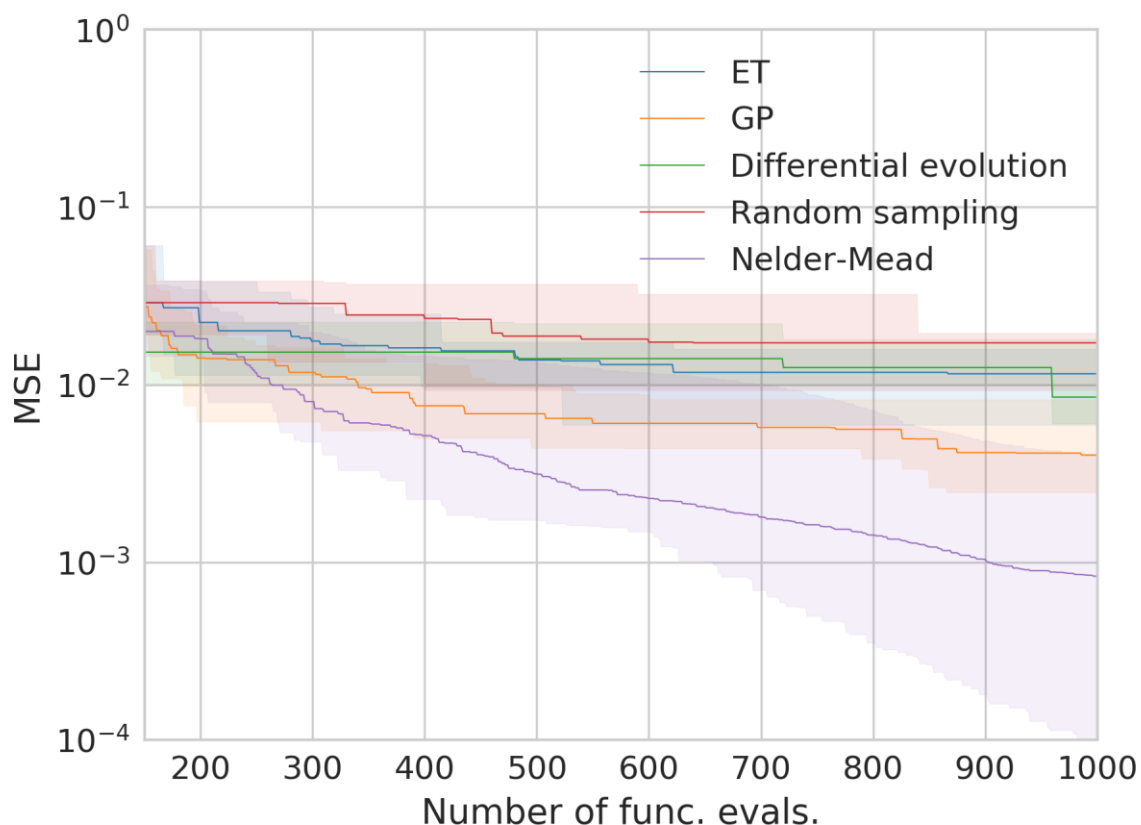


Figure 4-1 Convergence plots for two different regressors and two traditional optimization methods. Estimation of kinetic parameters from TGA experiment. The vertical axis shows the mean squared error and horizontal axis shows the number of function evaluations (FDS runs). The shaded area shows the minimum and maximum bounds while the continuous lines show the median.

The performance of the BO algorithm with GP surrogate is better than the Nelder-Mead method, especially in the first 200 or so iterations. The performance of the BO algorithm could

be further improved by using a more accurate optimizer for the acquisition functions. However, fitting a GP model is relatively slow and better optimization algorithms would incur an added cost to the computation.

The GP model needs to be fitted at every iteration and the cost of fitting the model increases as  $N^3$ , where  $N$  is the number of points used. For the present case, the 1000<sup>th</sup> iteration took about 1000 seconds. In contrast, the Nelder-Mead method used between 20-30 seconds per iteration. This simply means that the problem of determining TGA parameters is not costly enough for the BO algorithm to be useful. Things may change if the simulations would require more computational time. Figure 4-2 shows convergence plot, where an additional optimization method GP-DE is used. The GP-DE is otherwise exactly the same as GP but the acquisition function is optimized using the differential evolution algorithm. The option of using differential evolution for optimizing the acquisition function is not currently available in PyroPython as this would require modifying the the scikit-optimize package.

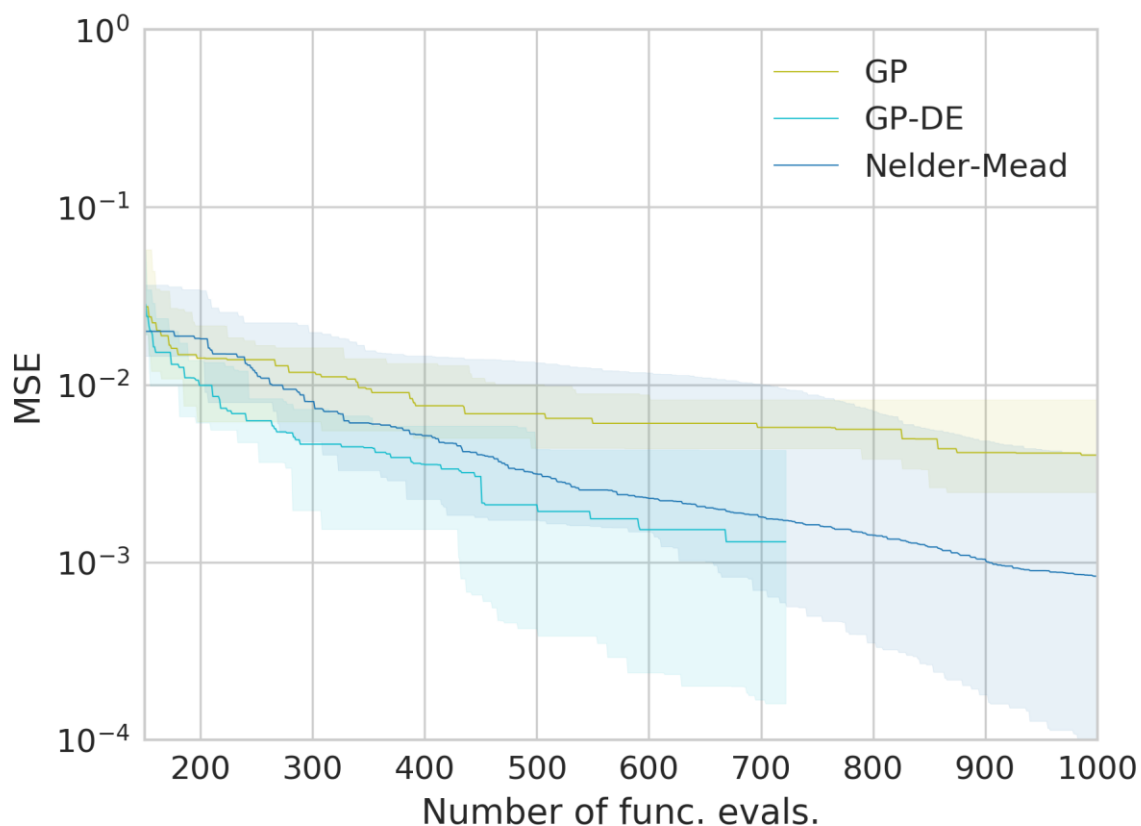
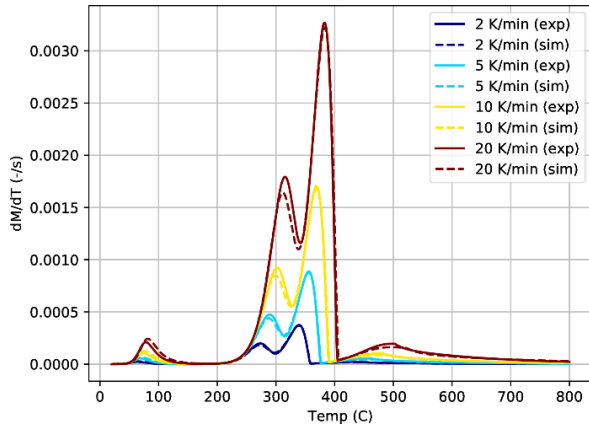


Figure 4-2 Convergence plots for BO algorithm using the GP and two different optimization methods for the acquisition function.

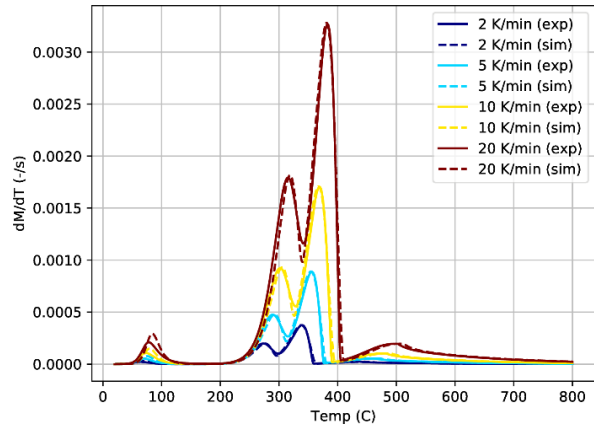
#### 4.1.2 Quality of the solutions.

Figure 4-3 shows the best solutions found by different optimization methods within the first 1000 iterations. Qualitatively, Nelder-Mead and GP models show the best match to experimental data. The result of the Nelder-Mead method matches the experimental data almost exactly.

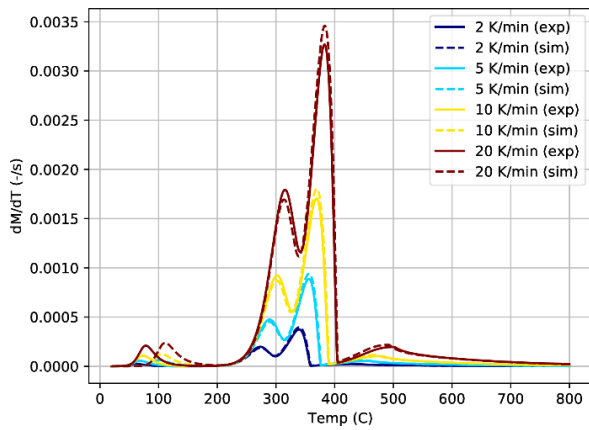
**skopt, Gaussian Process (GP)**



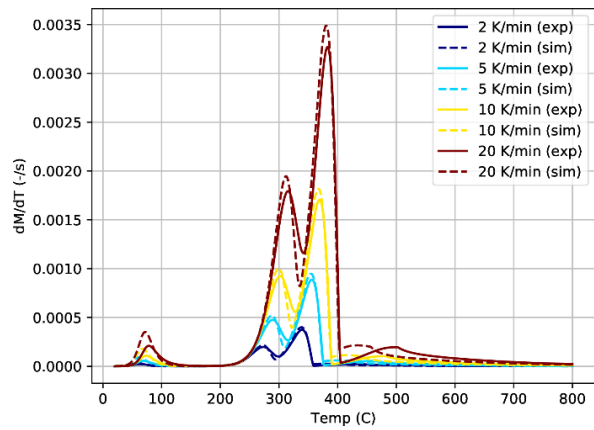
**skopt, ExtraRandomizedTrees (ET)**



**Random sampling (dummy)**



**Differential evolution**



**Nelder-Mead**

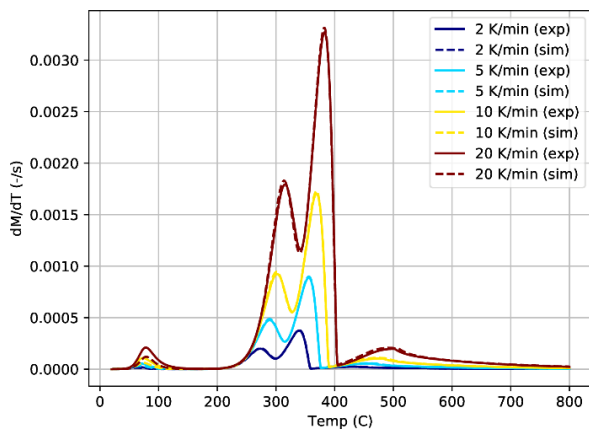


Figure 4-3 Best solution found within the first 1000 function evaluations for all the optimization methods

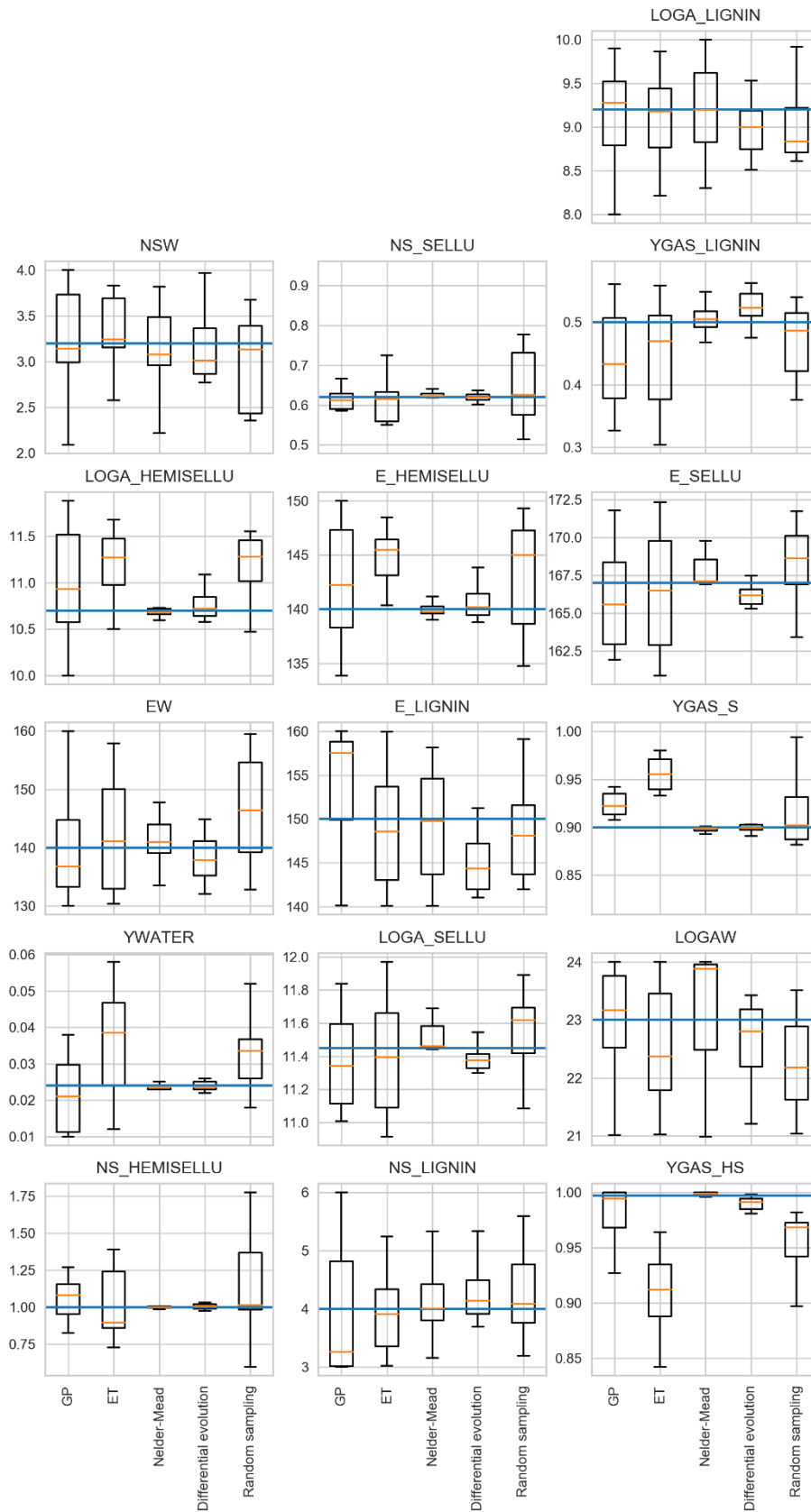


Figure 4-4 Distribution of parameter values from the test optimization.

## 5. Conclusions

---

This report described the theoretical underpinnings of the PyroPython tool. PyroPython was born out of the need for an easier to use version of PyroPlot. Unlike Pyroplot, PyroPython aims to be agnostic of the optimization method used. Four optimization methods are supported “out of the box” current version. Adding new solvers is a fairly straightforward task.

Several optimization methods were tested on a very challenging 16 parameter pyrolysis model fitting problem. It was found that, at least for the present optimization problem, the traditional optimization methods, Nelder-Mead simplex and differential evolution have better performance than the Bayesian Optimization methodology.

This conclusion may, however, change if the optimization problem at hand would be more costly to evaluate, say a long cone calorimeter experiment or a bench scale experiment.

## References

---

- Bal, N. and Rein, G., 2015. On the effect of inverse modelling and compensation effects in computational pyrolysis for fire scenarios. *Fire Safety Journal*, 72, pp.68-76.
- Bal, N. and Rein, G., 2013. Relevant model complexity for non-charring polymer pyrolysis. *Fire Safety Journal*, 61, pp.36-44.
- diBlasi, C. 1998. Physico-chemical processes occurring inside a degrading two-dimensional anisotropic porous medium. *International Journal of Heat and Mass Transfer* 41: 4139-4150.
- Jones, D.R., Schonlau, M. and Welch, W.J., 1998. Efficient global optimization of expensive black-box functions. *Journal of Global optimization*, 13(4), pp.455-492.
- Gao, F. and Han, L. Implementing the Nelder-Mead simplex algorithm with adaptive parameters. 2012. *Computational Optimization and Applications*. 51:1, pp. 259-277
- Storn, R and Price, K, Differential Evolution - a Simple and Efficient Heuristic for Global Optimization over Continuous Spaces, *Journal of Global Optimization*, 1997, 11, 341 - 359.
- Jones E, Oliphant E, Peterson P, et al. SciPy: Open Source Scientific Tools for Python, 2001-, <http://www.scipy.org/>
- Rasmussen C. and Williams C. 2006 *Gaussian Processes for Machine Learning* The MIT Press., ISBN 0-262-18253-X. <http://www.gaussianprocess.org/gpml/>
- Hastie, T., Tibshirani, R., & Friedman, J. H. 2009. *The elements of statistical learning: data mining, inference, and prediction*. <https://web.stanford.edu/~hastie/ElemStatLearn/>
- Lautenberger, C., 2007. *A Generalized Pyrolysis Model for Combustible Solids*, Ph.D Dissertation, Department of Mechanical Engineering, University of California, Berkeley.

---

Title	Determination of Fire Barriers reliability for fire risk assessment of Nuclear Power Plants. (FIREBAN) – Final Report
Author(s)	Patrick van Hees <sup>1</sup> Simo Hostikka <sup>2</sup> Topi Sikanen <sup>3</sup> Dan Lauridsen <sup>4</sup> Sebastian Levin <sup>5</sup>
Affiliation(s)	1. Lund University, Sweden 2. Aalto University, Finland 3. VTT Technical Research Institute, Finland 4. DBI Danish Institute of Fire and Security Technology, Denmark 5. Ringhals AB, Sweden
ISBN	978-87-7893-516-8
Date	July 2019
Project	NKS-R / FIREBAN
No. of pages	26 (without annexes)
No. of tables	0
No. of illustrations	9
No. of references	22
Abstract max. 2000 characters	Fires in nuclear power plants can be an important hazard for the overall safety of the facility. An important factor in reducing the spread of the fire is the use of fire barriers. However, it is important to be able to quantify the uncertainty of the result of the fire resistance of a fire barrier for fire risk assessment of nuclear power plants. The final report summarises the activities of the project at the different partners which means reliability of fire barriers by calculation tools, determination of uncertainty and sensitivity of input parameters with modelling of fire resistance of fire barriers.
Key words	Fire, nuclear power plants, fire barriers, modelling, uncertainty